UNIVERSITÉ DE STRASBOURG

ÉCOLE DOCTORALE DES SCIENCES CHIMIQUES

UMR-7177

THÈSE présentée par :

Alice Santoro

le 16 décembre 2019

Pour obtenir le grade de: **Docteur de l'université de Strasbourg**

Discipline: Sciences Chimiques

Métallothionéines et biomolécules capables de chélater et/ou de réduire le Cu et leur impact sur l'activité rédox et sur la stabilité des complexes de Cu d'intérêt médicinal

Etude de cas sur des complexes de Cu-peptide amyloïde ou sur des principes actifs à base de Cu

THÈSE dirigée par:	Prof. Peter Faller, Université de Strasbourg
RAPPORTEURS:	Prof. Claudia Blindauer, University of Warwick
	Dr. Olivier Seneque, CEA-Grenoble
AUTRES MEMBRES DU JURY:	Prof. Marine Desage-El-Murr, Université de Strasbourg

To my beloved family.

Acknowledgments

This manuscript is the result of the work I carried out during the past 3 years, not alone, but with the fundamental contribution and support of many people, that have made it possible. I wish to start it by expressing my gratitude to them, that from near and far, have been part of this challenging but full of achievements journey and contributed to the great fun of learning.

The first big thanks go to Peter, for having been an inspiring PhD advisor. The opportunities you have given me in these three years are unique and very much appreciated. I have learnt a lot from you, not only about science but also about many other aspects of life. You managed to teach me how to work independently but always supporting with stimulating discussions and useful advices. I feel lucky to have had the luck to enjoy your broad scientific knowledge, and your non-stop availability. You have been a great example of how to work efficiently and effectively and of how it is possible (and how important it is) to balance work with personal life. I am glad to have been part of your team!

I wish to thank Dr. Claudia Blindauer, Dr. Olivier Seneque and Dr. Marine Desage-El-Murr for offering their time to read and evaluate this manuscript and to be part of my dissertation committee.

During these years I had the luck to collaborate with many scientists outside from our group. I am extremely grateful to all of them for their essential contribution to the realization of the different projects, as this research work would have not been possible without your support.
Dr. Wojciech Bal, Dr. Nina Ewa Wezynfeld, Ewelina Stefaniak and Dawid Płonka for your contribution to the project concerning the reactivity of Cu-Aβ complexes with MT-3. Thank you for having provided the peptide, for your contribution in improving the manuscripts and for having warmly hosted me during the two very cold weeks I spent in Warsaw in your laboratories.
Dr. Artur Krezel, Dr. Adam Pomorski and Manuel David Peris-Dıáz, for providing MT samples. I was very pleased to have personally met you during the EuroBIC in Birmingham.
Dr. Oscar Palacios for helping with the ESI-MS experiments and taking care of me in Barcelona.
Dr. Bertrand Vileno, for your help with the EPR experiments. If this powerful technique is less a mystery now, it is also thanks to you. I've really enjoyed the days spent running EPR samples, entertained with inspiring discussions.
Dr. Gabriele Meloni and Jennifer Calvo for your contribution to the luminescence experiments.
Dr. Gaiddon Christian and Gilles Riegel for your contribution to the cell experiments with TSCs.
Dr. Isabelle Michaud-Soret, for hosting me in your laboratories at CEA in Grenoble, Dr Aurélien Deniaud and Roger Miras for teaching me how to express and purify Atox-1.
Dr. Romain Ruppert, for having provided many of the ligands without which a part of these studies would have not been possible. But also thank you for your constant positive humor! I've always enjoyed conversations with you.

I am really grateful to all the people that over these three years have been part of the 'BCB group' or better 'BCB family'. These years have not only been hard work and chemistry together but also a lot of apero, dinners, birthday parties, coffee breaks, breakfasts and conferences together. And it is because of all these moments together that I will leave with great memories and friendships to take with me.
The magic trio of the permanents: Laurent (my darling), Vincentito, Angelique. Thank you for your help in the lab, for sharing your suggestions and creative ideas for my projects. But also, for

your friendship and wise advices not related to science. A special thanks goes to Angelique for her essential help with the French part of thesis, grazie mille!
Thank you, Pau and Nina, who contributed to intellectually stimulating conversations about science and fun conversations about life in the office. It's been a great pleasure to discover Mexican and Polish cultures (mostly food and drinks, of course) with you.
Et voila, thank you, Gulshan for the short but intense stay in our lab!
Grazie Enrico, per aver portato un po'di Italia nel laboratorio. Le infinite conversazioni (pettegolezzi) rimaranno un ricordo indelebile nella mia memoria.
Thank you, Michael, Thibaut and Maxime, you've been a nice company in the office in the last two crazy months spent writing the manuscript.
Merci à Ryan de m'encourager toujours à parler français.
I also want to thank all the undergraduate students who have been in the lab in these years, Alex, Capucine, Elodie, Lucie, Wen li, Andres and Brice. A special thanks goes to Alex for his hard work and contribution to the study of the reactivity of Cu-Phen and Cu-Bipy complexes with GSH. It's been a great opportunity also for me to work with you!

Entertaining moments at the 4th floor have been shared with other awesome people that I would like to thank, Barbara, Michael, Christophe, Geordie, Elise, Moran, Dennis, Nolwen. Apero together will be deeply missed.

During these years I also had the luck to visit different floors of the Institute Le Bel, being the BCB group 'homeless' from time to time. I've been deeply impressed by the availability and hospitality of all the people that kindly offered to share their laboratories and offices with us.
8th floor – Équipe CLAC - Thank you Jean, Jennifer, Romain and Christophe and all the students of the team, Mary-Ambre, Thomas, Hervé, Jimmy. I got the luck to taste the greatest wines of Alsace and apero in Strasborg during your 'petite pot'. You are really amazing scientists and persons
9th floor - Équipe OMECA - Thank you Marine for having given us the chance to enjoy the best view of the cathedral, while working in the lab! Thanks again for accepting to be one of the members of my suivi de thèse and of my dissertation committee. Your availability has been really appreciated! But also, thanks to Agnideep and your numerous students! You have made the six months spent at 9th floor a nice time of my PhD journey.

My time in Strasbourg was also made enjoyable by many other friends outside from the lab that became part of my life. Thank you, Lilli e Mata, my best friends of this unforgettable experience. These years wouldn't have been the same without you! I am grateful to the big Italian family in Strasbourg that made me feel home far away from home. Thank you, Agnes, Cosimino, Matte, Ago e Marco for the memorable trips to the mountains, efforts have always been paid off with the best views (and not only) ever!

Grazie Ana e Dani, perchè è bastato poco tempo per scoprire degli amici sinceri!

Grazie ai miei Amichimici, Ire, Sofi, Angi, Dani, Nic1, Gio, Jacino e Nic2. Despite chemistry has spread us all over the world, we have been able to keep strong covalent bonds. You've been of great support during these years, although from far away.

Grazie Cami, Eli e Vio per avermi fatto sempre tornare il sorriso anche nei momenti piu duri. Grazie Sari per i tuoi indispensabili preziosi consigli. E grazie di cuore a Vale, Cheru e Sca che in questi anni hanno sempre mantenuto i contatti. Spesso succede che la distanza affievolisce i rapporti, ma nel nostro caso li ha resi piu forti!

Grazie Irene e Marco per avermi sempre su(o)pportato e fatto il regalo piu bello del mondo durante questo dottorato.

Grazie Elisina per il tuo sorriso che da quasi due anni è diventato lo sfondo stupendo delle mie giornate.

Grazie Mamma e Papà per avermi trasmesso l'importanza dello studio e della dedizione. Per avermi insegnato che 'la vita è fatta di sogni, progetti e realizzazioni' (cit) e che i sacrifici portano a grandi soddisfazioni. Grazie per avermi sempre seguito ed appogiato durante questi anni. La vostra presenza è la mia sicurezza.

E infine grazie a Marco, per aiutarmi ogni giorno a scegliere la strada migliore, che mi porta ad arrivare dove da sola non arriverei!

Table of Contents

List of publications in support of this thesis

Alice Santoro, Bertrand Vileno, Òscar Palacios, Manuel David Peris-Díaz, Gilles Riegel, Christian Gaiddon, Artur Krężeld and Peter Faller*, 'Reactivity of Cu(II)–, Zn(II)– and Fe(II)–thiosemicarbazone complexes with glutathione and metallothionein: from stability to dissociation to transmetallation', DOI: 10.1039/C9MT00061E, Metallomics, **2019**, 11, 994-1004.

Alice Santoro, Nina Ewa Wezynfeld, Ewelina Stefaniak, Adam Pomorski, Dawid Płonka, Artur Krężel, Wojciech Bal and Peter Faller*, 'Cu transfer from amyloid-β4–16 to metallothionein-3: the role of the neurotransmitter glutamate and metallothionein-3 Zn(II)-load states', DOI: 10.1039/C8CC06221H, Chem. Commun., **2018**, 54, 12634-12637.

Alice Santoro, Gulshan Walke, Bertrand Vileno, Prasad P. Kulkarni, Laurent Raibauta and Peter Faller*, 'Low catalytic activity of the Cu(II)-binding motif (Xxx-Zzz-His; ATCUN) in reactive oxygen species production and inhibition by the Cu(I)-chelator BCS', DOI: 10.1039/C8CC06040A, Chem. Commun., **2018**, 54, 11945-11948.

Elena Atrián-Blasco, Paulina Gonzalez, Alice Santoro, Bruno Alies, Peter Faller, Christelle Hureau*, 'Cu and Zn coordination to amyloid peptides: from fascinating chemistry to debated pathological relevance', DOI: 10.1016/j.ccr.2018.04.007, Coord. Chem. Rev., **2018**, 371, 38-55.

Elena Atrián-Blasco, Alice Santoro, Dean L. Pountney, Gabriele Meloni, Christelle Hureau and Peter Faller*, 'Chemistry of mammalian metallothioneins and their interaction with amyloidogenic peptides and proteins', DOI: 10.1039/C7CS00448F, Chem. Soc. Rev., **2017**, 46, 7683-7693.

Alice Santoro, Nina Ewa Wezynfeld, Milan Vašák, Wojciech Bal and Peter Faller*, 'Cysteine and glutathione trigger the Cu–Zn swap between Cu(II)-amyloid-$\beta_{4\text{-}16}$ peptide and $Zn(II)_7$-metallothionein-3', DOI: 10.1039/C7CC06802F, Chem. Commun., **2017**, 53, 11634-11637.

List of abbreviations

α_2M	α-2-macroglobulin
3-AP	3-aminopyridine-2-carboxaldehyde thiosemicarbazone
5,5'-DmBipy	5,5'-dimethyl-2,2'-dipyridyl
7-HO-CCA	7-hydroxycoumarin-3-carboxylic acid
Aβ	Amyloid β
Abs or A	Absorbance
AD	Alzheimer's disease
APDTC	Ammonium pyrrolidinedithiocarbamate
APP	Amyloid precursor protein
$AscH^-$	Ascorbate
$AscH^{\bullet-}$	Ascorbyl radical
Asp	Aspartic acid
Atox-1	Copper chaperone antioxidant 1
ATSM	Diacetylbis(4-methyl-3-thiosemicarbazone)
ATCUN	Amino terminal copper and nickel
BCS	Bathocuproine disulfonate
CCA	Coumarin-3-carboxylic acid
CCS	Copper chaperone for SOD
CD	Circular dichroism spectroscopy
CcO	Cytochrome c oxidase
Cox, Sco	Cytochrome c oxidase assembly proteins
CQ	Clioquinol
Cp	Ceruloplasmin
Ctr	Copper transport protein
Cys	Cysteine
DNA	Deoxyribonucleic acid
Dp44mT	Di-2-pyridylketone-4,4,-dimethyl-3-thiosemicarbazone
DTT	1,4-dithiothreitol
EDTA	Ethylenediamine tetraacetic acid
EPR	Electron paramagnetic resonance

ESI-MS	Electrospray ionization mass spectrometry
FAD	Familial Alzheimer’s disease
FDA	Food and drug administration
Fmoc	Fluorenylmethyloxycarbonyl
FNB	Food and nutrition board
Glu	Glutamate/Glutamic acid
GSH	Glutathione reduced
GSSG	Glutathione disulfide
GTSM	Glyoxal-bis(N4-methyl-3-thiosemicarbazone)
HEPES	4-(2-hydroxyethyl)-1-piperazineethanesulfonic acid
His	Histidine
HSA	Human serum albumin
HSAB	Hard soft acid base
L	Ligand
LFSE	Ligand field stabilization energy
LT	Low temperature
MD	Menkes disease
Met	Methionine
MT	Metallothionein
MTF1	Metal regulatory transcription factor 1
NHE	Standard hydrogen electrode
NMR	Nuclear magnetic resonance
PB	Phosphate buffer
PAR	4-(2-pyridylazo) resorcinol
PD	Parkinson’s diseases
POBN	A-(4-pyridyl N-oxide)-N-tert-butylnitrone
PrD	Prion disease
PT	Pyridine-2-carboxaldehyde thiosemicarbazone
Phen	1,10-phenantroline
Redox	Reduction-oxidation reduction
RNA	Ribonucleic acid
ROS	Reactive oxygen species
SOD1	Superoxide dismutase 1 or Cu/Zn superoxide dismutase

SAD	Sporadic Alzheimer’s disease
TCEP	Tris(2-carboxyethyl)phosphine
TGN	Trans Golgi network
TSC	Thiosemicarbazone
Uv-Vis	Ultraviolet visible spectroscopy
WD	Wilson’s disease
ZnT	Zn transporter

Abstract

Defects in copper (Cu) homeostasis have been linked to Alzheimer's disease (AD) and Cancer. In AD, Cu has been found to bind to Aβ-peptides in extracellular amyloid-plaques, and it has been proposed to impact the peptide aggregation process and mediate the production of reactive oxygen species (ROS). Increased Cu levels have also been implicated in tumor growth. This has led to the development of Cu-based therapeutics. Particularly, the use of pro-oxidant Cu-complexes, that can be harnessed to induce oxidative stress, appears to be a promising strategy in cancer. On the other hand, in AD, redox silencing chelators are warranted. In a biological environment, the kinetic and thermodynamic stability of a Cu-complex against physiological competitors, is a key aspect to consider. In particular, the role of Cu-binding and/or reducing biomolecules (including metallothioneins, gluathione, cystein and ascorbate) is of pivotal importance. Within this context, this thesis aims to investigate the impact of these molecules on the reactivity (redox-activity and stability) of several medicinal Cu-complexes. The studies carried out show that these molecules are key players for the fate of a Cu-complex, as they could lead to reactions of dissociation and transmetallation, abolishing also the Cu-dependent ROS production.

Key words: Copper, Metallothioneins, Thiols, Amyloid-β, Cu-based drug, redox-activity, Alzheimer's disease, Cancer, Spectroscopy.

Les dérèglements dans l'homéostasie du cuivre (Cu) ont été liés à la maladie d'Alzheimer et au cancer. Dans la maladie d'Alzheimer, il a été découvert que Cu se lie au peptide Aβ dans les plaques amyloïdes extracellulaires, ce qui a un impact sur le processus d'agrégation du peptide et sur la production d'espèces oxygénées réactives (ROS). L'augmentation de la présence de Cu a également été impliquée dans la croissance tumorale. Ceci a conduit au développement de thérapies à base de Cu. En particulier, l'utilisation de complexes de Cu pro-oxydants, qui peuvent être exploités pour induire un stress oxydant, semble être une stratégie prometteuse. A l'inverse, dans la maladie d'Alzheimer, des chélateurs qui bloquent l'activité redox du Cu sont nécessaires. Dans le cadre d'un environnement biologique, la stabilité cinétique et thermodynamique d'un complex de Cu par rapport à ses concurrents physiologiques, est un aspect essentiel à prendre en compte. En particulier, le rôle des biomolécules liant le Cu et/ou réductrices de Cu (telles que les métallothioneines, le gluathion, la cystéine et l'ascorbate) est d' une importance capitale. Dans ce contexte, cette thèse vise à étudier l' impact de ces molécules sur la réactivité (activité redox/ stabilité) de plusieurs complexes de Cu médicinaux. Les études réalisées montrent que ces molécules sont des acteurs essentiels du devenir d'un complex de Cu, car elles peuvent conduire à des réactions de dissociation et transmétallation, supprimant ainsi la production de ROS dépendantes du Cu.

Mots-clés: Cuivre, Métallothionéines, Thiols, Amyloïde-β, Médicament à base de Cu, Activité rédox, Maladie d'Alzheimer, Cancer, Spectroscopie.

Summary of the thesis in French

Le Cu, ainsi que le Zn, le Fe, le Mn, le Co et le Mo, est reconnu comme un micro-élément essentiel pour l'homme, même si la teneur totale dans le corps est plutôt faible, c'est-à-dire de l'ordre de 100 mg pour un adulte de 70 kg. Le Cu est un cofacteur catalytique indispensable, qui pilote un large éventail de processus biochimiques essentiels, nécessaires à la vie. Sa configuration électronique lui confère une grande capacité à accepter et à donner des électrons, en alternant entre les états rédox de Cu(I) ([Ar] $4s^0$, $3d^{10}$) et de Cu(II) ([Ar] $4s^0$, $3d^9$). Cette propriété redox convient au transfert d'électrons lors de réactions enzymatiques, mais elle permet également la production d'espèces oxygénées réactives (ROS) en présence d'un agent réducteur et O_2.

Pour cette raison, le fonctionnement physiologique de nos cellules nécessite un système métabolique très bien orchestré pour maintenir le niveau de Cu étroitement régulé. Le Cu sous forme hydraté n'existe pas à l'intérieur et à l'extérieur des cellules et un réseau de petites molécules/protéines a évolué pour l'apporter aux différentes enzymes dépendantes du Cu.

L'incapacité du corps à contrôler l'homéostasie en Cu est directement responsable de deux troubles génétiques humains (à savoir les maladies de Wilson et de Menkes), mais elle est également liée à la maladie d'Alzheimer et à la progression du cancer. Chez les patients atteints de la maladie d'Alzheimer, il s'est avéré que le Cu était lié aux peptides β-Amyloïde (les plus abondants identifiés à ce jour: $A\beta_{1\text{-}40/42}$, $A\beta_{4\text{-}42}$) qui s'accumulent dans des plaques amyloïdes extracellulaires. Le Cu influe sur le processus d'agrégation des peptides et engendre la production de ROS. Le rôle du Cu dans la croissance des tumeurs et son métabolisme modifié dans le cancer a été démontré. Les données suggèrent fortement que l'augmentation des quantités de Cu favorise i) la prolifération cellulaire, ii) la production de ROS, iii) l'angiogenèse et iv) les métastases.

Différents médicaments visant à cibler l'homéostasie du Cu ont été développés. Ceux-ci comprennent i) les ligands (chélateurs) de Cu, habituellement, utilisés pour éliminer cet ion métallique du corps en cas de surcharge en Cu, ii) les ligands de Cu capables de renverser les interactions anormales Cu-protéines et de redistribuer le Cu à travers les membranes biologiques et iii) les ligands de Cu qui favorisent la génération de ROS lors de la formation du complexe métallique. Dans ce dernier cas, le ligand peut déjà être injecté sous forme de complexe de Cu ou être injecté tel quel, et il est capable après de complexe le Cu. La production de ROS catalysée par le Cu est un mécanisme impliquant le couple redox Cu(II)/Cu(I), elle requiert un agent réducteur comme l'ascorbate (AscH-) et un oxydant, tel que O_2 ou H_2O_2 (**Image 1a**).

Les effets d'un complexe de Cu au niveau physiopathologique et/ou thérapeutique sont fortement influencés par la cinétique et la thermodynamique des réactions d'échange métal/ligand entre le complexe et les compétiteurs physiologiques. Parmi ceux-ci, par exemple, la métallothionéine (MT) et d'autres molécules plus petites contenant des thiols (par exemple, glutathionne, GSH, cystéine, Cys) sont très importantes car elles sont strictement impliquées dans la complexation et la régulation de Cu(I) dans le corps humain. Les MT sont des chélateurs de métaux et/ou des antioxydants bien connus avec une teneur élevée en Cys (20 Cys pour 60/68 AA en fonction de l'isoforme) qui interviennent dans la manipulation du Zn et du Cu. La liaison aux ions métalliques entraîne le repliement de la protéine dans une structure 3D (exemplifiée par la structure de $Zn(II)_7$MT-2), caractérisée par deux domaines en forme d'haltère, chacun contenant un groupe métal-thiolate (**Image 1b**). De plus, la complexation au Cu(I) résulte dans la formation d'un

complexe rédox-silencieux, protégeant ainsi la cellule de la production de ROS. Enfin, les MTs étant en général liées aux ions Zn(II) dans les conditions physiologiques, elles pourraient également effectuer un échange de métal avec un complexe de Cu, conduisant ainsi à la transmétallation entre le Cu et le Zn.

GSH et Cys sont des chélateurs plus faibles pour le Cu(I) par rapport aux MTs (K_d (MT) ~ 10^{-19} M, K_d (GSH) ~ 10^{-17} M), mais étant plus concentrés à l'intérieur et à l'extérieur des cellules, ils peuvent moduler leur interaction avec le Cu grâce à leur capacité à réduire le Cu(II) et à se lier fortement au Cu(I), via leur chaîne latérale (Cys). Ils peuvent donc devenir de sérieux concurrents des complexes de Cu d'intérêt médicinal et faire de médiateurs pour le transport de Cu(I) vers le MT.

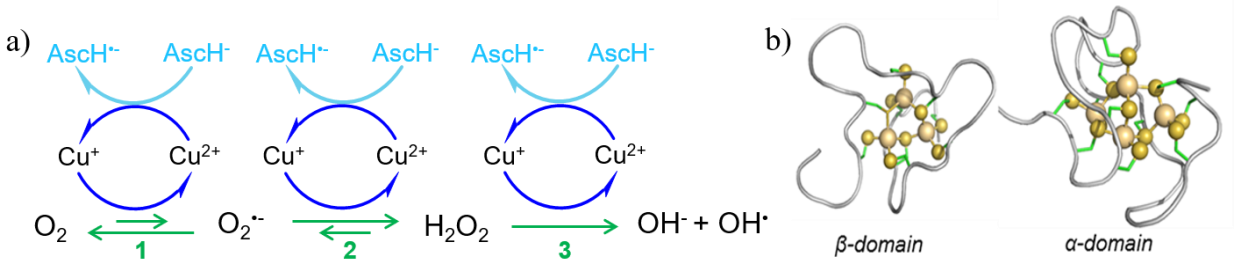

Image 1 - a) Mécanisme de production de ROS catalysé par le Cu en présence de $AscH^-$ et de O_2; b) Structure 3D des clusters de métaux divalents-thiolates dans les MT de mammifères (illustré par $Zn(II)_7$MT-2).

Dans ce contexte, ma thèse visait à étudier, au niveau moléculaire, la réactivité de complexes de Cu d'intérêt médicinal, d'un point de vue de leur activité redox et de leur stabilité, en présence de molécules physiologiques se liant au Cu et/ou réductrices (y compris la MT, le GSH, la Cys, l'$AscH^-$ et le Glutamate (Glu)). Deux études de cas seront présentées: i) pour un complexe physiopathologique du peptide Aβ dans le contexte de la maladie d'Alzheimer et ii) pour des complexes de Cu dans le contexte de traitements médicamenteux (agents anticancéreux, par exemple).

Dans la première partie de la thèse, nous discuterons des principaux résultats de l'étude de cas I concernant l'influence des biomolécules, GSH, Cys, Glu sur les réactions de transfert de Cu à partir de différentes espèces de peptides Aβ vers $Zn(II)_7$MT-3 (isoforme assez spécifique du cerveau). Les principaux problèmes que nous avons essayé de résoudre sont les suivants:

- Quel est l'impact de Cys et GSH sur la réaction? Pourraient-ils jouer le rôle d'agents réducteurs de Cu(II) et de navette pour le Cu(I) entre les deux biomolécules?
- Quelle est l'influence du neurotransmetteur Glutamate (Glu)? Comment la teneur en Zn(II) de MT-3 affecte-t-elle le taux de transfert de Cu? Plusieurs mécanismes peuvent-ils agir de manière coopérative?

Dans la deuxième partie, nous présenterons les principaux résultats de l'étude de cas II, qui traitent de la réactivité de différents médicaments à base de Cu (développés pour le traitement de diverses maladies, dont le cancer) dans i) la production catalytique de ROS et ii) avec leur stabilité (et, par conséquent, désactivation possible) en présence de $Zn(II)_7$MT-1 (isoforme exprimée de manière ubiquitaire) et GSH, dans les conditions trouvées dans le cytosol et le noyau. Les principales questions auxquelles nous avons essayé de répondre sont les suivantes:

- Quelle est l'activité des peptides Cu(II)-(Xxx-Zzz-His) (ATCUN) dans la production de ROS? Pourraient-ils jouer le rôle d'enzymes de Cu artificielles pour dégrader des biomolécules?

- Quelle est la réactivité des médicaments anticancéreux Cu(II)-Thiosemicarbazone avec GSH /$Zn(II)_7MT$ dans des conditions physiologiques présentes dans le cytosol/noyau? Le $Zn(II)_7MT$ peut-il être un désactivateur de ces médicaments?
- Serait-il possible d'avoir un médicament à base de Cu redox-actif en présence de concentrations physiologiques de GSH/$Zn(II)_7MT$, telles que celles trouvées dans le cytosol/noyau?

Nous avons commencé notre étude sur l'influence des biomolécules capables de se lier et/ou de réduire le Cu sur la réaction de transfert de Cu(II) de $A\beta_{4\text{-}16}$ (un peptide modèle de $A\beta_{4\text{-}42}$) vers $Zn(II)_7MT$-3, en présence de GSH et Cys. Des études antérieures, visant à étudier le rôle neuroprotecteur possible du $Zn(II)_7MT$-3 contre le complexe cytotoxique Cu(II)-$A\beta_{1\text{-}16/40}$, ont montré que le $Zn(II)_7MT$-3 pourrait retirer le Cu du complexe Cu(II)-$A\beta_{1\text{-}16/40}$, *via* la réduction de Cu(II) en Cu(I) et sa chélation ultérieure, avec la formation du complexe redox-silencieux**,** $Cu(I)_4Zn(II)_4MT$-3. Ce n'était pas le cas pour le composé Cu(II)-$A\beta_{4\text{-}16}$, qui était stable vis-à-vis de la réactivité de $Zn(II)_7MT$-3 et, par conséquent, aucun échange Cu/Zn n'avait eu lieu. Dans le cadre de cette thèse, nous avons exploré l'influence possible des ligands Cys et de GSH sur la réaction de transfert en considérant i) leurs propriétés mentionnées dans l'introduction et ii) que des fluctuations dans leur concentration pourraient se produire (par exemple, des dépôts extracellulaires de peptide Aβ auraient augmenté la concentration extracellulaire de Cys réduite).

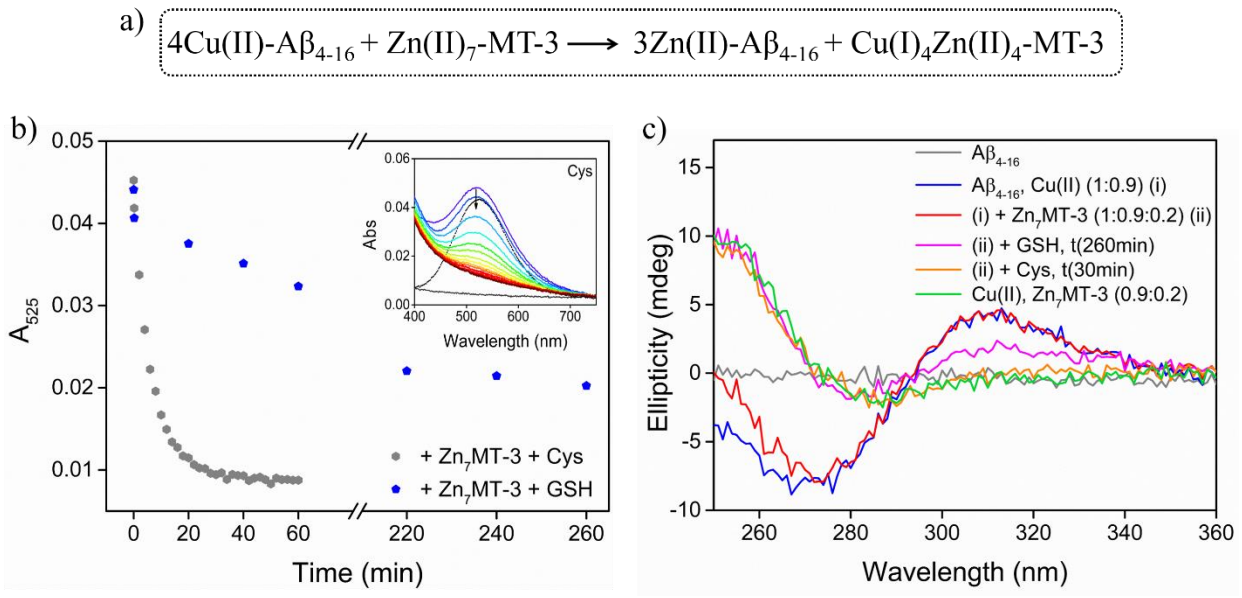

Image 2 - Effet de Cys/GSH sur la cinétique de transfert de Cu du complexe Cu(II)-$A\beta_{4\text{-}16}$ vers $Zn(II)_7MT$-3 dans un tampon phosphate 50 mM, pH 7,4. Dans a) schéma de la réaction; en b) les données sont exprimées en A_{525} (bande λ_{max} d-d de Cu (II)-$A\beta_{4\text{-}16}$ en fonction du temps). Encadré: spectres UV-Vis correspondants pour la réaction avec Cys. Conditions expérimentales: 500 µM $A\beta_{4\text{-}16}$, 450 µM Cu (II), 100 µM de $Zn(II)_7MT$-3 (1:0.9:0.2), 3 mM de Cys/GSH dans du PB 100 mM, pH 7,4. c) Spectre CD de la formation du $Cu(I)_4Zn(II)_4MT$-3 espèces des mélanges Cu(II)/$Zn(II)_7MT$-3, Cu(II)-$A\beta_{4\text{-}16}$/$Zn(II)_7MT$-3/GSH, Cu(II)-$A\beta_{4\text{-}16}$ /$Zn(II)_7MT$-3/Cys. Conditions expérimentales: 100 uM d'$A\beta_{4\text{-}16}$, 90 µM de Cu (II), 20 µM de $Zn(II)_7MT$-3, 3 mM de L-Cys ou GSH dans du PB 100 mM, pH 7.4.

En utilisant différentes méthodes spectroscopiques telles que l'absorbance, le dichroïsme circulaire et la ^{1}H-RMN, nous avons montré que Cys et GSH sont capables de déclencher le l'échange Cu/Zn entre Cu-$A\beta_{4\text{-}16}$ et $Zn(II)_7MT$-3 (**Image 2a**) *via* (i) la réduction de Cu(II) en Cu(I) (**Image 2b**), (ii) la complexation et le transfert de Cu(I) vers MT-3, avec la formation de $Cu(I)_4Zn(II)_4MT$-3 (**Image 2c**) et (iii) la libération de Zn(II) par MT-3, avec une liaison conséquente au peptide $A\beta_{4\text{-}16}$. Alors que Cys est capable de réduire quantitativement le Cu (II) et de transférer le Cu (I) sur $Zn(II)_7MT$-3, la réaction avec le GSH est plus lente et n'est pas terminée après 4 heures de réaction.

Considérant que les thiols déprotonés de Cys/GSH sont les formes susceptibles de subir une oxydation en cystine/ GSSG, ainsi que de se lier à des ions métalliques, la valeur de pK_a du groupe thiol dans Cys (pK_a ~ 8.2) est inférieure à celle dans GSH (pK_a ~ 9.2) et pourrait être un facteur déterminant pour leur activité.

Ensuite, nous avons exploré le rôle potentiel du neurotransmetteur Glu et comment la charge en Zn de MT-3 pourrait affecter cette réaction de transfert de Cu. Glu pourrait jouer un rôle important en étant stocké à une concentration d'environ 100 mM dans les vésicules des neurones glutamatergiques et libéré lors de la neurotransmission dans la fente synaptique, où les peptides Aβ et MT-3 sont souvent localisés dans l'espace extracellulaire. La charge en Zn de MT-3 peut au contraire affecter la vitesse de la réaction, étant donné que des espèces partiellement appauvries en Zn(II) (à savoir $Zn(II)_6$MT-3, $Zn(II)_5$MT-3 et $Zn(II)_4$MT-3) sont présentes dans des conditions physiologiques en même temps que $Zn(II)_7$MT-3, qui peuvent contenir des thiols Cys non coordonnés qui pourraient réduire davantage le Cu(II) que les thiolates liés au Zn(II). La présence de telles espèces partiellement chargées de Zn dépend de la quantité de Zn présente dans la cellule, de l'expression de la protéine et de la présence de potentiels compétiteurs du Zn(II) (biomolécules se liant au Zn(II)).

Par conséquent, nous avons utilisé l'EDTA comme imitateur, après avoir prouvé par ^{1}H-RMN que son addition en quantité stoechiométrique conduit à l'élimination quantitative de Zn(II) de $Zn(II)_7$MT-3, dans le temps de mélange, formant ainsi les especes $Zn(II)_{7-x}$MT-3 souhaité. Comme le montre le **Tableau 1**, Glu et l'EDTA ont tous deux étés en mesure d'accélérer le taux de transfert de Cu de $A\beta_{4-16}$ à MT-3.

Concernant la réaction avec Glu, nous avons démontré que, même si sa contribution à la répartition à l'équilibre des complexes Cu(II)-$A\beta_{4-16}$ et $Zn(II)_7$MT-3 est négligeable, elle pourrait néanmoins accélérer le transfert de Cu via un mécanisme associatif du complexe ternaire [Glu-Cu(II)-$A\beta_{4-16}$]). Concernant la réaction avec l'EDTA, les temps nécessaires pour le transfert obtenu, à savoir $Zn(II)_4$MT-3 > $Zn(II)_5$MT-3 > $Zn(II)_6$MT-3, a confirmé que la réaction était d'autant plus rapide que le nombre de groupes Cys-thiol pour la réduction/extraction de Cu(II).

Enfin, nous avons montré que leur effet était additif (**Tableau 1**), confirmant que Glu et EDTA agissent selon des mécanismes différents.

Tableau 1 - Valeurs $t_{1/2}$ représentatives des différentes réactions étudiées avec Glu et EDTA, calculées à partir de la cinétique expérimentale de disparition de la bande d-d de Cu (II)-$A\beta_{4-16}$. Les facteurs d'accélération (AF), rapportés avec les écarts types, ont été calculés en fonction de la réaction Cu(II)-$A\beta_{4-16}$ + $Zn(II)_7$MT-3.

Reaction	**$t_{1/2}$ (min x 10^2)**	**AF**
Cu(II)$A\beta_{4-16}$ + $Zn(II)_7$MT-3	7.94	1
Cu(II)$A\beta_{4-16}$ + $Zn(II)_7$MT-3 + Glu	4.06	2.15 ± 0.21
Cu(II)$A\beta_{4-16}$ + $Zn(II)_7$MT-3 + EDTA (3eq)	4.95	1.60 ± 0.04
Cu(II)$A\beta_{4-16}$ + $Zn(II)_7$MT-3 + EDTA (2eq)	6.44	1.21 ± 0.03
Cu(II)$A\beta_{4-16}$ + $Zn(II)_7$MT-3 + EDTA (1eq)	7.66	1.12 ± 0.09
Cu(II)$A\beta_{4-16}$ + $Zn(II)_7$MT-3 + EDTA (3eq) + Glu	2.15	3.27 ± 0.36

Sachant que de petites biomolécules physiologiques telles que GSH, Cys et Glu, ainsi que des molécules plus grosses telles que MT, peuvent jouer un rôle majeur dans le devenir des complexes physiopathologiques au Cu, nous avons étendu notre intérêt à la réactivité de différents médicaments à base de Cu (étude de cas II) représente en **Image 3**, qui ont été explorés pour plusieurs applications en médecine (par exemple dans le traitement du cancer, l'imagerie, le clivage ADN/ARN). Le GSH et les MTs pourraient en particulier être des modulateurs importants

pour ces médicaments, conduisant soit à la dissociation du complexe de Cu, soit à des réactions de transmétallation Cu/Zn. En plus de cela, comme expliqué dans l'introduction, la complexation de Cu(I) à la MT pourrait conduire à la désactivation complète du médicament à base de Cu, car le complexe $Cu(I)_4Zn(II)_4MT$-3 est inerte vis-à-vis de l'oxydo-réduction.

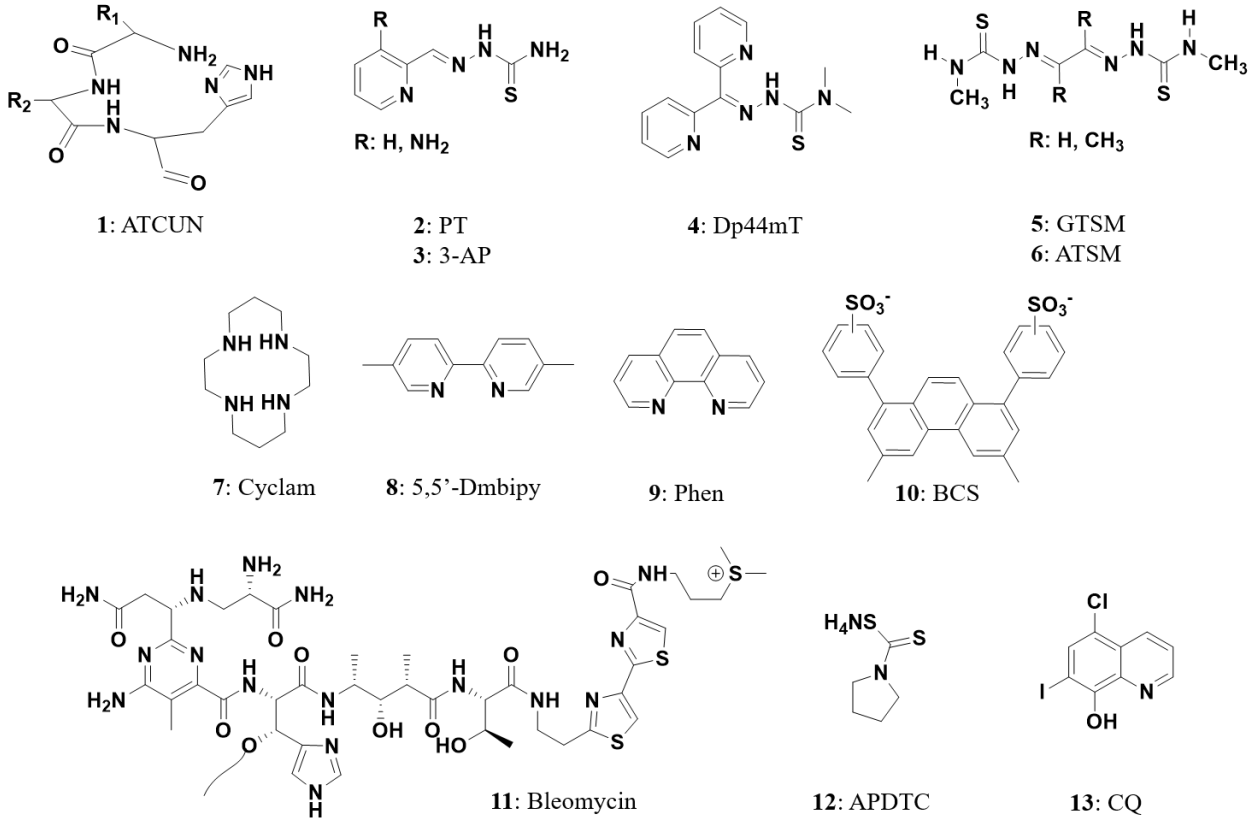

Image 3 - Liste des chélateurs de Cu étudiés dans cette thèse.

Parmi les différentes familles de ligands étudiées, la première est un simple motif peptidique H_2N-XxxZzzHis (XZH) (ligand 1, **Image 3**), appelé motif de liaison au Cu et au Ni (ATCUN) à l'extrémité amino-terminale, qui se lie fortement au Cu(II) dans un complexe plan carré (4N). Ce motif simple a été largement utilisé par plusieurs groupes de recherche pour équiper des peptides/protéines d'un de ce site de liaison au Cu(II), par des approches synthétiques ou recombinantes. D'une part, le motif ACTUN a été introduit pour ajouter une unité catalytique de ROS afin de dégrader les biomolécules, jouant ainsi le rôle de métalloenzyme artificielle. D'autre part, le même motif a été utilisé pour réduire ou pour rendre le Cu inactif dans l'activité redox ou le rendre redox-silencieux, par ex. en thérapie de chélation ou pour l'imagerie ^{64}Cu.

Pour éclaircir cette divergence, nous avons étudié l'activité rédox et la production de ROS de trois variantes communes de XZH (DAHK, le motif peptidique naturel issu de l'albumine du sérum, KGHK, l'un des motifs les plus efficaces pour la production de ROS et FRHD, le motif retrouvé dans $A\beta_{4\text{-}42}$) avec O_2, $AscH^-$ et/ou H_2O_2, en présence d'un chélateur de Cu(I), la bathocuproinedisulfonate, BCS (mimique de chélateurs de Cu(I) intracellulaires tels que les MT).

En mesurant i) la consommation du substrat, AscH-, par spectroscopie d'absorbance à λ_{max} = 265 nm (**Image 4a**) et ii) la production de $HO^{\bullet}$ par le suivi de la fluorescence du 7-HO-CCA (7-hydroxycoumaring-acide 3-carboxylique), nous avons montré que les activités complexes Cu(II)-XZH dans la production de ROS sont très faibles, c'est-à-dire inférieures à 0,7 turn-over par heure, dans nos conditions expérimentales. Comme le montre la **Image 4a**, d'autres complexes de Cu (II),

bien connus tels que Cu(II)-(DmBipy)$_2$, Cu (II)-(Phen)$_2$ et Cu (II)-(His)$_2$ (composés 8, 9 et 10, **Image 3**) ou de Cu(II) libre, étaient deux ordres de grandeur plus actifs que Cu(II)-XZH.

De plus, en utilisant le chélateur BCS, nous avons prouvé que la production lente de ROS avec Cu(II)-XZH se produit par un cycle redox entre Cu(II)/Cu(I) et qu'une telle faible activité peut être arrêtée par la chélation de Cu(I), comme le montre le piégeage de spin par RPE sur la **Image 4b**, limitant ainsi son application en tant qu'enzyme de Cu artificielle pour dégrader des biomolécules.

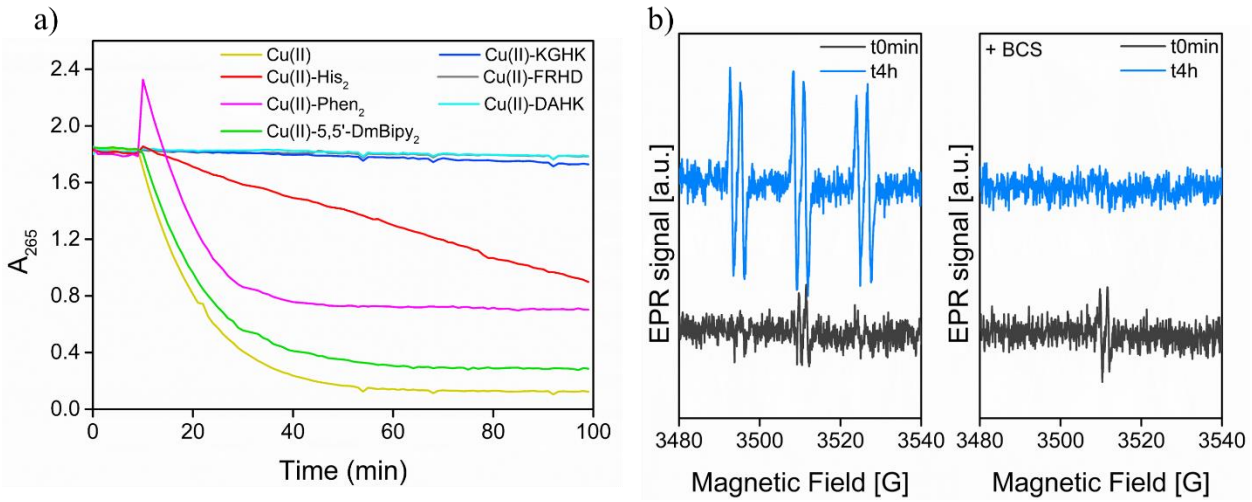

Image 4 - a) Évolution dans le temps de l'absorption de $AscH^-$ à λ_{max} = 265 nm, après addition au temps t =10 min de Cu(II) libre ou de complexes de Cu(II). Les concentrations initiales en Cu(II), peptide/ligands, $AscH^-$ et H_2O_2 étaient respectivement de 10 µM, 12 µM/24 µM, 100 µM et 100 µM dans du PB 50 mM, pH 7.4. b) Mesure indirecte de la production de HO• par RPE avec piégeage de spin, en utilisant POBN comme premier piègeur de spin, en présence (panneau de droite) et en absence (panneau de gauche) de BCS. Conditions expérimentales: KGHK 120 µM, Cu(II) 100 µM (1.2:1), $AscH^-$ 1 mM, H_2O_2 1 mM, PB 100 mM, pH 7.4, POBN 50 mM, ETOH 5%, BCS 300 µM.

La deuxième classe de ligands que nous avons examinés est celle des thiosemicarbazones (TSCs, ligands 2, 3, 4, **Image 3**). Les TSCs ont été explorés cliniquement pour diverses activités biologiques, mais principalement comme agents anticancéreux. Même si leur mécanisme d'action et leurs cibles biologiques sont encore flous, les métaux essentiels que sont le Cu, le Zn et le Fe semblent jouer un rôle central dans leur activité antitumorale. Un aspect négligé de leur l'activité des TSC avec ces métaux concerne leur stabilité en présence de GSH/Zn(II)$_7$MT-1 (isoforme de MT exprimée de manière omniprésente) dans des conditions trouvées dans le cytosol/noyau.

Nous avons donc étudié la réactivité des complexes Cu(II)/Zn(II)Fe(II) de trois TSC (à savoir PT, 3-AP et Dp44mT), en présence de GSH/Zn(II)$_7$MT-1 à des concentrations physiologiques pertinentes pour le cytosol/noyau, pour élucider leur stabilité face aux réactions de dissociation et de transmétallation.

Grâce aux spectroscopies d'absorbance, de dichroïsme circulaire, et de RPE (collaboration avec Dr. B. Vileno) et à la spectrométrie de masse ESI-MS (collaboration avec Prof. O. Placios), nous avons démontré que le GSH/Zn(II)$_7$MT-1 est un modulateur très important des médicaments à base de Cu(II)-TSC. Dans le cas de PT et de 3-AP (ligands 2 et 3, **Image 5**), après la formation rapide d'un adduit ternaire avec GSH, [PT/3-AP-Cu(II)-(SH)GSH], le complexe était rapidement réduit et dissocié et le Cu(I) était transféré sur MT-1, avec formation du complexe Cu(I)$_4$Zn(II)$_4$MT-1. Ainsi, comme montré avec l'étude du piégeage de spin par RPE, la production de ROS en présence de Cu, c'est-à-dire l'un des mécanismes proposés pour l'activité anticancéreuse de ces ligands, a été supprimée.

Avec Dp44mT (ligand 4, **Image 5**), une transmétallation est observée, ce qui indique que $Zn(II)_7$MT-3 pourrait transformer un le complexe de Cu(II) de départ en un complexe de Zn(II) correspondant.

De plus, nous avons étudié la réactivité des complexes Zn(II)/Fe(II) avec les trois ligands TSC et montré que seuls les complexes Fe(II)-PT/3-AP/Dp44mT pouvaient être stables en présence de concentrations physiologiques cytosoliques de GSH/$Zn(II)_7$MT-1, ce qui indique que Fe pourrait être le métal le plus important pour l'activité biologique des TSC.

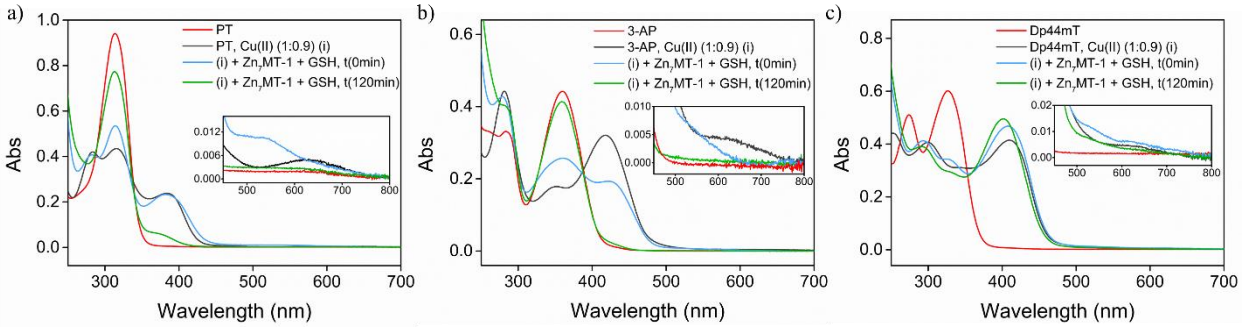

Image 5 - Spectres UV-Vis permettant le suivi de la réaction de a) Cu(II)-PT, b) Cu(II)-3-AP et c) Cu(II)-Dp44mT avec GSH/$Zn(II)_7$MT-1 à 0 et 120 min après addition de GSH et de $Zn(II)_7$MT-1 aux complexes Cu(II)-TSC préformés. Conditions expérimentales: L 30 µM, Cu(II) 27 µM (1.1:1), GSH 3 mM, $Zn(II)_7$MT-1 6 µM, tampon HEPES 100 mM, pH 7.4.

Dans la dernière partie de cette étude concernant la réactivité des médicaments à base de Cu, nous avons exploré et étudié la corrélation entre la stabilité vis-à-vis du GSH/$Zn(II)_7$MT-1, dans les conditions rencontrées dans le cytosol/noyau, et la consommation d'$AscH^-$ avec certains des complexes de Cu utilisés et étudiés pour le traitement du cancer (voir **Image 3** et **Tableau 2**), afin de savoir si un médicament à base de Cu pourrait exister et être actif en tant que complexe de Cu on catalyse redox dans des conditions trouvées dans le cytosol/noyau.

Tableau 2 - Valeurs $t_{1/2}$ (min ou s) du transfert de Cu des différents complexes de Cu étudiés dans ce travail, calculées à partir de la cinétique expérimentale de disparition des bandes CT de Cu (II) ou de Cu (I), observée par spectroscopie d'absorbance; les taux molaires-d'oxydation de $AscH^-$ (µM/min) et les potentiels rédox (mV).

Cu-complex	**$t_{1/2}$ transfer to MT-1 (with GSH)**	**r_{obs} $AscH^-$ oxidation (µM min^{-1})**	**Redox Potential (mV) [NHE]**
Background	/	0.11 ± 0.06	/
Cu(II)	< 30 sec	9.5 ± 1.4	160
Cu(II)-ATSM (6)	✗	0.05 ± 0.01	-403
Cu(II)-Cyclam (7)	✗	0.05 ± 0,02	-736 (E_{pc})
Cu(II)-Bleomycin (11)	✗	0.06 ± 0.02	-
Cu(II)-$(CQ)_2$ (13)	~ 20 min	0.16 ± 0.04	-
Cu(II)-$(APDTC)_2$ (12)	~ 5 min	/	-
Cu(II)-GTSM (5)	~ 50 min	0.49 ± 0.10	-241
Cu(II)-Dp44mT (4)	~ 4 min	0.92 ± 0.11	-210
Cu(II)-$(5,5'$-DmBipy$)_2$ (8)	< 30 sec	10.1 ± 1.0	120
Cu(II)-$(Phen)_2$ (9)	< 30 sec	12.4 ± 1.7	188 170
Cu(I)-$(BCS)_2$ (10)	< 30 sec	0.07 ± 0.01	618

Pour cela, nous avons mesuré l'activité catalytique des complexes de Cu dans la production de ROS *via* la consommation du substrat $AscH^-$ (hypothèse basée sur le schéma **Image 1a**), par spectroscopie d'absorbance à 265 nm et nous avons étudié leur stabilité vis-à-vis du GSH/

$Zn(II)_7$MT-1 par spectroscopies d'absorbance, de dichroïsme circulaire et de fluorescence à basse température.

Nous avons montré que la capacité d'un complexe de Cu ayant une activité pro-oxydante, en présence d'une concentration élevée de GSH/$Zn(II)_7$MT-1, telle que trouvée dans le cytosol et le noyau, dépend non seulement de la possibilité du complexe de Cu d'avoir une cyclage voir rédox rapide entre les états rédox Cu(I) et Cu(II) (E optimal ~ 200 mV vs NHE), mais aussi de l'affinité du ligand pour le Cu(I) (K_d optimal < 10^{-19}, soit < K_d (MT), voir ci-dessus). Une réaction de dissociation réductrice pourrait se produire, compte tenu de leur fort pouvoir réducteur et de leur affinité pour Cu (I). Par exemple, comme le montre le **Tableau 2**, les complexes Cu-(5,5'-$DmBipy)_2$ et Cu-$(Phen)_2$ oxydent $AscH^-$ très rapidement et sont donc très actifs dans la production de ROS, mais ils sont très rapidement dissociés par réduction avec le GSH/$Zn(II)_7$MT-1, qui sont des agents de chélation du Cu (I) plus faibles.

En conclusion, le but de la thèse était d'étudier l'impact des MT et de biomolécules plus petites, telles que GSH, Cys, AscH et Glu, sur la stabilité thermodynamique et cinétique de complexes de Cu. Les complexes de Cu ont été sélectionnés pour leur activité physiopathologique, ou pour leur potentiel médical à base de Cu, développés et étudiés en tant que produits thérapeutiques pour diverses maladies liées au dysmétabolisme du Cu.

Dans l'ensemble, nos résultats indiquent que ces biomolécules ont un impact majeur sur le devenir d'un complexe médicamenteux à base de Cu, qu'elles jouent un rôle neuroprotecteur contre les complexes de Cu toxiques, tels que le Cu(II)-Aβ, ou qu'elles sont modulatrices et désactivantes des médicaments à base de Cu. En effet, nos données montrent que ces molécules fonctionnent ensemble et peuvent conduire à la dissociation réductrice rapide d'un complexe de Cu(II), avec une complexation résultante de Cu (I) à la MT et à une inhibition de la production de ROS, dépendant de Cu.

Les réactions du transfert de Cu du complexe Cu(II)-$Aβ_{4-16}$ au $Zn(II)_7$-MT-3, étudiées dans ce travail, soulignent l'importance de prendre également en compte l'impact de biomolécules plus petites d'intérêt physiologique. Par exemple, Cys et GSH, malgré leurs capacités réductrice et chélatrice de Cu(I) inférieures, ont été en mesure d'accélérer le taux de transfert de Cu vers $Zn(II)_7$-MT-3, influant ainsi sur l'obtention d'un complexe rédox-silencieux $Cu(I)_4Zn(II)_4$-MT-3.

La compréhension des mécanismes d'échange d'ions métalliques (Cu/Zn) entre peptides Aβ, protéines et autres biomolécules, liées à la maladie d'Alzheimer, est extrêmement importante et devrait contribuer à répondre à la question de savoir pourquoi Cu/Zn est lié aux peptides Aβ dans les conditions de la maladie d'Alzheimer, mais pas dans les conditions physiologiques cérébrales normales.

L'étude de cas II sur la réactivité de plusieurs médicaments à base de Cu avec des agents de réduction et des réducteurs de Cu (I) intracellulaires pertinents, tels que le $Zn(II)_7$-MT-1 (ou BCS, un modèle de celui-ci), GSH et $AscH^-$, souligne le défi de concevoir un complexe de Cu pro-oxydant, dans les conditions rencontrées dans le cytosol/noyau. Ainsi, le $Zn(II)_7$-MT-1 et le GSH peuvent être considérés comme des modulateurs et des partenaires importants des médicaments à base de Cu. Globalement, ce type de chimie avec des molécules contenant des thiols pourrait être intéressant pour la conception de complexes de métaux et en particulier de Cu pour toutes les applications étendues de la biologie et de la médecine.

CHAPTER 1

Introduction to Cu at the crossroad of chemistry, biology and medicine

Even though approximately 97 % of the elemental composition of the human body by weight consists of only 6 non-metallic elements, i.e. C, O, H, N, P, S, a wide array of key biochemical processes would not occur without metal ions, e.g. ATP production, the cell's main energy source.

Metals are indispensable to ensure life and employed for normal metabolic processes. Some of them are required in quite large concentrations (bulk-elements, e.g. K, Na, Ca, Mg), whereas some others are only needed in very low amount (trace elements, e.g. Cu, Fe, Mn, Zn). Essential trace elements are usually required as catalytic or structural components of larger molecules, where they have specific functions.

In the next chapters of this thesis, we will mostly deal with the chemistry of one of the trace elements essential for our organism, i.e. Cu, at the interface with biology and medicine.

1.1 Cu, an essential metal in humans with unique chemical properties

1.1.1 Cu in the human body

As a trace element, an average adult male of 70 Kg contains only 100 mg of Cu.[1,2] Cu needs to be taken and absorbed from dietary sources, as it cannot be synthetized de novo. The average safe daily intake of Cu recommended by the Food and Nutrition Board (FNB) is of 1.5–3.0 mg, as only part of it is absorbed.[3,4] Dietary Cu absorption is affected by several parameters, such as age, sex, type of food (i.e. plant versus animal proteins), the amount of Cu in the diet, and the use of oral contraceptives.[5,6]

Although present in very small amount, Cu is an essential element for humans. Indeed, Cu is required for the activity of numerous enzymes involved in a broad spectrum of fundamental biological processes such as cell signaling, cellular respiration, free-radical defense, neurotransmitters and neuropeptides synthesis, iron metabolism, mostly by serving as catalytic and/or structural cofactor.[7–9] A list of the most studied Cu-dependent mammalian enzymes, with the corresponding catalyzed reaction, is reported in **Table 1**.[10–12]

Table 1 - Most studied human Cu-dependent enzymes, localization and corresponding catalyzed reaction.

Cu-Enzyme	Localization	Catalyzed reaction
Cu-Zn SOD (SOD 1)	Cytosol, nucleus	Disproportionation of superoxide to hydrogen peroxide and dioxygen
Cu-Zn SOD (SOD 3)	Secretory pathway/ Extracellular environment	
Cytochrome c oxidase (CCO)	Mitochondria	Dioxygen reduction to water
Dopamine β-hydroxylase (DBH)	Secretory pathway/ Extracellular environment	Conversion of dopamine to noradrenaline
Tyrosinase (TYR)	Secretory pathway/ Extracellular environment	Hydroxylation of tyrosine to DOPA (3,4-dihydroxyphenylalanine) and DOPA to DOPA-quinone
Peptidylglycine-α-amidating monooxygenase (PAM)	Secretory pathway/ Extracellular environment	Conversion of peptidyl-glycine substrates into α-amidated products
Lysyl oxidase (LOX, LOXL1-4)	Secretory pathway/ Extracellular environment	Formation of aldehydes from lysine in collagen and elastin precursors
Amine oxidase (AOC1-3)	Secretory pathway/ Extracellular environment	Oxidation of primary amines to aldehydes in catecholamine
Ceruloplasmin (Cp)	Secretory pathway/ Extracellular environment	Oxidation of Fe^{2+} to Fe^{3+}

A tight regulation of Cu metabolism in a characteristic range of concentrations is vital for our life.[11,13,14] A deficit of Cu would decrease the biosynthesis and activity of the aforementioned Cu-dependent enzymes and hence be detrimental to the organism. Likewise, an overload of Cu would be harmful, because of its inherent redox activity. Indeed, by catalyzing the production of high levels of ROS, Cu can trigger the non-specific oxidation of lipids, proteins and nucleic acids, ultimately resulting in cell death.

This important concept was mathematically formalized in 1912 by the French nutritionist Gabriel Bertrand, into the 'Bertrand's rule', represented in **Fig 1**. It shows that the dose-response curve of Cu (valid for all the essential micronutrients) varies non-monotonically with the concentration, i.e. increasing intake of Cu has an initial stage of increasing benefits (phase I), towards an optimal plateau (phase II), beyond which ingested excesses become toxic, because of the increasing costs of the corresponding regulatory mechanisms (phase III).[15]

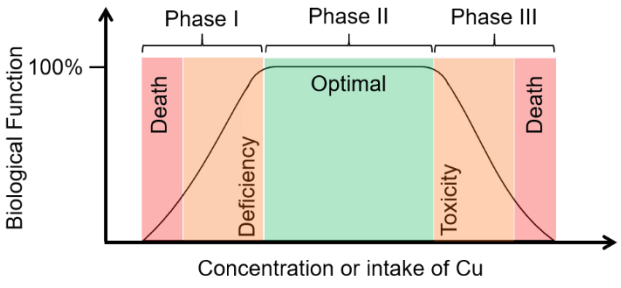

Fig 1 - Bertrand's rule: dependence of the biological function from the concentration or intake of Cu. A tight regulation of Cu concentration or intake is needed to maintain life.

1.1.2 Chemical properties of Cu important in biology

Among the essential metal ions, Cu has peculiar chemical properties, which make it essential for almost all living organisms.

In biological systems Cu ions are mainly found in two relatively stable valence states, i.e. the oxidized form Cu(II) (electronic configuration: [Ar]4s0, $3d^9$) and the reduced one Cu(I) (electronic configuration: [Ar]4s0, $3d^{10}$). Typically, under the oxidizing extracellular environment, Cu is present as Cu(II), but in the reducing conditions inside the cell, it mainly exists in the reduced Cu(I) oxidation state.[16]

The ability to exist in multiple valence states, makes Cu a redox-active metal, i.e. it can easily undergo reversible valency changes, between the reduced, Cu(I), and oxidized, Cu(II), states by accepting and/or donating electrons. By virtue of this electronic property, Cu is exploited as catalytic cofactor for the functioning of numerous enzymes (already reported in **Table 1**), mainly involved in oxidation-reduction (redox) reactions and oxygen activation.

Nevertheless, the essential redox-chemistry Cu(II)/Cu(I) makes Cu ions dangerous, if not handled properly by the cell (i.e. when free or loosely bound), as they become available for the catalytic production of ROS, including the Fenton type reaction. Cu-catalyzed ROS production requires the presence of an oxygen species (e.g. O_2 or H_2O_2), as well as of a reducing agent (e.g. $AscH^-$). Cu undergoes redox cycling, classically between reduction of Cu(II) to Cu(I), through the oxidation of $AscH^-$ to $AscH^{\bullet-}$. Then, O_2 is reduced by Cu(I) in one electron events to superoxide ($O_2^{\bullet-}$), hydrogen peroxide (H_2O_2) and finally hydroxyl radicals ($HO^{\bullet}$) (**Fig 2**).

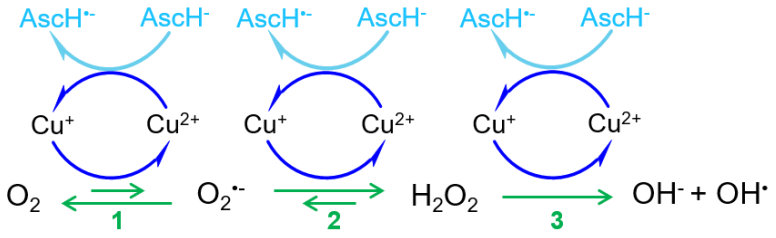

Fig 2 - Mechanism of Cu-catalyzed ROS production in the presence of O_2 and a reducing agent like $AscH^-$. The electron flow goes from $AscH^-$ to the O_2 species, catalyzed by Cu.

Cu(II)/Cu(I) redox cycling in Cu-dependent enzymes requires the presence of a Cu-binding donor ligand set that is capable of stabilizing both oxidation states. This is challenging as the preference of the two ions in coordination chemistry is distinct.

The different ligand preference of the two ions is well described by the ‘‘Hard and Soft Acids and Bases theory’’ (HSAB), developed by Pearson in the 1960s.[17] The theory elaborates that soft bases react preferentially with soft acids, resulting in adducts with a more covalent character, whereas hard acids prefer to bond with hard bases, and the resulting adduct tends to have more ionic character in its bonding. In its reduced state, Cu(I) is classified as a soft acid, whereas in its oxidized state, Cu(II), as a borderline acid. This depends on the polarizability of the ion, Cu(I) being larger with lower charge-density, while Cu(II) smaller with higher charge-density.

Hence, cupric centers, Cu(II), prefer electrostatic bonding to N and/or O ligands from hard Lewis bases (e.g carbonyl and carboxylate O from Asp and Glu, amide N), and borderline bases like imidazole N from His, whereas cuprous centers, Cu(I), prefer the more covalent environment of S donors from soft Lewis bases (e.g. thiolate or thioether sulfur from Cys and Met).

Moreover, based on the different number of valence d electrons, Cu(II) and Cu(I) ions prefer different coordination numbers and/or binding geometries. This preference is based on the ‘‘Ligand Field Stabilization Energy’’ (LFSE), with Cu(II) ions preferring coordination numbers of 4, 5, or 6, and Cu(I) ions of 2, 3, or 4. Cu(II) is a d^9 system that exhibits geometric preferences based in part on LFSE. This means that Cu(II) ions mostly adopt square planar, square pyramidal, or axially distorted octahedral geometries, the latter being the result of Jahn-Taller distortion. Cu(I) is a d^{10} system and therefore there is no LFSE from any particular geometry, giving to Cu(I) higher freedom to bind in any in geometric arrangement, adopting tetrahedral, trigonal, or even linear geometries.

Another important feature of the ligand set, both in terms of composition and geometric arrangement, is its influence on the reduction potential of the metal center. In case of Cu-dependent enzymes, this feature is critical as it influences the catalytic redox function. On the other hand, for Cu-transport proteins, this feature is critical for avoiding Cu(II)/Cu(I) redox cycling.[18–22]

In this respect, one of the most interesting and fascinating aspects of the biochemistry of Cu is to understand how it can function in rapid electron-transfer reactions, the two ions having such different ligand preference both in terms of donor atoms and binding geometries. Generally, the ligand donor groups chosen by the Cu-dependent redox enzymes tend to be a mix of the two classes of bases (i.e. hard and soft), with His, Met and Cys dominating. Instead, the binding geometry imposed by the protein tends to be finely tuned, so that to impose what Valle and Williams in 1968 called the ‘entatic state’, i.e. a state closer to a transition state, rather than to a conventional stable molecule.[23] In other words, the protein is capable of imposing a highly distorted geometry, not too unfavorable for both Cu(II)/Cu(I) oxidation states but favorable for rapid electron transfer. In many of the redox active Cu-dependent enzymes, the Cu center is predominantly found in a tetrahedral environment, in which the high energy Cu(I) geometry imposed to Cu(II), enhances its reactivity by increasing the redox potential.[22]

The above discussed fundamental chemical properties of Cu must be also considered when designing small Cu-coordination compounds to be used either to manipulate cellular Cu status, or as Cu-based drugs.

1.2 Regulation of Cu homeostasis in the human body

The essential yet toxic nature of Cu requires uncommon challenges for its transport in biology, both intra- and extracellularly.[24] Cu needs to be handled in a very carefully controlled manner, in order to minimize free Cu and keep its level tightly regulated.[25] As a result nature has evolved a sophisticated network of small molecular mass ligands and proteins to assist Cu in the complex journey of crossing the extracellular and intracellular membranes to reach the Cu-dependent enzymes.[11,26,27] Over the past few decades, intense investigation on the biomolecules that govern Cu homeostasis has led to huge progresses in our understanding of the mechanisms that allow our organism to acquire, transport, sequester and export Cu, hence preventing accumulation of toxic levels. This will be discussed in the following paragraphs.

1.2.1 Cu absorption and trafficking in the blood

Cu, taken in through the diet, is predominantly absorbed at the level of small intestine. Current physiologic models describe Cu uptake and distribution throughout the body as a biphasic process. In phase I, Cu is transported through the portal venous circulation, into the liver. Cu(I)-transporting P-type ATPase, ATP7A, is responsible for Cu exports from intestinal enterocytes. From the liver, Cu is imported into hepatocytes and redistributed throughout the body by excretion into the blood (phase II). Cu in excess is eliminated by the liver into the bile and discarded from the body via defecations (**Fig 3**). Cu excretion involves the Cu(I)-transporting P-type ATPase, APT7B.[28,29]

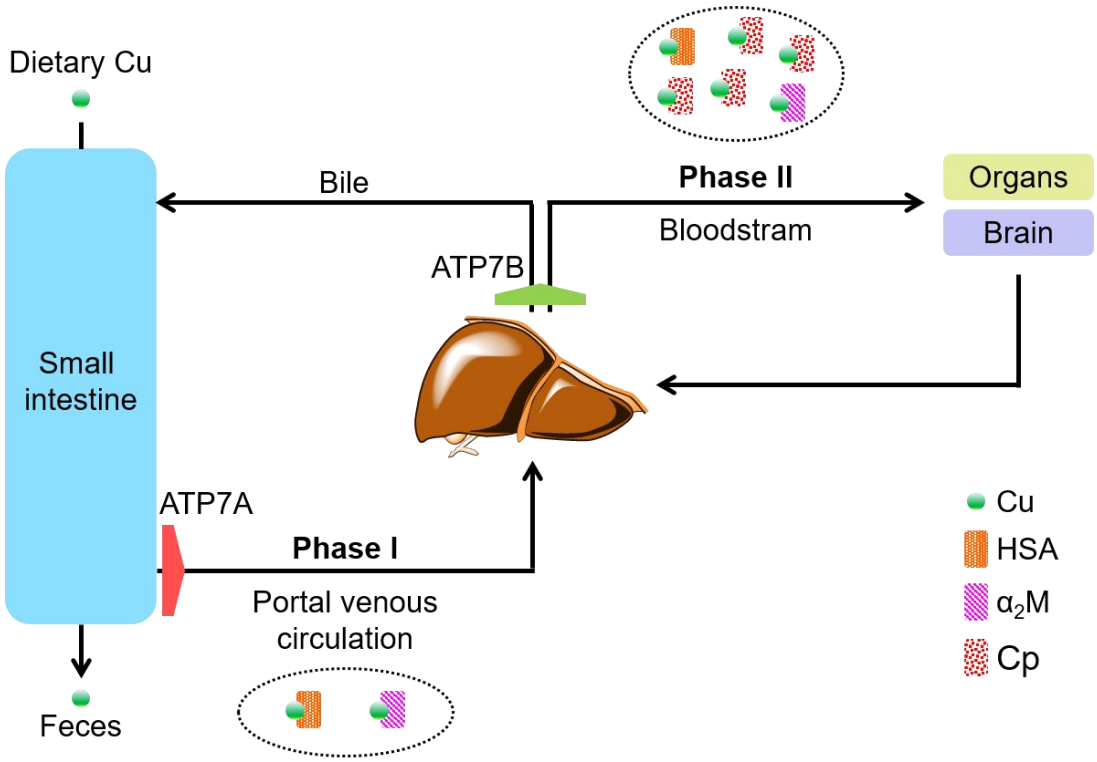

Fig 3 - Cu homeostasis in the whole body: schematic representation of Cu absorption from dietary sources and trafficking in the blood.

In adults, the reported total concentration of Cu in the blood plasma and serum is ~ 17 µM. Blood plasma components have been separated by many different techniques, ranging from native

electrophoresis and various kinds of chromatography. The so far identified Cu-binding components (proteins and small Cu-carriers) have been recently listed by M.C. Linder.[30] Three are the most important proteins that account for at least 90% of the total Cu-binding components, i.e. Ceruloplasmin (Cp), Albumin (HSA) and α-2-macroglobulin (α_2M).[31]

- Cp is the main Cu-binding glycoprotein in human blood plasma. ApoCp binds tightly 6 Cu atoms with a mixture of His, Cys and Met residues, in a compact 3-D structure.[1,32,33] The biosynthesis of holoCp occurs predominantly in the liver. Thus, phase II of Cu distribution is mostly marked by the excretion of holoCp into the blood. Cu bound to Cp is not easily exchangeable under physiological conditions, as buried into its structure. Using cultured human and mouse cells, incubated with purified human and mouse ^{64}Cu-radiolabeled Cp, respectively, it has been shown that the interaction with the cell surface makes possible holoCp conversion to apoCp, mediated by Cu transporter 1 (Ctr1), the main protein responsible for Cu import into cells.[34,35] Nevertheless, the importance of this interaction is still controversial.
- HSA is the most abundant protein in human blood plasma (typical concentration ~ 0.6 mM).[36] However, in the presence of Cp, only a small fraction (~ 1%, i.e. 6 µM) of it normally carries Cu.[37] It is composed of three homologous domains, containing two Cu(II) binding sites. The strongest binding site occurs at the N-terminus, where the sequence Asp-Ala-His-Lys provides the canonical amino terminal Cu, Ni (ATCUN) coordination sequence that binds Cu with 0.1 pM affinity at pH 7.4.[38] Like for Cp, studies on cell cultures showed that radiolabeled ^{64}Cu(II) loaded to HSA can be acquired by cells.[34,39] Moreover, recently, E. Stefaniak et al., spectroscopically demonstrated, using model peptides, that Ctr1 can collect Cu(II) from HSA.[40]
- α_2M is the third protein that has been found to tightly bind Cu in human blood plasma.[34] It is a tetrameric protein with 2 Cu binding sites, whose location is unknown yet.[41] α_2M was shown to bind Cu tightly even in the presence of HSA, thus suggesting a greater affinity for Cu.[42] Hence, α_2M was shown to exchange ^{64}Cu(II) with HSA and *in vitro* both α_2M and HSA to slowly release Cu to various buffers, even in the presence of high concentrations of His.[43,44] Thus, unlike Cp, the two proteins are considered to be part of the exchangeable Cu pool, which is present in the portal venous system, before entering the liver (Phase I).

1.2.2 Cu import and distribution intracellularly

The initial step in the intracellular Cu handling is its acquisition from the extracellular environment and transport across the plasma membrane. Then, Cu is distributed in several cells' compartments, *via* different pathways. The exact mechanisms of these processes are yet far from clear. A schematic illustration of the so far known major routes of intracellular Cu trafficking is presented in **Fig 4**.

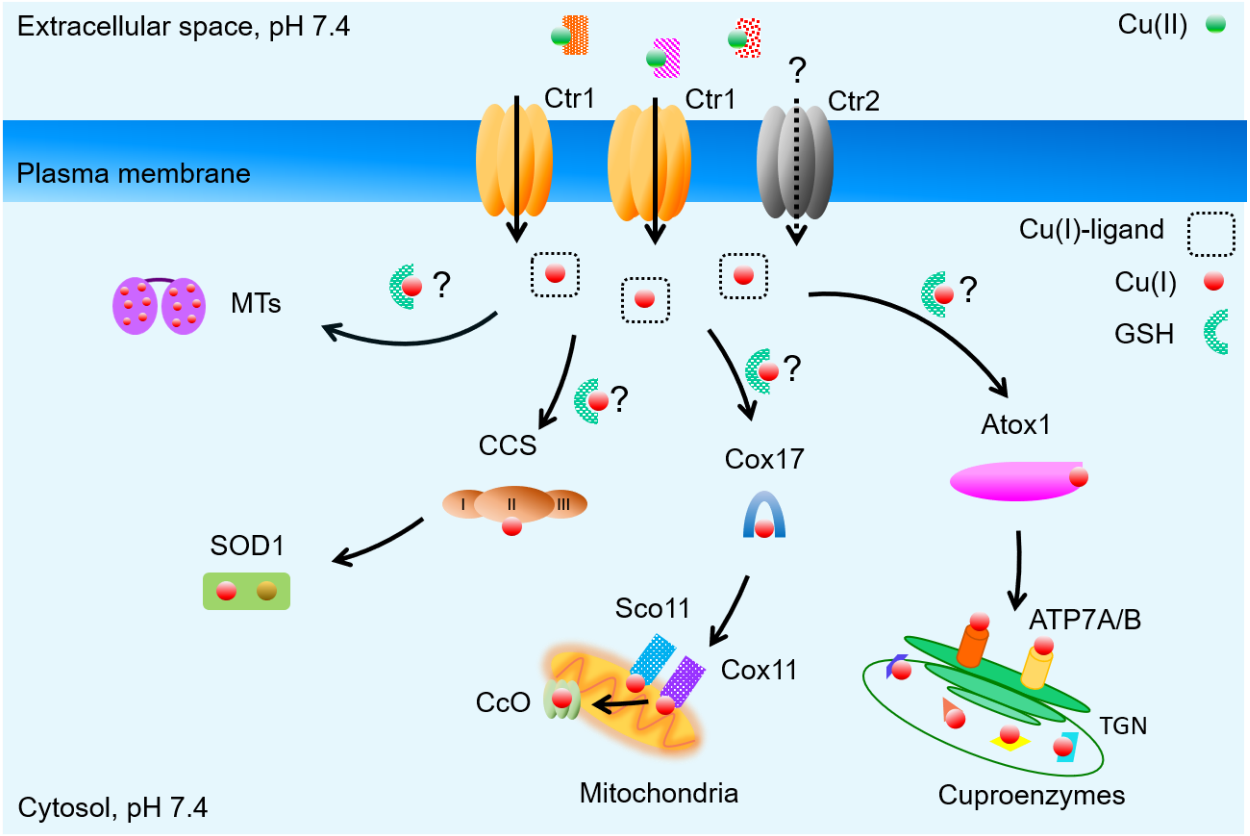

Fig 4 - Intracellular Cu trafficking after Cu uptake from the extracellular carriers *via* Ctr1/(Ctr2). Upon Cu entry, Cu-chaperones (CCS, Cox17 and Atox1) distribute it to different locations (i.e. cytosol, mitochondria or lumen of the Trans Golgi Network, TGN) for metalation of Cu-dependent enzymes. The GSH pool, present at mM concentrations, might transiently bind to Cu(I), as it exits the membrane, and facilitate Cu-dissociation from Ctr1/2. MTs may serve as a storage site, receiving excess of Cu directly from Ctr1 or *via* GSH.

To date, it is know that Cu enters the cell via the high-affinity mammalian Cu-transporter, Ctr1.[45,46] Ctr1 contains three transmembrane domains that homotrimerizes to form a narrow pore that widens on the intracellular side[47,48], and multiple Cu-binding sites (predominantly Met, His and Cys) with increasing affinity gradient from the entrance (extracellular environment) to the exit (intracellular environment).[49,50] A recent x-ray structure of the transmembrane domain of Ctr1 from *Salmo salar*, determined by Ren et al., revealed that the selectivity filter of Ctr1 is comprised by two layers of Met triads, which coordinate two Cu(I) ions close to the extracellular entrance.[48]

Ctr2 is a second possible mammalian Cu-transporter, mostly detected in lysosomes and late endosomes, but also at the plasma membrane.[51,52] Recently, Wezynfeld et al., using model peptides of Ctr2, suggested a maximal complementary role between the two transporters in Cu import, based on the 4 orders of magnitude lower affinity of Cu(II) to the extracellular N-terminal domain of Ctr2, compared to that reported for Ctr1.[53]

From Ctr1/(Ctr2), Cu is then distributed into at least three independent pathways *via* binding to chaperones. Chaperones are small intracellular proteins with high selectivity and affinity for Cu(I), that protect Cu along the pathway from the entry into the cell, through the cytoplasm, to its intracellular targets, thus preventing unwanted and dangerous oxidizing reactions.[54]

Variations in chaperones levels (down-regulation or over-expression) have been demonstrated to have little influence on the initial rate of Cu uptake, thus suggesting that a direct protein-protein interaction (Ctr1/(Ctr2)-metallochaperone) would not be essential for Cu uptake.[55] The GSH pool, present at mM concentrations, might transiently bind to Cu(I), as it exits the membrane, thus facilitating Cu-dissociation from Ctr1/2.[56]

Other Cys-rich proteins of low molecular weight, named Metallothioneins (MTs), occur intracellularly and bind Cu(I) with the highest binding affinity (K_d (MT) ~ 10^{-19} M)[57], even though for kinetic reasons they cannot remove Cu from enzymes. They may play special roles in the regulation of cellular Cu(I) distribution, especially under conditions of cellular Cu excess (a further discussion will be given in **1.5.1** Mammalian Metallothioneins (MTs)).[58]

Three are the Cu chaperones which have been identified so far in humans, responsible for shuttling Cu to various intracellular destinations, i.e. Cu-dependent enzymes in the cytosol, mitochondria, and the lumen of secretory pathway:

- CCS: it shuttles Cu to the radical scavenging enzyme, superoxide dismutase 1 (SOD1), mainly present in the cytosol. It is a multi-domain protein consisting of: i) domain I (with a Cu(I)-binding site, containing a Met-X-Cys-X-Ser-Cys motif), proposed to require Cu(I) from Ctr1 or GSH[59]; ii) domain II, required for the heterodimerization with SOD1, that facilitates Cu insertion into SOD1; iii) a C-terminal tail (with a Cys-x-Cys motif) which mediates Cu(I) transfer from domain I to SOD1 and simultaneously the formation of a disulfide bond within SOD1, which helps in the stabilization of the enzyme.[60–62]
- Cox17: it is involved in Cu transfer to Sco1 and Cox11, which in turn donate Cu to the CuB and CuA sites of cytochrome c oxidase (CcO). CcO is the terminal oxidase of the respiratory chain, located within the mitochondrial inner membrane.[63] Cox17 is a 62-residue protein, and contains 6 Cys residues, two of which (in position C22 and C23) have been proposed to be involved in Cu(I) binding, while the others constitute disulfide bridges.[64] Sco1 contain two essential Cys residues in a fully conserved Cys-X-X-X-Cys metal-binding motif, while Cox11 is known to form a dimer, where each monomer coordinates one Cu(I) via three Cys residues. Interactions of both Sco1 and Cox11 with Cox17 are likely to occur via complementary electrostatic surfaces, permitting Cu(I) transfer.[11,65]
- Atox1: it delivers Cu(I) to the N-terminus of the Cu(I)-transporting ATPases, ATP7A and ATP7B, located in the membranes of trans-Golgi network (TGN), and secretory vesicles. By transferring Cu(I) to ATPases, Atox1 assists the metalation of the downstream Cu-dependent enzymes, listed in **Table 1**, located in the lumen of secretory pathway which are then secreted in the extracellular environment.[10,66] Atox1 features the classic ferredoxin βαββαβ-fold with a Met-X-Cys-X-X-Cys motif at the N-terminus edge of α_1, acting as a high affinity Cu(I)-binding site.[67] With this Cu(I)-site, Atox1 directly interact with the Cu(I) binding domains of two Cu pumps, ATP7A/B, containing six copies of the Cys-X-X-Cys motif.[11,68]

1.3 Breakdown of Cu homeostasis: interconnection with human diseases

As seen in the previous paragraphs, a proper regulation of Cu metabolism is critical for our health. On the other hand, its mis-regulation can be lethal. The importance of keeping a tight regulation of Cu homeostasis, ensuring adequate Cu supplies, without any toxic effect, can be seen in the devastating consequences of several human pathologies associated with its breakdown.[3,69] Cu-related pathologies in organs, tissues and cells generally have their molecular foundations in defective transport and storage systems that interrupt Cu homeostasis.

Defects in Cu homeostasis are directly responsible for heritable human disorders, among which Wilson's and Menkes diseases (WD, MD), respectively related to a condition of Cu-overload or deficiency. Besides, alterations in Cu balance have been linked, but not causally associated, to other pathological states, including several neurodegenerative diseases (e.g. Alzheimer's, Parkinson's, prion diseases (AD, PD, PrD)), cancer, rheumatoid arthritis, gastrointestinal ulcers, epilepsy, diabetes. In the next paragraphs, the pathological role of Cu in WD and MD, as well as in AD and Cancer will be discussed.

1.3.1 Genetic disorders: Wilson's and Menkes diseases

The two best studied disorders in Cu regulation, with a genetic inherited component, are Wilson's and Menkes diseases:

- Wilson's disease (WD): it is an autosomal recessive disorder characterized by toxic accumulation of Cu primarily in the liver and subsequently in the brain and other organs. The causative gene ATP7B, encodes for a Cu(I)-transporting P-type ATPase, ATP7B, expressed most abundantly in the liver (**Fig 3**), where disruption of the protein function prevents the loading of apoCp with Cu to form holoCp (Cp biosynthesis) and elimination of excess of Cu from hepatocyte into the bile. Although missense mutations in ATP7B gene are most frequent, deletions, insertions, nonsense, and splice site mutations all occur.[70] In 40 to 50% of individuals with WD, hepatic dysfunction is the initial clinical manifestation of the disease. Besides, Cu accumulation in the brain can lead to neurological and psychiatric abnormalities like tremors, dystonia, abnormal behavior, personality changes and depression and ophthalmological manifestations such as the Kayser-Fleischer ring.[71,72]
- Menkes disease (MD): it is a X-linked disorder of impaired Cu absorption characterized by low Cu levels in the blood, affecting the metabolism of most major internal organs and ultimately leading to a severe Cu deficiency in the brain. The primary genetic defect occurs in the ATP7A gene, which encodes for the transmembrane protein ATP7A, expressed in most tissues, other than the liver. As ATP7A protein helps in controlling the absorption of Cu from food, as previously described in **1.2.1** Cu absorption and trafficking in the blood, its gene modification results in Cu accumulation in intestinal cells. The direct consequence is a reduced activity of the numerous Cu-dependent enzymes. Onset of the disease starts in utero and are fully manifested during the perinatal period (mainly in boys, because it is X linked). Patients affected with MD demonstrate mental retardation and nervous system deterioration, failure to thrive, coarse hair, and connective tissue abnormalities and usually do not survive to see their third birthday.[12,73,74]

1.3.2 Correlation with Alzheimer's diseases

Another disease in which a mis-regulation of Cu homeostasis (together with that of Zn, Fe) seems to play a pivotal role is AD.[75,76] This is supported by a multitude of *in vitro* and *in vivo* studies.[77–79] Nevertheless, the link between AD progression and Cu imbalance is still controversial.

AD is the most common form of neurodegenerative disease, currently affecting 47 million people worldwide, estimated to increase to 75 million by 2030 and to 131.5 by 2050.[80,81] Despite many years of intense research and great progresses in the knowledge of the molecular pathogenesis of AD, currently no drugs are available to cure or at least to stop the progression of the disease.[82]

95 % of all AD cases are sporadic (SAD), but inherited forms of the disease also exist (familial AD, FAD). FAD is mainly due to mutations in three major genes, i.e. amyloid precursor protein (APP) gene, presenilin1 (PSEN1) gene and presenilin 2 (PSEN2) gene. In contrast, many genetic and environmental factors may contribute to determining the SAD form.[83]

Patients progressively lose their cognitive function and gradually their short- and long-term memory, develop psychiatric disorders and die. Recent studies have shown that the pathology of the disease occurs several years before the onset of clinical symptoms, thus making it difficult to detect at an early stage.[84]

Although the pathophysiology of AD is extremely complex and heterogeneous, one of the characteristic hallmarks of the brains of people with AD is the buildup of senile (or amyloid) plaques, in the extracellular space of neurons. These proteinaceous deposits are composed of insoluble aggregates of the intrinsically disordered peptide Amyloid-β (Aβ).[85] According to the amyloid cascade hypothesis, formulated in the early 1990s, in AD brains, Aβ peptides aggregate first into small soluble oligomers and then in fibrils, consisting of repeating substructures of two layers of intermolecular β-sheets that run in the direction of the fiber axis. Fibrils clump together and finally form plaques.[86,87] Diffused smaller oligomeric aggregates are nowadays suggested to have higher neurotoxicity than the fully-grown amyloid fibrils.[88,89]

Aβ peptides are also present in heathy brains but in soluble and monomeric form. In this form they seem to be indispensable for brain physiology (e.g. for modulation of synaptic function, facilitation of neuronal growth), as their removal or reduction also causes dementia.[90]

Aβ peptides are proteolytic fragments formed during the amyloidogenic processing pathway of hydrolytic degradation of the transmembrane precursor protein (APP) (see **Fig 5**), whose physiological function is only partially understood.[91] The cleavage through this pathway (accounting for 10-20 %) requires two endoproteases, called β- and γ-secretases, which act in sequence and respectively cut at the N and C termini of Aβ. First β-secretase cleaves APP to secrete the large product sAPPβ, and CTFβ, which remains membrane bound. Then, CTFβ is cleaved by γ-secretase at multiple sites to produce a vast population of Aβ fragments, which undertake further hydrolytic and post-translational modifications.[92] The most abundant Aβ peptides identified so far in the brains of both normal and AD affected people are the full length $A\beta_{1\text{-}x}$ (x = 40, 42) and the N-truncated peptide, $A\beta_{4\text{-}x}$ (x = 42): $A\beta_{4–42} \sim A\beta_{1–42} > A\beta_{1–40} \gg$ other Aβ peptides.[93–95]

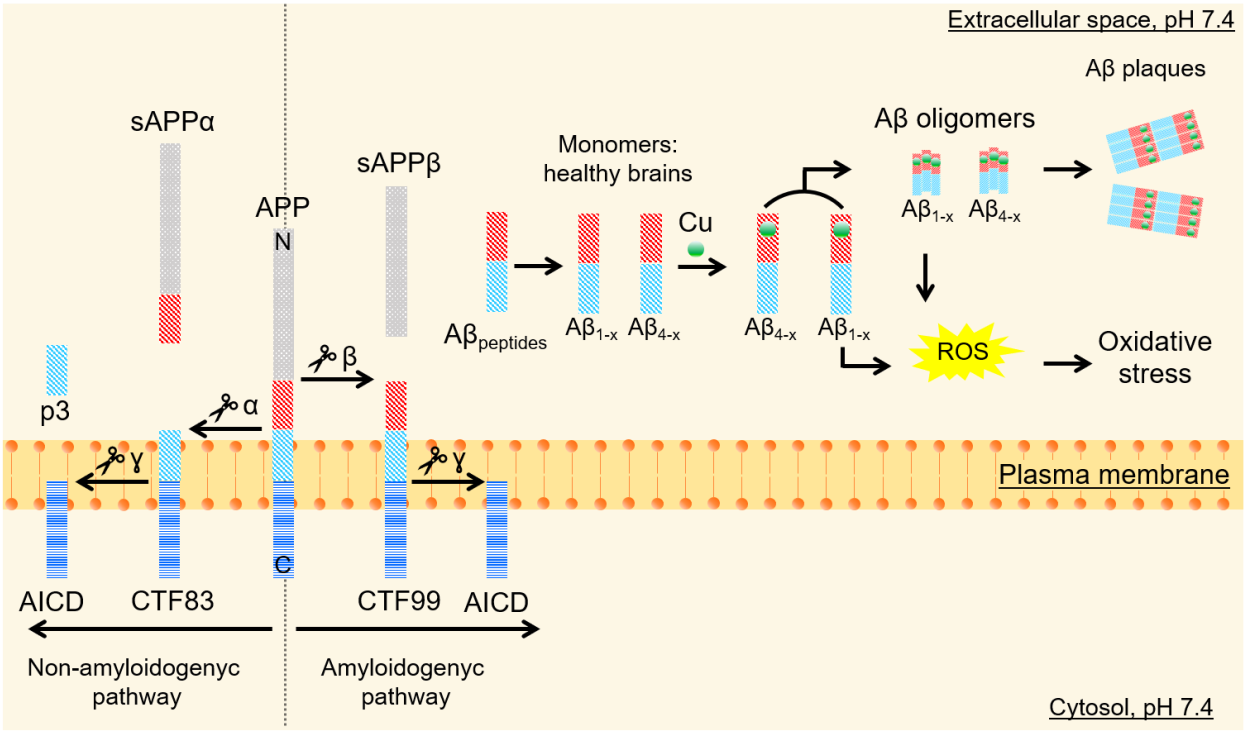

Fig 5 - Cu involvement in the amyloid cascade hypothesis.

On top of this, there is a large body of evidence that brains of AD victims are exposed to oxidative stress during the course of the disease. This is supported by high levels of oxidation of surrounding biomolecules, i.e. proteins, lipids, nuclear and mitochondrial DNA.[76,96]

Elevated amounts of Cu have been found in senile plaques (0.4 mM) and Raman studies indicate that Cu ions in plaques can coordinate Aβ peptides.[97–99] In addition, Cu ions have been detected in higher concentration in the CNS and in the region of hippocampus, while intra-neuronally Cu(I) deficiency has been reported.[98] Consequently, a mis-regulation in Cu-homeostasis might play a key role and be a key factor in AD. It has been suggested that Cu-coordination to Aβ peptides, with formation of Cu-Aβ complexes, can contribute to AD *via* induced structural changes and formation of more neurotoxic soluble oligomers and/or *via* catalyzing the production of ROS. Cu-complexes of $A\beta_{1\text{-}40/42}$ peptides have been implicated in both processes.[100,101] On the other hand, *in vitro* studies have shown that Cu(II)-$A\beta_{4\text{-}42}$ complex is completely inactive in ROS production in the presence of $AscH^-$, thus suggesting its involvement only in the aggregation process.[102] $A\beta_{4\text{-}42}$ peptide has been shown to aggregate faster than $A\beta_{1–42}$, forming toxic oligomers. Thus the N-terminal truncation is believed to render $A\beta_{1\text{-}42}$ peptides more neurotoxic than $A\beta_{1\text{-}40/42}$.[103] However, even though some studies have reported the effects of Cu(II) on the aggregation of some truncated Aβ peptides[104], the combination of Cu(II) and $A\beta_{4–42}$ has not been studied rigorously yet. Only preliminary results from Stefaniak et al., carried out with the C-truncated $A\beta_{4–40}$ peptide, are available, which suggest that Cu(II) ions slightly elongate the oligomer formation phase, probably by enhancing the oligomers stability, hence reducing fibril formation.[95]

As previously stated, a mis-regulation of other metal ions has been observed in AD. In particular for Zn, the link between Zn(II) dyshomeostasis and extracellular Aβ deposition has been established. Zn(II) ions have been found to accumulate in senile plaques at 1 mM concentration.[97] However, like for Cu, the role of Zn in the etiology of AD is not completely understood yet.

Zn(II) ions are redox-inert and thus do not participate directly in ROS production. Several studies have reported their involvement in the aggregation process of Aβ peptides, with rapid formation of amyloid fibrils.[105,106] Zn(II)-induced toxicity *in vitro* and *vivo* seems to be highly concentration dependent, i.e. only to occur at high concentration. A growing number of reports indicate that Zn(II) ions, at lower concentration (stoichiometric amount Zn(II):$A\beta_{1-40/42}$) lower Aβ-mediated cytotoxicity, thus having a neuroprotective role. Garai et al. observed reduced Aβ toxicity in the presence of Zn(II) by selectively precipitating aggregation intermediates. Zn(II) ions were found to destabilize soluble oligomeric intermediates and accelerate their aggregation kinetics.[107] Moreover, more recently, Zhang et al. showed that $A\beta_{1-42}$ aggregates found in the presence of Zn(II) were smaller in size, non-fibrillary and showed less β-sheet structures than aggregates formed in the absence of Zn(II).[108,109]

Throughout the years, the coordination of Cu(II), Cu(I) and Zn(II) ions to Aβ peptides ($A\beta_{1-x}$ and $A\beta_{4-x}$) in the monomeric form has been fully studied, even though there is still debate for some coordination modes. Here below, only the so far most accepted coordination modes, which have reached a consensus from many studies, will be discussed.

The C-terminally amidated $A\beta_{x-16}$ peptides have become appropriate models for studying the interaction with Cu(II), Cu(I) and Zn(II) ions, as they contain all the high affinity metal binding sites (except Met35, which is not known to participate in any complex with Aβ peptides). Besides, they have the advantages of having a higher solubility (mM range) and to maintain the monomeric state, hence allowing physicochemical studies.

Fig 6 shows the main coordination modes of $A\beta_{1-x}$ and $A\beta_{4-x}$ peptides for Cu(II), Cu(I) and Zn(II), at physiological pH:

- $A\beta_{1-x}$: two different binding modes can be found for Cu(II), at physiological pH, known as component I (favored at lower pH) and component II (favored at higher pH). They both present a distorted square-planar geometry and the coordination through the terminal amine of the Asp1 residue. In Component I, Cu(II) is also bound through the carbonyl from the Asp1-Ala2 amide bond, and the imidazole nitrogen atoms (Nim) from two histidine residues, His6 and His13 or His14 in equilibrium. In component II, the nitrogen atom from the Asp1-Ala2 amide bond is deprotonated and binds to Cu(II), together with the CO from the Ala2-Glu3 peptide bond and one imidazole nitrogen atom (Nim) with no preference.[110–112] The kinetic lability of His residues, makes Cu(II)-$A\beta_{1-x}$ complexes prone to form ternary adducts. Until now, two types of ternary complexes have been described in the literature: i) with small monodentate ligands, such as buffers, which occupy only one site around the Cu(II) center[113] or ii) with bigger tetradentate ligands, such as 2-(dimethylamino)-methyl-8-hydroxyquinoline), which occupy three sites around Cu(II).[114,115]

  Cu(I) is bound in a linear fashion by the Nim of His6, His13 and His14 in an equilibrium, in which His13 and His14 seem to be the preferred ligands.[116,117]

  According to a recent study performed by Alies et al., by means of ^{1}H-NMR and X-ray absorption, Zn(II) is bound to $A\beta_{1-x}$ in a tetrahedral binding with two His residues (His6 and His13 or His14) and two carboxylate residues (Glu11 and Asp1 or Glu3 or Asp7, with a preference for Asp1).[118]

- $A\beta_{4-x}$: Cu(II) binding sites in $A\beta_{4-x}$ are found within the first three AA. This is due to the presence of the Phe-Arg-His sequence, at the N-terminus, corresponding to the specific Cu(II)

binding motif, known as ATCUN (amino terminal Cu,Ni-motif), characterized by an His in 3rd position. Hence, Aβ4-x binds Cu(II) with the N-terminal amine, the two deprotonated N of the amide (between X-Z and Z-H), and the N(Pi) of the imidazole, forming a 4N complex with a square planar geometry. [95,119,120]

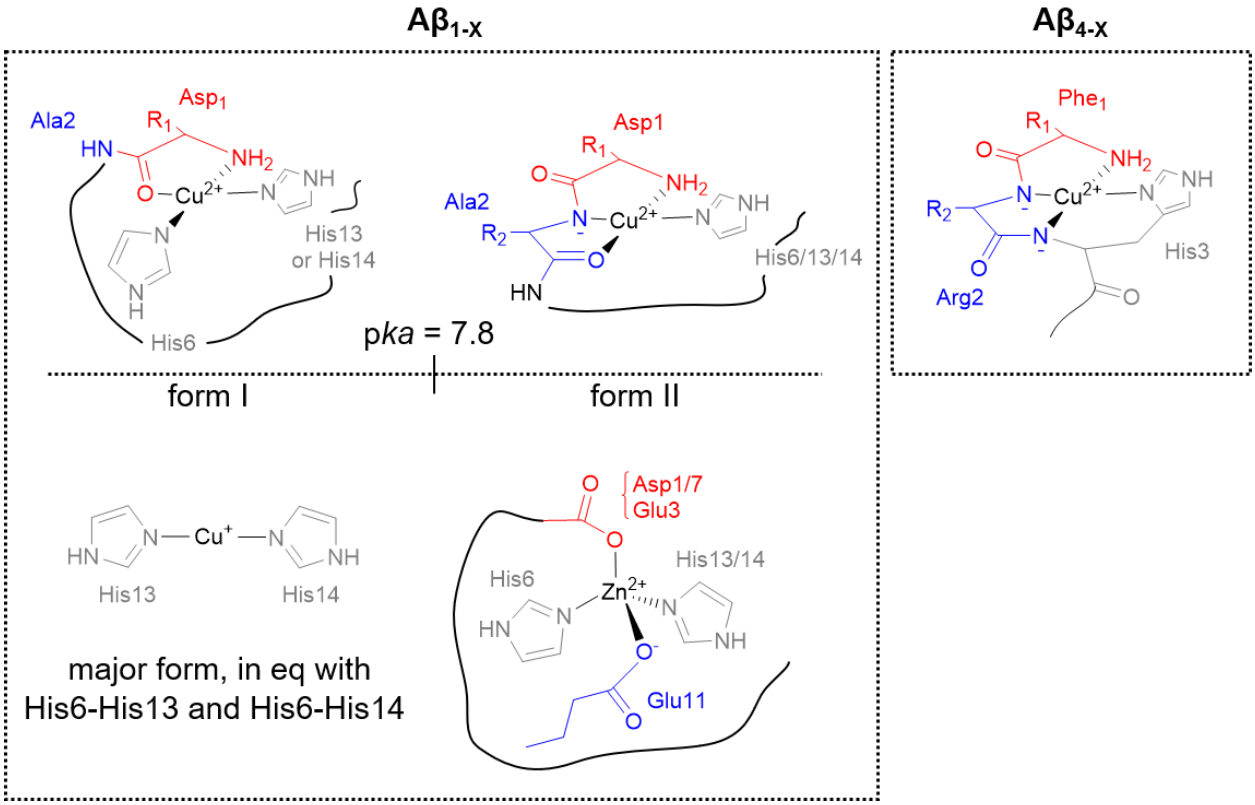

Fig 6 - Main coordination modes of Aβ1-x and Aβ4-x for Cu(II), Cu(I) and Zn(II), at physiological pH .

Conditional binding constants at physiological pH ($^cK_{7.4}$) of the above described complexes have been determined, using a number of methodologies, such as potentiometry, calorimetry, and spectroscopic techniques. Values are gathered together in **Table 2**.

Table 2 - Conditional binding constants at pH 7.4 ($^cK_{7.4}$) for the highest affinity binding sites of Aβ1-x and Aβ4-x.

Peptide	Cu(II)	Cu(I)	Zn(II)
Aβ1-x	10^9 - 10^{10} M^{-1}	10^7 - 10^{10} M^{-1} (121, 122)	10^5 M^{-1} (123, 124)
Aβ4-x	3×10^{14} M^{-1} (102)	-	-

1.3.3 Correlation with Cancer

Mis-regulation of Cu metabolism has long been known to occur in cancer cells.[125] Numerous reports have demonstrated increased Cu levels in several tumor cell types and blood serum of cancer patients.[126,127] Elevated Cu levels have been observed in a plethora of cancers, including stage I multiple myeloma[128], acute lymphoblastic leukemia[129], lung cancer[130], reticulum cell sarcoma, bronchogenic and laryngeal squamous cell carcinomas, cervical, breast, stomach.[131] Nevertheless, larger scale studies are needed to validate many other reports on other cancer types.

Weather Cu dyshomeostasis is cause or a consequence of cancer, like for AD, is still a matter of debate, as no clear associations between Cu levels and cancer incidence have been found so far. Wilde type mice have been exposed to 20 mM $CuSO_4$ in drinking water for up to 2 years, but no

increase in cancer incidence was registered, suggesting a non-carcinogenic role of Cu.[132] However, it was observed that such Cu concentration is unlikely to increase systemic Cu levels in mice, as they are able to eliminate surplus of Cu.[133] Thus, a more systemic controlled study would be required.

Data strongly suggest that increased Cu levels are involved in cancer development and progression, inducing i) cell proliferation ii) ROS production, with consequent induction of a state of oxidative stress and inflammation, iii) angiogenesis and iv) metastasis.[131,134,135]

Different studies have shown a relationship between expression of Cu-binding proteins/chaperones and cell proliferation. Expression of Cu-transporters such as Ctr1, Atox1, ATP7B, Cox 17 was found to be up-regulated in breast cancer, suggesting an increase Cu flow, and consequent Cu delivery to Cu-dependent enzymes.[136] Besides, Atox1 was proposed to act as a Cu-dependent transcription factor, that when activated by Cu, undergoes nuclear translocation, DNA binding, and transactivation, thereby contributing to cell proliferation.[137] On top of this, Cu may be involved in RAS-RAF-MEK-ERK signaling cascade, which is required for cancer development, as it may bind to the protein MEK1 (characterized by two Cu(II) binding sites), stimulating its interaction with ERK.[138]

However, one of the main processes by which Cu may enhance tumor growing is angiogenesis. Angiogenesis involves the migration, proliferation and differentiation of endothelial cells to form new blood vessels. This process is utilized by tumors to increase the supply of O_2 and nutrients, hence supporting their growth to a diameter larger than 1-2 millimeters.[139] The process is under control of multiple angiogenic stimulating factors. The molecular pathways that Cu may influence to induce angiogenesis are varied. Different studies have suggested that it may affect the angiogenic signaling cascade, both by binding to the proteins involved in the cascade and by regulating their expression/release. For instance, Cu has been found to activate angiogenic factors like vascular endothelial growth factor (VEGF), basic fibroblast growth factor (bFGF), transforming growth factor β (TGFβ), and cytokines (interleukin (IL-1, -6 and -8).[140] In addition, it has been shown to induce the induction of hypoxia-inducible factor 1 (HIF-1), which in turn regulate the expression of several angiogenic genes, such as Cp. Cp binds Cu and induces the formation of new blood vessels.[141]

As well as, a growing number of evidences support Cu direct influence in the ability of cancer cells to invade surrounding tissues and to spread to distant organs (metastasis). For instance, the activities of both lysyl oxidase (LOX) and lysyl oxidase-like (LOXL) proteins, which contribute to remodeling the extracellular matrix and to establishing a pre-metastatic niche, require Cu.[142,143] Additionally, more recently, the Cu-dependent protein MEMO, which requires Cu for its oxidase activity, was observed to play a significant role in the migratory capacity of breast cancer cells.[144]

1.4 Targeting Cu dysmetabolism: chemical approaches for Cu manipulation in medicine

Considering the pivotal role played by Cu dysmetabolism in the progression of a range of pathological conditions (as seen previously), a variety of chemical approaches and new ligands (exogenous compounds), that aim to target and manipulate Cu homeostasis, have been developed and explored since the last century.[145,146]

Generally, manipulation of the distribution of metal ions in biological systems, in a specific way, is a very difficult process, first of all because of the challenge of achieving metal binding selectivity. Selectivity is a measure of the ligand affinity for a particular metal ion over others (defined as the ratio of the affinity values of a ligand for two different metal ions). For instance, when one wants to have a specific Cu chelator to treat Cu-overload conditions, the risk is to bind and affect the concentration of another essential metal, such as Zn or Fe, thus inducing deficiencies of the latter. On top of this, it is extremely complicated to model and predict the metabolic stability and pharmacokinetics of a metal-complex, considering the variety of physiological conditions (e.g. pH) and all the biological contributors that might influence the reactivity and distribution characteristics of all parts of the coordination complex.

Cu-binding ligands that have been developed over the years can be split into three categories:

- traditional Cu-ligands (chelators), originally introduced and exploit for sequestration and elimination of endogenous Cu from the body in case of Cu-overload conditions (chelation therapy). This type of approach is one of treatment option currently in use for Wilson's disease. Some of the available Cu chelators are Penicillamine (first compound already introduced in 1956 by Walshe)[147], Trientine, and Tetrathiomolybdate. These chelating agents bind directly Cu in blood and tissues, thus preventing its accumulation, and facilitate its excretion *via* the stools and urine (**Fig 7a**).[71]

- Cu-ligands able to attenuate and disrupt specific and abnormal Cu-peptide/protein interactions (metal protein attenuating compounds, MPACs) additionally enabling Cu-redistribution with consequent normalization of its homeostasis. This type of compounds are supposed to work as metallophores, forming neutral and lipophilic complexes able to cross biological membranes (**Fig 7b).**[148] Different groups, have attempt to rationally design this type of binding agents, to be used as therapeutics to target the pathogenic Cu-Aβ peptides interaction in AD. With regard to this type of interaction, the ligands have to possess: i) an higher affinity for Cu ions than that of Aβ peptides (see **Table 2**), ii) Cu over Zn selectivity much higher than that of Aβ peptides (as Zn ions are much more concentrated in the synaptic cleft of neurons)[149] and iii) ability to cross the blood-brain barrier (BBB). Among the family of ligands developed in this context there are hydroxy- and aminoquinoline ligands and derivatives, tetraazamacrocycles, aminophenol-based ligands, aminopyridine-based ligands, phosphines and bis(thiosemicarbazonato) ligands (examples for each family are shown in **Fig 7b**).[150]

- Cu pro-oxidant ligands that enhance Cu-reactivity by forming of Cu-complex that promote Cu-redox cycling and generation of ROS, i.e. a catalytic metallodrug. In this case, the ligand can be injected already in form of Cu-complex, delivering exogenous Cu (ionophore), which exists extracellularly and then enters the cell, or it is applied as free ligand and is then able to pick up the metal inside the cell, thus forming in-situ the Cu-complex. This type of approach is of particular interest and has been considered for the development of anti-tumor Cu-based drugs.

Examples of select Cu-chelators are thiosemicarbazonato and bis-thiosemicarbazonato ligands, dithiocarbamate and analogs, phenanthrolines, bipyridines, which display antineoplastic activity *in vitro* and in mouse models.[134,151,152]

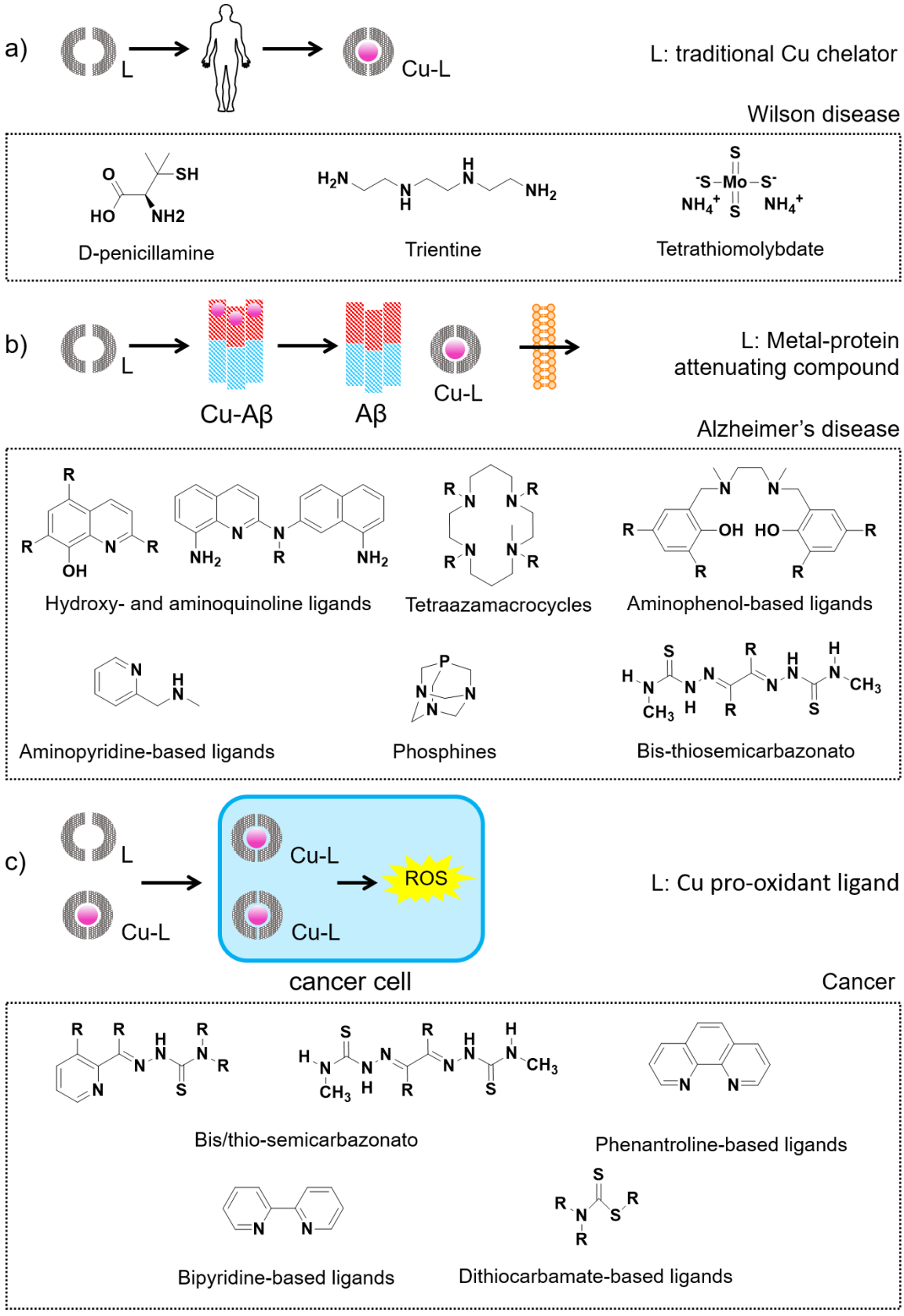

Fig 7 - Schematic representation of the chemical approaches for Cu-manipulation exploit in medicine.

1.5 The interplay between thiols containing biomolecules and medicinal Cu-complexes

Among the different factors that can influence the biological outcome of medicinal Cu-complex (both pathophysiological and/or therapeutic metallodrug), a key aspect to consider is its kinetic and thermodynamic stability in both ligand and metal exchange reactions, with potential physiological competitors in the biological environment. In this context, thiols containing biomolecules are of significant importance and could strongly impact the fate of a medicinal Cu-complex, as i) they have the potential to reduce Cu(II)-complexes and ii) are good chelators for Cu(I). In the next paragraphs, the properties of a group of metalloproteins, named Mammalian Metallothioneins (MTs), characterized by a high Cys-content, as well as those of low molecular weight thiol(ate) containing biomolecules, e.g. Glutathione (GSH) and Cysteine (Cys), will be considered.

1.5.1 Mammalian Metallothioneins (MTs)

a. General introduction

Mammalian MTs are low molecular weight proteins of about 7 KDa, with a characteristic amino acid composition, i.e. high Cys-content (~ 30%) and no aromatic amino acids (**Fig 8**), and a high metal ion content, occurring both intracellularly ($[MT]_{in}$ = 3-100 μM) and extracellularly ($[MT]_{ex}$ = ?).[58,153]

MT was first discovered as Cd(II)-containing protein in horse kidney, by Margoshes and Vallee, more than 60 years ago[154]. Quickly, further studies revealed that the most biologically relevant metal ions were Zn(II) and Cu(I). Only under environmental exposure, MTs can bind non-essential toxic metal ions, in particular Cd(II). These metal ions are coordinated through the thiolate sulfur of the Cys residues, resulting in the formation of two thiolates clusters, respectively in the β- and α-domains.

Mammalian MTs are present in four major isoforms, designated MT-1 to MT-4. While MT-1 and MT-2 are expressed in almost all tissues, MT-3 and MT-4 appear to be more tissue specific. MT-3 expression is primarily confined to the central nervous system (CNS), whereas MT-4 seems to be expressed exclusively in cornified and stratified squamous epithelia.[153]

The expression of MT-1 and MT-2 is under the control of the metal response element binding transcription factor 1 (MTF1).[155,156] Its activation depends on Zn, i.e. if the Zn concentration rises in the cell, Zn binds to MTF1 (which contains 6 Zn-fingers), and induces the transcription of MT genes as well as several Zn transporters. The de novo synthesized apo-MT (thionein, T) binds Zn in the cell until the Zn concentration drops to the point that Zn is released from at least 2 of the 6 zinc fingers present in MTF1. On the other hand, MT-3 and MT-4 seem to be relatively unresponsive to inducers like metals and a variety of chemical and physical conditions, but to be more tissue-specific. MT-4 isoform is the one less studied, whereas MT-3 is highly investigated as it possesses biological functions not shared by MT-1/MT-2/MT-4, i.e. extracellular growth inhibitory activity in neuronal primary cultures (attributed to the ^{5}TCPCP^{9} motif[157]) and involvement in neurodegenerative diseases.[158]

Nevertheless, the sequences are very similar, consisting of 60-68 amino acids and a conserved array of 20 Cys (**Fig 8**). When compared to the canonical MT-1 and MT-2 isoforms, MT-3

sequence contains 7 additional amino acids: a Thr insert at position 5 and a Glu/Ala-rich insert towards the C-terminus. In addition, it contains the conserved ^{6}CPCP^{9} motif, which is absent in all other members of the MT family.[159] Instead, MT-4 sequence has 62 amino acids with an insert of Glu at position 5.

Isofrom	Sequence
	1 10 20 31 32 40 50 60 68
MT-1	MDPN-CSCEA GGSCACAGSC KCKKCKCTSCK KSCCSCCPL GCAKCAQGCI CKGA------ SEKCSCCA
MT-2	MDPN-CSCAA GDSCTCAGSC KCKECKCTSCK KSCCSCCPV GCAKCAQGCI CKGA------ SDKCSCCA
MT-3	MDPETCPCPS GGSCTCADSC KCEGCKCTSCK KSCCSCCPA ECEKCAKDCV CKGGEAAEAE AEKCSCCQ
MT-4	MDPRECVCMS GGICMCGDNC KCTTCNCKTCK KSCCPCCPP GCAKCARGCI CKGG------ SDKCSCCP
	β-domain *α-domain*

Fig 8 - Amino acid sequences of human MT isoforms (numbering referring to MT-3). Cys residues are highlighted in red, the two inserts of MT-3 compared to MT-1/MT-2 in green. The boundary between the α- and β-domain is between amino acid 31 and 32.

b. Coordination chemistry

Metal ion content and selectivity: MT metalation state seems to be isoform specific. Under normal physiological conditions, MT-1 and MT-2 isoforms are isolated as homometallic species, containing seven Zn(II) ions (although some Zn(II) can be easily lost).[153,160] Only under exposure to high concentrations of other metals, i.e. Cd(II) or Cu(I), these can become the dominant ones. On the contrary, MT-3 as isolated from the human brain, presents a mixed Zn(II) and Cu(I) content, with about 4 Cu(I) ions in the N-terminal β-domain and 3-4 Zn(II) ions in the C-terminal α-domain, $Cu(I)_4Zn(II)_{3/4}$-MT-3.[161,162] Whether Cu(I) is bound during purification or is present natively is still unclear. According to a classification suggested by Capdevila and co-workers, MT-3 has a more Cu(I)-binding character compared to MT-1/MT-2, thus suggesting that Cu(I) is present natively.[163] This would be in agreement with the unique function of MT-3 in the CNS in modulating neuronal Zn and Cu metabolism. In general, the preference for discrete species, with distinct stoichiometries for Cu(I)-binding, arise from cooperativity, due to the formation of $Cu(I)_{4/6}$-thiolate clusters. *In vitro*, formation of MTs species with higher Cu(I) stoichiometry has been observed, i.e. $Cu(I)_8$, $Cu(I)_{10}$, up to $Cu(I)_{12}$ in solution[163,164], and up to $Cu(I)_{20}$ only in gas phase[165], obtained *via* thionein metalation or Cu(I) titration in $Cu(I)_4Zn(II)_4$MT-3, under reducing conditions. Formation of these species, *in vivo*, seems to be limited only to pathological conditions of Cu(I) overload. [166]

For Zn(II) (and also Cd(II)) seven binding sites have been classically described both for MT-1/MT-2 (both for isolated and *in vitro* reconstituted forms) and MT-3, although less well defined. In early studies it was shown that the seven Zn(II) ions bind to thionein with the same affinity, in the range of 10^{-12}-10^{-13} M, in terms of average K_d.[167] More recent investigations i) from Krezel and Maret on MT-2,with the Zn sensitive fluorescent probes FluoZin-3 and RhodZin-3, and ii) Carpenter et al. on MT-3, with ITC experiments, using EDTA as a competitor, revealed that not all the seven Zn(II) ions bind to MT-2/MT-3 with the same stability constant.[168,169] Conditional K_d calculated on MT-2 are reported in **Table 3**.

Table 3 - Conditional dissociation constants (at pH 7.4) for Zn(II)/Cd(II)/Cu(I) sites in MT-2.

Me-MT-2 complex	K_d **(M)**	**Reference**
$Zn(II)_7$MT-2 (1^{st}-4^{th} sites)	1.6×10^{-12}	[168]
$Zn(II)_7$MT-2 (5^{th} site)	3.5×10^{-11}	[168]
$Zn(II)_7$MT-2 (6^{th} site)	1.1×10^{-10}	[168]
$Zn(II)_7$MT-2 (7^{th} site)	2.0×10^{-8}	[168]
$Cd(II)_7$MT-2	5×10^{-15}	[168]
$Cu(I)_4Zn(II)_4$MT-2	4.3×10^{-19}	[170]

From a thermodynamic point of view, all MTs prefer Cu(I) over Zn(II). The MTs selectivity is directly linked to the HSAB theory (see **1.1.2** Chemical properties of Cu important in biology), i.e. thiolates bind preferentially to Cu(I) > Cd(II) > Zn(II), according to the softness of the overall metal ions. Nevertheless, MT bind Zn(II) in vivo, because Zn(II) is more bioavailable than Cu(I).

Overall, whether MTs bind Zn(II) and/or Cu(I) in vivo depends on the difference in affinity for Cu(I) over Zn(II) and on the bioavailability of these metals, which is influenced by its localization and physiological conditions. This means that although both MT-1/MT‑2 and MT-3 preferentially bind Cu(I) over Zn(II), the difference in affinity for Cu(I) over Zn(II) is larger for MT-3 than MT-1/MT‑2 (estimated K_d from $Cu(I)_4Zn(II)_4$-MT-3 ~ 10^{-19})[171], and hence in vivo Cu(I)-binding to MT-3 is more likely compared to that of MT-1/MT‑2, under normal physiological conditions. Moreover, depending on the Zn(II) and Cu(I) availability, the metal ion content can be different, not only with regard to the nature of the metal but also with regard to stoichiometry, as the affinities of each site are, at least for Zn(II), not the same.

On top of this, also isoform-specific key non-coordinating residues have been recently identified to play a significant role in controlling the Cu(I)/Zn(II) selectivity in MT-2 and MT-3 metal clusters, giving rise to the corresponding Zn(II)-thionein character to the C-terminal β-domain of MT-2 and increasing the Cu(I)-affinity in the N-terminal β-domain of MT-3.[170]

Structure: in the apo form, the protein is intrinsically disordered, thus making challenging structural studies on it. Upon metal ion binding, MTs acquire a defined 3D structure. Most of the current knowledge regarding the structural properties of MTs is based on NMR studies.[172,173] Only one X-ray structure of MT-2 containing Cd(II) and Zn(II) has been solved but not from humans.[174] For NMR analyses, Zn(II) is usually replaced by Cd(II), as Cd(II)-MTs possess better spectroscopic properties (i.e. isotopes with a nuclear spin I = ½), a less dynamic nature and higher protein affinity. Overall, the two molecules have been demonstrated to be structurally similar, both in terms of cluster geometry and overall shape.[175]

The MT-1/MT‑2 structure containing Zn(II) or Cd(II) is characterized by two separated domains in the form of a dumbbell, linked by a flexible region. Each domain contains a metal-thiolate cluster, one with 3 metal ions, $Me(II)_3$-S_9, in the N-terminal β-domain, and the other containing 4 metal ions, $Me(II)_4$-Cys_{11}, in the C-terminal α-domain (**Fig 9**). Therefore, all the 20 conserved cysteines are involved in metal coordination, forming a tetrahedral geometry and a tetrathiolate environment around each metal ion, where sulfur donors are bound to one or two (bridging donors) metal ions.

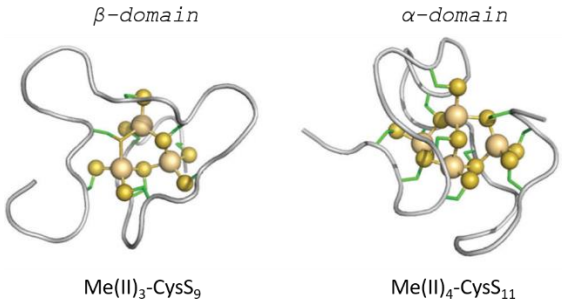

Fig 9 - Representation of the divalent metal-thiolate clusters in mammalian MTs as exemplified by the structure of human $Zn(II)_7$MT-2. Left: $Me(II)_3$-$CysS_9$ cluster in the N-terminal β-domain; right: $Me(II)_4$-$CysS_{11}$ cluster in the C-terminal α-domain. Me(II) (goldspheres) is either Zn(II) or Cd(II), and S (yellow spheres) represents the sulphur of the thiolate function from Cys residues (side chains in green).

Besides, Zn(II)-binding to MT-1/MT-2 has been recently demonstrated to follow a non-cooperative pathway at physiological pH, in which the formation of the Zn(II)-thiolate clusters is preceded by the formation of individual coordination sites, i.e. bead-like structures, where Zn(II) is only bound terminally to Cys thiolates.[176,177] On the other hand, Cd(II) binding to MT-1/MT-2 seems to be cooperative, also in the β-cluster, although the coordination dynamics in this cluster is more pronounced compared to the α-cluster.[178]

Concerning MT-3, the structural features have been investigated both for the recombinant human $Zn(II)_7$MT-3 and the native protein, containing Zn(II) and Cu(I), $Cu(I)_4Zn(II)_{3/4}$-MT-3.[179]

For $Zn(II)_7$MT-3 only the structure of the C-terminal α-domain, containing Cd(II) has been structurally solved by NMR[180], whereas the N-terminal β-domain has only been studied by absorbance, circular dichroism spectroscopies.[181,182] Both domains show similar $Me(II)_3$-Cys_9 and $Me(II)_4$-Cys_{11} clusters, $Me(II)_3$-S_9 having greater dynamic exchange than that in MT-1/MT-2.[183] This highly dynamic process has been assigned to the presence of the ^{5}TCPCP^9 motif, as engineering this motif into MT-1 yielded a MT with a similar dynamic to MT-3.[157]

Conversely, analysis of the native protein $Cu(I)_4Zn(II)_{3/4}$-MT-3 revealed the presence of two homometallic clusters, a $Cu(I)_4$-thiolate cluster in the N-terminal β-domain and a $Zn_{3/4}$-thiolate cluster in the C-terminal α-domain.[161,181] The localization of both clusters in the protein structure was established both with spectroscopic and immunochemical methods.[153] In the β-domain, Cu(I) ions are digonally or trigonally coordinated by Cys-thiolates.[184]

Generation of $Cu(I)_4Zn(II)_4$-MT-3 species in the aerobic reaction between $Zn(II)_7$MT-3 and free Cu(II), revealed the presence of a $Cu(I)_4$-Cys_5 cluster, containing five reduced thiolates and two disulfides. The Cu(I)-thiolate cluster was found to be stable in air oxygen and redox-silent. The reason for this in not known. Structural constraints and the short Cu(I)-Cu(I) distances (< 2.8 Å) in the $Cu(I)_4$-thiolate cluster, leading to peculiar metal-metal interactions, have been postulated as important factors for its stability. Regarding the inability of Cu contained in the $Cu(I)_4Zn_4$MT-3 to catalyze the production of ROS, this has been related to the unfeasible formation of the complex between the $Cu(I)_4$-thiolate cluster and oxygen or to the increased redox potential of the $Cu(I)_4$-thiolate cluster.[171,185]

Metal buffering capacity: as highlighted in **Table 3**, MT-2 affinities for Zn(II) in the β- and α-domains are not all the same. These values indicate that under physiological conditions MTs possess appropriate metal-binding properties for buffering fluctuations in free Zn(II) concentration in the cell, considering its natural fluctuations in the range of 10^{-11} to 10^{-9} M. Thus, under cellular

conditions MT-2 can exist in unsaturated forms ranging from $Zn(II)_4$MT-2 to $Zn(II)_7$MT-2, which have been recently characterized for the first time by Drodz et al.[177] They can serve as a Zn(II) donors and/or acceptors at the same time and regulate cellular Zn(II) free concentration, together with other Zn(II) transporters.[186,187] Their buffering capacity stems from their capability to accommodate a dynamic transition from tetrathiolate coordination in partially metallated MTs (in which Zn can be coordinated exclusively by terminal thiolate ligands) to fully metallated forms.

c. Reactivity

In general, the reactivity of the two clusters of MTs is similar, in terms of final products, although the kinetics of the reactions can be different. As already mentioned, often the β-cluster is more reactive, likely due to the higher flexibility and solvent exposure, and the difference is more pronounced for MT-3 compared to MT-1/MT-2. For instance, study of the reactivity of $Zn(II)_7$MT-2 and $Zn(II)_7$MT-3 towards 4 eq. of Cu(II), led in both cases to Cu(I) binding to the β-domain, with concomitant release of 3 Zn(II) ions (formation of $Cu(I)_4Zn_4$MT-2/3), but with a faster kinetic of Cu(I)-binding to MT-3 compared to MT-2.[170]

Reactions of exchange of metal ions between the two domains and between two MTs can occur and be relatively fast (faster than minutes), despite the high binding affinities. They require associative mechanisms, as a dissociative metal ion transfer would be too slow ($t_{1/2}$ of Cu(I) dissociation of days to years, estimated based on a K_d of ~ 10^{-19} M). Thus, MTs can be considered as unique metalloproteins with high thermodynamic stability but with kinetic lability.

Most of the other reactions involving the thiol(ate) sulfur atoms are redox reactions that result in their oxidation (disulfide formation). Thus, despite Zn(II) does not exhibit redox activity, the thiolate ligands confer redox activity on the Zn(II) clusters. The redox potential of ~ 0.37 V vs Ag/AgCl reported by Maret and Vallee for the Zn(II) clusters is lower than that of other well-known reducing biomolecules such as GSH, NADH or thioredoxin. This means that Zn(II)-MTs can be oxidized by mild cellular oxidants, leading to the release of the coordinated Zn(II) ions. This reaction is reversible and is a very important connection, linking metal binding ability to redox reactions. Other ways to oxidize Cys, include i) the reaction with Cu(II), as seen above, and ii) oxidation triggered by ROS in particular, H_2O_2, $O^{\bullet-}$ or $HO^{\bullet}$.

Cysteines are good nucleophiles and hence reactions with electrophiles consume the thiol/thiolates leading to the release of metal ions. This can apply to several organic reagents such as alkylating reagents or $NO^{\bullet}$ and metal ions such as Pt(II), Ag(I), Hg(II).[183]

d. Functions

The chemical properties of MTs, linked to the presence of thiol(ate) sulfur atoms of the Cys residues, which have been described in the previous paragraphs, are useful and can be exploited by MTs in a variety of physiological processes. Thus, from a functional point of view, MTs have been reported to play roles in:

- regulation of Zn and Cu homeostasis
- detoxification from excess of toxic metal ions (mostly Cd)
- cellular defense against oxidative stress
- modulation of neuronal growth (MT-3)

control of aberrant Cu-amyloidogenic peptides interactions, linked to the progression of neurodegenerative disorders, e.g. AD and Parkinson disease (MT-3).

1.5.2 Low molecular weight thiol(ate) containing biomolecules

Besides MTs, low molecular weight thiol(ate) containing biomolecules, can also play a crucial role on the stability and redox activity of medicinal-relevant Cu-complexes. One of the most relevant biomolecule for the intracellular environment is the tripeptide GSH (composed of Glu, Cys and Gly, with the unusual amide linkage between the γ-carboxylate of Glu and the amine of Cys) (**Fig 10**). GSH, in its reduced form, is present at very high concentrations in the cytosol or nucleus, which are often reported in the range of 1-10 mM, and together with corresponding oxidized form glutathione disulfide (GSSG), it is considered to be the major thiol-disulfide redox buffer of the cell (GSH/GSSG redox couple).[188–190] Nevertheless, in the reduced form GSH is also present extracellularly where it has been proposed to act as a neurotransmitter. However, in the extracellular space the most abundant thiol(ate) containing biomolecule is the amino acid Cys (**Fig 10**) Cys occurs also intracellularly but it becomes less relevant considering the high GSH concentration.[188]

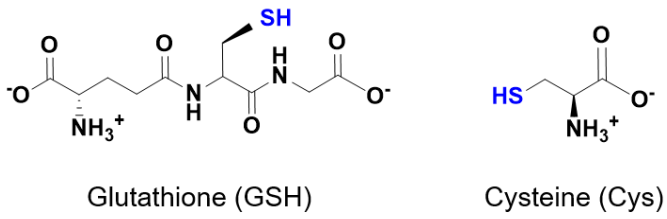

Fig 10 - Chemical structure of the two most relevant low molecular weight thiol(ate) containing biomolecules: GSH and Cys

GSH and Cys have two important features, like MTs: i) they are reducing agents, thus can potentially reduce a Cu(II)-complex ($E°_{GSH}$ = -240 mV, $E°_{Cys}$ = -220 mV vs Ag/AgCl, in the cell as GSH/GSSG and Cys/Cystine ≥ 10000). This can have a major impact on the stability of the complex, and hence its fate. ii) They are metal-chelators and can coordinate Cu(I) *via* their Cys side chain. The stability and nature of the Cu(I)-GSH/Cys complexes formed under biological relevant conditions are less clear than for MTs. GSH has been reported to form the tetranuclear cluster $Cu(I)_4$-$(GS)_6$ with a K_d(GSH) ~ 10^{-17} M.[56] Besides, GSH complexes have proposed to act as Cu(I)-shuttles between proteins, like Ctr1 and Cu-chaperons, and the *in vitro* studies have shown that the Cu(I)‑GSH complex can transfer Cu(I) to MT-1.[55,191]

1.6 Aim and objectives of the thesis

Within this context, the studies carried out in the present thesis aimed to investigate the reactivity of medicinal-relevant Cu-complexes, either pathophysiological and/or therapeutic metallodrug, in terms of redox activity and stability towards physiological Cu-binding and/or reducing molecules (including Zn(II)-MTs, GSH, Cys, $AscH^-$, Glu).

Indeed, as discussed above, a key aspect to consider for the biological outcome of a Cu-complex is its kinetic and thermodynamic stability in both ligand and metal exchange reactions, with potential physiological competitors.

Two case studies will be presented: i) for a pathophysiological Cu-complex of Aβ peptide in the context of AD and ii) for Cu-based metallodrugs studied as therapeutics for medicinal applications (e.g. anticancer agents).

The thesis has been organized in the following way. In the first section (chapter II) we will discuss the principal findings of the first case study, which concerns the influence of the biomolecules GSH, Cys and Glu on Cu transfer reactions from/off the N-truncated Aβ species, $Aβ_{4-42,}$ to $Zn(II)_7$MT-3. The main issues we tried to address are stated below.

❖ Case study 1: pathophysiological Cu(II)-Aβ complex of the N-truncated Aβ peptide, $Aβ_{4-16}$ (model for $Aβ_{4-42}$)

- What is the impact of Cys and GSH on this transfer? Could they play the role of Cu(II) reducing agents and Cu(I)-shuttles between the two biomolecules?
- What is the influence of the neurotransmitter Glutamate (Glu)? How does the Zn(II) content of MT-3 affect the rate of Cu-transfer? May multiple mechanisms act cooperatively?

Understanding of the mechanisms of Cu (and Zn)-trafficking between Aβ peptides, proteins and other biomolecules, related to AD, is extremely important and should contribute to answer the question why Cu/Zn are bound to Aβ peptides under AD conditions but not under normal brain physiology.

In the second section (chapter III) we will present the main findings of the second case study, dealing with the reactivity of different Cu-based metallodrugs developed for the treatment of diverse diseases, including cancer, in i) the catalytic production of ROS and ii) with their stability (and consequent possible deactivation) against $Zn(II)_7$MT and GSH, under conditions found in the cytosol and nucleus. The main questions we tried to reply are the following stated below.

❖ Case study 2: Cu-based drugs

- How active are Cu(II)-Xxx-Zzz-His (ATCUN) peptides in ROS production? Could they be applied as artificial Cu-enzymes to degrade biomolecules?
- What is the reactivity of Cu(II)-Thiosemicarbazone anticancer drugs with GSH/$Zn(II)_7$MT under physiological conditions found in the cytosol/nucleus? Is $Zn(II)_7$MT a possible deactivator of these drugs?
- Would it be possible to have a redox-active Cu-drug in the presence of relevant concentrations of GSH/$Zn(II)_7$MT as found in the cytosol/nucleus?

Overall, this type of chemistry with thiols containing molecules could be of interest for the design of metal- and in particular Cu-complexes for all the wide applications in biology and medicine.

In order to answer the questions above and be able to monitor Cu (and Zn) transfer reactions, various spectroscopic and analytical techniques, including absorbance, circular dichroism, low temperature fluorescence, ^{1H}NMR, EPR, and ESI-MS have been employed.

1.7 Reference list

1 C. A. Linder, M.C. & Goode, *Biochemistry of Copper*, Springer-Verlag New York, LLC, New York, 1991.

2 W. Maret, *Int. J. Mol. Sci.*, 2016, **17**, 1–8.

3 National Academy of Sciences, *Copper in Drinking Water*, National Academy Press, 2101 Constitution Ave., N.W. Washington, D.C., 2000.

4 Food and Nutrition Board, *Recommended Dietary Allowances, 10th Edition*, 1989.

5 J. R. Turnlund, C. A. Swanson and J. C. King, *J. Nutr.*, 1983, **113**, 2346–2352.

6 M. Bost, S. Houdart, M. Oberli, E. Kalonji, J. F. Huneau and I. Margaritis, *J. Trace Elem. Med. Biol.*, 2016, **35**, 107–115.

7 J. Kardos, L. Héja, Á. Simon, I. Jablonkai, R. Kovács and K. Jemnitz, 2018, **3**, 1–21.

8 E. I. Solomon, U. M. Sundaram and T. E. Machonkin, *Chem. Rev.*, 1996, **96**, 2563–2606.

9 J. A. Tainer, E. D. Getzoff, J. S. Richardson and D. C. Richardson, *Nature*, 1983, **306**, 284–287.

10 Y. Hatori, S. Inouye and R. Akagi, *IUBMB Life*, 2017, **69**, 246–254.

11 B. Kim, T. Nevitt and D. J. Thiele, *Nat. Chem. Biol.*, 2008, **4**, 176–85.

12 M. DiDonato and B. Sarkar, *Biochim. Biophys. Acta*, 1997, **1360**, 3–16.

13 S. Lutsenko, *Curr. Opin. Chem. Biol.*, 2010, **14**, 211–217.

14 R. R. Crichton, *Biological Inorganic Chemistry*, Elsevier, 2012.

15 W. Mertz, *Science*, 1981, **213**, 1332–1338.

16 R. Malkin and B. G. Malmström, *Adv. Enzymol. Relat. Areas Mol. Biol.*, 1970, **33**, 177–244.

17 R. G. Pearson, *J. Am. Chem. Soc.*, 1963, **85**, 3533–3539.

18 R. D. Hancock and A. E. Martell, *Chem. Rev.*, 1989, **89**, 1875–1914.

19 A. E. Martell and R. D. Hancock, *Metal complexes in aqueous solutions*, 1996.

20 M. E. Helsel and K. J. Franz, *Dalt. Trans.*, 2015, **44**, 8760–8770.

21 K. L. Haas and K. J. Franz, *Chem. Rev.*, 2009, **109**, 4921–4960.

22 J. T. Rubino and K. J. Franz, *J. Inorg. Biochem.*, 2012, **107**, 129–143.

23 B. L. Vallee and R. J. Williams, *Proc. Natl. Acad. Sci.*, 1968, **59**, 498–505.

24 I. Bertini, G. Cavallaro and K. S. McGreevy, *Coord. Chem. Rev.*, 2010, **254**, 506–524.

25 T. D. Rae, P. J. Schmidt, R. A. Pufahl, V. C. Culotta and T. V. O'Halloran, *Science*, 1999, **284**, 805–808.

26 L. A. Finney and T. V. O. Halloran, *Science*, 2003, **300**, 931–937.

27 H. Öhrvik, J. Aaseth and N. Horn, *Metallomics*, 2017, **9**, 1204–1229.

28 P. V. E. Van Den Berghe and L. W. J. Klomp, *Nutr. Rev.*, 2009, **67**, 658–672.

29 J. H. Kaplan and S. Lutsenko, *J. Biol. Chem.*, 2009, **284**, 25461–25465.

30 M. C. Linder, *Metallomics*, 2016, **8**, 887–905.

31 A. Cabrera, E. Alonzo, E. Sauble, Y. L. Chu, D. Nguyen, M. C. Linder, D. S. Sato and A. Z. Mason, *BioMetals*, 2008, **21**, 525–543.

32 P. Bielli and L. Calabrese, *Cell. Mol. Life Sci.*, 2002, **59**, 1413–1427.

33 I. Zaitseva, V. Zaitsev, G. Card, K. Moshkov, B. Bax, A. Ralph and P. Lindley, *J. Biol. Inorg.*

Chem., 1996, **1**, 15–23.

34 T. Z. Kidane, R. Farhad, K. J. Lee, A. Santos, E. Russo and M. C. Linder, *BioMetals*, 2012, **25**, 697–709.

35 D. Ramos, D. Mar, M. Ishida, R. Vargas, M. Gaite, A. Montgomery and M. C. Linder, *PLoS One*, 2016, **11**, 1–23.

36 T. Peters, *Adv. Protein Chem.*, 1985, **37**, 161–245.

37 A. G. Bearn and H. G. Kunkel, *Exp. Biol. Med.*, 2013, **85**, 44–48.

38 A. K. Bossak-ahmad, T. Frączyk, W. Bal and S. Drew, *ChemBioChem*, , DOI:10.1002/cbic.201900435.

39 M. Moriya, Y. Ho, A. Grana, L. Nguyen, A. Alvarez, R. Jamil, M. L. Ackland, A. Michalczyk, P. Hamer, D. Ramos, S. Kim, J. F. B. Mercer and M. C. Linder, *Am J Physiol Cell Physiol*, 2008, **295**, C708–C721.

40 E. Stefaniak, D. Płonka, S. C. Drew, K. Bossak-Ahmad, K. L. Haas, M. J. Pushie, P. Faller, N. E. Wezynfeld and W. Bal, *Metallomics*, 2018, **10**, 1723–1727.

41 A. A. Rehman, H. Ahsan and F. H. Khan, *J. Cell. Physiol.*, 2013, **228**, 1665–1675.

42 C. Linder, *Am. J. Physiol. Physiol.*, 1985, **249**, E77–E88.

43 N. Liu, L. S. Lo, S. H. Askary, L. Jones, T. Z. Kidane, T. Trang, M. Nguyen, J. Goforth, Y. Chu, E. Vivas, M. Tsai, T. Westbrook and M. C. Linder, 2007, **18**, 597–608.

44 C. Linder, *Am. J. Clin. Nutr.*, 1996, **63**, 767S-811S.

45 J. F. Eisses and J. H. Kaplan, *J. Biol. Chem.*, 2005, **280**, 37159–37168.

46 Y.-M. Kuo, B. Zhou, D. Cosco and J. Gitschier, *Proc. Natl. Acad. Sci.*, 2002, **98**, 6836–6841.

47 C. J. De Feo, S. G. Aller, G. S. Siluvai, N. J. Blackburn and V. M. Unger, *Proc. Natl. Acad. Sci.*, 2009, **106**, 4237–4242.

48 F. Ren, B. L. Logeman, X. Zhang, Y. Liu, D. J. Thiele and P. Yuan, *Nat. Commun.*, 2019, **10**, 1–9.

49 K. L. Haas, A. B. Putterman, D. R. White, D. J. Thiele and K. J. Franz, *J. Am. Chem. Soc.*, 2011, **133**, 4427–4437.

50 D. Kahra, M. Kovermann and P. Wittung-Stafshede, *Biophys. J.*, 2016, **110**, 95–102.

51 P. V. E. van den Berghe, D. E. Folmer, H. E. M. Malingré, E. van Beurden, A. E. M. Klomp, B. van de Sluis, M. Merkx, R. Berger and L. W. J. Klomp, *Biochem. J.*, 2007, **407**, 49–59.

52 J. Bertinato, E. Swist, L. J. Plouffe, S. P. J. Brooks and M. R. L'Abbé, *Biochem. J.*, 2008, **409**, 731–740.

53 N. E. Wezynfeld, B. Vileno and P. Faller, *Inorg. Chem.*, 2019, **58**, 7488–7498.

54 T. V. O'Halloran and V. C. Culotta, *J. Biol. Chem.*, 2000, **275**, 25057–25060.

55 E. B. Maryon, S. A. Molloy and J. H. Kaplan, *Am. J. Physiol. Physiol.*, 2013, **304**, C768–C779.

56 M. T. Morgan, L. A. H. Nguyen, H. L. Hancock and C. J. Fahrni, *J. Biol. Chem.*, 2017, **292**, 21558–21567.

57 L. Banci, I. Bertini, S. Ciofi-Baffoni, T. Kozyreva, K. Zovo and P. Palumaa, *Nature*, 2010, **465**, 645–648.

58 C. A. Blindauer, in *RSC Metallobiology Series No. 2*, eds. W. Maret and A. G. Wedd, 2014, pp. 606–665.

59 J. M. Leitch, P. J. Yick and V. C. Culotta, *J. Biol. Chem.*, 2009, **284**, 24679–24683.

60 P. J. Schmidt, C. Kunst and V. C. Culotta, *J. Biol. Chem.*, 2000, **275**, 33771–33776.

61 A. . Lamb, A. K. Wernimont, R. A. Pufahl, V. C. Culotta, T. V. O'Halloran and A. C. Rosenzweig, *Nat. Struct. Biol.*, 1999, **6**, 724–729.

62 N. J. Blackburn, N. A. N. Yan and S. Lutsenko, in *RSC Metallobiology Series No. 2*, eds. W. Maret and A. Wdd, 2014, pp. 524–555.

63 T. Tsukihara, H. Aoyama, E. Yamashita, T. Tomizaki, K. Shinzawa-itoh, R. Nakashima, R. Yaono and S. Yoshikawa, *Science*, 1995, **269**, 1063–1064.

64 L. Banci, I. Bertini, S. Ciofi-Baffoni, A. Janicka, M. Martinelli, H. Kozlowski and P. Palumaa, *J. Biol. Chem.*, 2008, **283**, 7912–7920.

65 G. Inesi, *IUBMB Life*, 2017, **69**, 211–217.

66 S. Lutsenko, *Metallomics*, 2016, **8**, 840–852.

67 Y. Hatori and S. Lutsenko, *Antioxidants*, 2016, **5**, 25–41.

68 F. Hussain, J. S. Olson and P. Wittung-Stafshede, *Proc. Natl. Acad. Sci. U. S. A.*, 2008, **105**, 11158–63.

69 E. D. Harris, *Crit. Rev. Clin. Lab. Sci.*, 2003, **40**, 547–586.

70 A. B. Shah, I. Chernov, H. T. Zhang, B. M. Ross, K. Das, S. Lutsenko, E. Parano, L. Pavone, O. Evgrafov, K. Westermark, I. A. Ivanova-smolenskaya, F. H. Urrutia, G. K. Penchaszadeh, I. Sternlieb, I. H. Scheinberg, T. C. Gilliam and K. Petrukhin, *Am. J. Hum. Genet.*, 1997, **61**, 317–328.

71 O. Bandmann, K. H. Weiss and S. G. Kaler, *Lancet Neurol.*, 2015, **14**, 103–113.

72 D. Huster, *Gastroenterologe*, 2018, **13**, 199–214.

73 S. G. Kaler, *Nat. Publ. Gr.*, 2011, **7**, 15–29.

74 E. Madsen and J. D. Gitlin, *Annu. Rev. Neurosci.*, 2007, **30**, 317–339.

75 Y. Liu, M. Nguyen, A. Robert and B. Meunier, *Acc. Chem. Res.*, 2019, **52**, 2026–2035.

76 M. A. Greenough, J. Camakaris and A. I. Bush, *Neurochem. Int.*, 2013, **62**, 540–555.

77 P. Wang and Z. Y. Wang, *Ageing Res. Rev.*, 2017, **35**, 265–290.

78 J. S. Cristòvao, R. Santos and C. M. Gomes, *Oxid. Med. Cell. Longev.*, 2016, **2016**, 1–13.

79 K. Reybier, S. Ayala, B. Alies, J. V. Rodrigues, S. Bustos Rodriguez, G. La Penna, F. Collin, C. M. Gomes, C. Hureau and P. Faller, *Angew. Chemie - Int. Ed.*, 2016, **55**, 1085–1089.

80 *World Alzheimer Report 2018. Alzheimer's Disease International (ADI), London*, 2018.

81 Alzheimer's Association. Alzheimer's Disease Facts and Figures, 2018, www.alz.org/alzheimers-dementia/facts-figures.

82 S.-Y. Hung and W.-M. Fu, *J. Biomed. Sci.*, 2017, **24**, 47.

83 I. Piaceri, N. Benedetta and S. Sandro, *Front. Biosci.*, 2013, **5**, 5–7.

84 O. Klementieva, K. Willén, I. Martinsson, B. Israelsson, A. Engdahl, J. Cladera, P. Uvdal and G. K. Gouras, *Nat. Commun.*, 2017, **8**, 14726.

85 F. Chiti and C. M. Dobson, *Annu. Rev. Biochem.*, 2017, **86**, 27–68.

86 H. John and H. Gerald, *Science*, 1992, **256**, 184–185.

87 R. Riek and D. S. Eisenberg, *Nature*, 2016, **539**, 227–235.

88 U. Sengupta, A. N. Nilson and R. Kayed, *EBioMedicine*, 2016, **6**, 42–49.

89 S. Lesné, T. K. Ming, L. Kotilinek, R. Kayed, C. G. Glabe, A. Yang, M. Gallagher and K. H. Ashe, *Nature*, 2006, **440**, 352–357.

90 G. M. Bishop and S. R. Robinson, *Drugs and Aging*, 2004, **21**, 621–630.

91 U. C. Müller, T. Deller and M. Korte, *Nat. Rev. Neurosci.*, 2017, **18**, 281–298.

92 G. F. Chen, T. H. Xu, Y. Yan, Y. R. Zhou, Y. Jiang, K. Melcher and H. E. Xu, *Acta Pharmacol. Sin.*, 2017, **38**, 1205–1235.

93 E. Portelius, M. K. Gustavsson, I. Volkmann and H. Zetterberg, *Acta Neuropathol.*, 2013, **120**, 185–193.

94 O. Wirths, S. Walter, I. Kraus, H. W. Klafki, M. Stazi, T. J. Oberstein, J. Ghiso, J. Wiltfang, T. A. Bayer and S. Weggen, *Alzheimer's Res. Ther.*, 2017, **9**, 1–12.

95 E. Stefaniak and W. Bal, *Inorg. Chem.*, , DOI:10.1021/acs.inorgchem.9b01399.

96 C. Cheignon, M. Tomas, D. Bonnefont-Rousselot, P. Faller, C. Hureau and F. Collin, *Redox Biol.*, 2017, **14**, 450–464.

97 L. M. Miller, Q. Wang, T. P. Telivala, R. J. Smith, A. Lanzirotti and J. Miklossy, *J. Struct. Biol.*, 2006, **155**, 30–37.

98 E. Atrián-Blasco, A. Conte-Daban and C. Hureau, *Dalt. Trans.*, 2017, **46**, 12750–12759.

99 J. Dong, C. S. Atwood, V. E. Anderson, S. L. Siedlak, M. A. Smith, G. Perry and P. R. Carey, *Biochemistry*, 2003, **42**, 2768–2773.

100 S. Ayala, P. Genevaux, C. Hureau and P. Faller, *ACS Chem. Neurosci.*, 2019, **108**, 3366–3374.

101 E. Atrián-Blasco, M. Del Barrio, P. Faller and C. Hureau, *Anal. Chem.*, 2018, **90**, 5909–5915.

102 M. Mital, N. E. Wezynfeld, T. Frączyk, M. Z. Wiloch, U. E. Wawrzyniak, A. Bonna, C. Tumpach, K. J. Barnham, C. L. Haigh, W. Bal and S. C. Drew, *Angew. Chemie Int. Ed.*, 2015, **54**, 10460–10464.

103 E. Cabrera, P. Mathews, E. Mezhericher, T. G. Beach, J. Deng, T. A. Neubert, A. Rostagno and J. Ghiso, *Biochim. Biophys. Acta - Mol. Basis Dis.*, 2018, **1864**, 208–225.

104 P. Faller, *ChemBioChem*, 2009, **10**, 2837–2845.

105 X. Huang, C. S. Atwood, R. D. Moir, M. A. Hartshorn, J. P. Vonsattel, R. E. Tanzi and A. I. Bush, *J.Biol.Chem.*, 1997, **272**, 26464–26470.

106 J. Durand, G. Meloni, C. Talmard, M. Vašák and P. Faller, *Metallomics*, 2010, **2**, 741.

107 K. Garai, B. Sahoo, S. K. Kaushalya, R. Desai and S. Maiti, *Biochemistry*, 2007, **46**, 10655–10663.

108 T. Zhang, T. Pauly and L. Nagel-Steger, *Int. J. Biol. Macromol.*, 2018, **113**, 631–639.

109 M. Rana and A. K. Sharma, *Metallomics*, 2019, **11**, 64–84.

110 J. W. Karr, L. J. Kaupp and V. A. Szalai, *J. Am. Chem. Soc.*, 2004, **126**, 13534–13538.

111 P. Dorlet, S. Gambarelli, P. Faller and C. Hureau, *Angew. Chemie - Int. Ed.*, 2009, **48**, 9273–9276.

112 B. Alies, H. Eury, C. Bijani, L. Rechignat, P. Faller and C. Hureau, *Inorg. Chem.*, 2011, **50**, 11192–11201.

113 M. Rózga, A. M. Protas, A. Jabłonowska, M. Dadlez and W. Bal, *Chem. Commun.*, 2009, 1374–1376.

114 V. B. Kenche, I. Zawisza, C. L. Masters, W. Bal, K. J. Barnham and S. C. Drew, *Inorg. Chem.*, 2013, **52**, 4303–4318.

115 Y. Bin, Z. Jiang and J. Xiang, *Appl. Biochem. Biotechnol.*, 2015, **176**, 56–65.

116 J. Shearer and V. A. Szalai, *J. Am. Chem. Soc.*, 2008, **130**, 17826–17835.

117 C. Hureau, V. Balland, Y. Coppel, P. L. Solari, E. Fonda and P. Faller, *J. Biol. Inorg. Chem.*, 2009, **14**, 995–1000.

118 B. Alies, A. Conte-Daban, S. Sayen, F. Collin, I. Kieffer, E. Guillon, P. Faller and C. Hureau, *Inorg. Chem.*, 2016, **55**, 10499–10509.

119 C. Harford and B. Sarkar, *Acc. Chem. Res.*, 1997, **30**, 123–130.

120 P. Gonzalez, B. Vileno, K. Bossak, Y. El Khoury, P. Hellwig, W. Bal, C. Hureau and P. Faller, *Inorg. Chem.*, 2017, 2–11.

121 B. Alies, B. Badei, P. Faller and C. Hureau, *Chem. - A Eur. J.*, 2012, **18**, 1161–1167.

122 T. R. Young, A. Kirchner, A. G. Wedd and Z. Xiao, *Metallomics*, 2014, **6**, 505–517.

123 C. Talmard, A. Bouzan and P. Faller, *Biochemistry*, 2007, **46**, 13658–13666.

124 S. Noël, S. Bustos Rodriguez, S. Sayen, E. Guillon, P. Faller and C. Hureau, *Metallomics*, 2014, **6**, 1220–1222.

125 F. B. De Jorge, C. Canato and D. Delascio, *Matern. Infanc. (Sao Paulo)*, 1965, **24**, 649–654.

126 *Prog Clin Biol Res*, 1988, **259**, 161–75.

127 A. Gupte and R. J. Mumper, *Cancer Treat. Rev.*, 2009, **35**, 32–46.

128 M. H. Khadem-Ansari, M. Asoudeh, H. F. K. Gheshlaghi, S. Nozari, M. Zarringol, N. F. Maroufi and Y. Faridvand, *Horm. Mol. Biol. Clin. Investig.*, 2019, **37**, 1–6.

129 C. Akhgarjand, K. Djafarian, H. Rezvani, E. Azargashb and M. Vafa, *Am. J. Blood Res.*, 2018, **8**, 21–28.

130 X. Zhang and Q. Yang, *J. Int. Med. Res.*, 2018, **46**, 4863–4873.

131 K. C. Park, L. Fouani, P. J. Jansson, D. Wooi, S. Sahni, D. J. R. Lane, D. Palanimuthu, H. C. Lok, Z. Kovačević, M. L. H. Huang, D. S. Kalinowski and D. R. Richardson, *Metallomics*, 2016, **8**, 874–886.

132 S. Ishida, P. Andreux, C. Poitry-Yamate, J. Auwerx and D. Hanahan, *PNAS*, 2013, **110**, 19507–19512.

133 D. M. Y. Cheah, Y. J. Deal, P. F. A. Wright, N. E. Buck, C. W. Chow, J. F. B. Mercer and K. J. Allen, *BioMetals*, 2007, **20**, 751–757.

134 D. Denoyer, S. Masaldan, S. La Fontaine and M. A. Cater, *Metallomics*, 2015, **7**, 1459–1476.

135 A. De Luca, A. Barile, M. Arciello and L. Rossi, *J. Trace Elem. Med. Biol.*, 2019, **55**, 204–213.

136 D. Denoyer, S. A. S. Clatworthy, S. Masaldan, P. M. Meggyesy and M. A. Cater, *Prostate*, 2015, **75**, 1510–1517.

137 S. Itoh, H. W. Kim, O. Nakagawa, K. Ozumi, S. M. Lessner, H. Aoki, K. Akram, R. D. McKinney, M. Ushio-Fukai and T. Fukai, *J. Biol. Chem.*, 2008, **283**, 9157–9167.

138 M. Dankner, A. A. N. Rose, S. Rajkumar, P. M. Siegel and I. R. Watson, *Oncogene*, 2018, **37**, 3183–3199.

139 P. Carmeliet and R. K. Jain, *Nature*, 2000, **407**, 249–257.

140 Q. Pan, K. L. Van Golen, J. Irani, K. M. Bottema, G. J. Brewer, S. D. Merajver, C. G. Kleer, D. M. Robins, R. D. Dick, C. Bias, M. De Carvalho and E. A. Mesri, *Cancer Res.*, 2002, **62**, 4854–4859.

141 R. H. Wenger, F. Martin, T. Linden, D. M. Katschinski, F. Oehme, I. Flamme, C. K. Mukhopadhyay, K. Eckhardt, J. Tröger, S. Barth and G. Camenisch, *Blood*, 2005, **105**, 4613–4619.

142 J. T. Erler, K. L. Bennewith, T. R. Cox, G. Lang, D. Bird, A. Koong, Q. T. Le and A. J. Giaccia, *Cancer Cell*, 2009, **15**, 35–44.

143 H. E. Barker and J. T. Erler, *Futur. Oncol.*, 2011, **7**, 707–710.

144 N. E. Hynes, *Sci. Signal.*, 2014, **7**, 1–13.

145 L. E. Scott and C. Orvig, 2009, 4885–4910.

146 M. Tegoni, D. Valensin, L. Toso and M. Remelli, *Copper Chelators: Chemical Properties and Biomedical Applications*, 2014, vol. 21.

147 J. M. Walshe, *Am. J. Med.*, 1956, **21**, 487–495.

148 C. Esmieu, D. Guettas, A. Conte-Daban, L. Sabater, P. Faller and C. Hureau, *Inorg. Chem.*, 2019, acs.inorgchem.9b00995.

149 A. Conte-Daban, A. Day, P. Faller and C. Hureau, *Dalt. Trans.*, 2016, **45**, 15671–15678.

150 M. G. Savelieff, G. Nam, J. Kang, H. J. Lee, M. Lee and M. H. Lim, *Chem. Rev.*, 2018, **119**, 1221–1322.

151 R. Tabti, N. Tounsi, C. Gaiddon, E. Bentouhami and L. Desaubry, *Med. Chem. (Los. Angeles).*, 2017, **07**, 875–879.

152 K. Gaur, A. Vázquez-Salgado, G. Duran-Camacho, I. Dominguez-Martinez, J. Benjamín-Rivera, L. Fernández-Vega, L. Carmona Sarabia, A. Cruz García, F. Pérez-Deliz, J. Méndez Román, M. Vega-Cartagena, S. Loza-Rosas, X. Rodriguez Acevedo and A. Tinoco, *Inorganics*, 2018, **6**, 126.

153 M. Vašák and G. Meloni, *J. Biol. Inorg. Chem.*, 2011, **16**, 1067–1078.

154 M. Margoshes, B. L. Vallee, Y. Kojima, C. Berger, J. H. R. Kägi and Piscator, *JACS*, 1957, **79**, 4813–4814.

155 G. Westin and W. Schaffner, *EMBO J.*, 1988, **7**, 3763–3770.

156 G. Dong, H. Chen, M. Qi, Y. Dou and Q. Wang, *Mol. Med. Rep.*, 2015, **11**, 1582–1586.

157 N. Romero-Isart, L. T. Jensen, O. Zerbe, D. R. Winge and M. Vaák, *J. Biol. Chem.*, 2002, **277**, 37023–37028.

158 J. Bousleiman, A. Pinsky, S. Ki, A. Su, I. Morozova, S. Kalachikov, A. Wiqas, R. Silver, M. Sever and R. Austin, *Int. J. Mol. Sci.*, 2017, **18**, 1133.

159 Y. Uchida, K. Takio, K. Titani, Y. Ihara and M. Tomonaga, *Neuron*, 1991, **7**, 337–347.

160 A. Krezel, Q. Hao and W. Maret, *Arch. Biochem. Biophys.*, 2007, **463**, 188–200.

161 R. Bogumil, P. Faller, D. L. Pountney and M. Vasák, *Eur. J. Biochem.*, 1996, **238**, 698–705.

162 B. Roschitzki and M. Vašák, *Biochemistry*, 2003, **42**, 9822–9828.

163 E. Artells, Ò. Palacios, M. Capdevila and S. Atrian, *FEBS J.*, 2014, **281**, 1659–1678.

164 D. L. Pountney, I. Schauwecker, J. Zarn and M. Vašák, *Biochemistry*, 1994, **33**, 9699–9705.

165 J. S. Scheller, G. W. Irvine, D. L. Wong, A. Hartwig and M. J. Stillman, *Metallomics*, 2017, **9**, 447–462.

166 J. Calvo, H. Jung and G. Meloni, *IUBMB Life*, 2017, **69**, 236–245.

167 J. D. Otvos, D. H. Petering and C. F. Shaw, *Structure-Reactivity Relationships of Metallothionein, a Unique Metal-Binding Protein*, 1989, vol. 9.

168 A. Krezel and W. Maret, *J. Am. Chem.Soc*, 2007, **129**, 10911–10921.

169 M. C. Carpenter, A. Shami Shah, S. DeSilva, A. Gleaton, A. Su, B. Goundie, M. L. Croteau, M. J. Stevenson, D. E. Wilcox and R. N. Austin, *Metallomics*, 2016, **8**, 605–617.

170 J. S. Calvo, V. M. Lopez and G. Meloni, *Metallomics*, 2018, **10**, 1777–1791.

171 G. Meloni, V. Sonois, T. Delaine, L. Guilloreau, A. Gillet, J. Teissié, P. Faller and M. Vašák, *Nat. Chem. Biol.*, 2008, **4**, 366–372.

172 B. A. Messerle, A. Schäffer, M. Vašák, J. H. R. Kägi and K. Wüthrich, *J. Mol. Biol.*, 1990, **214**, 765–779.

173 J. D. Otvos and I. M. Armitage, *Proc. Natl. Acad. Sci. U. S. A.*, 1980, **77**, 7094–7098.

174 A. H. Robbins, D. E. McRee, M. Williamson, S. A. Collett, N. H. Xuong, W. F. Furey, B. C. Wang and C. D. Stout, *J. Mol. Biol.*, 1991, **221**, 1269–1293.

175 B. A. Messerle, A. Schäffer, M. Vašák, J. H. R. Kägi and K. Wüthrich, *J. Mol. Biol.*, 1992, **225**, 433–443.

176 G. W. Irvine, T. B. J. Pinter and M. J. Stillman, *Metallomics*, 2016, **8**, 71–81.

177 A. Drozd, D. Wojewska, M. D. Peris-Díaz, P. Jakimowicz and A. Krężel, *Metallomics*, 2018, **10**, 595–613.

178 M. Good, R. Hollenstein, P. J. Sadler and M. Vasak, *Biochemistry*, 1988, **27**, 7163–7166.

179 M. Vašák and G. Meloni, *Int. J. Mol. Sci.*, 2017, **18**, 1117.

180 H. Wang, Q. Zhang, B. Cai, H. Li, K. H. Sze, Z. X. Huang, H. M. Wu and H. Sun, *FEBS Lett.*, 2006, **580**, 795–800.

181 B. Roschitzki and M. Vašák, *J. Biol. Inorg. Chem.*, 2002, **7**, 611–616.

182 D. W. Hasler, P. Faller and M. Vašák, *Biochemistry*, 1998, **37**, 14966–14973.

183 P. Faller, *FEBS J.*, 2010, **277**, 2921–2930.

184 R. Bogumil, P. Faller, P. A. Binz, M. Vasak, J. M. Charnock and C. D. Garner, *Eur. J. Biochem.*, 1998, **255**, 172–177.

185 G. Meloni, P. Faller and M. Vašák, *J. Biol. Chem.*, 2007, **282**, 16068–16078.

186 A. Krężel and W. Maret, *Int. J. Mol. Sci.*, 2017, **18**, 1237.

187 D. H. Petering and A. Mahim, *Int. J. Mol. Sci.*, 2017, **18**, 1289.

188 R. Banerjee, *J. Biol. Chem.*, 2012, 287, 4397–4402.

189 R. Environment, O. F. The, C. As and V. Through, *Free Radic. Biol. Med.*, 2001, **30**, 1191–1212.

190 A. J. Meyer and R. Hell, *Photosynth. Res.*, 2005, **86**, 435–457.

191 A. M. D. C. Ferreira, M. R. Ciriolo, L. Marcocci and G. Rotilio, *Biochem. J.*, 1993, **292**, 673–676.

CHAPTER 2

Cu transfer reactions from/off $A\beta_{4-16}$ to $Zn(II)_7$MT-3 in Alzheimer's Disease: the influence of other physiological relevant biomolecules

2.1 State of the art and aim of the study

As already discussed in the introduction (**1.3.2** Correlation with Alzheimer's diseases), in AD patients Cu and Zn ions have been found to accumulate at high levels in extracellular amyloid plaques, bound to Aβ peptides,[1] thereby potentially participating in their aggregation and in the production of ROS.[2,3] Evidence from the literature suggests that Cu might be pumped by the Cu-transporter ATPase7A into synaptic vesicles and upon stimulation of the glutamate receptor NMDA it could be released into the synaptic cleft *via* vesicle fusion.[4] Zn, instead, has been shown to be stored in high amounts (mM) in synaptic vesicles of a subset of glutamatergic neurons, where it is transported *via* the ZnT3 transporter. Upon neuronal activation, these vesicles fuse with the cell membrane and Zn is released into the synaptic cleft. At the peak of neuronal activity, transient concentrations of up to several hundred μM have been detected.[5] Even though not demonstrated, the Cu and Zn pools bound to Aβ peptides in amyloid plaques, might arise from Cu and Zn released into the synaptic cleft.
One of the key questions still unsolved in studying Cu and Zn involvement in AD is to find out when and how various Aβ peptides bind Cu and Zn ions in normal brain physiology and under AD conditions.

Besides its intraneuronal localization, cell culture studies have revealed that also MT-3 occurs in comparable amounts extracellularly and hence potentially in the synaptic cleft of neurons.[6]
As MTs are major key players in Zn and Cu homeostasis, during the last decades, interest has arisen on the interaction of Cu-complexes of Aβ peptides with MTs, since MT-3, the isoform highly expressed in the central nervous system, was found to be downregulated under AD conditions.[7,8] Furthermore, in cell cultures studies, $Zn(II)_7$-MT-3 was shown to protect neurons from the toxicity of Aβ species, by an unknown mechanism.[9]
As before mentioned, MTs are also well-known antioxidants, being efficient ROS scavengers.[10] Oxidative stress occurs in AD, due to an imbalance between ROS production and defense, leading to an accumulation of ROS.[11,12] This may also explain the upregulation of MT-3 in AD. However, as for Cu, Zn ions and Aβ peptides, whether MT-3 dysregulation in AD is a cause or a consequence is unclear.

Considering what stated above, MT-3 could encounter and interact with synaptic Zn and Cu ions, release upon neuronal excitation, as well as with Aβ peptides (**Fig 11**).[13] Here, reaction of Cu/Zn exchange between the two biomolecules could occur.
Very little is known about the exact concentrations of Aβ and MT-3 in the extracellular space, and especially in the synaptic cleft. Recently W. Goch et al. have shown that such reacting species might have micromolar or even higher concentrations as lower concentrations would be physically impossible for this small brain structure, due to volume constraints.[14]

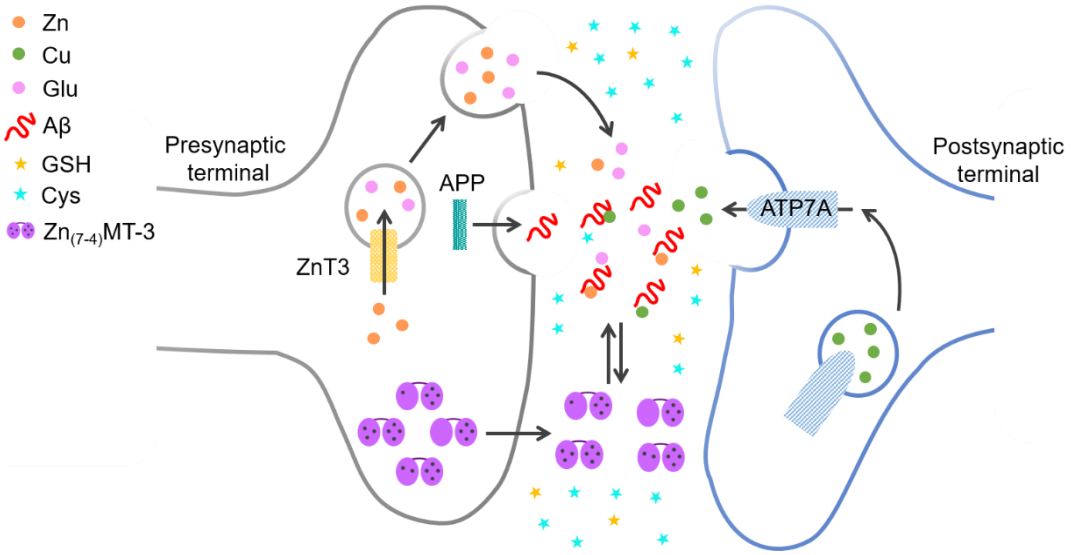

Fig 11 - Schematic representation of the synaptic cleft of some glutamatergic neurons where Aβ peptides, Cu, Zn(II) ions, $Zn(II)_{(7-4)}$-MT-3 and/or other small biomolecules like GSH, Cys, Glu might encounter. Figure adapted from[15,16]

Previous studies have already investigated the reactivity *in vitro* of the Zn(II) saturated form of MT, $Zn(II)_7$-MT-3, with the two Cu(II)-complexes of the major species of Aβ peptides found in amyloid plaques, i.e. $Aβ_{1-x}$ (x = 40, 42) and the N-truncated peptide, $Aβ_{4-x}$ (x = 42). Spectroscopic studies are usually carried out using model peptides $Aβ_{x-16}$ (including x = 1 or 4), which are widely accepted to represent the metal binding properties of the whole Aβ peptide sequences as monomers, as all the amino acids involved in Cu(II), Cu(I) and Zn(II) binding are located within the first 14 residues.[17–19]

In case of the full length peptide $Aβ_{1-x}$, the Cu(II)-complex, Cu(II)-$Aβ_{1-16/40}$ (for Cu(II) coordination to $Aβ_{1-x}$, see **Fig 6**), was shown to react rapidly with $Zn(II)_7$-MT-3 by a swap of metal ions, that resulted in Cu(I) binding to MT-3 and Zn(II) binding to $Aβ_{1-16/40}$.[20] During this process, Cu(II) contained in Cu(II)-$Aβ_{1-16}$ is reduced to Cu(I) by the thiolate system of $Zn(II)_7$-MT-3. At stoichiometric ratios of 4 Cu(II)-$Aβ_{1-16}$ per MT-3 the reaction yields a relatively defined species, i.e. $Cu(I)_4Zn(II)_4$-MT-3, in agreement with the reduction of 4 Cu(II), concomitant release of 3 Zn(II) ions from $Zn(II)_7$-MT-3. Previously, as mentioned in the introduction (**1.5.1** Mammalian Metallothioneins (MTs)) only the $Zn(II)_3S^-_9$ cluster in the β-domain was shown to react, leading to the formation of a $Cu(I)_4$-$(CysS^-)_5$ cluster, with two disulfides (**Fig 12a**).[21]

This molecular mechanism has been suggested to be responsible of the neuroprotective role of $Zn(II)_7$-MT-3 from the ROS-related induced cell toxicity of Cu(II)-$Aβ_{1-x}$. Indeed, Cu(I)-binding to the N-terminal β-domain of MT-3, in the heterometallic $Cu(I)_4Zn(II)_4$-MT-3 species, results in an oxygen stable and redox-stable Cu(I)-thiolate complex ($Cu(I)_4S^-_5$ cluster). The reason for this is not known yet but the structural constraints and the short Cu(I)-Cu(I) distances (< 2.8 A˚) in the $Cu(I)_4S^{-5}$ cluster, which lead to peculiar metal-metal interactions, have been proposed to be important factors for the observed stability in air.[21]

In contrast, $Aβ_{4-16}$, which binds Cu(II) ions ~ 3000 times more strongly than $Aβ_{1-16}$ at pH 7.4, due to the presence of the Cu(II)-specific H_2N-Xxx-Zzz-His motif[18,22,23] (for Cu(II) coordination to $Aβ_{4-16}$, see **Fig 6**), was stable against $Zn(II)_7$-MT-3, as no copper transfer was observed over 30 min (**Fig 12b**).[24] The reason for this may be ascribed to a lower off rate of Cu(II) from the N-truncated peptide $Aβ_{4-16}$, compared to $Aβ_{1-16}$. Only the addition very high non-physiological concentrations of $AscH^-$ (i.e. 20 mM) resulted in the complete transfer of Cu from $Aβ_{4-16}$ to $Zn(II)_7$-

MT-3. Consequently, Wezynfeld et al. proposed that the full-length peptide, $A\beta_{4-42}$ might play a parallel role with MT-3 as Cu(II)-scavenger into the synaptic cleft, under physiological conditions.[24]

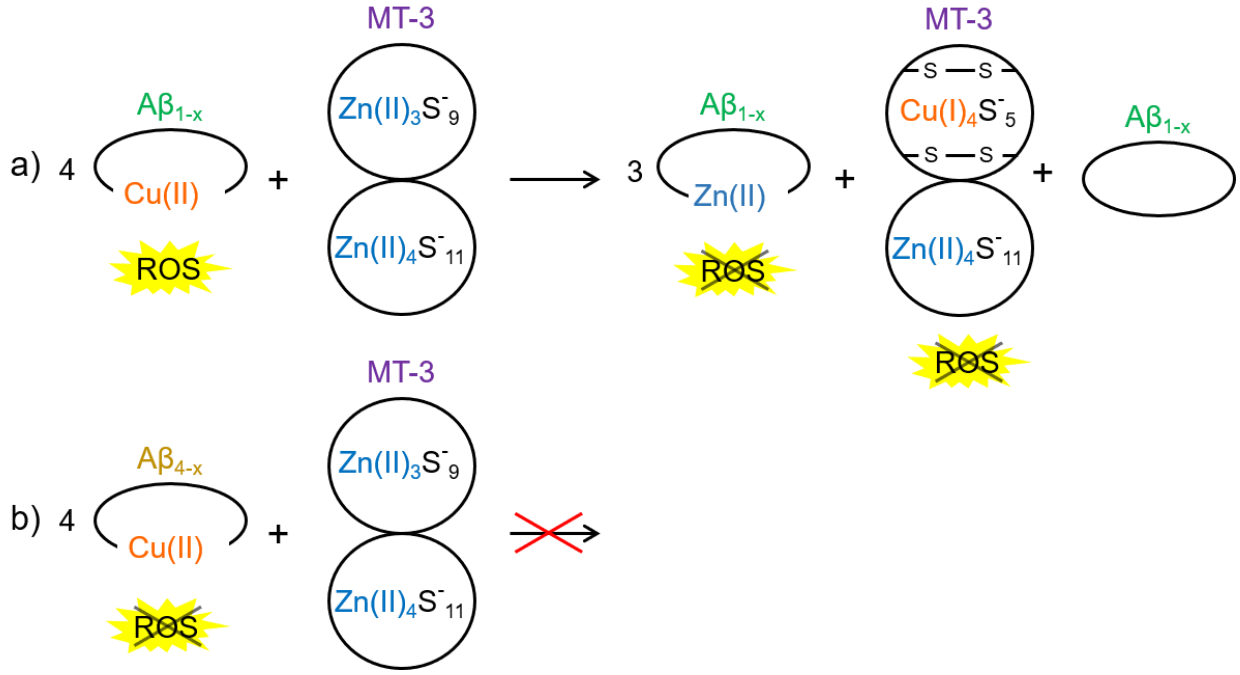

Fig 12 - Reactivity of a) Cu(II)-$A\beta_{1-x}$ and b) Cu(II)-$A\beta_{4-x}$ complexes with $Zn(II)_7$MT-3.

Within this context, we were interested in other physiological molecules that might be found in the same location as Aβ peptides and $Zn(II)_7$-MT-3, and could influence the rate of Cu transfer from/off the Cu(II)-complexes of the N-truncated Aβ species, $A\beta_{4-16}$, to $Zn(II)_7$-MT-3 and consequently their interaction on the level of both Cu/Zn ions. Besides, we studied the reactivity of physiological partially depleted $Zn(II)_{7-x}$-MT-3 species, i.e. $Zn(II)_4$-MT-3, $Zn(II)_5$-MT-3, $Zn(II)_6$-MT-3, towards Cu(II)-$A\beta_{4-16}$ to form $Cu(I)_4Zn(II)_4$-MT-3. The physiological existence of these species depends on the protein expression, the cellular Zn(II) availability and the presence of Zn(II) competitors. Hence, we generated such species using the Zn(II)-chelator EDTA, as mimic of Zn(II) binding biomolecules.

2.2 Influence of Cys and GSH

2.2.1 Introduction

We started our investigation by exploring the potential role of GSH and Cys on the reactivity between Cu(II)-$A\beta_{4-16}$ and $Zn(II)_7$-MT-3. Besides their potential influence on the physiological stability of Cu(II)-Aβ complexes because of their properties already mentioned in the introduction (**1.5.2** Low molecular weight thiol(ate) containing biomolecules), the biological relevance of Cys and GSH stems from the reported intracellular and extracellular fluctuations in their concentration.[25] For instance, the extracellular deposition of Aβ peptides has been reported to increase the extracellular concentration of reduced Cys.[26]

Therefore, the first objective of this thesis was to investigate the impact of Cys and GSH, concerning i) their ability to reduce and extract Cu(II) from Cu(II)-$A\beta_{4-16}$ in the presence of $Zn(II)_7$-MT-3 and ii) to probe their role as shuttles for the Cu(I)-transfer between the two biomolecules.

Thus, we employed different spectroscopic techniques, i.e. absorbance spectroscopy, circular dichroism, ^{1}H-NMR, that allowed us to study the different steps of the two reactions.

2.2.2 Results and discussion

a. Cu(II) reduction and release from Cu(II)-Aβ$_{4-16}$

The ability of Cys and GSH to reduce Cu(II) and extract Cu(I) in the reaction mixture Cu(II)-Aβ$_{4-16}$/Zn(II)$_7$-MT-3 was investigated by i) absorbance spectroscopy and ii) circular dichroism, through the characteristic band of Cu(II)-Aβ$_{4-16}$ at λ_{max} = 525 nm, due to the Cu(II) d-d transition.

First of all, we repeated the reaction between Cu(II)-Aβ$_{4-16}$ and Zn(II)$_7$-MT-3, to confirm what was previously reported. Cu(II)-Aβ$_{4-16}$ complex was generated in PB, pH 7.4, with a Cu(II) to peptide ratio of 0.9:1, to avoid the presence of free Cu. Zn(II)$_7$-MT-3 was then added to the preformed Cu(II)-complex and the course of the reaction monitored for 30 min. As shown in **Fig 13a/b** (purple profiles)/**d** (blue profile) the band was stable, in line with absence of an unassisted Cu-transfer from Cu(II)-Aβ$_{4-16}$ to Zn(II)$_7$-MT-3.

Next, we added Cys or GSH to the mixture Cu(II)-Aβ$_{4-16}$/Zn(II)$_7$-MT-3 and the d-d band decreased in a time dependent manner. In case of Cys (**Fig 13a/c/d**), the band completely disappeared in 30 min, meaning that Cys is able to react with Cu(II)-Aβ$_{4-16}$, by reducing Cu(II) to Cu(I), with concomitant release of Cu from the peptide. The ability of Cys to reduce and dissociate the Cu(II)-Aβ$_{4-16}$ complex was also confirmed based on the appearance of the characteristic CT absorption band of the CysS-Cu(I) species at λ_{max} = 260 nm with shoulder at λ_{max} = 300 nm[27], observed when Cys alone was added to Cu(II)-Aβ$_{4-16}$ (**FigS 1a/b**).

The analogous experiment with GSH, resulted in a qualitatively similar behavior but the reaction was slower and did not reach completion after 260 min (**Fig 13b/c/d**). The higher reactivity of Cys compared to GSH could be mainly related to the lower pK_a value of the thiol function in Cys than in GSH (pK_a (Cys) ~ 8.2, pK_a (GSH) ~ 9.2)[28], as the deprotonated thiol is the form undergoing the oxidation to cystine/GSSG, as well as the form that can bind metal ions.

Hence, these experiments strongly suggest that Cys and GSH are able to reduce Cu(II) from Cu(II)-Aβ$_{4-16}$ to Cu(I) and extract Cu(I).

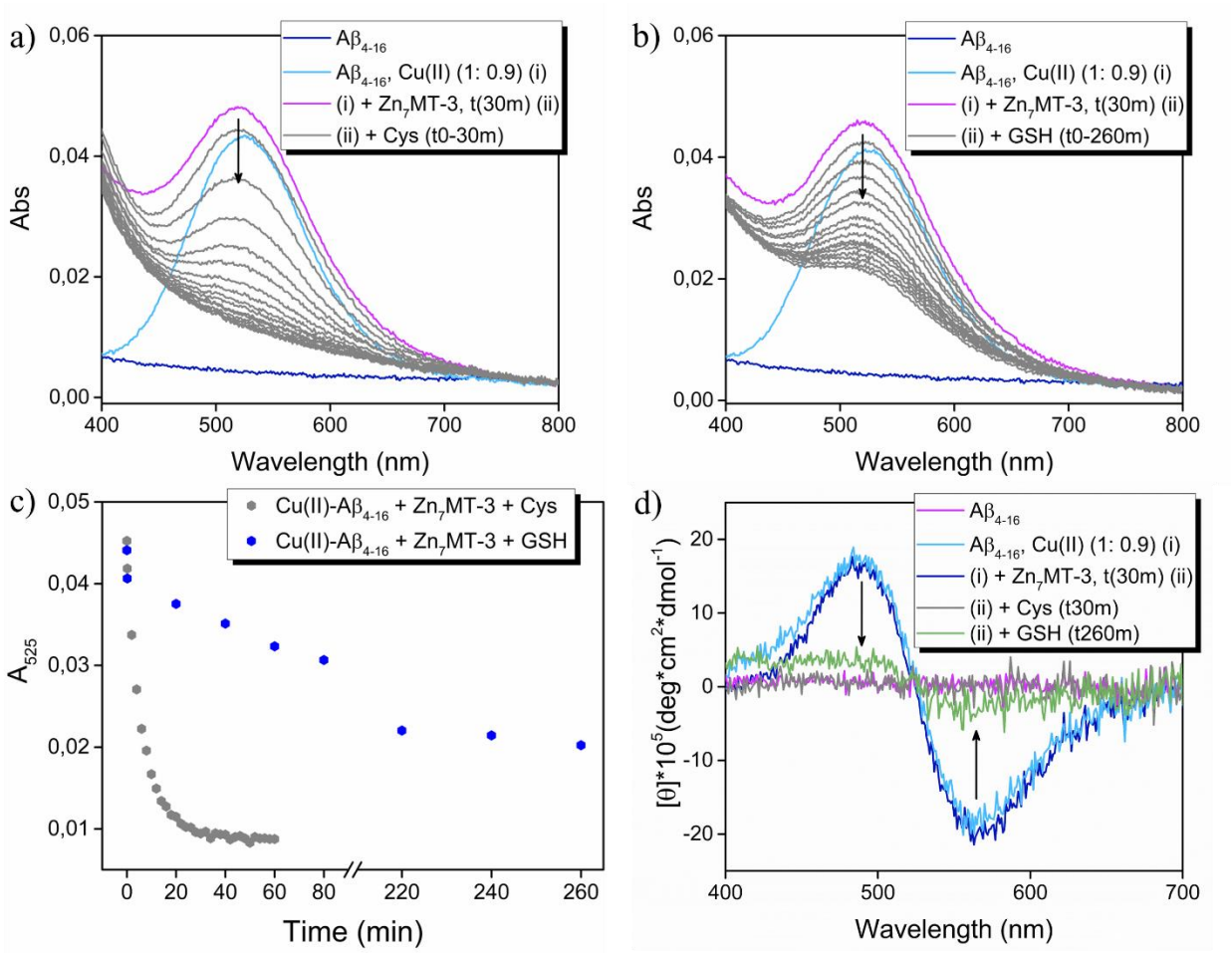

Fig 13 - Evidence of Cu(II) reduction and release from Cu(II)-Aβ$_{4-16}$ in the presence of Zn(II)$_7$-MT-3. In a) and b) absorption spectroscopy for the reaction with Cys and GSH respectively is shown. Each intermediate spectrum was collected at 2 min intervals in a) and at 10 min intervals in b). c) Corresponding kinetics for the two reactions with Cys and GSH: absorbance at λ_{max} = 525 nm versus time. d) Circular dichroism (Vis-region, 400-700 nm) for the reaction with Cys (grey profile) and GSH (green profile). Reaction conditions for Uv-Vis and CD experiments: Aβ$_{4-16}$ 500 µM, Cu(II) 450 µM, Zn(II)$_7$-MT-3100 µM (ratio Aβ$_{4-16}$/Cu(II)/Zn(II)$_7$-MT-3, 1:0.9:0.2), a) Cys 3 mM, b) GSH 3 mM, PB 50 mM, pH 7.4.

b. Cu(I) shuttling over MT-3 and formation of Cu(I)$_4$Zn(II)$_4$MT-3 species

In order to elucidate whether the extracted Cu(I) from Cu(II)-Aβ$_{4-16}$ was transported to Zn(II)$_7$MT-3, with consequent generation of the Cu(I)$_4$Zn(II)$_4$-MT-3 complex, we employed i) absorbance spectroscopy and ii) circular dichroism.

First, to confirm the Cys and GSH induced Cu(I) transfer from Cu(II)-Aβ$_{4-16}$ to Zn(II)$_7$-MT-3 we compared the reaction with Cys, with and without Zn(II)$_7$MT-3 in the reaction mixture, (**Fig 14a**, **FigS 1**). Addition of Cys to preformed Cu(II)-Aβ$_{4-16}$ complex resulted in the initial disappearance of the d-d band of Cu(II)-Aβ$_{4-16}$, in line with Cu(II) reduction and dissociation from Aβ$_{4-16}$ (blue profile).

However after ~ 18 min, the re-formation of the Cu(II)-Aβ$_{4-16}$ complex was observed and after 60 min the intensity of the d-d band was almost the same as the initial one. This agrees with the instability of the generated CysS-Cu(I) complex in the presence of O_2. The re-oxidation of CysS-Cu(I) to Cu(II) and cystine, allowed the complete re-formation of Cu(II)-Aβ$_{4-16}$ complex, indicating that Aβ$_{4-16}$ was not degraded during the reaction.

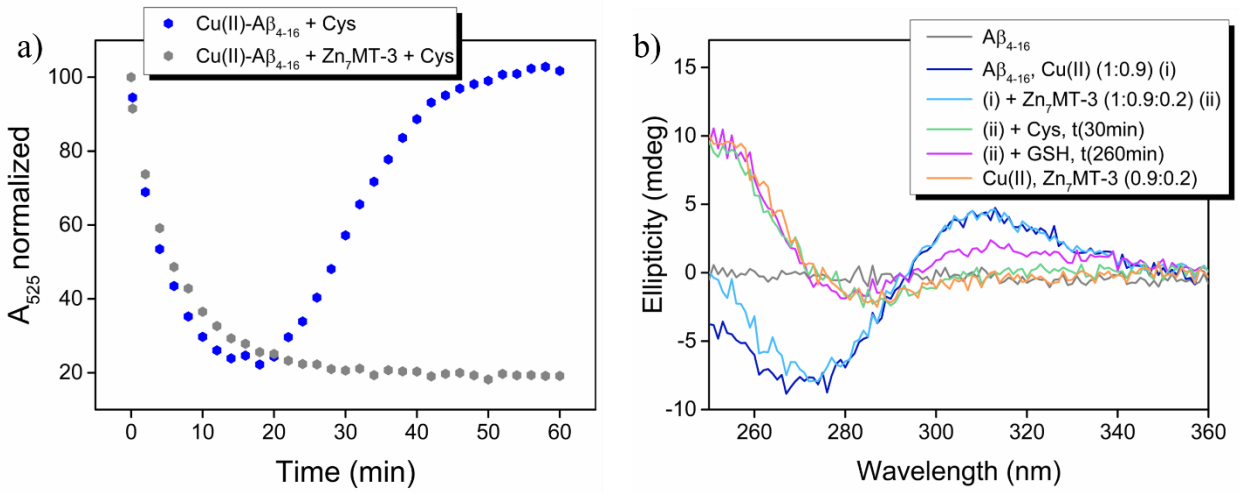

Fig 14 - Evidence for A) Cu(I) shuttling to MT-3 and B) formation of the $Cu(I)_4Zn(II)_4$-MT-3 complex. In a) kinetics of Cu(II) release from Cu(II)-$A\beta_{4-16}$ with Cys in the presence (grey profile) and absence (blue profile) of $Zn(II)_7$-MT-3 are shown: normalized absorbance at λ_{max} = 525 nm versus time. In b) circular dichroism for the reaction with Cys or GSH. CD spectra were respectively recorded after 30 min (grey profile) and 260 min (purple spectra) after their addition to the mixture Cu(II)-$A\beta_{4-16}$/$Zn(II)_7$-MT-3. Reaction conditions for i) UV-Vis experiments: Ab_{4-16} 500 µM, Cu(II) 450 µM, Cys 3 mM ± $Zn(II)_7$-MT-3 100 µM, PB 50 mM, pH 7.4; ii) CD experiments: Ab_{4-16} 100 µM, Cu(II) 90 µM, $Zn(II)_7$-MT-3 20 µM, Cys/GSH 3 mM, PB 50 mM, pH 7.4 (ratio $A\beta_{4-16}$/Cu(II)/$Zn(II)_7$-MT-3, 1:0.9:0.2).

In contrast, in the presence of $Zn(II)_7$-MT-3, the reaction was not reversible, suggesting Cu(I) binding to MT-3 and formation of the $Cu(I)_4Zn(II)_4$-MT-3 complex, which remained stable towards air oxidation.

We can see that the kinetics of disappearance of the d-d band were identical, within experimental error, regardless of the presence of $Zn(II)_7$-MT-3. This indicates that the rate limiting step in the Cu-transfer reaction from Cu(II)-$A\beta_{4-16}$ to $Zn(II)_7$-MT-3 is the reduction of Cu(II)-$A\beta_{4-16}$ by Cys, rather than the formation of CysS-Cu(I) complex or the Cu(I) transfer to $Zn(II)_7$-MT-3. In line with this, also the kinetic of disappearance of the d‑d band of Cu(II)-$A\beta_{4-16}$ for the reaction with GSH was independent on the presence of $Zn(II)_7$-MT-3 (results not shown).

Furthermore, to confirm the formation of the $Cu(I)_4Zn(II)_4$-MT-3 species, we monitored the reaction by circular dichroism (**Fig 14b**).
Cu(II)-$A\beta_{4-16}$ complex was again generated in 0.9:1 ratio (blue profile). Then, $Zn(II)_7$-MT-3 was added to the mixture and its lack of reactivity monitored for 30 min. Indeed, the CD spectrum observed (light blue profile) overlapped with that of Cu(II)-$A\beta_{4-16}$, except for the region 250-270 nm, where the increase in ellipticity is due to the $Zn(II)_7$-MT-3 absorption in this region (**FigS 2**), blue profile). Then, Cys or GSH was added to the mixture Cu(II)-$A\beta_{4-16}$/$Zn(II)_7$-MT-3.

After the reaction with Cys was mainly completed, i.e. 30 min, the characteristic CD bands of $Cu(I)_4Zn(II)_4$-MT-3 complex at about (+) 255 and (-) 285 nm, due to CysS-Cu(I) charge-transfer transitions, were detected. The newly developed CD bands were identical in size and position to those observed in the reaction of free Cu(II) with $Zn(II)_7$-MT-3 (orange profile) (the CD profile of Cys or GSH alone and Cu(II)/Cys, Cu(II)/GSH mixtures are shown in **FigS 2**) and to those reported in the literature for the reaction of free Cu(II) or Cu(II)-$A\beta_{1-16}$ with $Zn(II)_7$-MT-3.[20,21]

By comparison, the CD spectrum obtained after 260 min from GSH addition to Cu(II)-$A\beta_{4-16}$/$Zn(II)_7$-MT-3 (purple profile), confirmed that GSH could not quantitatively reduce Cu(II) to Cu(I) from Cu(II)-$A\beta_{4-16}$ and that the Cu-transfer to $Zn(II)_7$-MT-3 was not complete. Thus, Cu was still distributed between the biomolecules, as Cu(II) in $A\beta_{4-16}$ and as Cu(I) in $Cu(I)_xZn(II)_4$-MT-3.

c. Zn(II) release from Zn(II)$_7$-MT-3 and binding to Aβ$_{4-16}$

As already discussed above (**2.1** State of the art and aim of the study)**,** Cu(I) binding to the β-domain of Zn(II)$_7$-MT-3 results into the release of three Zn(II) ions. Thus, we investigated whether Zn(II) was bound or not to Aβ$_{4-16}$ peptide at the end of the reaction, by employing ^{1}H-NMR. Indeed, we expected that Zn(II) binding to Aβ$_{4-16}$ would impact the ^{1}H-NMR signatures of the coordinating groups in the peptide, like it was the case for Zn(II)-binding to Aβ$_{1-16/28/40}$.[19] Zn(II) binding to the N-truncated Aβ peptide, Aβ$_{4-x,}$ has not been studied in detail yet but the same residues that have been proposed to be involved in Zn(II)-binding to the full length Aβ peptide, Aβ$_{1-x}$, are also present in Aβ$_{4-x.}$

Since MT-3 does not have aromatic amino acids in the sequence, whereas Aβ$_{4-16}$ does (for the details of the amino acid residues of Aβ$_{4-16}$ see **Fig 15a)**, we monitored the overall reaction through the aromatic region of the ^{1}H-NMR spectra. As shown in **Fig 15**, signals from the protons of Aβ$_{4-16}$ from His(6,13,14), Phe4 and Tyr10 are present in the spectrum between 6.6-8 ppm (light blue line).

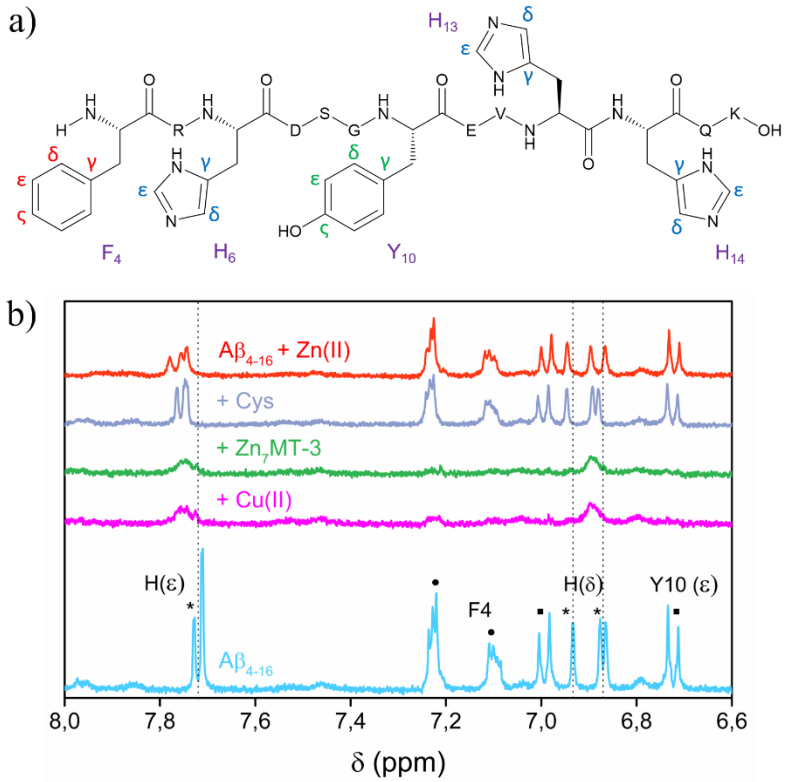

Fig 15 - a) Aβ$_{4-16}$ peptide sequence (FRHDSGYEVHHQK-NH$_2$) with the aromatic amino-acid residues nomenclature. b) ^{1}H-NMR displaying the Zn(II) binding to Aβ$_{4-16}$. Aromatic region of the spectrum of Aβ$_{4-16}$ (light blue line) and after the addiction of (i) Cu(II) (purple line), (ii) Zn(II)$_7$-MT-3 (green line), (iii) Cys (grey line); control of Aβ$_{4-16}$ after the direct addiction of 0.6 eq. of Zn(II) (red line). Reaction conditions: Aβ$_{4-16}$ 300 μM, Cu(II) 270 μM, Zn(II)$_7$-MT-3 60 μM, Cys 3 mM (ratio Aβ$_{4-16}$/Cu(II)/Zn(II)$_7$MT-3, 1:0.9:0.2). Spectra were obtained from 10% D$_2$O/90% H$_2$O solutions in PB 50 mM, pH 7.4, at ν = 400MHz.

Addition of paramagnetic Cu(II) to Aβ$_{4-16}$ resulted in the broadening of His protons and disappearance of those from Phe and Tyr, due to the paramagnetic effect of Cu(II)[29,30] (purple line). As expected, upon Zn(II)$_7$-MT-3 addition to Cu(II)-Aβ$_{4-16}$, no change in the spectrum was observed, in line with the lack of reactivity of Zn(II)$_7$-MT-3 (over 30 min) in the Cu-Zn swap with Aβ$_{4-16}$ (green line). Instead, when Cys was added to the mixture Cu(II)-Aβ$_{4-16}$/Zn(II)$_7$-MT-3 we observed the recovery of the signals of the Aβ$_{4-16}$ peptide (grey line), in agreement with Cu(II)

reduction to diamagnetic Cu(I) and release from $A\beta_{4\text{-}16}$. However, compared to the spectrum of $A\beta_{4\text{-}16}$ at the beginning, the signals of the protons of the three His (i.e. His(δ), His (ε)) were slightly down shifted. This was assigned to an at least partial binding of Zn(II) to $A\beta_{4\text{-}16}$ peptide, as direct addition of Zn(II) into $A\beta_{4\text{-}16}$, gave rise to similar shifts of the His resonances (red line) (Zn(II) titration to $A\beta_{4\text{-}16}$ shown in **FigS 3**. In line with the Zn(II)-related shifts of the His protons of $A\beta_{4\text{-}16}$, addition of EDTA to the 1:1 complex Zn(II)-$A\beta_{4\text{-}16}$ resulted into the recovery the signature of the unbound-peptide.
It is important to highlight that Cys and cystine, as well as GSH or GSSG, could be possible binding sites for Zn(II) released from $Zn(II)_7$-MT-3, hence a partial binding also to these species cannot be excluded.[31,32]

Overall, the data suggest a Cu-Zn swap between $A\beta_{4\text{-}16}$ and MT-3 triggered by Cys or GSH (^{1}H-NMR experiment not shown for the reaction with GSH).

2.3 Influence of Glu and MT-3 Zn(II)-load states

2.3.1 Introduction

After Cys and GSH, we studied if and how Glu and MT-3 at various physiological Zn(II)-load states (i.e. $Zn(II)_4$-MT-3, $Zn(II)_5$-MT-3, $Zn(II)_6$-MT-3) could affect the rate of Cu transfer from/off Cu(II)-$A\beta_{4\text{-}16}$.

Glu is one of the main neurotransmitters in the brain, stored at ~ 100 mM concentration in the vesicles of glutamatergic neurons.[33] During neurotransmission, these vesicles fuse with the cell membrane and Glu is released into the synaptic cleft (**Fig 11**). Its concentration in the extracellular space of these synapses has been stated to exceed 1 mM.[34] As AD pathology initially affects glutamatergic synapses, and Glu has already been reported to compete for Cu(II) from Cu(II)-$A\beta_{1\text{-}16}$[35] at physiological concentrations, we thought that it might also play an important role in the reactivity between Cu(II)-$A\beta_{4\text{-}16}$ and $Zn(II)_7$-MT-3.

Besides, as already introduced in paragraph **1.5.1** Mammalian Metallothioneins (MTs) a variety of partially Zn(II)-depleted MT species, i.e. $Zn(II)_4$-MT-3, $Zn(II)_5$-MT-3 and $Zn(II)_6$-MT-3, could be present under physiological cellular conditions together with the zinc saturated $Zn(II)_7$-MT-3, depending on the Zn(II) status of the cell.[36–38] Since such species may contain un-coordinated Cys thiols, that are more reactive than Zn(II)-bound thiolates[20,21], we studied whether this could affect the reactivity with Cu(II)-$A\beta_{4\text{-}16}$.

Thus, by means of absorbance spectroscopy, we monitored the kinetics of Cu(II) reduction and release from Cu(II)-$A\beta_{4\text{-}16}$ in the presence of i) Glu and $Zn(II)_7$-MT-3 ii) MT-3 at various Zn(II)-load states ($Zn(II)_{6/5/4}$-MT-3) and iii) Glu and the partially Zn(II)-depleted, $Zn(II)_4$-MT-3. Furthermore, by circular dichroism and ^{1}H-NMR we characterized the eventual Cu(I) binding to MT-3 and Zn(II) binding to $A\beta_{4\text{-}16}$.

2.3.2 Results and discussion

a. Effect of Glu

As discussed so far and reported in a previous study[24], Cu(II)-Aβ$_{4-16}$ was stable in the presence of Zn(II)$_7$MT-3, with no Cu transfer occurring over 30 min. However, when the kinetics was followed longer (i.e. 800 min, ~ 13 h), we realized that a slow Cu transfer could be observed.

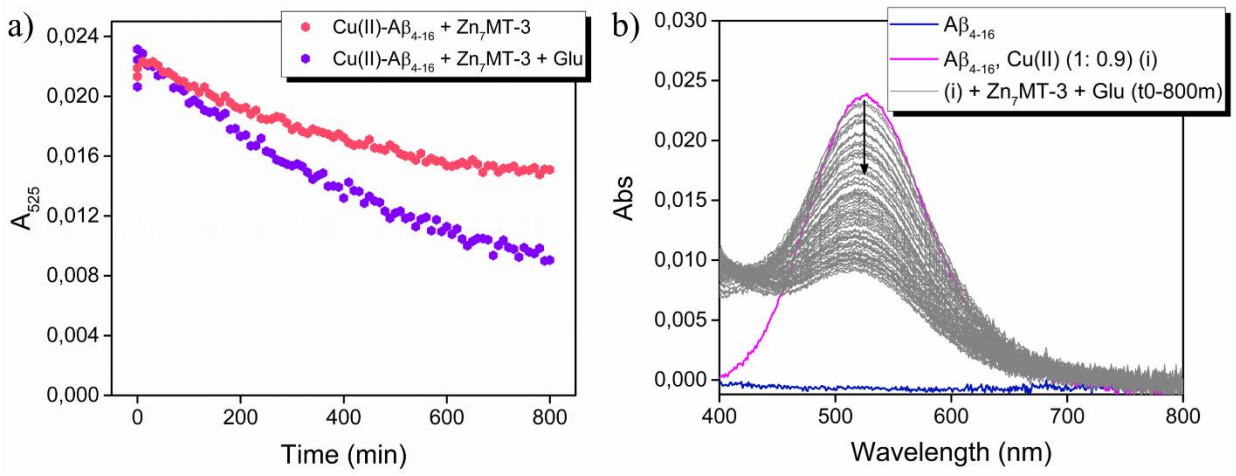

Fig 16 - a) Time course of Cu(II) release from Cu(II)-Aβ$_{4-16}$ to Zn(II)$_7$-MT-3 in the presence and absence of Glu in the reaction mixture, monitored by absorbance spectroscopy at λ_{max} = 525 nm. b) Source of UV-Vis spectra for the reaction of Cu(II)-Aβ$_{4-16}$ with Zn(II)$_7$MT-3 and Glu, added together at t(0m) to the preformed Cu(II)-Aβ$_{4-16}$ complex (purple profile). Reactions conditions: Aβ$_{4-16}$ 250 µM, Cu(II) 225 µM, EDTA 150 µM, ± Glu 5 mM, PB 50 mM, pH 7.4.

As shown in **Fig 16b**, the Cu(II)-Aβ$_{4-16}$ d-d band at λ_{max} = 525 nm decreased with a $t_{1/2}$ of ~ 700 min (**FigS 4b** and **FigS 6a** for determination of $t_{1/2}$), in line with a partial Cu transfer to MT-3, which was confirmed by the appearance of new absorption features in the UV-region, above 250 nm, due to CysS-Cu(I) charge-transfer transitions (**FigS 4a**).[20] Then, to the mixture Cu(II)-Aβ$_{4-16}$/Zn(II)$_7$-MT-3 we added Glu and monitored its impact on the kinetic of Cu transfer from Aβ$_{4-16}$ to Zn(II)$_7$-MT-3, through the Cu(II)-Aβ$_{4-16}$ d-d band (**Fig 16**). Addition of 5 mM Glu (estimated Glu concentration in the synapse) accelerated the transfer by a factor of about 2 (**FigS 6b**, **Fig 19, TableS 1**).

Cu(I) transfer to Zn(II)$_7$-MT-3 was confirmed by circular dichroism (**Fig 17a**), whereas Zn(II) binding to Aβ$_{4-16}$, after release from MT-3, by ^{1}H-NMR (**Fig 17b**), as it was the case of the reaction with Cys and GSH (see discussion above).

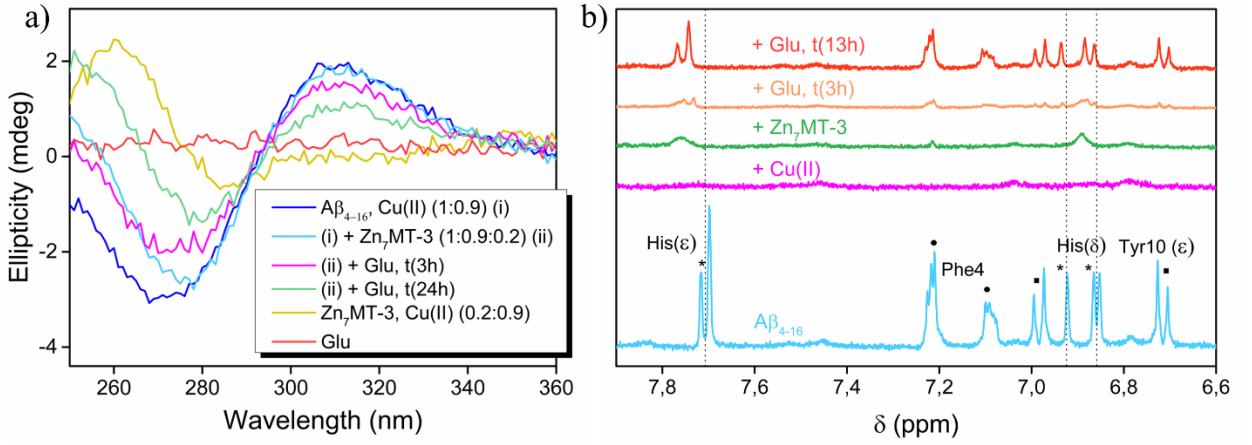

Fig 17 - Reaction between Cu(II)-Aβ$_{4\text{-}16}$ and Zn(II)$_7$-MT-3 with Glu. In a) reaction monitored by circular dichroism (UV-region 250-360 nm). After addition of Glu to the mixture Cu(II)-Aβ$_{4\text{-}16}$/Zn(II)$_7$-MT-3 a CD spectrum was recorded at t(3h) (purple profile) and t(24h) (green profile). Reactions conditions: Aβ$_{4\text{-}16}$ 35 µM, Cu(II) 31.5 µM, Zn(II)$_7$-MT-3 7 µM (ratio Aβ$_{4\text{-}16}$/Cu(II)/Zn(II)$_7$-MT-3, 1:0.9:0.2), Glu 5mM. In b) reaction monitored by ^{1}H-NMR, through the aromatic region of the spectra. Reactions conditions: Aβ$_{4\text{-}16}$ 300 µM, Cu(II) 270 µM, Zn(II)$_7$-MT-3 60 µM (ratio Aβ$_{4\text{-}16}$/Cu(II)/Zn(II)$_7$-MT-3, 1:0.9:0.2), Glu 5mM. Spectra were obtained from 10 % D_2O/90 % H_2O solutions in 50 mM PB, ν=400 MHz.

The acceleration of Cu transfer by Glu was not huge but significant, and raised interesting questions concerning the mechanism of the reaction. Three different mechanisms could be imagined:

- Dissociative mechanism *via* competition for Cu(II) from Cu(II)-Aβ$_{4\text{-}16}$: Cu(II) bound to Glu would be faster reduced by Zn(II)$_7$-MT-3 than that bound to Aβ$_{4\text{-}16}$, since Aβ$_{4\text{-}16}$ binds Cu(II) in a square planar geometry, disfavoring Cu(II) reduction to Cu(I).[23,39] If Glu could intercept even a tiny fraction of Cu(II)-bound Aβ$_{4\text{-}16}$, this might be sufficient to support a slow transfer and subsequent reduction to Cu(I) by MT-3. The very high affinity of MT-3 for Cu(I) and hence the formation of Cu(I)$_4$Zn(II)$_4$-MT-3 complex (stable against oxidation) would in turn make irreversible the reaction.[40]

- Dissociative mechanism *via* competition for Zn(II) from Zn(II)$_7$-MT-3: this would lead to the generation of the aforementioned partially Zn(II)-loaded species, Zn(II)$_{(7\text{-}x)}$-MT-3, yielding non-coordinated thiols. Consequently, MT might have a higher Cu(II) reducing activity that could speed up the Cu(II) reduction and transfer from Cu(II)-Aβ$_{4\text{-}16}$ to Zn(II)$_{(7\text{-}x)}$-MT-3.

- Associative mechanism *via* formation of a transient ternary complex with Cu(II)-Aβ$_{4\text{-}16}$, i.e. [Glu-Cu(II)-Aβ$_{4\text{-}16}$], during the Cu(II) dissociation process. This could change the redox potential of the Cu(II)-Aβ$_{4\text{-}16}$ complex, and Cu(II) be easier reduced from [Glu-Cu(II)-Aβ$_{4\text{-}16}$] than from Cu(II)-Aβ$_{4\text{-}16}$ and consequently transferred to MT-3.

We calculated the contribution of Glu to the equilibrium distributions of Cu(II)-Aβ$_{4\text{-}16}$ and Zn(II)$_7$-MT-3, for concentrations used in the kinetic experiments (**TableS 2**). We found out that such contributions are negligible, as Cu(II)-Glu, Cu(II)-Glu$_2$, Zn(II)-Glu and Zn(II)-Glu$_2$ complexes are very weak compared to Cu(II)-Aβ$_{4\text{-}16}$ and Zn(II)$_7$-MT-3 species, respectively. Thus, this excludes the two possible dissociative mechanisms *via* i) competition for Cu(II) from Cu(II)-Aβ$_{4\text{-}16}$ and ii) competition for Zn(II) from Zn(II)$_7$-MT-3, and suggests an associative one *via* transient formation of the ternary complex [Glu-Cu(II)-Aβ$_{4\text{-}16}$]. Indeed, a dissociative mechanism where Cu(II)-Aβ$_{4\text{-}16}$ releases Cu(II) first (or Zn(II)$_7$-MT-3 releases Zn(II)) and then Cu(II) (or Zn(II)) binds to Glu,

would not lead to any acceleration on the rate of Cu transfer, as the dissociation process would be too slow and hence the rate determining step of the reaction.

In order to assess possible mechanisms, we also replaced $Zn(II)_7$-MT-3 with EDTA as Cu acceptor (**Fig 18**). EDTA cannot reduce Cu(II) to Cu(I), excluding the redox-dependent mechanism of MT-3, but its Cu(II) complex is nearly 1000 times stronger at pH 7.4 (log ${}^{C}K$ (EDTA) = 16.39, vs. log ${}^{C}K$ ($A\beta_{4\text{-}16}$) =13.53), enabling a non-redox transfer.[41]

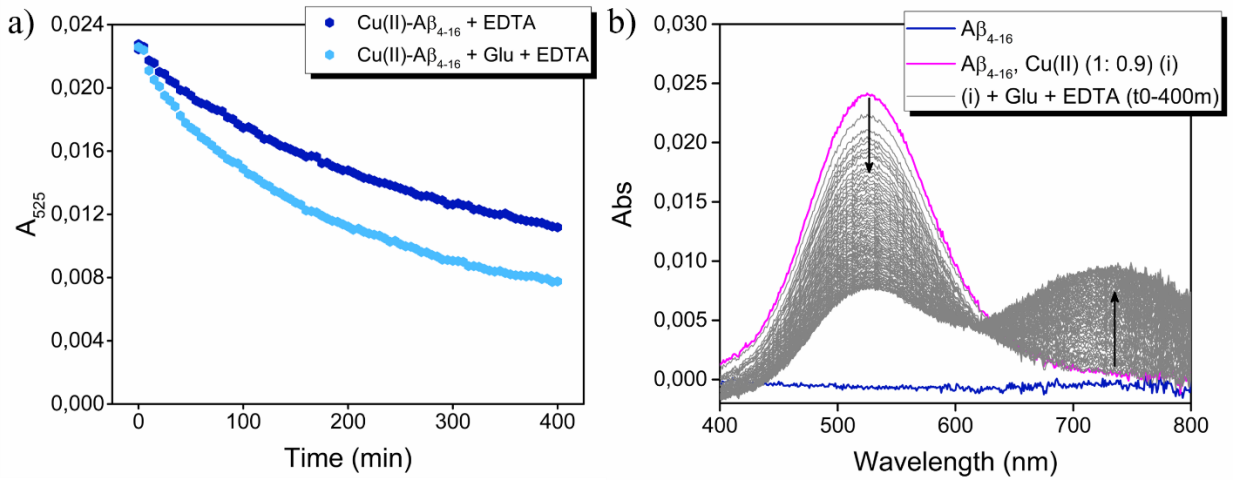

Fig 18 - a) Time course of Cu(II) release from Cu(II)-$A\beta_{4\text{-}16}$ to EDTA in the presence (light blue profile) or absence (blue profile) of Glu in the reaction mixture, monitored by absorbance spectroscopy at λ_{max} = 525 nm. b) Source of UV-Vis spectra for the reaction of Cu(II)-$A\beta_{4\text{-}16}$ with EDTA and Glu, added together at t(0m) to the preformed Cu(II)-$A\beta_{4\text{-}16}$ complex (purple profile). Reactions conditions: $A\beta_{4\text{-}16}$ 250 µM, Cu(II) 225 µM, EDTA 150 µM, ± Glu 5 mM, PB 50 mM, pH 7.4.

In **Fig 18a** the time courses of the reactions in the absence (blue profile) or presence (light blue profile) of EDTA are shown. Addition of Glu and EDTA together to the preformed Cu(II)-$A\beta_{4\text{-}16}$ complex, accelerated the rate of Cu(II) release to EDTA by ~ 2 times (**Fig 19**, ,**TableS 1**). Cu(II) binding to EDTA was confirmed by the appearance of the characteristic Cu(II)-EDTA d-d band at λ_{max} = 738 nm, coupled with the disappearance of the Cu(II)-$A\beta_{4\text{-}16}$ d-d band (**Fig 18b** and **FigS 5**).

Therefore, this experiment indicated that, despite its inability to compete Cu(II) out of Cu(II)-$A\beta_{4\text{-}16}$, Glu can nevertheless influence the rate of Cu transfer to $Zn(II)_7$-MT-3, hence helping in the shuttling of Cu. The likely explanation can be found in the kinetic studies of Cu(II) release from non-ATCUN peptide complexes by Margerum et al., who demonstrated that amino acid molecules could interfere with intermediate species formed transiently during the Cu(II) dissociation process *via* an associative mechanism.[42]

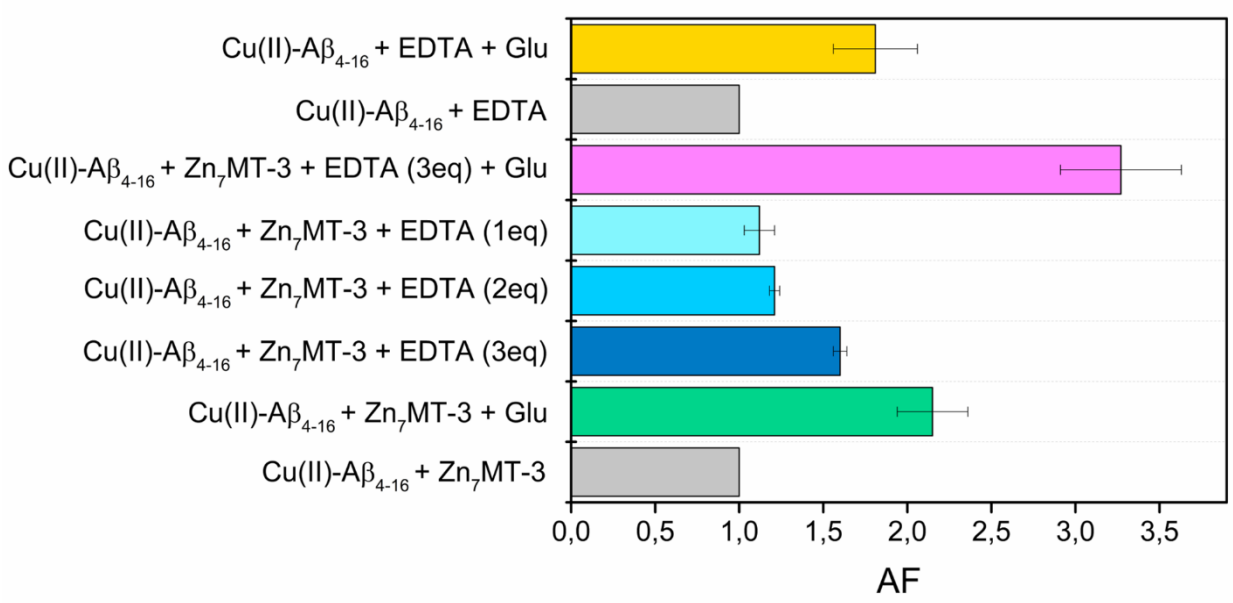

Fig 19 - Acceleration factors (AFs) calculated with respect to the reactions Cu(II)-Aβ$_{4-16}$ + Zn(II)$_7$-MT-3 (in case of the reactions in the presence of Zn(II)$_7$-MT-3) and Cu(II)-Aβ$_{4-16}$ + EDTA (for the reaction Cu(II)-Aβ$_{4-16}$ + EDTA + Glu). AFs are reported with the corresponding standard deviation error (reactions performed in triplicate).

b. Effect of MT-3 Zn(II)-load state

Physiologically relevant partially Zn(II)-loaded species, i.e. Zn(II)$_4$-MT-3, Zn(II)$_5$-MT-3 and Zn(II)$_6$-MT-3, were generated using the specific Zn(II)-chelator EDTA.
The correctness of our approach was confirmed by ^{1}H-NMR (**Fig 20**): EDTA removed Zn(II) from Zn(II)$_7$-MT-3 in the mixture Zn(II)$_7$-MT-3 quantitatively and within the sample mixing time, yielding the desired partially Zn(II) depleted MT-3 species (In **FigS 7**, Zn(II) titration experiment

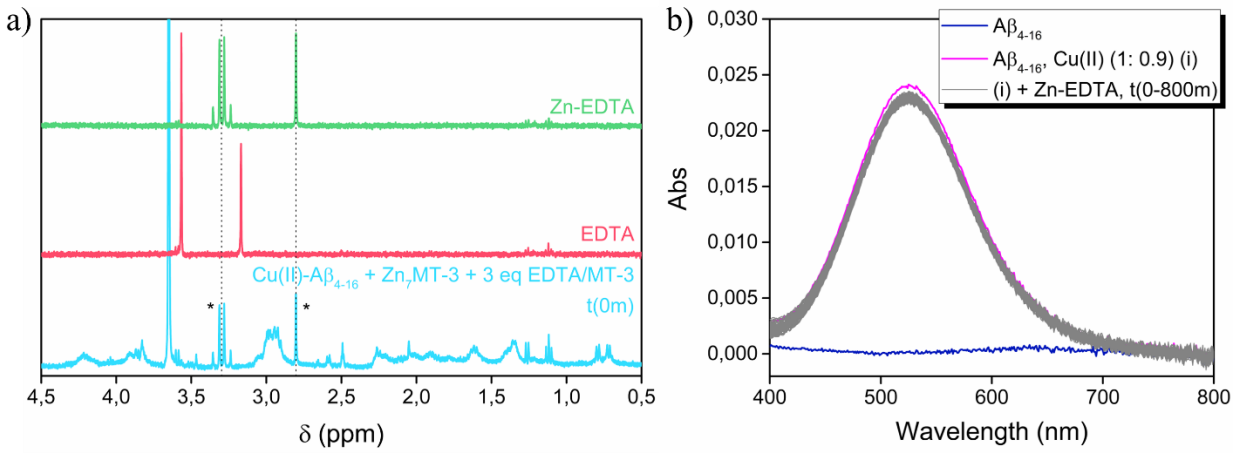

Fig 20 - a) ^{1}H-NMR of the Zn(II) binding to EDTA in the mixture Cu(II)-Aβ$_{4-16}$/Zn(II)$_7$-MT-3 at t = 5 min: spectra of Cu(II)-Aβ$_{4-16}$/Zn(II)$_7$-MT-3 after the addition of 3 eq. of EDTA/MT-3 (light blue), free EDTA (red) and Zn(II)-EDTA, ratio 1:1 (green). Reaction conditions: Aβ$_{4-16}$ 300 µM, Cu(II) 270µM, Zn(II)$_7$-MT-3 60 µM, EDTA 180 µM (3 eq EDTA/MT-3). Spectra were obtained from 10 % D_2O/90 % H_2O solutions in 50 mM PB, ν=400 MHz. b) UV-Vis spectra for the reaction of Cu(II)-Aβ$_{4-16}$ with the preformed complex Zn(II)-EDTA. The reaction was monitored over time from t(0-800m). Intermediate spectra were collected at 10 min intervals. Reaction conditions: Aβ$_{4-16}$ 250 µM, Cu(II) 225 µM, Zn(II)-EDTA 150 µM, PB 50 mM, pH 7.4.

of EDTA monitored by ^{1}H-NMR to characterize the changes observed upon generation of the Zn(II)-EDTA complex). Then, to study weather partially Zn(II)-loaded species accelerate the rate of Cu transfer from Cu(II)-Aβ$_{4-16}$, we followed the reactions by absorbance spectroscopy.

Stoichiometric amounts of EDTA to pull out respectively 1, 2, and 3 mol equiv. of Zn(II) from $Zn(II)_7$-MT-3, hence generating the corresponding partially metallated species $Zn(II)_6$-MT-3, $Zn(II)_5$MT-3, $Zn(II)_4$-MT-3, were added to the preformed Cu(II)-$A\beta_{4\text{-}16}$ complex at t(0m), together with $Zn(II)_7$-MT-3, and the reactions monitored over time for 800 min through the d-d band of Cu(II)-$A\beta_{4\text{-}16}$.

Uv-Vis spectra for the reaction with $Zn(II)_4$-MT-3, $Zn(II)_5$-MT-3 and $Zn(II)_6$-MT-3 are shown in **Fig 21b** and **FigS 8**, while the corresponding kinetics of disappearance of the Cu(II)-$A\beta_{4\text{-}16}$ d-d band in **Fig 21**.

The transfer rate order of Cu acquisition by $Zn(II)_{7\text{-}X}$-MT-3 species and the corresponding acceleration factors calculated with respect to the reaction Cu(II)-$A\beta_{4\text{-}16}$ + $Zn(II)_7$-MT-3 (**Fig 19**), followed the order $Zn(II)_4$-MT-3 > $Zn(II)_5$-MT-3 > $Zn(II)_6$-MT-3 > $Zn(II)_7$-MT-3. This confirmed the expected relationship, i.e. the more thiol groups of MT-3 were available for Cu(II) reduction and extraction from $A\beta_{4\text{-}16}$, the fastest the reaction was.

Cu(II) reduction and release from $A\beta_{4\text{-}16}$ from the mixture Cu(II)-$A\beta_{4\text{-}16}$/$Zn(II)_7$-MT-3/EDTA (3 eq/MT-3) and the consequent Cu(I) binding to MT-3 was also confirmed by circular dichroism as shown in **FigS 9**.

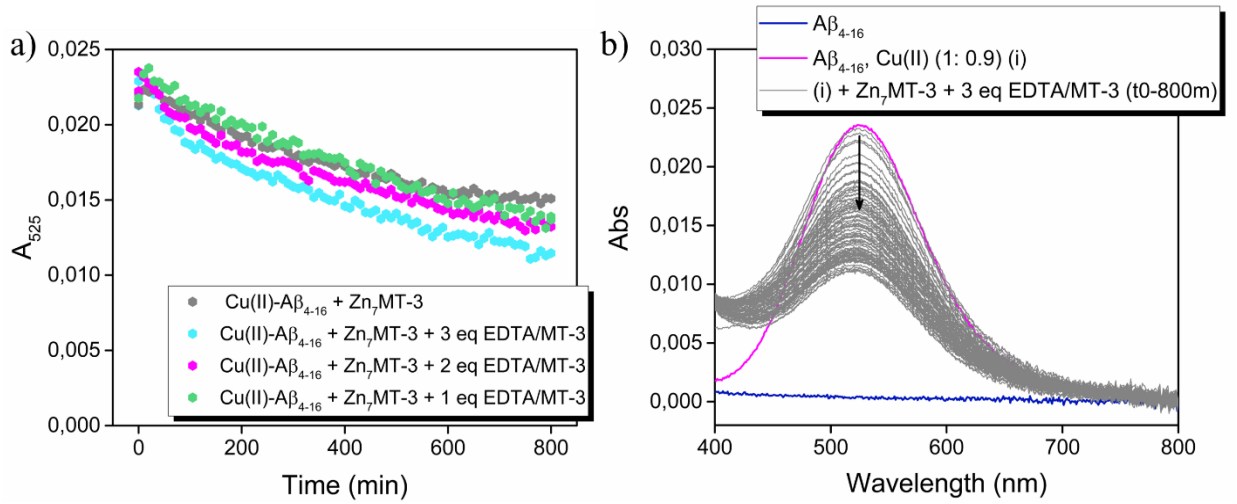

Fig 21 - a) Time course of Cu(II) release from Cu(II)-$A\beta_{4\text{-}16}$ to $Zn(II)_7$-MT-3 (grey profile), $Zn(II)_4$-MT-3 (cyan profile), $Zn(II)_5$-MT-3 (purple profile), $Zn(II)_6$-MT-3 (green profile) monitored by absorbance spectroscopy at λ_{max} = 525 nm. 3, 2 and 1 eq of EDTA/MT-3 were respectively added together with $Zn(II)_7$-MT-3 to the preformed Cu(II)-$A\beta_{4\text{-}16}$ complex to generate the desired partially Zn(II)-loaded species. b) Source of UV-Vis spectra for the reaction of Cu(II)-$A\beta_{4\text{-}16}$ with $Zn(II)_7$-MT-3 and 3 eq EDTA/MT-3. Reactions conditions: $A\beta_{4\text{-}16}$ 250 µM, Cu(II) 225 µM, $Zn(II)_7$-MT-3 50 µM (ratio $A\beta_{4\text{-}16}$/Cu(II)/$Zn(II)_7$-MT-3, 1:0.9:0.2), EDTA 150 µM (3 eq/MT-3)/EDTA 100 µM (2 eq./MT-3)/EDTA 50 µM (1 eq./MT-3), PB 50 mM, pH 7.4.

However, EDTA could also play the role of Cu(II)-shuttle between Cu(II)-$A\beta_{4\text{-}16}$ and $Zn(II)_7$-MT-3, by competing for Cu(II) from Cu(II)-$A\beta_{4\text{-}16}$. Two arguments were against this: i) upon addition of EDTA to the mixture Cu(II)-$A\beta_{4\text{-}16}$/$Zn(II)_7$-MT-3, the characteristic d-d band of Cu(II)-EDTA complex at λ_{max} = 738 nm, was not detected during the entire kinetics, showing that only very small amounts of Cu could be bound to EDTA; ii) Zn(II)-EDTA, which is formed immediately and quantitatively (**Fig 20a**), was not able to retrieve a significant amount of Cu(II) from Cu(II)-$A\beta_{4\text{-}16}$ (**Fig 20b**). Indeed, addition of equimolar Zn(II)-EDTA to Cu(II)-$A\beta_4$-16 yielded no changes in the Uv-Vis spectrum of Cu(II)-$A\beta_{4\text{-}16}$ during the 800 min time window of the reaction.

Besides, we carried out a control experiment for the reaction Cu(II)-$A\beta_{4\text{-}16}$ + $Zn(II)_7$-MT-3 with 3 eq of EDTA to investigate whether the sequence of additions to the preformed Cu(II)-$A\beta_{4\text{-}16}$

complex could interfere with the results obtained. Thus, 3 eq of EDTA where first added to the preformed Cu(II)-Aβ$_{4-16}$ complex and after mixing for 30 sec, Zn(II)$_7$-MT-3 was added. As EDTA does not compete significantly with Cu(II) from Cu(II)-Aβ$_{4-16}$ in the mixing time (not more than 1%), the same rate of Cu(II) transfer to MT-3 is expected, since after Zn(II)$_7$-MT-3 addition, the partially Zn(II)-depleted species, Zn(II)$_4$-MT-3 would be instantaneously generated as well. As shown in **FigS 10** the sequence of additions did not interfere with the results and Cu(II) was reduced and transfer over MT-3 with the same kinetic, within the experimental error.

Hence, EDTA by lowering the Zn(II) status of Zn(II)$_7$-MT-3 could speed up the rate of Cu transfer from Cu(II)-Aβ$_{4-16}$.

c. Additive effect of Glu and MT-3 Zn(II)-load state

To further demonstrate that Glu and Zn(II)-depletion from Zn(II)$_7$-MT-3 (*via* EDTA addition) accelerate the rate of Cu transfer from Cu(II)-Aβ$_{4-16}$ according to separate mechanisms, both compounds were added simultaneously to the preformed Cu(II)-Aβ$_{4-16}$ complex with Zn(II)$_7$-MT-3.

The kinetics of Cu release from Aβ$_{4-16}$ from the mixture Cu(II)-Aβ$_{4-16}$/Zn(II)$_7$-MT-3/Glu/EDTA (3 eq/MT-3) was monitored over 800 min by absorbance spectroscopy through the Cu(II)-Aβ$_{4-16}$ d-d band. As illustrated in **Fig 22** and **Fig 19**, Glu and EDTA (3 eq/MT-3) accelerated the transfer of a factor of about 3 ($t_{1/2}$ ~ 200 min). Thus, their effect was additive meaning that the two mechanisms could complement each other (leading to additive effects).

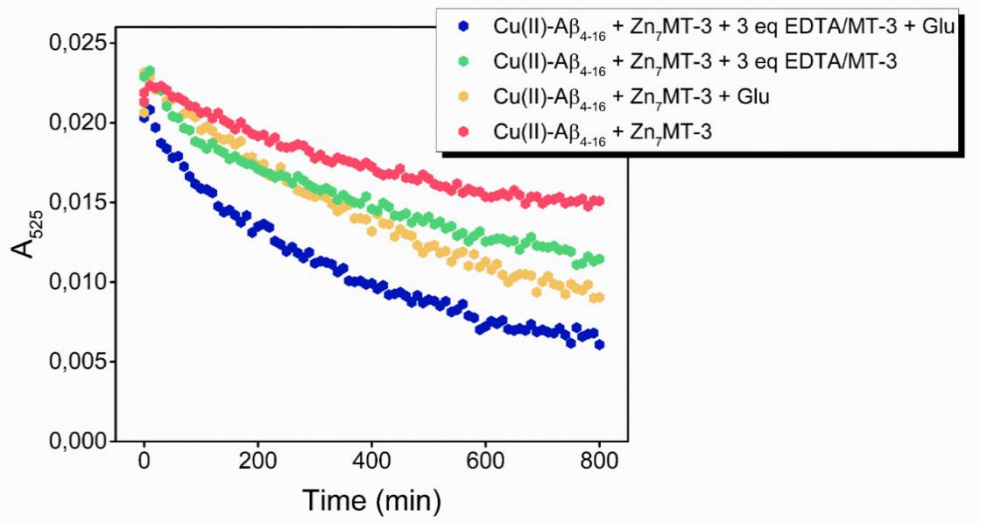

Fig 22 - Additive effect of EDTA and Glu on the Cu transfer from Cu(II)-Aβ$_{4-16}$ to MT-3. Data are expressed as the kinetics of Cu(II)-release from Cu(II)-Aβ$_{4-16}$ (absorbance of the λ_{max} of the d⁻d band of Cu(II)-Aβ$_{4-16}$ as a function of time). Experimental conditions: Aβ$_{4-16}$ 250 µM, Cu(II) 225 µM, Zn(II)$_7$-MT-3 50 µM (1:0.9:0.2), Glu 5 mM, EDTA 150 mM (3 eq/Zn(II)$_7$-MT-3), PB 50 mM, pH 7.4.

2.4 Summary of the main findings

In conclusion, from these experiments, with the complementary use of absorbance and circular dichroism spectroscopies we demonstrate that Cu transfer from Cu(II)-Aβ$_{4-16}$ complex to Zn(II)$_7$-MT-3 can be accelerated by a) Cys or GSH b) Glu and/or c) by lowering the Zn(II)-load of MT-3 with EDTA (**Fig 23**).

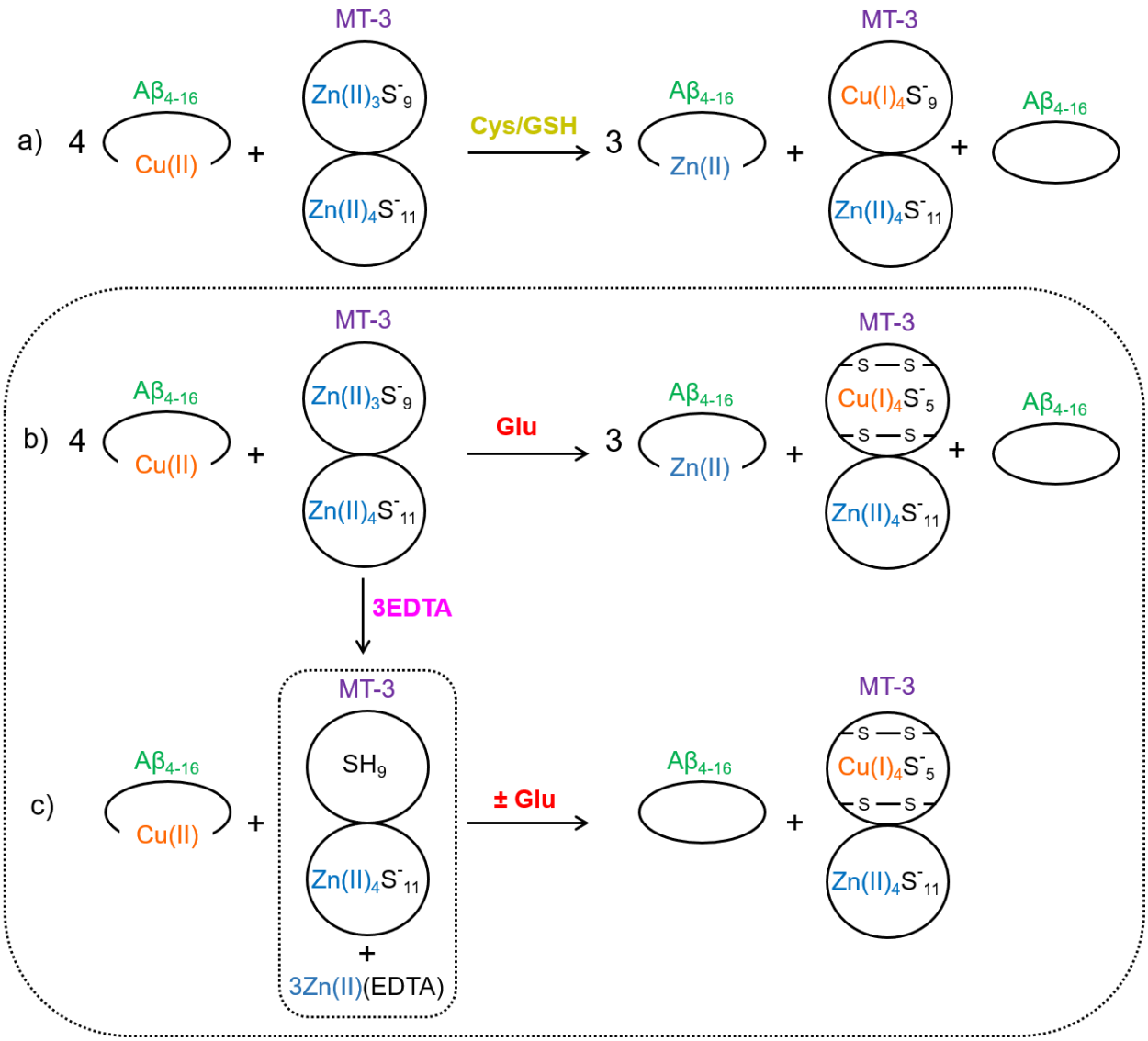

Fig 23 - Scheme summarizing the reactions of Cu transfer from/off Cu(II)-Aβ$_{4-16}$ to Zn(II)-MT-3 studied in this thesis. Influence of a) Cys or GSH, b) Glu; c) Zn(II)-load state of MT-3 (reaction with Zn$_4$MT-3 reported as example). Multiple mechanism may act simultaneously as shown for reaction b) and c), *via* interaction with Cu(II) from Cu(II)-Aβ$_{4-16}$ and by lowering the Zn(II)-status of MT-3 with a Zn(II)-chelator (EDTA).

Concerning the reaction with the amino acid Cys and the tripeptide GSH, we assessed that, under our *in vitro* conditions, the two molecules can induce i) the reduction (rate limiting step of the reaction) and ii) release of Cu(II) from Cu(II)-Aβ$_{4-16}$ in the presence of Zn(II)$_7$-MT-3. Besides, we proved that in the reaction mixture Cu(II)-Aβ$_{4-16}$/Zn(II)$_7$-MT-3 the extracted Cu(I) ions are shuttled to Zn(II)$_7$-MT-3 in form of Cu(I) bound to Cys/GSH, thus generating the species Cu(I)$_4$Zn(II)$_4$-MT-3, in which an air stable Cu(I)-thiolate cluster is present. The full transfer of Cu(II) bound to Aβ$_{4-16}$ was observed for Cys over a period of 30 min, whereas GSH under the same conditions

reacted slower and only a partial transfer could be detected. Even though sluggish under our *in vitro* experimental conditions, the reaction with GSH is noteworthy as it suggests the possibility of coupling the Cu(II)-$A\beta_{4-16}$ biology with physiological processes mediated by GSH neurotransmission.

In case of the reaction with the amino acid and neurotransmitter Glu we demonstrated that despite its low affinity for Cu(II) and Zn(II) compared to $A\beta_{4-16}$ peptide and the metalloprotein $Zn(II)_7$-MT-3, not sufficient to enable the permanent existence of Cu(II)-Glu or Zn(II)-Glu complexes, Glu can nevertheless accelerate the kinetic of Cu transfer to MT-3, *via* an associative mechanism, i.e. transiently forming a ternary complex [Glu-Cu(II)-$A\beta_{4-16}$]. Thus, this mechanism does not depend on the acceptor molecule MT-3. Although the effect is not large, i.e. $t_{1/2}$ (Cu(II)$A\beta_{4-16}$ + $Zn(II)_7$-MT-3) ~ 700 min,vs $t_{1/2}$ (Cu(II)$A\beta_{4-16}$ + $Zn(II)_7$-MT-3 + Glu) ~ 330 min), it paves the way for further research, taking into account the multitude of different small molecules in biological media, present at high concentration, which may collectively be physiologically relevant.

Regarding the mechanism of Cu transfer acceleration by lowering the Zn(II)-content in MT-3 with the specific Zn(II)-chelator EDTA, this is specific for the acceptor molecule $Zn(II)_{7-x}$-MT-3: proportionally to the extent of Zn(II) depletion, and hence on the amount of unbound-thiol groups, partially Zn(II)-loaded species acquires Cu(I) faster, i.e. $Zn(II)_4$-MT-3 > $Zn(II)_5$-MT-3 > $Zn(II)_6$-MT-3 > $Zn(II)_7$-MT-3.

Furthermore, by reducing Cu(II) from Cu(II)-$A\beta_{4-16}$ and shuttling Cu(I) over MT-3 or by interacting with Cu(II)-$A\beta_{4-16}$ *via* transient formation of the ternary complex [Glu-Cu(II)-$A\beta_{4-16}$], Cys, GSH and Glu indirectly affected the Zn(II) distribution between the two species. Indeed, ^{1}H-NMR experiments were consistent with the hypothesis that Zn(II) released from $Zn(II)_7$-MT-3 is at least partially bound to $A\beta_{4-16}$ at the end of the reaction. Hence, Cys, GSH and Glu are modulators of both the Cu and Zn-distribution between the two biomolecules.
In the same way, the reaction with EDTA is interesting as it couples Cu and Zn metabolism. Indeed, this mechanism will depend on the cellular Zn(II) demand, as on Zn(II)-binding biomolecules that can abstract Zn(II) from $Zn(II)_7$-MT-3 MT-3, which might be able to indirectly influence Cu trafficking from Cu(II)-$A\beta_{4-16}$.
Moreover, the reaction Cu(II)-$A\beta_{4-16}$ + $Zn(II)_7$-MT-3 + EDTA (3eq) + Glu shows that depending on external stimuli or stresses, multiple mechanisms may act together, exemplifying the complexity of the metal distribution in a biological environment.

2.5 Reference list

1 L. M. Miller, Q. Wang, T. P. Telivala, R. J. Smith, A. Lanzirotti and J. Miklossy, *J. Struct. Biol.*, 2006, **155**, 30–37.

2 K. J. Barnham and A. I. Bush, *Chem. Soc. Rev.*, 2014, **43**, 6727–6749.

3 J. Nasica-Labouze, P. H. Nguyen, F. Sterpone, O. Berthoumieu, N. V. Buchete, S. Coté, A. De Simone, A. J. Doig, P. Faller, A. Garcia, A. Laio, M. S. Li, S. Melchionna, N. Mousseau, Y. Mu, A. Paravastu, S. Pasquali, D. J. Rosenman, B. Strodel, B. Tarus, J. H. Viles, T. Zhang, C. Wang and P. Derreumaux, *Chem. Rev.*, 2015, **115**, 3518–3563.

4 M. L. Schlief, *J. Neurosci.*, 2005, **25**, 239–246.

5 J.-Y. Lee, T. B. Cole, R. D. Palmiter, S. W. Suh and J.-Y. Koh, *Proc. Natl. Acad. Sci.*, 2002, **99**, 7705–7710.

6 Y. Uchida, F. Gomi, T. Masumizu and Y. Miura, *J. Biol. Chem.*, 2002, **277**, 32353–32359.

7 W. H. Yu, W. J. Lukiw, C. Bergeron, H. B. Niznik and P. E. Fraser, *Brain Res.*, 2001, **894**, 37–45.

8 Y. Uchida, K. Takio, K. Titani, Y. Ihara and M. Tomonaga, *Neuron*, 1991, **7**, 337–347.

9 Y. Irie and W. M. Keung, *Biochem. Biophys. Res. Commun.*, 2001, **282**, 416–420.

10 M. Sato and I. Bremner, *Free Radic. Biol. Med. Med.*, 1992, **14**, 325–337.

11 X. Huang, R. D. Moir, R. E. Tanzi, A. I. Bush and J. T. Rogers, *Ann. N. Y. Acad. Sci.*, 2004, **1012**, 153–163.

12 C. Cheignon, P. Faller, D. Testemale, C. Hureau and F. Collin, *Metallomics*, 2016, **8**, 1081–1089.

13 B. Masters, C. Quaife, J. Erickson, E. Kelly, G. Froelick, B. Zambrowicz, R. Brinster and R. Palmiter, *J. Neurosci.*, 1994, **14**, 5844–5857.

14 W. Goch and W. Bal, *PLoS One*, 2017, **12**, 1–24.

15 E. Atrián-Blasco, A. Santoro, D. L. Pountney, G. Meloni, C. Hureau and P. Faller, *Chem. Soc. Rev.*, 2017, 46, 7683–7693.

16 S. L. Sensi, P. Paoletti, A. I. Bush and I. Sekler, *Nat. Rev. Neurosci.*, 2009, **10**, 780–791.

17 B. Alies, H. Eury, C. Bijani, L. Rechignat, P. Faller and C. Hureau, *Inorg. Chem.*, 2011, **50**, 11192–11201.

18 M. Mital, N. E. Wezynfeld, T. Frączyk, M. Z. Wiloch, U. E. Wawrzyniak, A. Bonna, C. Tumpach, K. J. Barnham, C. L. Haigh, W. Bal and S. C. Drew, *Angew. Chemie Int. Ed.*, 2015, **54**, 10460–10464.

19 B. Alies, A. Conte-Daban, S. Sayen, F. Collin, I. Kieffer, E. Guillon, P. Faller and C. Hureau, *Inorg. Chem.*, 2016, **55**, 10499–10509.

20 G. Meloni, V. Sonois, T. Delaine, L. Guilloreau, A. Gillet, J. Teissié, P. Faller and M. Vašák, *Nat. Chem. Biol.*, 2008, **4**, 366–372.

21 G. Meloni, P. Faller and M. Vašák, *J. Biol. Chem.*, 2007, **282**, 16068–16078.

22 C. Harford and B. Sarkar, *Acc. Chem. Res.*, 1997, **30**, 123–130.

23 P. Gonzalez, K. Bossak, E. Stefaniak, C. Hureau, L. Raibaut, W. Bal and P. Faller, *Chem. - A Eur. J.*, 2018, 8029–8041.

24 N. E. Wezynfeld, E. Stefaniak, K. Stachucy, A. Drozd, D. Płonka, S. C. Drew, A. Krężel and W. Bal, *Angew. Chemie - Int. Ed.*, 2016, **55**, 8235–8238.

25 R. Banerjee, *J. Biol. Chem.*, 2012, **287**, 4397–4402.

26 R. Garg, Sanjay K., Vitvitsky, Victor, Albin, Roger and Banerjee, *Antioxidants Redox Signal.*, 2011,

14, 2385–2397.

27 A. Rigo, A. Corazza, M. Luisa Di Paolo, M. Rossetto, R. Ugolini and M. Scarpa, *J. Inorg. Biochem.*, 2004, **98**, 1495–1501.

28 S. G. Tajc, B. S. Tolbert, R. Basavappa and B. L. Miller, *J. Am. Chem. Soc.*, 2004, **14642**, 10508–10509.

29 I. Bertini, L. Claudio and A. Rosato, *Science*, 1997, **66**, 43–80.

30 I. Bertini and R. Pierattelli, *Pure Appl. Chem.*, 2004, **76**, 321–333.

31 A. Krezel and W. Bal, *Bioinorg. Chem. Appl.*, 2004, **2**, 293–305.

32 A. Krezel, J. Wójcik, M. Maciejczyk and W. Bal, *Chem. Commun.*, 2003, **37**, 704–5.

33 B. S. Meldrum, *J. Nutr.*, 2000, **130**, 1007S–15S.

34 N. C. Danbolt, *Prog. Neurobiol.*, 2001, **65**, 1–105.

35 T. Fraczyk, I. A. Zawisza, W. Goch, E. Stefaniak, S. C. Drew and W. Bal, *J. Inorg. Biochem.*, 2016, **158**, 5–10.

36 A. Krezel and W. Maret, *J. Am. Chem.Soc*, 2007, 10911–10921.

37 A. Krężel and W. Maret, *Int. J. Mol. Sci.*, 2017, **18**, 1237.

38 A. Drozd, D. Wojewska, M. D. Peris-Díaz, P. Jakimowicz and A. Krężel, *Metallomics*, 2018, **10**, 595–613.

39 M. Z. Wiloch, U. E. Wawrzyniak, I. Ufnalska, A. Bonna, W. Bal, S. C. Drew and W. Wróblewski, *J. Electrochem. Soc.*, 2016, **163**, G196–G199.

40 L. Banci, I. Bertini, S. Ciofi-Baffoni, T. Kozyreva, K. Zovo and P. Palumaa, *Nature*, 2010, **465**, 645–648.

41 E. W. Baumann, *J. Inorg. Nucl. Chem.*, 1974, **36**, 1827–1832.

42 D. W. Margerum and G. R. Dukes, *Metal Ions in Biological Systems*, Dekker, New York, 1974.

CHAPTER 3

Redox-activity and stability of Cu-based drugs with Cu-binding and/or reducing biomolecules under conditions found in the cytosol/nucleus

3.1 State of the art and aim of the study

In the first part of the thesis (case study I), we have seen and proven that physiological small molecules such as GSH, Cys and Glu, together with MTs, can have a major role on the fate of pathophysiological Cu-complexes. From these results, we extended our interest to the reactivity of different Cu-based drugs, which have been explored for a variety of medicinal applications, from cancer and AD treatment, to imaging and DNA/RNA cleavage.

As seen in the introduction, the stability of a metal-complex *in vivo* is a key factor for its clinical application, because an administered metallodrug must reach its target in its active form.
GSH and MTs in particular, could have a major impact on the reactivity of Cu-containing drugs which have targets in the cytosol or nucleus as they can be found in elevated concentrations ($[GSH]_{in}$ = 1-10 mM, $[MT]_{in}$ = 1-300 µM]. Because they are strong reducing agents and Cu(I)-chelators, they could lead very fast to the reductive dissociation of a Cu-complex and to its complete deactivation, as Cu(I)-binding to MT results in a redox-silent complex. Besides, MTs have the potential to perform Cu/Zn transmetallation reactions, thus transforming a Cu-complex into the corresponding Zn-complex. In this context, the main issue we wanted to address is whether, in the highly reducing environment found inside the cytosol/nucleus, a Cu-complex, designed to induce catalytically the production of ROS, might be active and stable in form of metallodrug.

The strategy of using Cu-based drugs able to induce the catalytic cleavage or modification of a target biomolecule has been quite a lot investigated since the pioneering work of Sigman and coworkers in the late 70', when they discovered that [Cu-$(Phen)_2$] (ligand 9, **Fig 24**) could induce oxygen-dependent catalytic cleavage of DNA and RNA by attacking the sugar groups.[1,2] Following this example, over the years a variety of families of Cu-pro-oxidant ligands have been investigated.[3,4] They have been explored for many applications but mostly for the development of antitumor-based drugs.[5] Indeed, they are an attractive option, compared to metallodrugs based on non-essential metal ions such as Pt, Co, Ru.[6] As we have seen Cu and essential metal ions in general are tightly regulated by transporters, carriers, binding-proteins, and hence our organism is able to deal with fluctuating amounts of them. Thus, they may be less toxic to normal cells, giving rise to less toxic effects. Nevertheless, so far Cu-containing drugs have not transitioned into clinical use yet. The glycopeptide antibiotic Bleomycin (ligand 11, **Fig 24**) is the only FDA approved drug that has been suggested to chelate essential metal ions (mainly Fe but also Cu has been considered), forming a redox-active complex that is capable of cleaving DNA.[7]

Different families of Cu-chelators which have been developed in the past years have been chosen and studied in this thesis (**Fig 24**). The redox potentials of the corresponding Cu-complexes, associated with the redox couple Cu(II)/Cu(I), vary significantly (~ from -0.8 to 0.5 V vs NHE)

and give an indication of the possibility of a Cu-complex to fast redox cycling between Cu(I) and Cu(II) redox states, with physiological redox partners. Their reactivities in terms of efficiency in ROS production and stability with physiological relevant Cu-binding and/or reducing biomolecules, i.e. $AscH^-$, MT, GSH, under conditions found in the cytosol/nucleus, will be discussed in the next paragraphs.

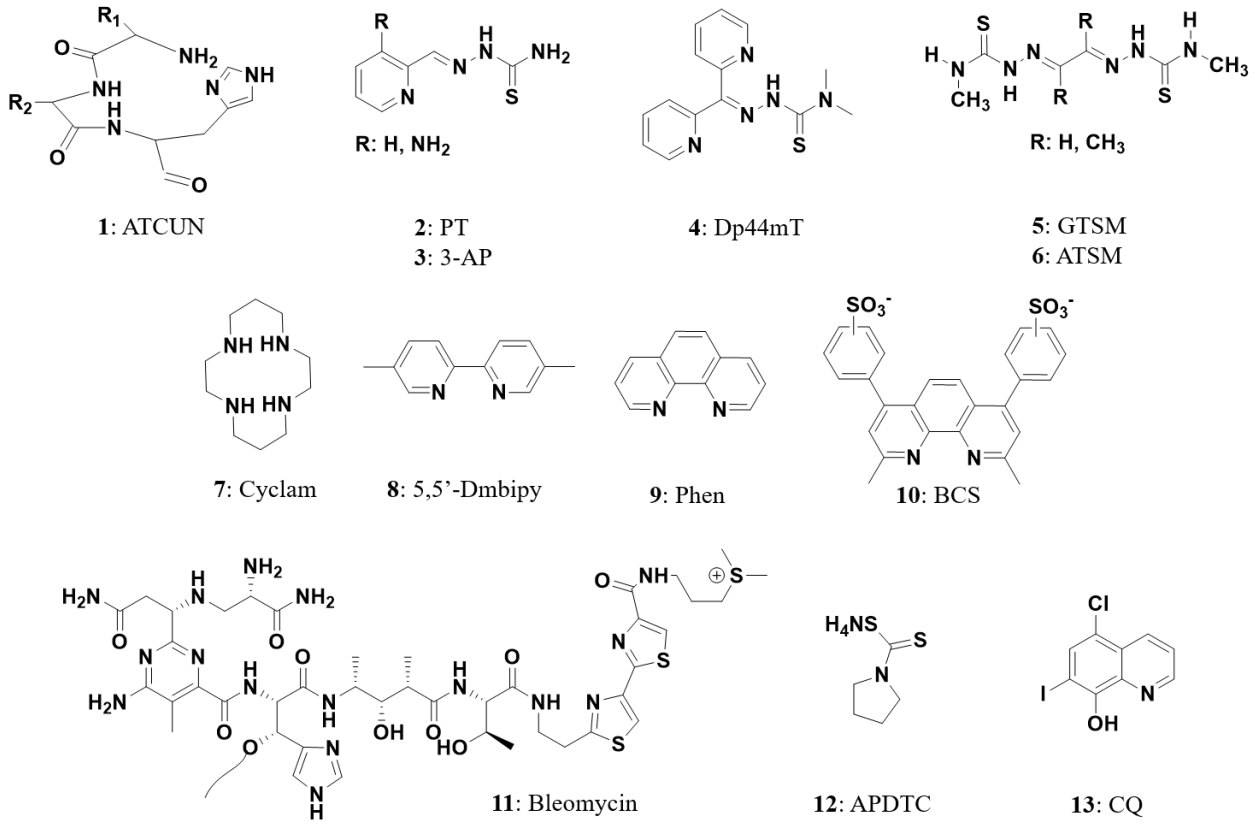

Fig 24 - List of the Cu-chelators studied in this thesis and discussed in next paragraphs.

3.2 Case study of Cu-XZH (ATCUN) peptides: investigation of their application as artificial metalloenzymes

3.2.1. Introduction

Among the different families of ligands investigated, the first one is the peptide motif H_2N-Xxx-Zzz-His (XZH) (ligand 1, **Fig 24**), known as amino-terminal Cu and Ni-binding motif (ATCUN) and already seen at the of N-terminus of $A\beta_{4-x}$ (**Fig 6**).[8] This simple motif has been widely used by different research groups to add a strong Cu(II)-binding site to peptides, proteins or organic ligands, for a vast variety of biological and medicinal applications. Indeed, it can be easily inserted by synthetic or recombinant approaches, just by adding the three amino acids or by mutating the third amino acid to a His. The binding through the N-terminal amine and the presence of an His in third position, which binds with the imidazole nitrogen at the delta ring position, N(δ), provide the strongest bond for Cu(II), because they create stable 5- and 6-membered chelate rings with the in-between amide nitrogen's. Instead, X and Z can be any amino acid except for Pro for Z, because it is a secondary amine and its nitrogen would not carry a dissociable H, when involved in the peptide bond, that could be replaced by Cu(II).[9] However, despite their side chains do not directly participate in equatorial Cu(II)-coordination, they can have an impact on the Cu(II)-affinity and on the reactivity of the resulting Cu(II)-XZH complex.

Thus, in several studies the concept of the Cu(II)-XZH motif, attached at the N-terminus, has been used to introduce a ROS catalytic unit, in the context of nuclease (DNA, RNA cleavage), protease (proteins cleavage), glycosidase (sugars cleavage), in cancer research and as antimicrobial agent, hence playing the role of an artificial enzyme.[4,9,10] As already seen, the cleavage of biomolecules catalyzed by Cu is a redox dependent mechanism (**Fig 2**), generally involving Cu(I) and Cu(II) redox states (although the formation of a higher oxidation state of Cu, i.e. Cu(III), has been suggested[11]).[4]
More recent research suggests novel biological functions, based on the redox inertness of Cu(II) in the ATCUN motif. For instance, peptides and proteins with XZH motif have been used to suppress the ROS production induced by Cu-$A\beta_{1-x}$, in the presence of $AscH^-$ and O_2. This approach is based on the retrieval of Cu from $A\beta_{1-x}$ peptide and strong stabilization of Cu(II) in the 4N square planar complex at physiological pH.[12] Besides, the motif XZH has been used for ^{64}Cu imaging (PET) by Miyamoto et al, with the idea of a redox-inert Cu(II)‑XZH. Based on their results, they concluded that the structural bulkiness and hydrophobicity of the residues XZ are key parameters for the stability of Cu(II)-ATCUN peptides in blood plasma, as they likely contribute to limiting the ^{64}Cu-transchelation of the ATCUN peptides with other proteins.[13]

Hence, according to what reported in the literature, there is an inherent discrepancy about the redox activity of this motif. On the one hand Cu(II)-XZH motif has been used to produce ROS, for which an efficient redox cycling of Cu is warranted. On the other hand, the same motif has been used to redox silence Cu, based on an arrest of its redox-cycling once Cu is bound to it, in form of Cu(II). In order to gain insight into this discrepancy, we selected three canonical variants of XZH motif, i.e.:

- DAHK: the natural motif found in human serum albumin;
- KGHK: one of the motifs mostly studied and efficient to perform cleavage of biomolecules;

- FRHD: the motif found in the N-truncated Aβ peptide, $A\beta_{4-x}$, and reported to redox silence Cu efficiently;

and quantified the corresponding redox-activity of the three Cu(II)-XZH complexes, under the most classical conditions, i.e. with $AscH^-$ as reducing agent and O_2, and/or H_2O_2. Moreover, we compared their activities to that of other redox active Cu-complexes of organic ligands (i.e. 5,5'-DmBipy: 5,5'-dimethyl-2,2'-dipyridyl, Phen: 1,10-Phenantroline), which have been used as catalytic Cu-based-drugs to produce ROS[14], and to that of the natural occurring His containing Cu(II)-complex, i.e. Cu(II)-$(His)_2$. Then, we investigated the redox states of Cu that is/are eventually involved in the catalytic redox reaction. Finally, we explored the ability of Cu(II)-XZH complexes to catalyze the production of ROS in the presence of the Cu(I)-binding ligand BCS (ligand 10, **Fig 24**), used as mimic of abundant intracellular Cu(I) chelators (such as GSH and MTs).

3.2.2 Results and discussion

a. Quantification of Cu(II)-XZH redox-catalytic activity with O_2, $AscH^-$ and H_2O_2, via $HO^\bullet$ trapping

The ability and efficiency of the three Cu(II)-XZH complexes (Cu(II)-DAHK, Cu(II)-KGHK, Cu(II)-FRHD) to catalyze the production of ROS was first studied with Fluorescence and EPR spectroscopies, *via* $HO^\bullet$ trapping.

To start, Cu(II)-titrations experiments of XZH ATCUN peptides were carried out, to determine the exact concentration of the peptides and the ratio Cu(II):peptide. This is extremely important, as the presence of non-peptide-bound Cu, would impact the measurements, being very efficient in catalyzing the production of ROS. Titrations were monitored by absorbance spectroscopy through the characteristic d-d band of the 1:1 complex Cu(II)-ATCUN at λ_{max} = 525 nm. As shown in **FigS 11**, titrations experiments confirmed the stoichiometry of the Cu(II) to peptide complexes, with a breaking point exactly at 1.

Then, we monitored the $HO^\bullet$ production, catalyzed by the three Cu(II)-XZH complexes, by following the kinetics of fluorescence of 7-HO-CCA (7-hydroxycoumarin-3-carboxylic acid). Coumarin-3-carboxylic acid (CCA) reacts with $HO^\bullet$ to produce 7-HO-CCA, which is fluorescent at 450 nm upon excitation at 390 nm (**Fig 25**). Under the experimental conditions used in the assay the intensity of the fluorescence signal is proportional to the number of 7-OH-CCA molecules formed. Measurements were performed under three conditions, i.e. in the presence of i) $AscH^-$ and H_2O_2, and ii) $AscH^-$ or iii) H_2O_2 only. In the presence of both $AscH^-$ and H_2O_2, the scheme in **Fig 2**, is mainly limited to the last part.

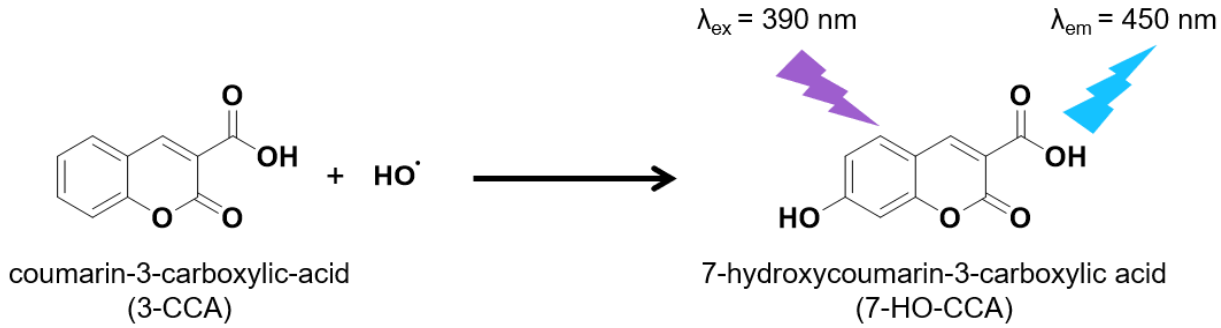

Fig 25 - 3-CCA used to detect $HO^\bullet$ by fluorescence: $HO^\bullet$ reacts with 3-CCA to form 7-HO-CCA, which is fluorescent at 450 nm, upon excitation at 390 nm.

Fig 26 shows the representative kinetics of 7-OH-CCA fluorescence, used to detect the time course of $HO^\bullet$ production, for Cu(II), Cu(II)-DAHK, Cu(II)-KGHK and Cu(II)-FRHD, with 250 µM a) $AscH^-$ and H_2O_2, b) $AscH^-$ or c) H_2O_2, in PB. Control experiments were carried out in the presence of the peptides only (i.e. without Cu), in buffer (results not shown). Both for $AscH^-$ and H_2O_2, concentrations of hundreds µM were used, which are physiologically relevant for $AscH^-$, whereas the concentration of H_2O_2 is normally much lower.[15,16]

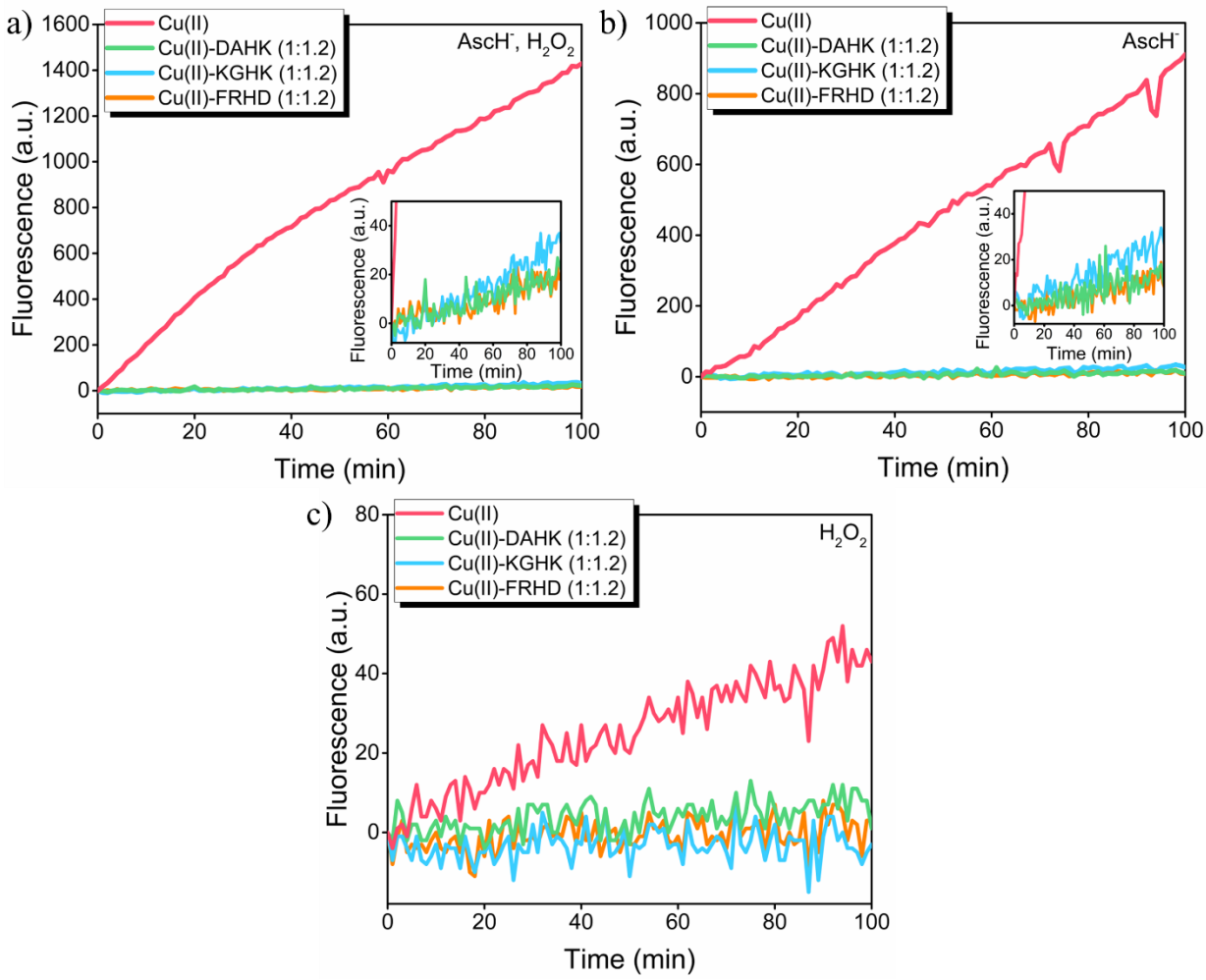

Fig 26 - Evolution of fluorescence of the HO• adduct of CCA, i.e. 7-HO-CCA (excitation: λ = 390 nm; emission λ = 450 nm) as a function of time in the presence of a) $AscH^-$ and H_20_2, b) $AscH^-$ and c) H_20_2. Cu(II)-XZH complexes (H-DAHK-OH, H-KGHK-OH, H-FRHD-NH_2) were preformed with a ratio Cu(II):peptide, 1:1.2 (to avoid the presence of free Cu), in PB 50 mM, pH 7.4. Reactions were triggered by the addition of a) $AscH^-$ and H_20_2, b) $AscH^-$ and c) H_20_2. Insets in a) and b) are a zoom on the kinetics with the three Cu(II)-XZH complexes. Experimental conditions: Cu(II) 25 µM, peptide 30 µM, $AscH^-$ 250 µM, H_2O_2 250 µM and CCA 0.5 mM, in 50 mM pB, pH 7.4.

The following observations can be made, i.e.:

- under the three conditions (i.e. $AscH^-$ and H_2O_2, $AscH^-$, H_2O_2) Cu in buffer was much more efficient in HO• production than the three Cu(II)-XZH complexes, by about 2 orders of magnitude;
- HO• production was more efficient in the presence of both $AscH^-$ and H_2O_2 (**Fig 25a**), about twice as fast as with $AscH^-$ alone. In case of free Cu(II), also H_2O_2 alone produced HO•, but very slowly, at least an order of magnitude slower than $AscH^-$ alone;
- although Cu-XZH complexes showed very little activity, in all repetitions of the experiments, Cu(II)-KGHK was slightly more active than Cu(II)-DAHK and Cu(II)-FRHD (insets in **Fig 26a/b**). However, this difference is just around the statistical error, and hence is just a tendency.

The efficiency in HO• production catalyzed by Cu(II)-XZH ATCUN complexes, with the example of Cu(II)-KGHK, was also confirmed *via* HO• trapping with the spin-trap POBN (α-[4-pyridyl-1-oxide]-N-tert-butylnitrone), by EPR spectroscopy (**Fig 27**). EPR characterization was carried out in collaboration with Dr. Vileno Bertrand from University of Strasbourg.

POBN was used as a primary spin-trap, while EtOH was added as a secondary one, in order to enhance the EPR signal S/N. Decomposition of EtOH with HO• results in the formation of a carbon centered radical, which then reacts with the spin-trap POBN, to form the more stable spin-adduct POBN-CH_3 that gives a signal as the one shown in **Fig 27** (green profile, g = 2.0056, A_H = 2.7 G, A_N = 16 G). The activity of Cu(II)-KGHK was measured at different ratios of Cu(II):peptide, i.e. 1:1, 1.1.2, 1.2, 1.3. The experiments confirmed the much lower efficiency of Cu(II)-KGHK complex in HO• production, when compared to Cu in buffer. Besides, it showed that only at stoichiometric ratio Cu(II):peptide (i.e. 1:1, purple line) there was still a residual activity of non-peptide-bound Cu. This is the reason why experiments were carried out at a slight over-stoichiometry of peptide (Cu(II):XZH, 1:1.2).

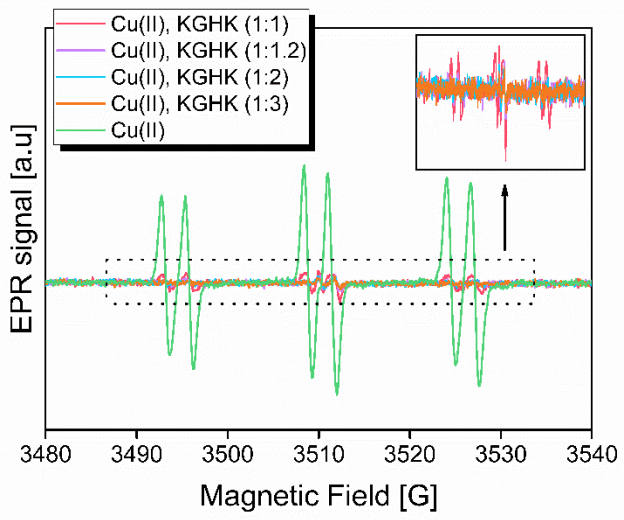

Fig 27 - Indirect evidence of HO• generation by Cu(II)-KGHK complexes: EPR spectra of the POBN-CH_3 spin-adduct collected for the different Cu:KGHK ratios, i.e. 1:1, 1:1.2, 1:2, 1:3, and for Cu in buffer, after triggering the reaction with $AscH^-$. Experimental conditions: Cu(II) 100 µM, KGHK 100 µM (1:1), 120 µM (1:1.2), 200 µM (1:2), 300 µM (1:3), $AscH^-$ 1 mM, H_2O_2 1 mM, POBN 50 mM and EtOH 5% v/v, in PB 50 mM, pH 7.4, at room temperature (RT).

b. Quantification of Cu(II)-XZH redox-catalytic activity with O_2, $AscH^-$ and H_2O_2, *via* consumption of the substrate $AscH^-$

The measurement of HO• production *via* CCA or POBN used to evaluate the redox activity of Cu(II)-XZH complexes are not quantitative. Indeed, they rely on one molecule to trap the radical, which is extremely reactive, and could also be quenched or scavenged by other molecules in solution, like the peptide itself or buffer.

For this reason, we also measured the consumption of the substrate, $AscH^-$, by absorption spectroscopy. $AscH^-$ has an absorption band with λ_{max} = 265 nm (ε = 14500 $M^{-1}cm^{-1}$), whereas the the oxidized form, $AscH^{\bullet -}$, does not absorb at this wavelength. Hence, it is possible to follow the oxidation of $AscH^-$, from the decrease in absorbance at 265 nm (see **Fig 28a**).

The activities of Cu(II)-XZH complexes in $AscH^-$ oxidation were compared to that of Cu(II) in buffer and to those of other Cu(II)-complexes, known to produce ROS *via* Cu-dependent mechanism, i.e. Cu(II)-(5,5'-DmBipy)$_2$, Cu(II)-(Phen)$_2$ and Cu(His)$_2$. Experiments were performed with (**Fig 28**) and without (**FigS 12**) H_2O_2 in the reaction mixture.

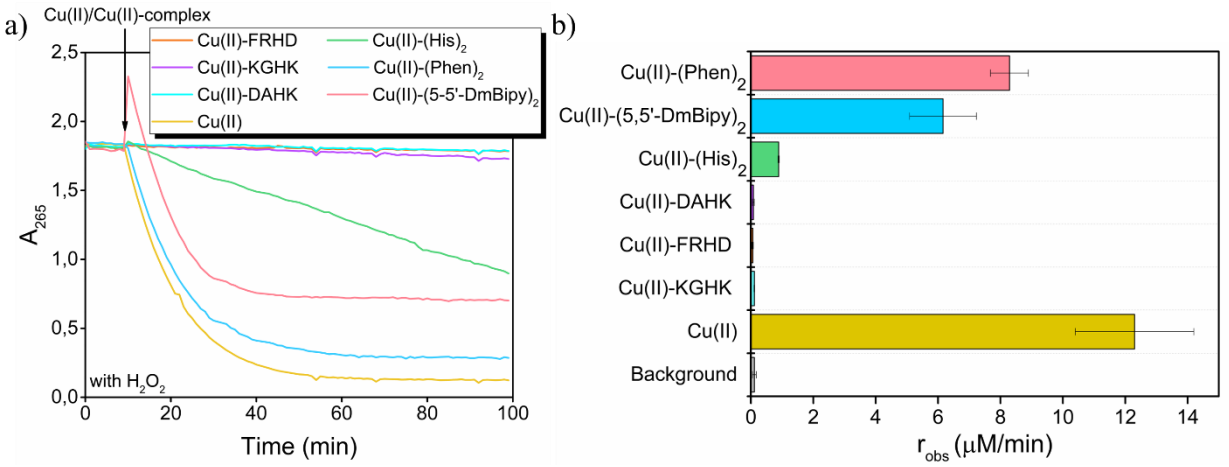

Fig 28 - a) Time course of $AscH^-$ oxidation: evolution of the $AscH^-$ absorption (λ_{max} = 265 nm) as a function of time, after exposure to Cu(II), Cu(II)-XZH, Cu-$(His)_2$, Cu(II)-(5,5'-DmBipy)$_2$, and Cu(II)-$(Phen)_2$ complexes ,with H_2O_2. $AscH^-$ oxidation was started by the addition of free Cu(II) or the preformed Cu(II)-complex after 10 min. Experimental conditions: Cu(II) 10 µM, XZH peptide/ligand 12 µM/24 µM, $AscH^-$ and H_2O_2 100 µM, in PB 50 mM, pH 7.4. b) Histogram of the corresponding molar $AscH^-$ oxidation rates (µM/min). Measurements were performed in triplicate, with different solutions at different days, thus average values of r_{obs} (µM/min) with standard deviations have been calculated.

The results obtained, overall parallel those of $HO^\bullet$ trapping shown above:

- Cu in buffer oxidizes $AscH^-$ rapidly (with, **Fig 28**, or without, **FigS 12**, H_2O_2) with an initial rate of 12.3 ± 1.9 µM/min under the given conditions. In contrast, Cu bound to the XZH ATCUN peptides almost completely blocked the $AscH^-$ oxidation, with rates of 0.08-0.11 µM/min. These values obtained are similar to that of the background of $AscH^-$ oxidation, in which no Cu and peptide are present.
- Comparison with the activities of Cu(II)-(5,5'-DmBipy)$_2$, Cu(II)-$(Phen)_2$ (**Fig 28**) and Cu(II)-$(His)_2$ confirms that Cu(II)-XZH complexes are very slow catalysts for the production of ROS, even under the most favorable conditions, i.e. $AscH^-$ and H_2O_2. Indeed, all three complexes were one or two orders of magnitude faster than Cu(II)-XZH, whereas both Cu(II)-(5,5'-DmBipy)$_2$ and Cu(II)-$(Phen)_2$ were about as active as free Cu(II), under these experimental conditions (i.e. at 10 µM Cu(II), 100 µM $AscH^-$ and H_2O_2).
- Cu(II)-KGHK was slightly more active than Cu(II)-DAHK and Cu(II)-FRHD. Nevertheless, less than 7 µM $AscH^-$ was consumed over 1 h. This corresponds to a maximal turnover rate of about 0.7 per hour with 100 µM $AscH^-$ and H_2O_2. Subtraction of the background of $AscH^-$ yields even a lower activity.
- Addition of H_2O_2 did not increase the rate of $AscH^-$ oxidation both in case of free Cu(II) and Cu-XZH complexes (**FigS 12**). This means that the rate determining step of the reaction is not O_2 reduction to $O_2^{\bullet-}$ (thermodynamically up-hill reaction), but rather the reduction of Cu(II)/Cu(II)-XZH complex by $AscH^-$.

Besides, we measured the oxidation of $AscH^-$, catalysed by Cu(II)-KGHK at different ratios Cu(II):peptide, i.e. 1:0, 1:0.4, 1:0.6, 1:0.8, 1:1, 1:1.2, 1:2, 1:3, both in PB and HEPES buffer. Results are shown in **FigS 13**. $AscH^-$ oxidation rate of Cu(II)-KGHK at 1:1.2 ratio was comparable in the two buffers tested (purple kinetics, **FigS 13a/c**), although Cu in HEPES was more active than in PB (18.9 µM/min *vs* 12.3 µM/min). Hence, Cu(II)-KGHK was very inefficient in $AscH^-$ oxidation and hence almost completely stopped the catalytic production of $HO^\bullet$ at 1:1 ratio,

Cu(II):KGHK. In case of HEPES buffer the rates of $AscH^-$ oxidation for the ratios Cu(II):peptide, 1:1, 1:1.2, 1:2, 1:3 were the same, while in PB, Cu(II)-KGHK at 1:1 ratio was slightly more active (0.28 µM/min) compared to the ratios 1:1.2, 1:2 and 1:3 (~0.11 µM/min). This can be assigned to a slight competition of PB for Cu during the redox cycling Cu(II)/Cu(I). This is also the reason why, in PB, in case of the ratios Cu(II):KGHK, 1:0.4, 1:0.6, 1:0.8, a proportional decrease in the rate of $AscH^-$ oxidation was not observed.

The very low reactivity of Cu(II)-KGHK (and in general Cu(II)-XZH complexes) was also confirmed by measuring (for 1h) the effect of very high concentrations of $AscH^-$ and H_2O_2 (i.e. 20 times excess) on the Cu(II) d-d band, by absorbance spectroscopy (**Fig 29**). In case of a strong reactivity with the substrate one would expect the disappearance of the d-d band, either due to reduction to Cu(I) by $AscH^-$ or oxidation to Cu(III) by H_2O_2. For Cu(III) the appearance of new d-d bands could also be expected. As shown in Fig 6, no significant reduction of the d-d band was observed, neither in the presence of $AscH^-$ and H_2O_2, nor of $AscH^-$ or H_2O_2 only.

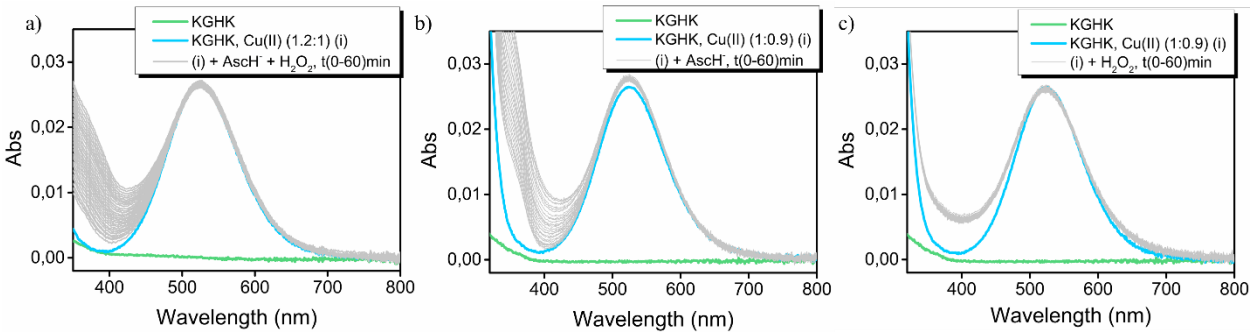

Fig 29 - Uv-Vis spectra for the reaction of Cu(II)-KGHK (ratio 1:1.2, Cu(II):KGHK) with a) $AscH^-$ and H_2O_2 , b) $AscH^-$ and c) H_2O_2. Reaction conditions: Cu(II) 250 µM, KGHK 300 µM, $AscH^-$ and H_2O_2 5 mM, in PB 50 mM, pH 7.4.

Under the conditions with $AscH^-$, i.e. $AscH^-$ and H_2O_2 (a) and $AscH^-$ only (b), a new band around 370 nm appeared in line with the literature.[17] After a longer incubation up to 15h, the band around 370 nm steadily increase and then decrease (**FigS 14a**). Thus the tail of the band started to overlap with the d-d band of Cu(II)-KGHK and apparently that the d-d band started to decrease. However, as shown by a low temperature EPR experiment (**FigS 14b**), this apparent decrease in the d-d band is not due to a reduction or oxidation of Cu(II), but rather to a degradation of the peptide and hence a change in the Cu(II)-coordination site.

c. Investigation of the Cu-redox states involved in the catalytic reaction and of the stability against intracellular Cu(I)-chelators

Next, we investigated the redox state(s) of Cu that is/are involved in the slow catalytic reaction of Cu(II)-XZH with $AscH^-$ and/or H_2O_2. In the presence of $AscH^-$, it is generally assumed that the ROS production occurs *via* redox cycling Cu(II)/Cu(I) (according to the scheme reported in Fig 2 of paragraph 1.1.2), as $AscH^-$ is a reducing agent. However, from electrochemical studies it is known that Cu(II)-XZH complex is very difficult to reduce and that XZH motif can support the redox couple Cu(II)/Cu(III) but not Cu(I)/Cu(II). Indeed, Cu(I) does not bind to the XZH motif, as it is not acidic enough to deprotonate the amides and it prefers a tetrahedral rather than a square planar coordination geometry, that instead is well adapted for Cu(III). Thus, the reorganization energy for Cu(II)/Cu(III) would be very low and hence the redox activity could be very efficient.[18]

Therefore, we hypothesized that if the $HO^{\bullet}$ production of the Cu(II)-XZH complexes passes *via* Cu(I), this Cu(I) is not strongly bound and could be retrieved from the peptide. To address this, we used bathocuproinedisulfonate (BCS), a well-known Cu(I)-ligand/chromophore ($\log\beta_2$ [Cu(I)-$(BCS)_2]^{3-}$ = 19.8)[19], and monitored the reactions by absorbance spectroscopy (**Fig 30**, **FigS 15**) and EPR through a spin-trapping experiment (**Fig 31**). Non-physiological high concentrations of $AscH^-$ and H_2O_2 (up to 10 mM) have been used to facilitate the reactions.

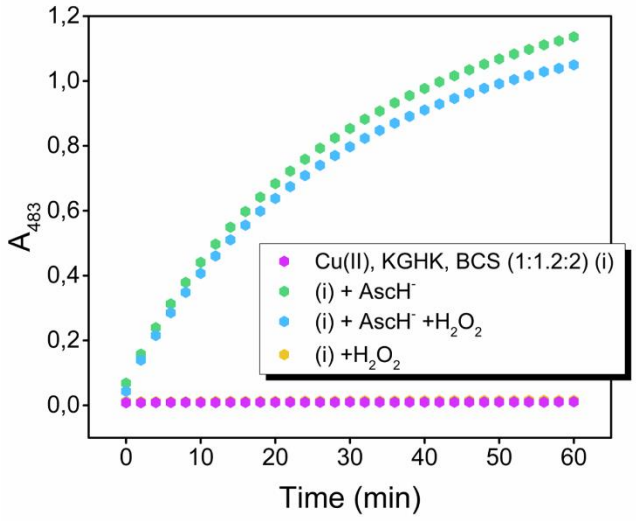

Fig 30 - Kinetics representing the tendency of formation of free or loosely bound Cu(I) from Cu(II)-KGHK in the presence of (i) $AscH^-$ and H_2O_2 (light blue profile), (ii) $AscH^-$ (green profile), (iii) H_2O_2 (yellow profile) and (iv) blank, i.e. no $AscH^-$and H_2O_2 (purple profile), in the presence of the Cu(I) chelator BCS. Corresponding UV-Vis spectra are reported in **FigS 15**. Experimental conditions: Cu(II) 100 µM, KGHK 1200 µM, $AscH^-$ and H_2O_2 10 mM, BCS 200 µM, in PB 50 mM, pH 7.4

In **FigS 15** and **Fig 30**, the UV-Vis spectra and corresponding kinetics of formation of the typical $[Cu(I)\text{-}(BCS)_2]^{3-}$ complex (λ_{max} = 483 nm), for the reaction of Cu(II)-KGHK with i) $AscH^-$ and H_2O_2 (ii) $AscH^-$, (iii) H_2O_2 and (iv) blank, i.e. no $AscH^-$and H_2O_2, in the presence of BCS, are reported. Addition of BCS to Cu(II)-KGHK led to a very small increase of λ_{max} = 483 nm, which corresponds to 0.2 µM $[Cu(I)\text{-}(BCS)_2]^{3-}$ complex formed after 1 h. However, after addition of i) $AscH^-$ and H_2O_2 and (ii) $AscH^-$ only, the band at λ_{max} = 483 nm increased steadily due to the Cu(I)-binding to BCS. This indicates that the formation of Cu(I) is directly linked to $HO^{\bullet}$ production.
In the analogous experiment in the presence of H_2O_2 alone, $[Cu(I)\text{-}(BCS)_2]^{3-}$ was also formed, clearly more than in the background reaction, and its amount parallel the $HO^{\bullet}$ production efficiency, measured with CCA (**Fig 26c**). This means that also in the case of H_2O_2 only (i.e. a strong oxidant), the $HO^{\bullet}$ production takes place *via* Cu(I) and not Cu(III). An explanation, in line with the very slow kinetic, is that H_2O_2 is reducing Cu(II)-XZH, in a one electron reaction, thus forming $O_2^{\bullet-}$. This is in line with what shown for Cu in buffer, i.e. H_2O_2 could slowly and inefficiently reduce Cu(II) to Cu(I), with formation of $O_2^{\bullet-}$ (reaction 1). Then $O_2^{\bullet-}$ can reduce Cu(II) to Cu(I) much faster, and thus the depletion of the product of reaction 1 slowly drags this reaction. Subsequently, the generated Cu(I) can do the Fenton type reaction (reaction 3).[20]

- 1) $H_2O_2 + Cu(II) \rightarrow Cu(I) + O_2^{\bullet-} + 2H^+$ (slow)
- 2) $O_2^{\bullet-} + Cu(II) \rightarrow Cu(I) + O_2$ (fast)
- 3) $Cu(I) + H_2O_2 \rightarrow Cu(II) + HO^{\bullet}$

If Cu(III) would be easily reached, a fast reaction of Cu(II) with H_2O_2 would occur (at least one turnover), i.e.:

- 4) $Cu(II) + H_2O_2 \rightarrow Cu(III) + HO^{\bullet}$

Instead, no indication for Cu(III)-KGHK was observed during absorption even at high H_2O_2 concentration (see **Fig 29**). Cu(III) has a d^8 electronic configuration, hence it is expected to have a much stronger d-d band than the corresponding Cu(II)-complex. Overall, these observations, together with the very high redox-potential of the Cu(II)/Cu(III)-XZH redox couple (i.e. 1 V vs NHE), much higher than that of $H_2O_2/HO^{\bullet}$ (i.e. 0.32 V), point to the involvement of Cu(I) in the mechanism of ROS production catalyzed by Cu(II)-XZH complexes.

To confirm the relation of Cu(I) formation to the $OH^{\bullet}$ production, we measured the $OH^{\bullet}$ in the presence of BCS. As BCS could interfere with CCA fluorescence because of their absorptions at the same spot we used EPR spectroscopy. Thus, if the formed Cu(I) is the key species for the $OH^{\bullet}$ formation, in the presence of BCS no $OH^{\bullet}$ should be produced, because it is known that $[Cu(I)-(BCS)_2]^{3-}$ is very redox inert and hence does not react with O_2 under aerobic conditions.
Fig 31 (left panel) shows the $OH^{\bullet}$ production catalyzed by Cu(II)-KGHK, measured with POBN as primary spin-trap (for the mechanism of $OH^{\bullet}$ trapping with POBN see above). After 4 hours of incubation with $AscH^-$ and H_2O_2, a signal originating from POBN-CH_3 adduct could be detected. In the presence of BCS (right panel), after 4h, no signal was detected, supporting the mechanism that the Cu(I)/Cu(II) redox couple (and not Cu(II)/Cu(III)) is involved in the slow catalytic reaction. Hence, when the formed Cu(I) from Cu(II)-KGHK is chelated by BCS no $OH^{\bullet}$ is detected anymore.

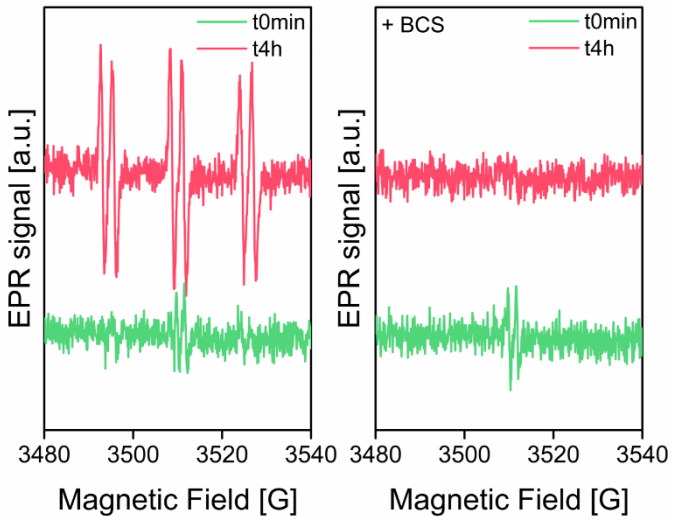

Fig 31 - Indirect evidence of $HO^{\bullet}$ production by Cu(II)-KGHK, measured by EPR spin trapping with POBN in the presence (right panel) and absence (left panel) of BCS. The POBN-CH3 spin adduct was observed after 4h of mixing Cu(II)–KGHK (at 1 : 1.2 ratio) with $AscH^-$ and H_2O_2. The two lines observed at t=0 are ascribed to the ascorbyl radical. Experimental conditions: KGHK 120 µM, Cu(II) 100 µM (1.2 : 1), $AscH^-$ 1 mM, H_2O_2 1 mM, PB 100 mM, pH 7.4, POBN 50 mM, ETOH 5%, ± BCS 200 µM.

Moreover, the experiments in the presence of BCS, mimic of intracellular Cu(I) chelators like GSH and MTs, indicate that in the highly reducing environment found in the cytosol/nucleus Cu(I) from Cu(II)-XZH is strongly accessible for other Cu(I)-chelators that would be able to retrieve Cu(I) during the redox cycle and completely abolish the low ROS production.

3.2.2 Summary of the main findings

In summary, the data presented and discussed indicate that the ROS production of Cu(II)-XZH ATCUN complexes is very slow and that Cu(II)-KGHK is tentatively the most active complex, with 0.7 turnover per hour in the presence of both $AscH^-$ and H_2O_2, under the used conditions. Cu in buffer or other well-known redox-active Cu(II)-complexes, i.e. Cu(II)-(5,5'-DmBipy)$_2$ and Cu(II)-(Phen)$_2$ had two orders of magnitude higher initial turnover rates. Moreover, the experiments with BCS suggest that Cu(I) is involved in the catalytic mechanism, indicating that the redox couple Cu(I)/Cu(II) is predominant and not Cu(II)/Cu(III). This is also supported by the much lower $HO^\bullet$ production activity observed in the presence of H_2O_2 alone.
Overall, this indicates that the cleavage of biomolecules by Cu(II)-XZH ATCUN complexes with $AscH^-$ and H_2O_2 is catalytically not very efficient but possible. However, a real limit for the application of the XZH ATCUN motif to produce ROS, could be the fact that a Cu(I) chelator (like GSH and MTs) would be able to retrieve Cu(I) during the redox cycle and totally suppress this ROS production (mechanism of reductive Cu-dissociation) (**Fig 32**).

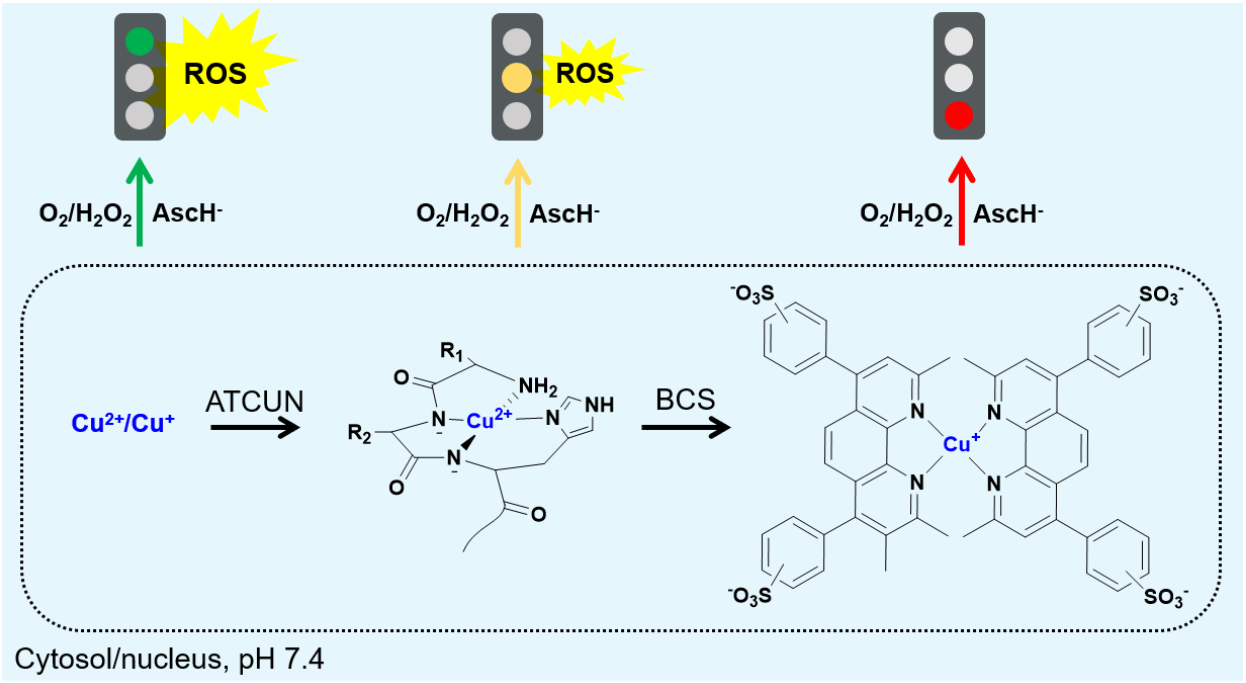

Fig 32 - Schematic representation of the main findings: the catalytic redox activity of Cu(II)-XZH ATCUN motif, with $AscH^-$ and H_2O_2/O_2, compared to Cu in buffer, is very low and can be stopped *via* Cu(I)-chelation with BCS.

Thus, considering the slow rate of ROS production by Cu(II)-XZH ATCUN complexes and the reductive Cu-dissociation by physiologically relevant reducing agents, it seems very difficult to use the ATCUN motif efficiently in catalysis for targets such as DNA/RNA or proteins in the cytosol or nucleus.
Concerning the other applications, for which a redox inertness of Cu(II) is warranted, the XZH motif seems to be quite efficient in keeping Cu(II) redox stable, but not completely, as a small activity in ROS production remains. This is line with previous results which have shown that DAHK can suppress efficiently, but non completely, the ROS production of Cu(II)-Aβ_{1-x} peptides.[12] As shown in the above experiments, the ROS production activity of XZH motif might be sequence dependent, but maximal in a modest way. Nevertheless, there might be space to further improve the redox inertness of Cu(II)-XZH by changing X and Z and the amino acids after the His at position 3.

3.3 Case study of Cu-Thiosemicarbazone (TSC) anticancer drugs: insight into the mechanism of the reaction

3.3.1. Introduction

The second class of ligands we studied is the one of thiosemicarbazones (TSCs, ligands 2, 3, 4, **Fig 24**). During the past decades, TSCs have been clinically developed for a variety of diseases, including tuberculosis, viral infections, malaria and cancer.[5,22] The first clinically approved drug belonging to the family of TSC was p-acetamidobenzaldehyde TSC, introduced in the late 1940' and still in use for the treatment of multidrug-resistant tuberculosis.[23] The clinical anticancer research mainly focused on α-N-heterocyclic TSC (usually containing a pyridyl moiety). 2-pyridinecarboxaldehyde TSC (PT, ligand 2, **Fig 24**) was already reported to show activity against leukemia in mice in 1956.[24] Further optimization led to the development of 3-aminopyridine- 2-carbaldehyde TSC, commonly named Triapine (3-AP, ligand 3, **Fig 24**), which has been tested in more than 30 clinical phase I and II trials.[25,26] Despite the promising activity against hematologic tumors, 3-AP proved to be unresponsive against solid tumors. The reason for this is still not fully understood but possible explanations are i) the very short plasma half-life (< 1 h in humans), ii) the rapid metabolism and extraction and/or the ii) fast development of drug resistance.[27] Nevertheless, it has remained the focus of interest mostly in combination therapy with other drugs, such as cisplatin.[28] To overcome these issues, the series of di-2-pyridylketone TSC, i.e. di-2-pyrydilketone 4,4-dimethyl-3-TSC (Dp44mT, ligand 4, **Fig 24**) and di-2-pyridylketone 4-cyclohexyl-4-methyl-3-TSC (DpC) have been developed which showed the impressive property of being able to overcome drug resistance.[5,29]

TSCs are basically bidentate ligands but are often equipped with a further coordinating moiety to improve stability *via* tridentate ligation, like in case of α -N-pyridyl TSCs. In general, α-N-pyridyl TSCs possess two dissociable protons, the first one from the pyridinium unit (pK_1 ~ 3-4) and the second one from the hydrazinic N-H group of the thiosemicarbazide moiety (pK_2 ~ 10.5-11.5). Based on the pK_a values, at physiological pH all α-N-pyridyl TSCs are charged neutral (HL), thus enabling an easier passage across the cell membrane. In case of pK_2, the resulting negative charge in mainly localized on the S atom *via* the thione-thiol tautomeric equilibrium (**Fig 33**), overall resulting in a N, N, S donor set.

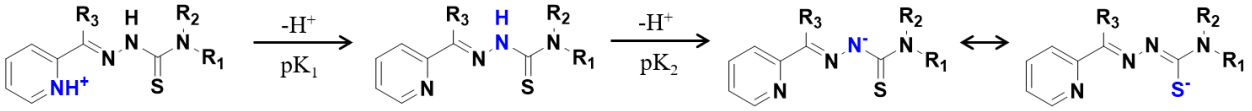

Fig 33 - General scheme of the deprotonation of α-N-pyridyl TSCs like ligands from the form H_2TSC existing at acidic pH.

TSCs were initially developed with the aim of targeting the enhanced requirement of cancer cells for Fe, but rapidly the complex formation with other biologically relevant metals has been suggested (e.g. Cu, Zn), as these compounds have relatively strong metal binding abilities. Especially, Cu complexation has been suggested in the mode of action of several α-N-pyridyl TSCs as they form more stable 1:1 Cu(II)-complexes compared the corresponding Fe-complexes.[30] In case of some di-2-pyridylketone TSC compounds, the Zn(II)-complex showed generally higher antitumor activity, but its toxicity was attributed to the corresponding Cu(II)-complex, formed

after the Zn(II)-complex crossed the cytosol and underwent transmetallation in the lysosomal compartment.[31]
This shows that metal-TSCs could be transformed into apo-TSCs or transmetallated. Thus, apo-TSC could potentially pick up metals, depending on the availability of different metal ions, which is compartment dependent.

The mechanism responsible for the anticancer activity of TSCs is not fully understood yet and different derivatives may have different types of action. In some cases, the TSC alone was found to be as active as the metal complex, and in other cases metal complexes showed higher activity.[32,33] Initially, the activity of TSCs has been attributed only to the inhibition of ribonucleotide reductase (RR), an Fe-containing enzyme involved in the rate limiting step of DNA synthesis, but whether this involves chelation of Fe in this enzyme or chelation of Fe beforehand and inhibition *via* the preformed redox-active Fe(II)-TSC complex, remains unclear.[34,35] Also, a non-Fe dependent mechanism has been suggested, involving quenching of the tyrosine radical in RR by the non metallated-TSC.[36] Moreover other targets have been proposed, such as the thioredoxin system.[37] Concerning Cu, the major mode of action underlying the anticancer activity of Cu(II)-TSC complexes has been related to the intracellular production of ROS.[38] The reactivity of varies Cu(II)-TSC complexes has been studied mainly with the reducing agent GSH. It has generally been observed that GSH can reduce Cu(II)-TSCs and often Cu(I) is then released when an excess of GSH is present. During this process Cu(II)-TSCs can produce ROS.[39–41]

A neglected aspect of the activity of TSCs with these essential metal ions (mainly Cu), deals with their stability with GSH and MTs under conditions found in the cytosol/nucleus. Indeed, Cu-complexes of TSCs have not been investigated for their reactivity with MT, with or without GSH, in a test tube, despite its potential importance. However, Petering and co-workers showed the formation of Cu(I)-MT in cells exposed to the bisTCS called kts (3-ethoxy-2-oxobutyraldehyde bis-thiosemicarbazone).[42] This shows clearly that MT could also be an important player in the reactivity of Cu(II)-TSCs.
As seen before, GSH and MTs have two important features: i) they are reducing agents, and thus can potentially reduce Cu(II) to Cu(I) and Fe(III) to Fe(II); ii) they are metal chelators, having MT S thiolate ligands and GSH thiolate S, O (carboxylate) and N (amine). Despite the affinity of the metal-complexes formed with GSH, under biological relevant conditions, is general lower compared to the respective metalloproteins (Cu(I), Zn(II) and Fe(II) seem to form preferentially $Cu(I)_4$-$(GS)_6$, Zn(II)-$(GSH)_2$ and Fe(II)-GSH complexes, respectively)[43–45], GSH present in much higher concentration in the cytosol and nucleus (~1-10mM). Hence, it could become a serious competitor for metal-binding of exogenous metal-complexes, formed with essential metal ions, mediating the transport of these metal ions to or from proteins.

Therefore, we selected three α-N-pyridyl TSCs, i.e. PT, 3-AP, Dp44mT (ligands 2, 3 and 4, **Fig 24**) and studied the reactivity of their Cu(II)-, Zn(II)- and Fe(II)-complexes in the presence of physiological relevant i) GSH, ii) $Zn(II)_7MT$ and iii) GSH/$Zn(II)_7MT$ concentrations for the cytosol and nucleus, to evaluate their stability against dissociation and potential transmetallation reactions with consequent inhibition of the Cu/Fe-dependent ROS production. Different spectroscopic and analytical techniques have been employed, i.e. absorbance, circular dichroism, EPR spectroscopies and ESI-MS analysis.

There are two different schemes to consider: (i) a preformed metal-TSC complex existing extracellularly enters the cell. In this case, the oxidized form, Cu(II) and Fe(III) will be the more relevant oxidation states; (ii) TSC is applied as a ligand only and enters the cell and is then able to

pick up a metal ion. Here, Cu(I) and Fe(II) will be the more relevant forms since they are the most prevalent intracellularly. Generally, Fe(III)-TSCs have a much lower affinity compared to the main extracellular Fe(III)-binding protein transferrin. Considering that transferrin is only partially loaded with Fe(III), it is expected to withdraw Fe(III) from TSCs.[46,47] Similarly, TSCs are very poor Cu(I)-ligands.[48] Hence, we investigated the more likely existing Fe(II) and Cu(II)-TSC complexes, which are also the better characterized forms. We chose the $Zn(II)_7$MT-1 isoform of MT since it is the one ubiquitously expressed in all cell tissues. Besides, we used the $Zn(II)_7$MT-2a and $Zn(II)_7$MT-3 isoforms to evaluate potential differences in their behavior.

3.3.2 Results and discussion

a. Reactivity of Cu(II)-TSCs with GSH

To start our study, we evaluated the reactivity of the three Cu(II)-TSCs complexes with GSH alone. Although the interactions of some Cu(II)-TSCs with GSH have been studied in the past, the aim was to repeat the reactions to confirm previous results and compare the following experiments with $Zn(II)_7$MT-1. As seen, GSH can use its thiol function to reduce Cu(II) to Cu(I), and bind Cu(I) quite strongly, thus leading itself to the reductive dissociation of a Cu(II)-complex.
The reactivity of each Cu(II)-TSC complex (Cu(II)-PT/3-AP/Dp44mT) with GSH was initially studied by absorbance spectroscopy through the corresponding characteristic CT and d-d bands.

First, to elucidate the stoichiometry of the Cu(II)-complexes formed under our experimental conditions and to characterized their spectroscopic features, Cu(II)-titration experiments were carried out (**FigS 16**). Cu(II)-complexes with a binding stoichiometry of 1:1 were obtained for the three ligands, although in case of the Dp44mT, the formation of a 1:2 (Cu(II):2L) was also observed, based on a red-shift of 8 nm of the CT band, after the addition of 0.5 eq of Cu(II) per L.

Table 4 - Table summarizing the λ_{max} values of absorbance of the different species observed in the reaction of Cu(II)-PT/3-AP/Dp44mT with GSH (TSC, Cu(II)-TSC, [TSC-Cu(II)-GSH])

	λ_{max}				
	TSC	**Cu(II)-TSC**		**GSH-Cu(II)-TSC**	
		d-d band	**CT band**	**d-d band**	**CT band**
PT	313	628	382	530	386
3-AP	359	606	418	528	425
Dp44mT	328	608	411	526	416

Then, Cu(II)-TSC complexes were generated in HEPES buffer with a Cu(II) to ligand ratio of 0.9:1 to avoid the presence of free Cu(II), and GSH in 3 mM concentration was added, monitoring the reaction over time. For the three Cu(II)-TSCs exposed to 3 mM GSH, the instantaneous formation of a ternary adduct [TSC-Cu(II)-GSH] was detected (**Fig 34**), based on a blue shift of ~80 nm of the d-d band together with a small red shift of the corresponding CT band (**Table 4**). A similar shift in the CT band was already observed for a pyridoxal-TSC upon binding of GSH.[49]

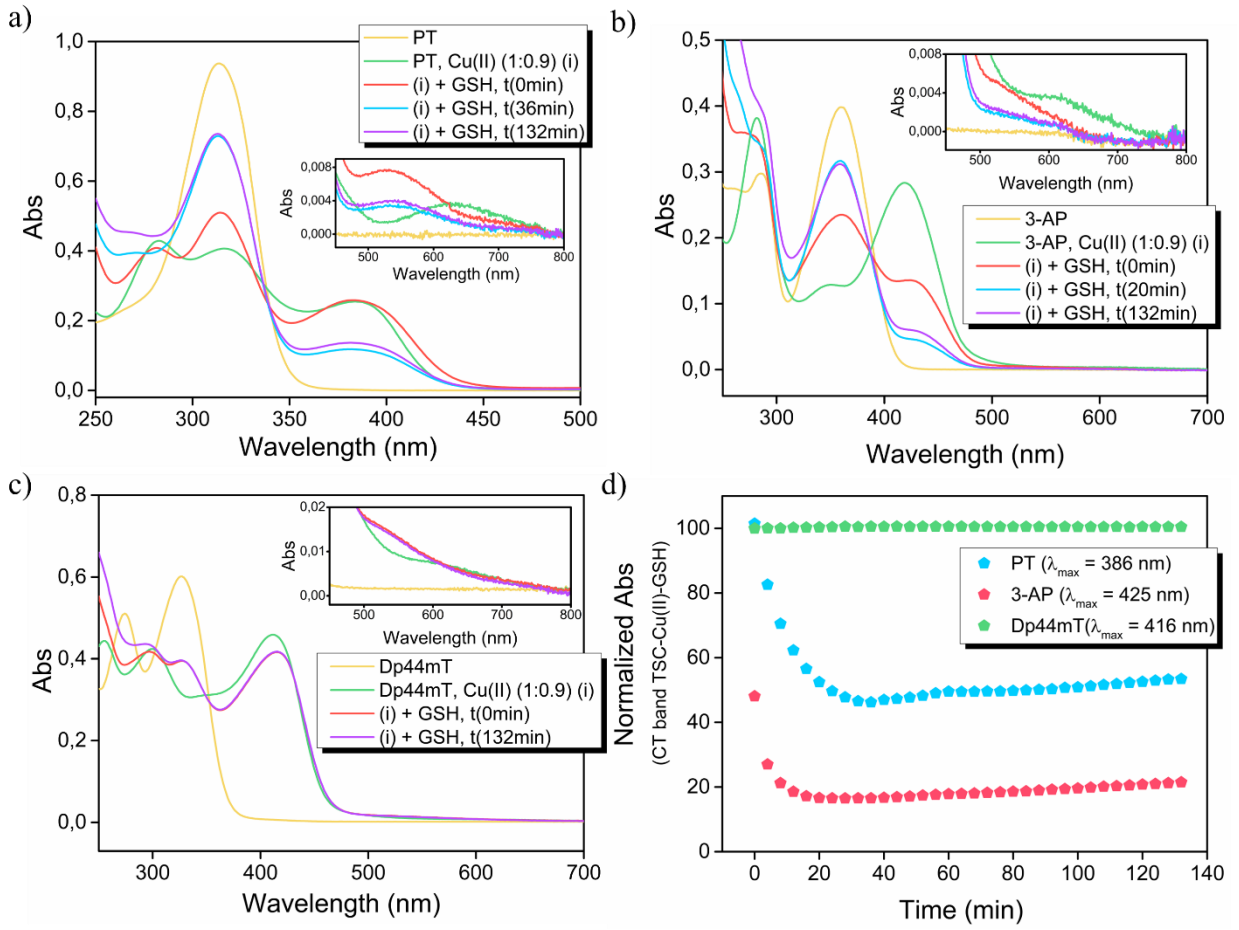

Fig 34 - Reaction of a) Cu(II)-PT, b) Cu(II)-3-AP and c) Cu(II)-Dp44mT complexes with GSH monitored over time by absorbance spectroscopy. Insets refer to the Vis region of the spectra (450-800 nm), in which the d-d bands are present; d) normalized absorbance of the λ_{max} of the CT bands of the [TSC-Cu(II)-GSH] ternary adducts as a function of time. Intermediate spectra were collected at 4min intervals. Experimental conditions: 30 µM TSC, 27 µM Cu(II) (ratio TSC:Cu(II), 1:0.9), 3 mM GSH, 100 mM HEPES buffer, pH 7.4.

The formation of ternary adducts was confirmed by EPR spectroscopy at low temperature (100 K) with the example of Cu(II)-PT complex (**Fig 35**). Cu(II)-PT showed a typical axial Cu(II) EPR spectrum (orange line). Upon the addition of GSH, a significant shift in the g parallel values was observed from ~ 2.205 to 2.142 together with a noticeable change within the superhyperfine structure (green line) (simulation parameters are given in **TableS 3**).

These changes observed are consistent with the substitution of an equatorial ligand (likely H_2O or buffer molecule) by a thiolate from GSH.[50]

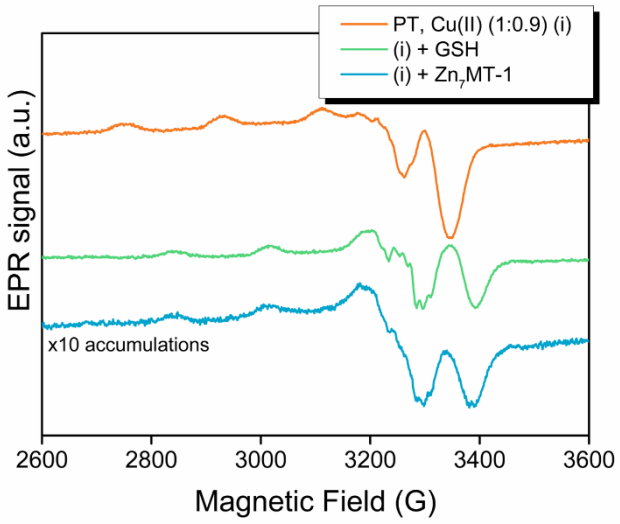

Fig 35 - EPR spectra of snap-frozen solutions of the Cu(II)-PT complex (orange line), at t_0 min after the addition of GSH (green line) and after the addiction of $Zn(II)_7MT$-1 (light blue line). Experimental conditions: 1 mM PT, 900 µM Cu(II), 3 mM GSH or 200 µM $Zn(II)_7MT$-1 (ratio PT/Cu(II)/$Zn(II)_7MT$-1 1:0.9:0.2), HEPES buffer 100 mM, pH 7.4 and T = 100 K. All samples were supplemented by 10% v/v glycerol.

After the fast formation of a ternary adduct of GSH with all three Cu(II)-TSCs, very marked differences in terms of further reactivity could be observed (**Fig 34**). The addition of GSH to the preformed Cu(II)-Dp44mT complex resulted in the immediate binding of GSH to the complex, but no changes in the spectrum of the ternary adduct [Dp44mt-Cu(II)-GSH] could be detected over a period of 132 min. Thus, the Cu(II)-Dp44mT complex did not dissociate in the presence of GSH. On the contrary, the addition of GSH to the preformed Cu(II)-PT and Cu(II)-3-AP complexes resulted in the immediate formation of the ternary adduct [TSC-Cu(II)-GSH], from which Cu(II) was rapidly (several minutes) reductively dissociated to form the Cu(I)-GSH species. Indeed, a decrease in intensity of the CT and d-d bands of the ternary adducts [PT-Cu(II)-GSH] and [3-AP-Cu(II)-GSH] was observed over time along with an increase in the intensity of the band of the free ligands. The kinetic of Cu(II) reduction and release of Cu(I) from the ternary adduct with 3-AP was faster compared to that with PT. The reason for this is not known but the assumed limiting step of the reaction is the reduction of Cu(II) to Cu(I). Redox potentials reported for Cu(II)-3-AP and Cu(II)-PT are respectively -0.19 and -0.14 mV vs NHE;[41] thus, Cu(II)-PT should be easier to reduce. However, these potentials were obtained in 66% organic solvent and in the absence of the relevant ternary complexes with GSH.

Cu(I)-dissociation from the ligands PT and 3-AP in the ternary adducts [PT/3-AP-Cu(II)-GSH] with consequent Cu(I) binding to GSH was confirmed based on the appearance of the characteristic CT absorption band of the Cu(I)-GSH species at 265 nm under a saturated argon atmosphere (**FigS 17**) and on the disappearance of the EPR signature of the [PT-Cu(II)-GSH] species after 30 min from the addition of GSH to the preformed Cu(II)-PT complex at RT (**FigS 18**). Under an O_2 atmosphere, after around 36 min (PT) and 20 min (3-AP) the slow re-oxidation of Cu(I) to Cu(II) and re-formation of the Cu(II)-complex started to be observed (**Fig 34**). This was not detected in the absence of O_2, but when O_2 was vigorously bubbled through the sample, the oxidation was faster with the regeneration of the ternary adducts, [PT/3-AP-Cu(II)-GSH] (**FigS 17**).

Afterwards, we tested other physiological relevant GSH concentrations, i.e. 6 and 9 mM (**FigS 19**). As expected, at higher concentration of GSH, a faster release of Cu(I) from the Cu(II)-PT complex was observed and in line with the higher amount of reduced GSH available in solution,

the re-oxidation of Cu(I) to Cu(II) and consequently the re-formation of the Cu(II)–PT complex was slower and hence it was not observed over a period of 120 min.

Overall, the data obtained lead to the proposition of the following reactions:

- 5) $[Cu(II)\text{-}TSC]^+ + GSH \rightarrow [TSC\text{-}Cu(II)\text{-}GS^-] + H^+$
- 6) $[TSC\text{-}Cu(II)\text{-}GS^-] + xGSH \rightarrow Cu(I)\text{-}GS_x^- + TSC + ½\ GSSG + xH^+$

where x is likely 1.5 due to the formation of $Cu(I)_4\text{-}(GS)_6$ clusters. Thus, PT and 3-AP undergo reactions 5) and 6), where 5) is faster than 6). Cu(II)-Dp44mT seems to perform reaction 6) much slower than PT and 3-AP. Overall, this suggests that the fate of Cu(II)-TSCs with mM GSH concentrations, as encountered in the cytosol/nucleus of cells, is quite different. Cu(II)-Dp44mT does not dissociate, and undergoes only a very slow redox cycle with GSH and O_2. In contrast, the Cu(II)-complexes of PT and 3-AP dissociate with Cu(I)-bound to GSH. This makes Cu(I) available for its sequestration by Cu-binding proteins.

b. Reactivity of Cu(II)-TSCs with $Zn(II)_7$-MT-1

Before investigating the effect of both GSH and $Zn(II)_7$MT-1, we evaluated the reactivity of Cu(II)-PT, 3-AP and Dp44mT, with $Zn(II)_7$MT-1 alone. Like for GSH, MT could reduce Cu(II) from Cu(II)-TSCs and form ternary adducts with the complexes. The Cu(II)-complexes were exposed to 6 µM $Zn(II)_7$MT-1, which is in the lower range of values reported in the cytosol and nucleus. Reactions were followed by absorbance, circular dichroism spectroscopies and ESI-MS.

Fig 36 shows the UV-Vis spectra for the reactions of the three complexes. All of them, reacted very fast with $Zn(II)_7$MT-1 *via* the formation of a ternary complex, [TSC-Cu(II)-$Zn(II)_7$MT-1], by binding of a thiolate from $Zn(II)_7$MT-1 to Cu(II)-TSCs, based on the blue shift of the d-d bands (insets in **Fig 36** and **Table 4**).
This was also supported by EPR spectroscopy (shown for PT), i.e. shift in the g parallel values from ~ 2.205 to 2.147, along with changes within the superhyperfine structure, and the loss in the EPR intensity (light bue line, **Fig 35** and **TableS 3** for the EPR simulation parameters).

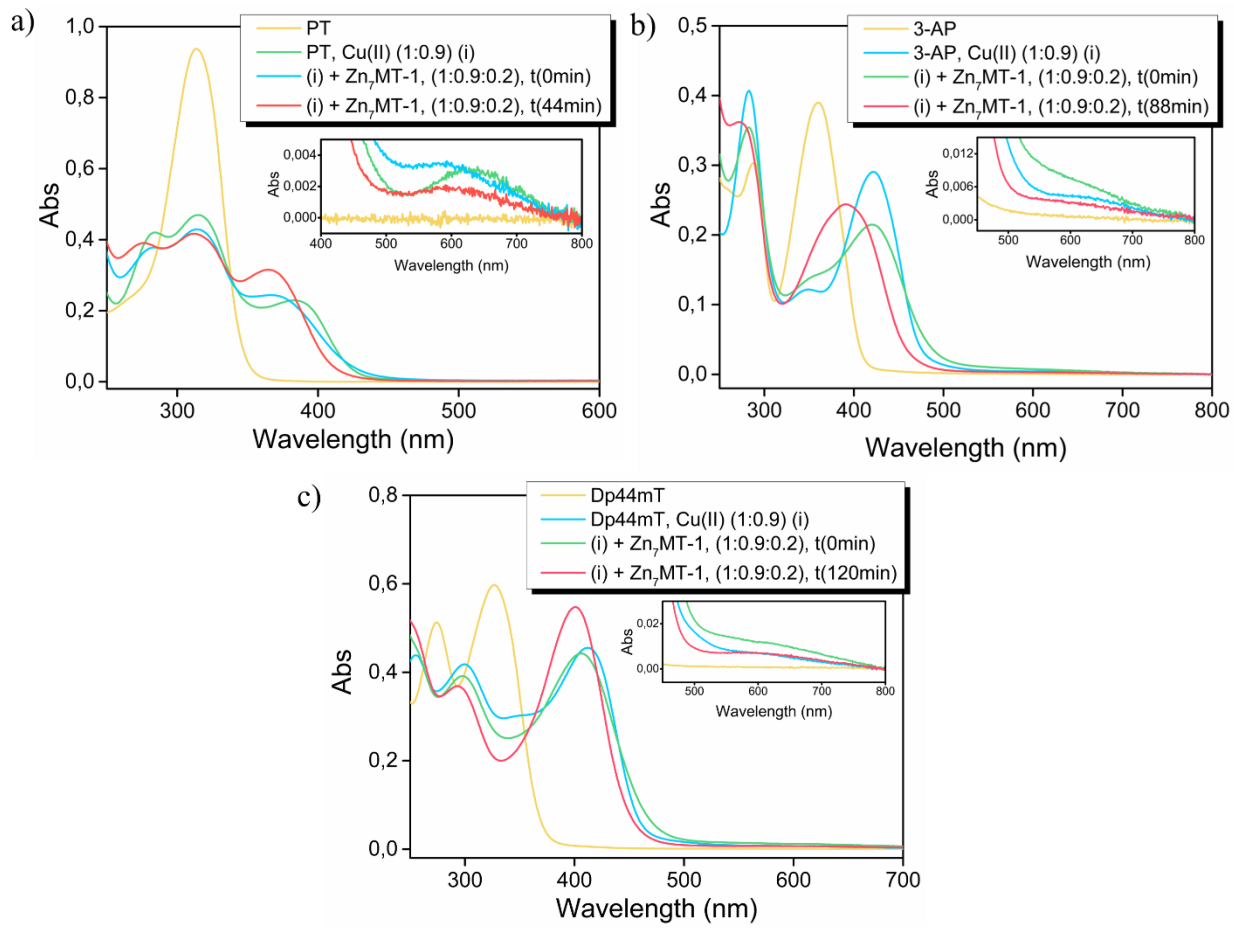

Fig 36 - UV-Vis spectra of the reaction of $Zn(II)_7MT$-1 with a) Cu(II)-PT, b) Cu(II)-3-AP and c) Cu(II)-Dp44mT monitored over time after $Zn(II)_7MT$-1 addition to the preformed Cu(II)-TSC complex. Intermediate spectra were collected at 4 min intervals. Insets refer to the Vis region of the spectra (450–800 nm) for the corresponding reaction. Experimental conditions: 30 µM TSC, 27 µM Cu(II), 3 µM $Zn(II)_7MT$-1 (ratio TSC:Cu(II):$Zn(II)_7MT$-1, 1:0.9:0.2), 100 mM HEPES buffer, pH 7.4.

Hence, $Zn(II)_7MT$-1 was able to reduce Cu(II) to Cu(I) via its cysteines and to chelate Cu(I) finally. This was supported by circular dichroism spectroscopy (shown for 3-AP in **Fig 37**), with the appearance of the typical spectrum observed for $Cu(I)_4Zn(II)_4MT$-1, i.e. CD bands at about (+) 255 and (-) 285 nm. This CD spectrum has been already observed in the past after reaction of MTs with Cu(II) and Cu(II)-compounds (see previous reactions of Cu(II)-$A\beta_{4-16}$)

Cu(I) binding to MT-1 was also confirmed by ESI-MS for the reaction of $Zn(II)_7MT$-1 with Cu(II)-3-AP (**Fig 38** and **FigS 20a**) and Cu(II)-Dp44mT (**FigS 20b**). Experiments were carried out in collaboration with Dr. Oscar Palacios from Autonomous University of Barcelona.
The main peak in a) of m/z ~ 6610 has the mass expected for $Zn(II)_7MT$-1 at neutral pH; upon the addition of $Zn(II)_7MT$-1 to the preformed Cu(II)-3-AP and Cu(II)-Dp44mT complexes (b and c), the immediate appearance of the main peak at m/z ~ 6671 (after deconvolution of the spectra), which corresponds to the substitution of three Zn(II) ions with four Cu(I) ions, i.e. to the formation of $Cu(I)_4Zn(II)_4MT$-1 complex.

Besides, in the experiments monitored by absorbance spectroscopy, a band in the region 360-400 nm was detected during the reactions, which is typical for the Zn(II)-TSC complexes (**Fig 36** and see **FigS 26** for Zn(II) titration experiments). This is line with the fact that Cu(I)-binding to

$Zn(II)_7MT$ results in the release of Zn(II), and suggest the possibility of Cu/Zn transmetallation reaction.

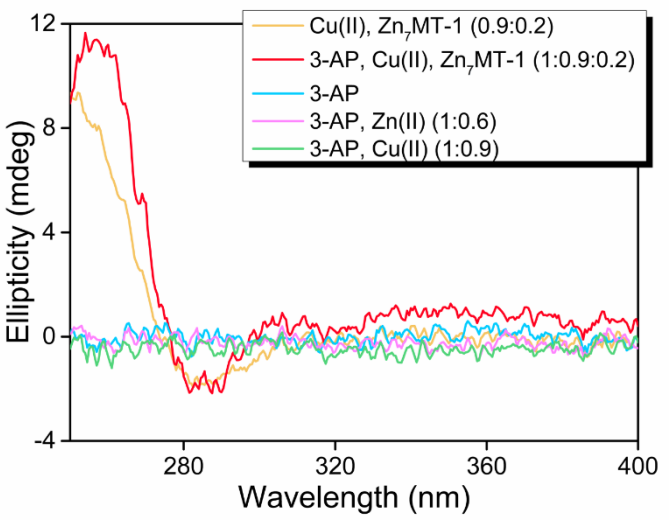

Fig 37 - CD spectra of 3-AP (light blue line); 3-AP/Cu(II), 1:0.9 (green line); 3-AP/Zn(II), 1:0.6 (purple line); 3-AP/Cu(II)/$Zn(II)_7MT$-1, 1:0.9:0.2 (red line, spectrum registered after 120 min from the addition of $Zn(II)_7MT$-1 to the preformed Cu(II)‑3-AP complex), and Cu(II)/$Zn(II)_7MT$-1, 0.9:0.2 (yellow line). Experimental conditions: 100 µM PT, 90 µM Cu(II), 20 µM $Zn(II)_7MT$-1 (ratio 3-AP:Cu(II):$Zn(II)_7MT$-1, 1:0.9:0.2), 100 mM HEPES buffer, pH 7.4.

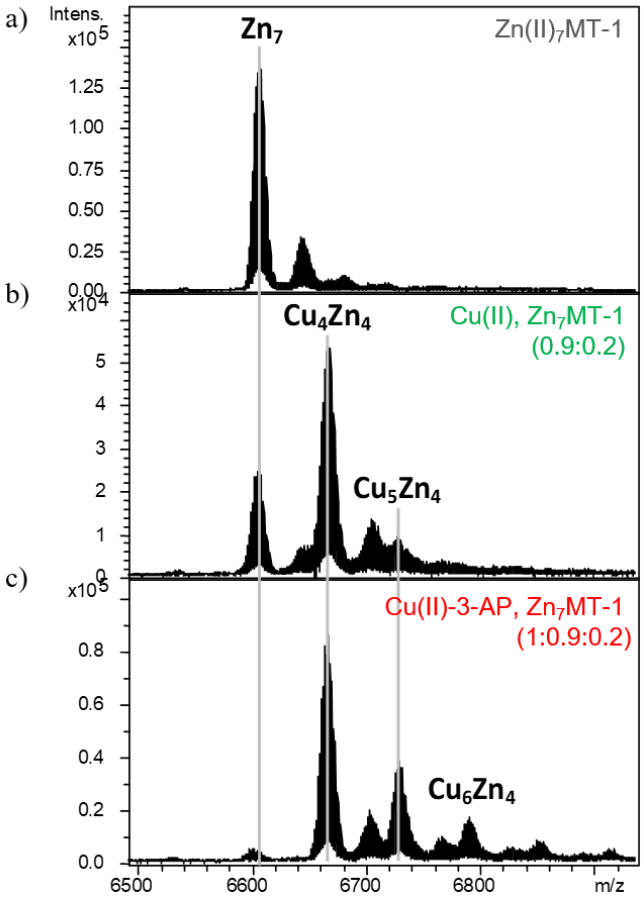

Fig 38 - Deconvoluted ESI-MS spectra a) of $Zn(II)_7MT$-1, b) Cu(II)/$Zn(II)_7MT$-1, 0.9:0.2, and c) 3-AP/Cu(II)/$Zn(II)_7MT$-1, 1:0.9:0.2 (spectrum registered after 120 min from the addition of $Zn(II)_7MT$-1 to the preformed Cu(II)-3-AP complex). Experimental conditions: 50 µM 3-AP, 45 µM Cu(II), 10 mM $Zn(II)_7MT$-1 (ratio 3-AP:Cu(II):$Zn(II)_7MT$-1, 1:0.9:0.2), 50 mM ammonium acetate, pH 7.4.

Overall, for the three complexes the following reaction occurs with $Zn(II)_7MT$-1:

- 7) $4Cu(II)\text{-}TSC + Zn(II)_7MT\text{-}1 \rightarrow Cu(I)_4Zn(II)_4MT\text{-}1 + 3Zn(II)\text{-}TSC + TSC$

It is important to highlight that with $Zn(II)_7MT$-1, Cu(II)‑Dp44mT also reacted, not only Cu(II)‑PT and Cu(II)‑3-AP. This is in contrast to GSH, which was not able to withdraw Cu(II) from Dp44mT, but only formed a stable ternary complex. The reason for this is not known, but may be due to the more reducing potential of MT.

c. Reactivity with of Cu(II)-TSCs with GSH and $Zn(II)_7$-MT-1

In the end, the reactivity of the Cu(II)‑TSC complexes with GSH and $Zn(II)_7MT$-1 together was investigated by absorbance spectroscopy and ESI-MS. The results are shown in **Fig 39** and **FigS 21** and are consistent with the previous ones, for GSH and $Zn(II)_7MT$-1 only.

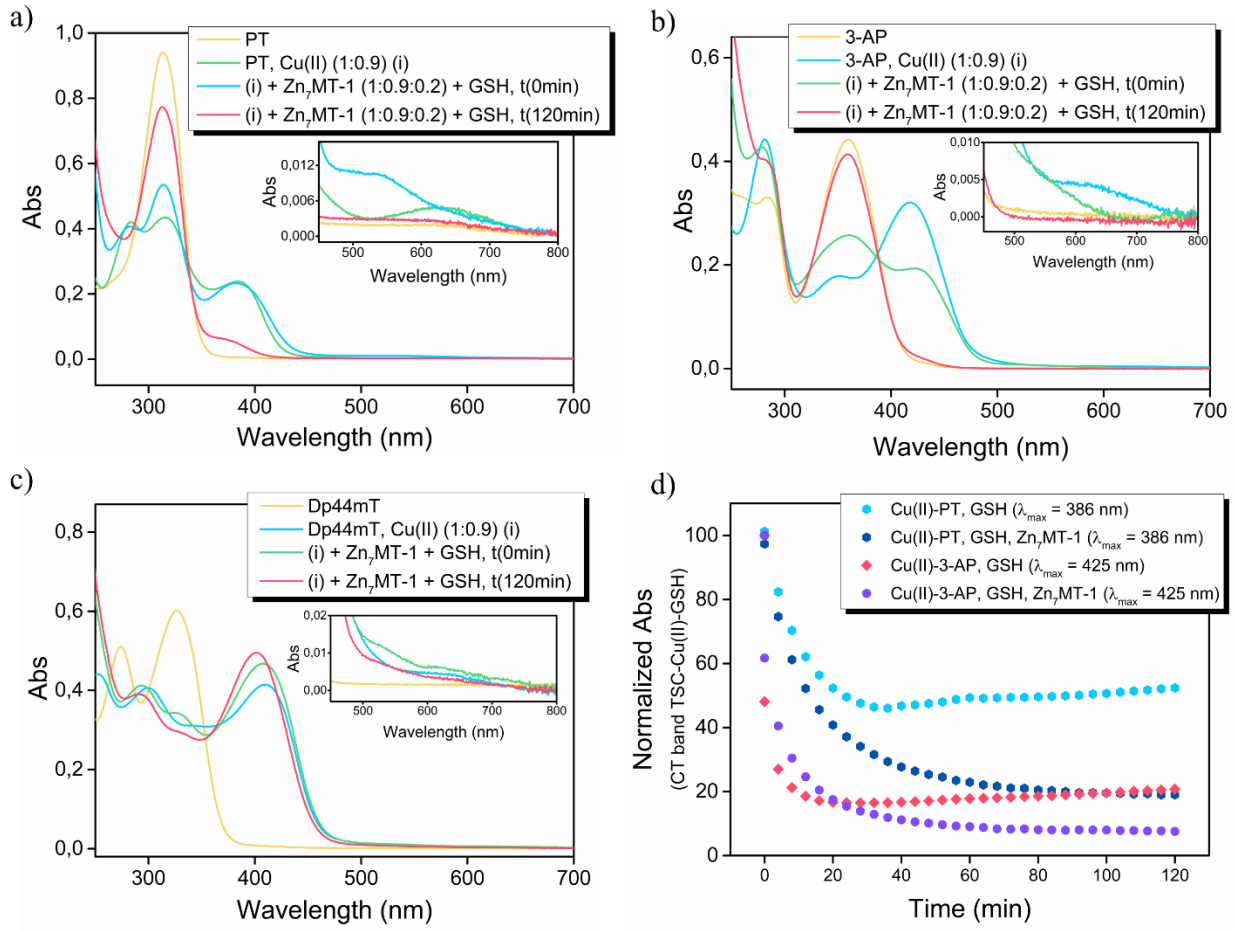

Fig 39 - UV-Vis spectra of the reaction of a) Cu(II)-PT, b) Cu(II)-3-AP, and c) Cu(II)‑Dp44mT with GSH/$Zn(II)_7MT$-1 monitored over time after GSH and $Zn(II)_7MT$-1 additions to the preformed Cu(II)-TSC complexes. Insets refer to the Vis region of the spectra (450‑800 nm) for the corresponding reactions. d) Kinetics of Cu(II) release from Cu(II)-PT/3-AP with GSH in the presence (PT: blue profile; 3-AP: violet profile) and absence (PT: light blue profile; 3-AP: magenta profile) of $Zn(II)_7MT$-1. Data are expressed as normalized absorbance of the λ_{max} of the CT bands of [PT/3-AP-Cu(II)-GSH] ternary adducts as a function of time. Experimental conditions: 30 µM TSC, 27 µM Cu(II), 3 µM $Zn(II)_7MT$-1 (ratio TSC:Cu(II):$Zn(II)_7MT$-1, 1:0.9:0.2), 3 mM GSH, 100 mM HEPES buffer, pH 7.4

GSH/$Zn(II)_7MT$-1 can reduce Cu(II) to Cu(I) from Cu(II)-TSCs and then Cu(I) is transferred to $Zn(II)_7MT$-1, where it is stabilized in the form of Cu(I) by the formation of the $Cu(I)_4Zn(II)_4MT$-1 species. These reactions have a half-time of about 5 and 10 min for 3-AP and PT respectively, and for Dp44mT of about 4 min (**TableS 4**). In the latter case, due to the simultaneous generation of the corresponding Zn(II)-$(Dp44mT)_2$ complex (**FigS 22**), the $t_{1/2}$ could not be accurately

determined. Cu(I) binding to MT-1 was confirmed by ESI-MS for the reaction of $Zn(II)_7$MT-1/GSH with Cu(II)‑3-AP (**FigS 21**a) and Cu(II)‑Dp44mT (**FigS 21b**).

For PT and 3-AP, when comparing the kinetics of the reduction of Cu(II) to Cu(I) via the CT band (**Fig 39d**) with (PT: blue; 3-AP: violet) and without $Zn(II)_7$MT-1 (PT: light blue; 3-AP:purple), it can be observed that the kinetics at the beginning of the reactions are very similar. This implies that GSH reduces Cu(II) to Cu(I) from Cu(II)-PT/3-AP and then shuttles Cu(I) to $Zn(II)_7$MT-1. Moreover, it can be observed the Cu(II)-PT/3-AP complexes are not re-formed over time. Hence, when $Zn(II)_7$MT-1 is present in solution, the reaction is not reversible, confirming the Cu(I) binding to MT-1 and consequent formation of the $Cu(I)_4Zn(II)_4$MT-1 species, which is stable towards oxidation in air/with dioxygen. However, the spectrum of the Zn(II)-PT/3-AP complex was not observed under these conditions, suggesting that Zn(II) released from $Zn(II)_7$MT-1 was not bound to PT or 3-AP. Indeed, further experiments showed that 3 mM GSH can withdraw Zn(II) from Zn(II)-PT/3-AP (**Fig 40** and **FigS 27**), suggesting that Zn(II) was bound to GSH at the end of the reaction.

Thus, the overall reaction of Cu(II)-PT and Cu(II)-3-AP complexes with GSH/$Zn(II)_7$MT-1 is the following:

- 8) $4Cu(II)\text{-}PT/3\text{-}AP + xGSH + Zn(II)_7MT\text{-}1 \rightarrow Cu(I)_4Zn(II)_4MT\text{-}1 + 4PT/3\text{-}AP + 2GSSG + 3Zn\text{-}GS_{(x-4)/3} + xH^+$

In contrast, for Cu(II)-Dp44mT the reactivity was different from PT/3-AP. First, the overall reaction leads to the binding of Zn(II) to Dp44mT, as indicated by the presence of the CT band at λ_{max} = 398 nm, characteristic of the Zn(II)-$(Dp44mT)_2$ complex. This means that a transmetallation reaction occurs, by a swap of metal ions, as follows:

- 9) $4Cu(II)\text{-}Dp44mT + xGSH + Zn(II)_7MT\text{-}1 \rightarrow Cu(I)_4Zn(II)_4MT\text{-}1 + 3Zn(II)\text{-}Dp44mT_2 + xGSSG + xH^+$

The higher affinity of Dp44mT for Zn(II) with respect to GSH was confirmed by a direct competition experiment. Indeed, 3 mM GSH could not retrieve more than 5% Zn(II) from Zn(II)-$Dp44mT_2$, and even at 10 mM GSH ~84% of the Zn(II)-$Dp44mT_2$ complex was still present.

Thus, Cu(II)-Dp44mT was stable in the presence of GSH but when $Zn(II)_7$MT-1 was added, the complex dissociated like Cu(II)-PT/3-AP. In terms of mechanism, two possibilities can be imagined: (i) $Zn(II)_7$MT-1 plays the role of reducing agent and not GSH, even though it is present at much lower concentration (i.e. 6 µM $Zn(II)_7$MT-1 against 3 mM GSH) or ii) GSH can reduce, likely slowly, Cu(II) in Dp44mT, but Cu(I) binds stronger to Dp44mT than to GSH or it is immediately re-oxidized before dissociation. In the presence of $Zn(II)_7$MT-1, $Zn(II)_7$MT-1 can pull out Cu(I) from Dp44mT since it is a stronger ligand than GSH, and/or trap Cu(I) before re-oxidation to Cu(II) occurs.

We also tested the same reactivity but with different MT isoforms, i.e. GSH/$Zn(II)_7$MT-2a and GSH/$Zn(II)_7$MT-3 isoforms (**FigS 23**, **FigS 24**, **FigS 25**). The results only differ in terms of their kinetics. The half-times for the reactions with $Zn(II)_7$MT-3 were generally more rapid than that for $Zn(II)_7$MT-1/2 (3 min for PT and 2 min for 3-AP). This is consistent with the faster kinetics of Cu(I)/Zn(II) exchange for MT-3 already reported.[51]

d. Interaction of TSCs with other essential metals (i.e. Zn, Fe)

As seen above, the three TSCs differed in their capacity to bind Zn(II), released from $Zn(II)_7$MT-1, in the presence of GSH. To confirm these results and also because different Zn(II)-TSC complexes have been considered as anticancer drugs[31,52], we investigated the reactivity of the Zn(II)-TSC complexes with GSH.

To start, we characterized *via* absorbance spectroscopy, with titration experiments, the Zn(II) binding behavior to the ligands under our experimental conditions (**FigS 26**). Only for Dp44mT the formation of a complex Zn(II)-$(Dp44mT)_2$ with a distinct 1:2 stoichiometry was detected.

Fig 40 and **FigS 27** show the competition of GSH for Zn(II) from the three Zn(II)-TSC complexes. Zn(II)-$(Dp44mT)_2$ complex did not completely dissociate even at 10 mM GSH (only ~16%). In contrast, 1 mM GSH was enough to retrieve more than 50% of Zn(II) bound to 3-AP and almost half from PT. The reaction was very rapid (<1 min, the mixing time). This indicates that only Zn(II)-$(Dp44mT)_2$ complex could be stable against GSH concentration found in the cytosol/nucleus, whereas Zn(II)-PT and Zn(II)-3-AP rapidly dissociate.

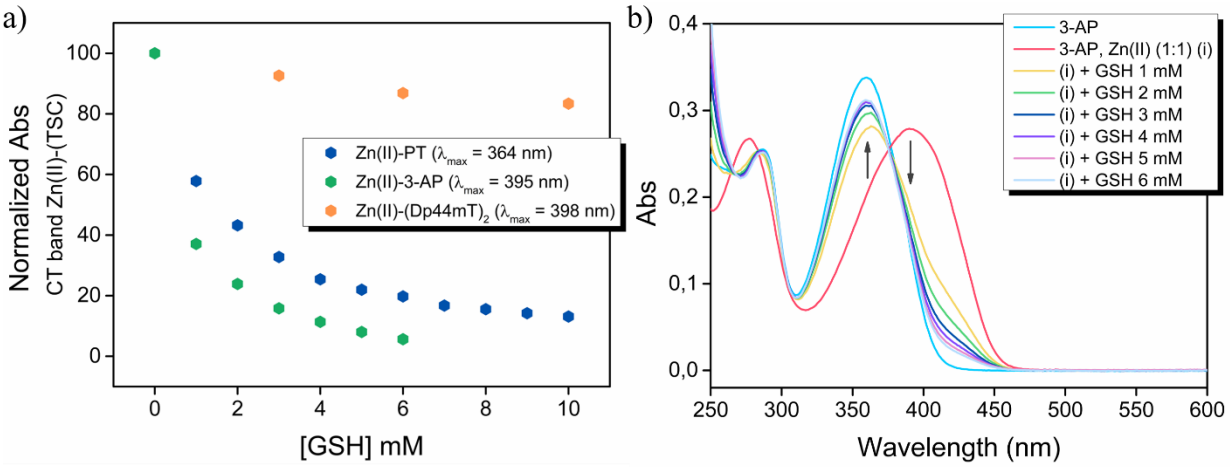

Fig 40 - Reaction of Zn(II)-TSC complexes with GSH monitored by absorbance spectroscopy. A concentrated stock solution of GSH was titrated into the preformed Zn(II)-TSC complexes ([GSH] = 1-10 mm). In a) data are expressed as normalized absorbance of the λ_{max} of the Zn(II)-PT, Zn(II)-3-AP, and Zn(II)-$(Dp44mT)_2$ complexes (at 364 nm, 395 nm, 398 nm respectively) as a function of GSH concentration (mM). In b) UV-Vis spectra for the reaction of Zn(II)-3-AP with GSH are reported. Experimental conditions: 30 µM TSC, 30 µM or 15 µM (in case of Dp44mT) Zn(II), HEPES buffer 100 mM, and pH 7.4. 1 µl aliquots of a 100 mM stock solution of GSH were added to obtain the desired GSH concentration (from 1 to 10 mM).

Then, we investigate the reactivity the three Fe(II)-$(TSC)_2$ complexes with $Zn(II)_7$MT-1 and GSH. To the preformed Fe(II)-$(PT)_2$, Fe(II)-3-AP_2 and Fe(II)-$(Dp44mT)_2$ complexes, $Zn(II)_7$MT-1 was first added and the reaction monitored over time. Then, to the Fe(II)-$(TSC)_2$/$Zn(II)_7$MT-1 mixture, GSH was added (**Fig 41a/b/c** for PT, 3-AP and Dp44mT respectively).
The three Fe(II)-$(TSC)_2$ complexes did not dissociate over time both in the presence of $Zn(II)_7$MT-1 alone and after the addition of GSH. The absence of reactivity with $Zn(II)_7$MT-1 is consistent with the biologically non-relevant Fe binding capacity of the protein. The inability of GSH to dissociate Fe(II)-$(TSC)_2$ may be ascribed to the inability of GSH to form ternary adducts with the complex and to the lower stability of the Fe(II)-GSH complex compared to Fe(II)-$(TSC)_2$.

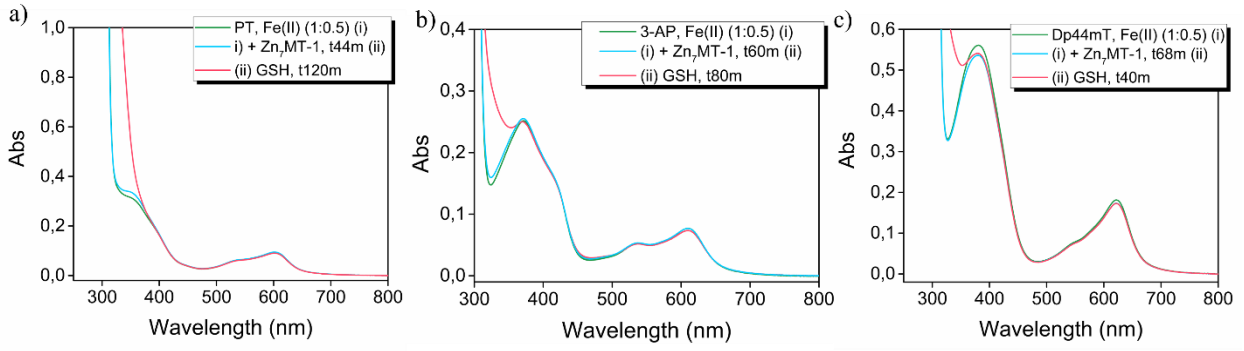

Fig 41 - Uv-Vis spectra for the reaction of a) Fe(II)-$(PT)_2$, b) Fe(II)-$(3\text{-}AP)_2$, c) Fe(II)-$(Dp44mT)_2$ with $Zn(II)_7$-MT-1 and GSH. To the preformed Fe(II)-$(TSC)_2$ complexes, $Zn(II)_7$-MT-1 and then GSH were added one after the other, and the reactions monitored over time. Experimental conditions: 30 µM TSC, 15 µM Fe(III), $AscH^-$ 5 mM (formation of the Fe(II)$^-$ $(TSC)_2$ complex with a ratio TSC:Fe(II), 2:1), 100 mM HEPES buffer, pH 7.4. Addition of $Zn(II)_7$MT-1 6 µM and GSH 3 µM.

e. Catalytic-redox activity of Cu-TSC and Fe-TSC_2 with O_2, GSH and $Zn(II)_7$-MT-1

As introduced previously, one of the proposed mechanisms of action responsible for the anticancer activity of Cu-TSCs and Fe-$(TSCs)_2$ is the intracellular production of ROS, based on the reduction of Cu(II) and Fe(III) by reducing agents such as $AscH^-$ and GSH.

Hence, we investigated the ROS production catalyzed by Cu(I)-TSC and Fe(II)-$(TSCs)_2$, with the example of PT, with a EPR spin-trapping investigation (**Fig 42**), in the absence (left panels) and presence (right panels) of $Zn(II)_7$MT-1. Cu(II)-PT was able to induce the production of $HO^{\bullet}$ in the presence of only GSH, concomitant with a significant loss in the Cu(II)-PT background (baseline left panel of **Fig 42a**). Both features indicate the reduction of Cu(II) to Cu(I) by GSH followed by the reduction of O_2 to ROS by Cu(I)-PT or Cu(I)-GSH. In the same way, Fe(III)-PT was also able to produce $HO^{\bullet}$.

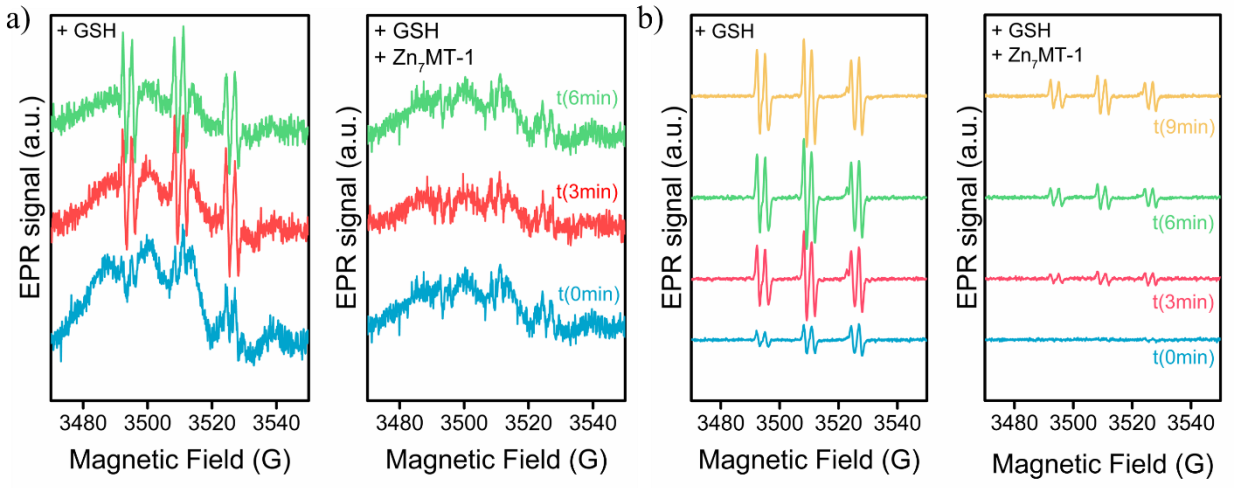

Fig 42 - EPR spin-trap experiments (at RT) for the reactions of a) Cu(II)-PT and b) Fe(III)-$(PT)_2$ with GSH (left panels), and with GSH and $Zn(II)_7$MT-1 (right panels). 4-POBN was used as primary spin trap and DMSO (from the ligand stock solution, ~ 5%) as secondary spin-trap. Experimental conditions a): 1 mM PT (stock solution in DMSO), 900 µM Cu(II), ± 200 µM $Zn(II)_7$MT-1 (ratio PT:Cu(II):$Zn(II)_7$MT-1 (1:0.9:0.2)), GSH 3 mM, HEPES buffer 50 mM, pH 7.4, and POBN 50mM. Experimental conditions b): 1 mM PT (stock solution in DMSO), 500 µM Fe(III), ± 200 µM $Zn(II)_7$MT-1 (ratio PT:Cu(II):$Zn(II)_7$MT-1 (1:0.9:0.2)), GSH 3 mM, TRIS buffer 50 mM, pH 7.4, and POBN 50 mM.

After addition of GSH and $Zn(II)_7$MT-1 to Cu(II)-PT and Fe(III)-PT no signal above the background, originating from HO•, was observed for Cu(II)-PT (right panel, **Fig 42a**), whereas a partial signal was still detected for Fe(III)-$(TSC)_2$.
This indicates that, Cu(I) transfer to MT-1 completely abolished the Cu(II)-PT mediated ROS production observed. In contrast $Zn(II)_7$MT-1 was only able to partially reduce the Fe(III)-$(TSC)_2$ mediated ROS production in the presence of GSH. This is in line with the fact that $Zn(II)_7$MT-1 can suppress the metal-catalyzed ROS production *via* two mechanisms:

- Mechanism 1): ROS scavenging, i.e. by destruction of the product (antioxidant effect);[53]
- Mechanism 2): metal-binding with concomitant redox-silencing of the complex and hence complete suppression of the metal-mediated ROS production (neutralization of the catalyst).[54]

Thus, $Zn(II)_7$MT-1 is able to completely suppress the production of HO• by Cu(I)-PT *via* binding and redox-silencing of Cu(I) (mechanism 2), but it is only able to inhibit the ROS produced by Fe(II)-PT because it cannot withdraw Fe, but is able to scavenge HO• (mechanism 1). This indicates that $Zn(II)_7$MT-1 is a more efficient ROS scavenger for Cu(I)-TSCs compared to Fe(II)--TSCs.

3.3.3 Summary of the main findings

The results described above for the reactivity of Cu(II)-Zn(II)-Fe(II)-PT/3-AP/Dp44mT complexes are summarized in **Table 5**. The reactivity depends not only on the type of ligand but also on the type of metal ion.

Table 5 - Table summarizing the reactivity of the Cu(II)/Zn(II)/Fe(II)-PT/3-AP/Dp44mT complexes with i) GSH, ii) $Zn(II)_7MT$-1 and ii) GSH in the presence of $Zn(II)_7MT$-1. Stability in the cytosol/nucleus refers to the metal complexes existing in the cytosol after reaction with GSH and $Zn(II)_7MT$-1 under physiological-like conditions.

TSC	M	Resistance to:			Stability in the cytosol/nucleus
		GSH	$Zn(II)_7MT$-1	GSH/$Zn(II)_7MT$-1	
PT	Cu(II)	✗	✗	✗	$Fe(II)-(PT)_2$
	Zn(II)	✗	-	-	
	Fe(II)	✓	✓	✓	
3-AP	Cu(II)	✗	✗	✗	$Fe(II)-(3\text{-}AP)_2$
	Zn(II)	✗	-	-	
	Fe(II)	✓	✓	✓	
Dp44mT	Cu(II)	✓	✗	✗	Zn(II)-Dp44mT $Fe(II)-(Dp44mT)_2$
	Zn(II)	✓	-	-	
	Fe(II)	✓	✓	✓	

All the three $Fe(II)-(TSC)_2$ complexes were i) stable in the presence of GSH/$Zn(II)_7MT$-1, indicating that a $Fe(II)-(TSC)_2$ complex could exist for a longer time in the cytosol/nucleus and ii) able to catalyze the production of ROS. Indeed, $Zn(II)_7MT$-1 could only partially suppress the ROS production catalyzed by $Fe(II)-(PT)_2$ *via* $HO^{\bullet}$ scavenging. This supports the notion that Fe may be the most important metal complex in the biological activity of TSCs, with respect to these environments.

Concerning the $Zn(II)-(TSC)_2$ complexes, their reactivity with GSH was different depending on the TSC ligand. Zn(II)-PT and -3-AP dissociate partially within seconds in the presence of mM GSH, although not totally from Zn(II)-PT (~ 90%). However, considering that other Zn sites exist in a cell, which are often unoccupied, it is well possible that Zn dissociates almost completely and rapidly from Zn(II)-PT, entering the cytosol.[55] In contrast, $Zn(II)-(Dp44mT)_2$ dissociates very little, even at 10 mM GSH concentration (~ 16%). However, this dissociation is very rapid, so Zn(II) could be rapidly transferred to stronger Zn-binding sites if available in the cell.

The most complex behavior was observed for the Cu(II)-TSC complexes (**Fig 43**). Overall, Cu(II)-PT and -3-AP have very similar behaviors, where they only differ slightly by their kinetics, with 3-AP reacting faster than PT. Cu(II)-PT and -3-AP react within a few minutes with GSH and/or $Zn(II)_7MT$-1. First, a ternary complex with a thiolate is formed (*via* the cysteine of GSH or MT-1), then Cu(II) is reduced and dissociated from PT/3-AP. If $Zn(II)_7MT$-1 is present, Cu(I) ends up in MT-1, whereas if only GSH is present, Cu(I) binds to GSH. The fast reductive dissociation of Cu(II)-TSCs indicates that the lifetime of Cu(II)-PT/3-AP in the cytosol/nucleus may be quite short (couple of minutes), which limits quite significantly the time to produce ROS in these environments. Moreover, our data indicate that the ROS production by Cu-TSC is not very efficient. Thus, the question that arises is if it is really the complex Cu(II)-PT/3-AP/Dp44mT that is responsible for the biological activity or the combination of Cu(II)/Cu(I) on one side and free ligand PT/3-AP on the other side. Of course, this is only valid under the conditions found in the cytosol and nucleus, where high concentrations of GSH and $Zn(II)_7MT$-1 are present. In other

compartments, with less GSH and/or Zn(II)$_7$MT-1, Cu(II)-PT/3-AP may be stable and exhibit activity.

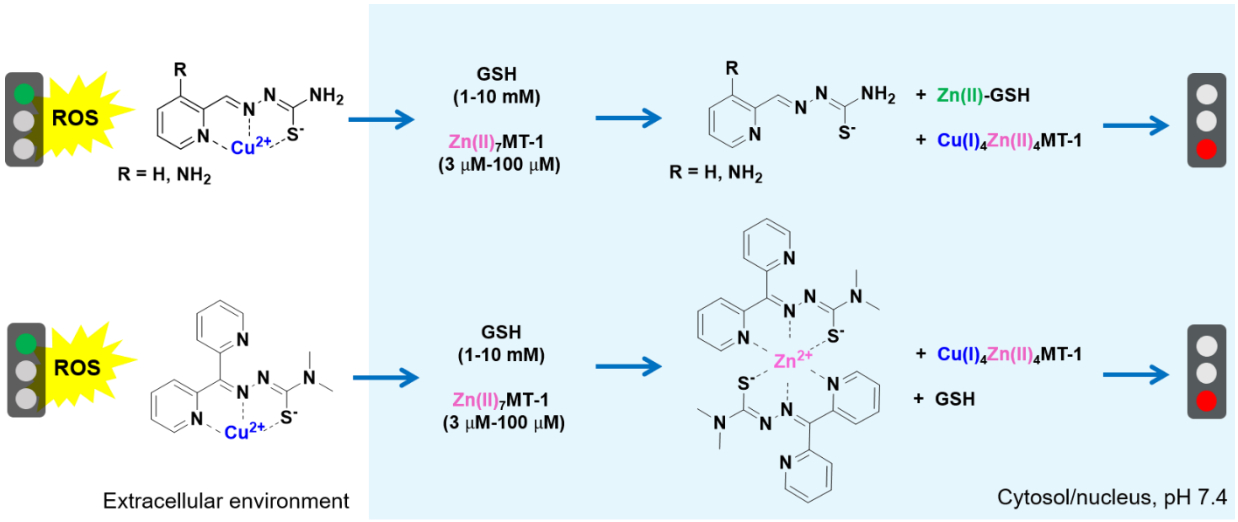

Fig 43 - Schematic representation of the reactivity of Cu(II)-TSCs complexes in the presence of physiological concentrations of GSH and Zn(II)$_7$MT-1 found in the cytosol and nucleus (pH 7.4).

On the other hand, Cu(II)-Dp44mT rapidly forms a ternary complex with GSH, [Dp44mT-Cu(II)-GSH], but this complex is stable and no transfer of Cu(I) to GSH is observed. This can be explained by the expected lower redox potential of Cu(II)-Dp44mT compared to 3-AP and PT due to the additional electron donating groups (2 methyl groups and one pyridine), stabilizing Cu(II), compared to Cu(I). Reduction to Cu(I) is a prerequisite for Cu transfer to GSH. However, Zn(II)$_7$MT-1 can react rapidly with Cu(II)-Dp44mT, also *via* first (i) formation of a ternary complex [Dp444mT-Cu(II)- Zn(II)$_7$MT-1], (ii) reduction of Cu(II) to Cu(I) and (iii) its transfer to MT-1. This indicates that with GSH and Zn(II)$_7$MT-1 concentrations typically found in cytosol and nucleus, Cu(II)-Dp44mT dissociates quite rapidly. The reason why Zn(II)$_7$MT-1 at only 6 µM concentration but not GSH at 3 mM can extract Cu(II) from Cu(II)-Dp44mT may be related to the lower reduction potential of MT and hence its greater efficiency in reducing Cu(II) to Cu(I) from Cu(II)-Dp44mT, and the stronger affinity of MT-1 for Cu(I) compared to GSH.

Another remarkable point is that after the reaction of Cu(II)-Dp44mT with Zn(II)$_7$MT-1, the released Zn(II) from Zn(II)$_7$MT-1 can bind to Dp44mT even when GSH is present. Hence, it is possible that in the case of Cu(II)-Dp44mT a transmetallation occurs when entering the cytosol or nucleus, with Cu(II)-Dp44mT being transformed into Zn(II)-(Dp44mT)$_2$. Of course the stability of the Zn(II)-(Dp44mT)$_2$ complex also depends on other competitors, as discussed above.

Besides, the EPR spin-trap experiment indicate that the mechanism of reductive dissociation of Cu(II)-TSCs with GSH and Zn(II)$_7$MT-1 leads to the complete deactivation of the Cu-based drugs as Cu(I)-binding to Zn(II)$_7$MT-1 fully ceases the formation of HO$^{\bullet}$, induced by Cu(II)-TSCs

The anticancer activity of some Zn(II)-TSCs has been attributed to the localization of the Zn(II)-TSC to the lysosome and subsequent transmetallation with Cu(II). From our data, the existence of a Zn(II)-TSC complex in the cytosol is possible for Dp44mT, but less likely for Zn(II)-3-AP and -PT, which will more likely enter the lysosome without Zn(II). GSH and MT concentrations in the lysosome are not well known. However, it is clear that the affinity of GSH and MT for Cu(I) and Zn(II) ions at lower pH ~ 5, as found in lysosomes, will dramatically decrease. Also the metal affinities of TSCs decrease with a decrease in pH, but to a lesser extent because metal-binding to

TSCs is possible for protonated TSCs since the protonated nitrogen is not involved directly in the Cu(II)-coordination.[27] Hence, from the data presented above, the proposed mechanism of formation of Cu(II)-TCS complexes in the lysosome and its induced lysosomal membrane permeabilization and cytotoxicity is not contradicted.[31] They rather support this view. Moreover, they are consistent with the study by Kraker et al., which showed the transfer of Cu(II) to MT from the Cu(II)-complex of 3-ethoxy-2-oxobutyraldehyde bis(thiosemicarbazonato) after being taken up by cells.[42]

3.4 Cu-based drugs: catalytic redox-activity in ROS generation *vs* stability under cytosol/nucleus like conditions

3.4.1 Introduction and aim of the study

As already discussed, Cu metabolism appear to be severely altered in neoplastic diseases and this has led to the research, development and investigation of several Cu-based drugs which are able to target and kill cancer cells. In this respect, pro-oxidant ligands, that are able to enhance Cu-reactivity by forming a Cu-complex that promote Cu-redox cycling and generation of ROS, have been particularly investigated.

Therefore, in the last part of this study, we tried to understand whether a Cu-based drug might be stable as Cu-complex and at the same time efficiently catalyze the production of ROS, under conditions found in the cytosol/nucleus, i.e. in the presence of elevated concentrations of Cu-binding and/or reducing biomolecules. Hence, we explored and investigated the correlation between stability against GSH/$Zn(II)_7$MT-1 and redox-activity in the presence of $AscH^-$, with some of the Cu-complexes (containing different families of ligands) which have been developed and studied for their anticancer activity.[56,57] As the redox-potential of a Cu-complex (associated with the redox-couple Cu(II)/Cu(I)) gives an indication of the possibility of a Cu-complex to fast redox cycling between Cu(I) and Cu(II) redox states, with physiological redox partners, we included in our study several Cu-complexes with redox potentials that vary significantly from ~ -0.6 to 0.6 V vs NHE. The ligands which have been included in this study are shown in **Fig 24**:

- Cyclam (L7), Bleomycin (L11), ATSM (L6), CQ (L13) APDTC (L12) (redox potential Cu-complexes: < - 400 mV vs NHE);
- GTSM (L5), Dp44mT (L4) (redox potential Cu-complexes ~ - 200 mV vs NHE)
- Phen (L9), 5,5'DmBipy (L8) (redox potential Cu-complexes ~ 200 mV vs NHE)
- BCS (L10) (redox potential Cu-complex ~ 600 mV vs NHE)

The catalytic activity in ROS production of the Cu-complexes was studied *via* consumption/oxidation of the substrate $AscH^-$ by absorbance spectroscopy at λ_{max} = 265 nm, whereas their stability with GSH/$Zn(II)_7$MT-1 was investigated by absorbance and luminescence spectroscopy at 77K.

3.4.2 Results and discussion

a. Evaluation of the catalytic redox-activity of the Cu-complexes with O_2 and $AscH^-$

To start our investigation, we addressed the question concerning the Cu(II)/Cu(I)-redox-activity of all the selected Cu-complexes, in the presence of $AscH^-$ as reducing agent, at pH 7.4. $AscH^-$ is one of the highest concentrated reducing agents, from 100 µM to several mM. Based on the reaction scheme reported in *Fig 2*, the ability of a Cu-complex to fast oxidizing $AscH^-$, correlates with an efficiency in redox-cycling between Cu(II) and Cu(I) redox states and hence in catalyzing the generation of ROS (pro-oxidant activity).

Measurements were performed by monitoring the consumption of the substrate $AscH^-$ at λ_{max} = 265 nm ($\varepsilon = 14500\ M^{-1}cm^{-1}$), as already shown for Cu(II)-XZH ATCUN complexes. The activities of the Cu-complexes were compared to that of free Cu(II) in buffer.
At first, experiments were carried out triggering the oxidation of $AscH^-$ with the preformed Cu-complexes after 10 min as highlighted by the black arrow (**Fig 44a**). The histogram in **Fig 44b** and **Table 6** show the corresponding initial molar $AscH^-$ oxidation rates in µM/min, with the corresponding standard deviation errors.

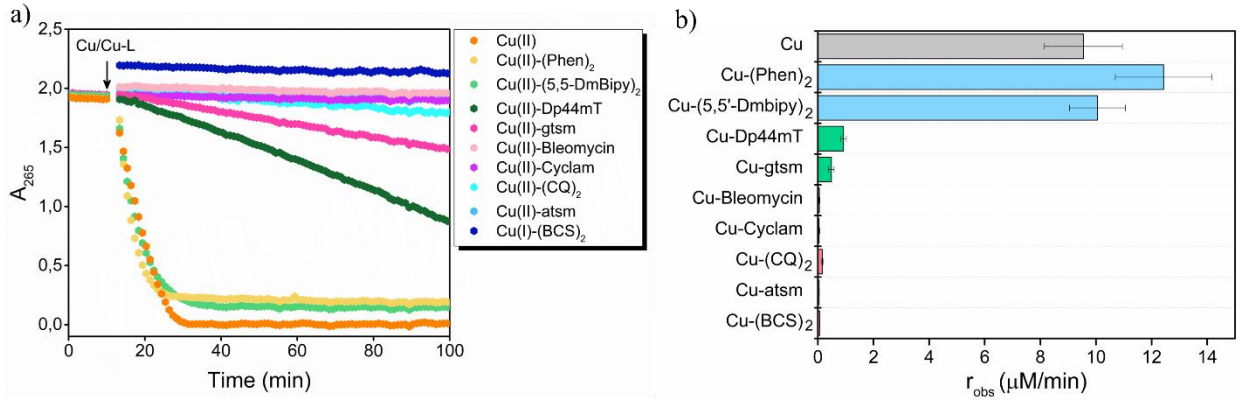

Fig 44 - a) Time course of $AscH^-$ oxidation monitored by absorbance spectroscopy at λ_{max}= 265 nm. $AscH^-$ oxidation was started by the addition of the preformed Cu(II)-complexes after 10 min (black arrow). b) Histogram of the corresponding molar $AscH^-$ oxidation rates (µM/min). Measurements were performed in triplicate, with different solutions at different days, thus average values of r_{obs} (µM/min) with standard deviations are reported. Experimental conditions: Cu(II) 5 µM, L 6 µM/12 µM or 10 µM (CQ), $AscH^-$ 100 µM, in HEPES 50 mM, pH 7.4.

Based on the efficiency in $AscH^-$ oxidation in the presence of O_2, under the given experimental conditions, i.e. 100 µM $AscH^-$ and 5 µM Cu-complex at pH 7.4, the studied Cu-complexes can be divided into three groups, i.e.:

- Group 1: Cu(II)-$(Phen)_2$, Cu(II)-$(5,5'DmBipy)_2$ (light blue bars, **Fig 44b**):

  They oxidize $AscH^-$ slightly more rapidly or as rapidly as free Cu, with initial rates of 12.4 ± 1.7 and 10.1 ± 1.0 µM/min (see **Table 6)** respectively. If we assume that the ROS production correlates with $AscH^-$ consumption (based on scheme reported in **Fig 2**), Cu(II)-$(Phen)_2$ and Cu(II)-$(5\text{-}5'DmBipy)_2$ would be much more efficient catalysts for the production of ROS, compared to the other Cu-complexes. This correlates with the favourable redox-potentials of Cu(II)-$(Phen)_2$ and Cu(II)-$(5,5'DmBipy)_2$ complexes for Cu(II) reduction to Cu(I) (i.e. ~ 0.2 V vs NHE) in the presence of $AscH^-$ ($E°\ AscH^-/AscH^{\bullet-}$ = 0.28 V).

- Group 2: Cu(II)-Dp44mT, Cu(II)-gtsm (green bars, **Fig 44b**):

  They oxidize $AscH^-$ but very slowly with initial rates of about less than one order of magnitude than complexes of group 1. This correlates with their more negative redox potentials. Thus, reduction of Cu(II)-Dp44mT and Cu(II)-gtsm to Cu(I)-Dp44mT and Cu(I)-gtsm, which represents the step 1 to start the Cu(II)-catalysed ROS production in presence of $AscH^-$ is thermodynamically less favoured.

- Group 3: Cu(I)-$(BCS)_2$, Cu(II)-$(CQ)_2$, Cu(II)-Cyclam, Cu(II)-Bleomycin (pink bars, **Fig 44b**)

  They are very inefficient catalysts to produce ROS and thus almost completely block the oxidation of $AscH^-$, with values of initial rates even lower or similar in case of Cu(II)-$(CQ)_2$ to that of the background of $AscH^-$ oxidation, in which no Cu and ligands are present (**Table 6**). The very low catalytic redox-activity of the Cu-complexes of this group relates to their either too negative (Cu(II)-$(CQ)_2$, Cu(II)-Cyclam, Cu(II)-Bleomycin) or too positive (Cu(I)-$(BCS)_2$, redox-potentials, not accessible for $AscH^-/AscH^{\bullet -}$ redox-couple.

In case of Cu(II)-$(APDTC)_2$ complex it was not possible to measure the activity in $AscH^-$ oxidation because of solubility issues. Thus, we decided to follow $AscH^-$ oxidation catalyzed by all the Cu-complexes generated *in situ*, i.e. triggering the reaction with free Cu, after (**Fig 45a**) or before (**Fig 45b**) the addition of the ligand in solution. Experiments were performed at lower concentration i.e. 1 µM Cu.

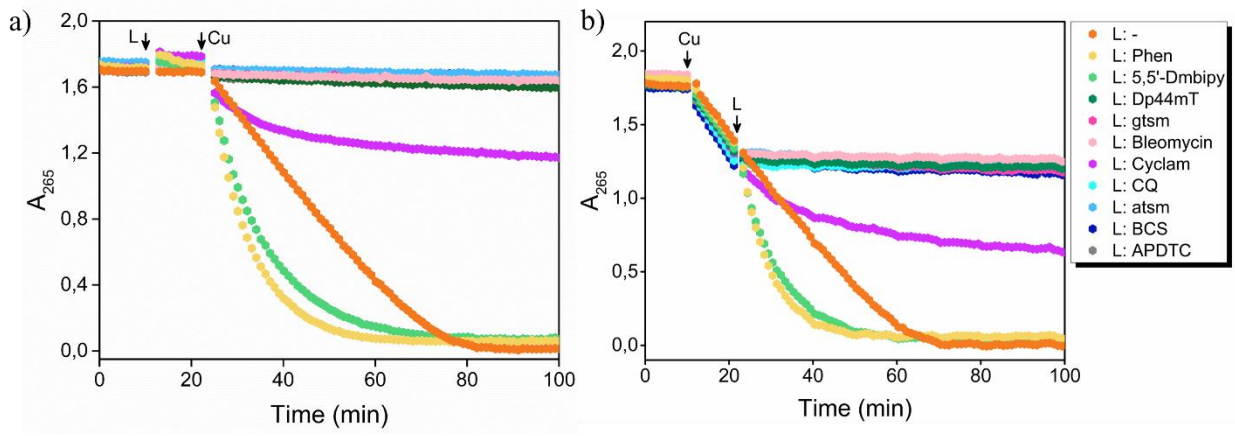

Fig 45 - Time course of $AscH^-$ oxidation monitored by absorbance spectroscopy at λ_{max}= 265 nm. $AscH^-$ oxidation was started by the addition of free Cu(II) a) after or b) before the addition of the ligand in solution (generation in-situ of the Cu-complexes). Experimental conditions: Cu(II) 1 µM, L 1.2 µM/2.4 µM or 2 µM in case of CQ, APDTC (ratio 1:1.2/1:2.4, 1:2.0), $AscH^-$ 100 µM, in HEPES 50 mM, pH 7.4.

The following observations can be made:

- APDTC completely stops the Cu-induced oxidation of $AscH^-$, meaning that Cu(II)/(I)-$(APDTC)_2$ redox-cycling is very inefficient. This is again in line with the thermodynamically unfavorable reduction of Cu(II)-$(APDTC)_2$ to Cu(I)-$(APDTC)_2$.[58] Indeed, although being a sulfur-containing ligand, APDTC does not stabilize well Cu(I). This is likely due to low π-acceptor character of the ligand.

- Cyclam does not arrest the oxidation of $AscH^-$ immediately. This is in line with the slow kinetic of complexation of Cu(II) observed for unsubstituted tetraazamacrocycles.[59] Nevertheless, once the Cu(II)-Cyclam is formed, it cannot be reduced by $AscH^-$ as probed by the absence of $AscH^-$ oxidation (**Fig 44**).

- At 1 µM concentration, Cu(II)-$(Phen)_2$, Cu(II)-$(5,5'DmBipy)_2$ oxidize $AscH^-$ much more rapidly than Cu in buffer. This result was confirmed also at lower concentration than 1 µM (results not shown). This indicates that at concentration of Cu(II)-$(Phen)_2$, Cu(II)-$(5,5'DmBipy)_2$ higher than 1 µM, the activity of the catalyst is not kinetically determinant, likely because the catalyst is not completely saturated.

b. Evaluation of the stability of the Cu-complexes with GSH and $Zn(II)_7$MT under cytosol/nucleus like conditions

Next, we investigated the stability of the Cu-complexes in the presence of physiological concentrations of GSH and Zn(II)-MT, found in the cytosol and nucleus. As already seen with the example of Cu(II)-TSC complexes in the previous study, in the presence of GSH and MT reactions of reductive dissociation can occur and lead very fast to the deactivation of the drug. The reactivity of the Cu-complexes with GSH/Zn(II)-MT was studied by i) absorbance spectroscopy, in order to be able to estimate the $t_{1/2}$ of Cu transfer to MT-1, and ii) luminescence at 77 K, to confirm Cu(I) binding to MT.

Low temperature luminescence represents a powerful tool in the structural investigation of Cu(I)-MTs, because of the characteristic luminescence properties of inorganic Cu(I)-thiolate clusters. The luminescence emission spectra of tetra-, hexanuclear and other similar clusters in MT have been deeply investigated.[60–62] In case of the $Cu(I)_4$-thiolate cluster found in $Cu(I)_4Zn(II)_4$MT-3 the LT emission spectrum is characterized by two emissive bands, one at high energy centered at 425 nm and one at low energy with maximum between 560-595 nm. The luminescence bands decay according to single exponential functions with lifetimes of ~ 40 and 130 ms respectively, which is consistent with their origin from two triplet-excited-states. The presence of two emissive bands has been correlated with the short internuclear Cu-Cu distances (< 2.8 Å), which allow metal-metal interactions and hence a d^{10}-d^{10} orbital.[54,63]

The luminescence characterization of Cu(I), Zn(II)MT species was carried out in collaboration with Prof. Gabriele Meloni and Jennifer Calvo at University of Texas, Dallas. Experiments monitored by absorbance spectroscopy were performed with MT-1 isoform, whereas those by LT luminescence with MT-2. Indeed, as shown before, the two isoforms have a similar behavior in terms of kinetic of Cu acquisition. Besides, in order to have a better resolution of the emission spectra, the concentration of MT used was 4 times higher compared to the conditions employed when the reactions were followed by absorbance spectroscopy (i.e. 2.5 µM Zn(II)MT-1 (ratio Cu-complex, Zn(II)MT-1).

In **Fig 46** the UV-Vis spectra for the reactions of the Cu-complexes with i) GSH and Zn(II)-MT-1 or ii) only GSH are shown. In **Fig 47** the corresponding LT luminescence spectra for the reaction with GSH and Zn(II)-MT-2 at t(0.5h) and t(4h) are reported. **FigS 28**, **FigS 29**, **FigS 30**, **FigS 31**, **FigS 32**, **FigS 33**, **FigS 34**, **FigS 35**, **FigS 36**, **FigS 37** show the LT luminescence spectra for the reaction with Zn(II)-MT-2 and GSH/Zn(II)-MT-2 at t(0.5h) and t(4h) for Cu(I)-$(BCS)_2$, Cu(II)-$(APDTC)_2$, Cu(II)-$(5,5'$-$DmBipy)_2$, Cu(II)-$(Phen)_2$, Cu(II)-ATSM, Cu(II)-Bleomycin, Cu(II)-$(CQ)_2$, Cu(II)-Cyclam, Cu(II)-GTSM and Cu(II)-Dp44mT respectively.

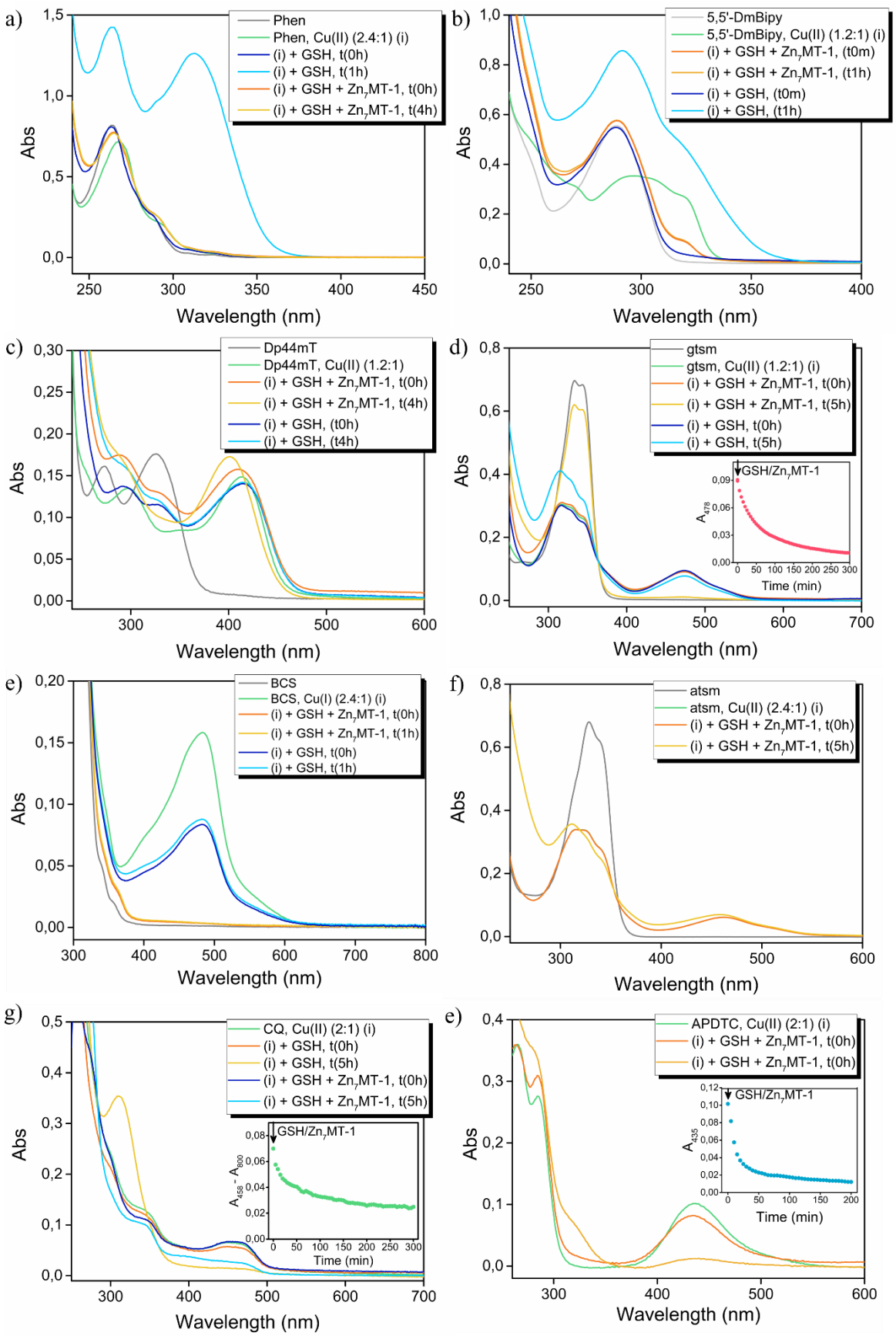

Fig 46 - Reactivity of the Cu-complexes with GSH/Zn(II)$_7$-MT-1 or GSH only monitored by absorbance spectroscopy. Experimental conditions: preformed Cu-complexes at 10 µM concentration were mixed with 2.5 µM Zn(II)$_7$-MT-1/3 mM GSH (ratio Cu-complex: Zn(II)$_7$-MT-1, 1:0.25), in 50 mM HEPES, pH 7.4, in the presence of 60% DMSO for Cu(II)-(CQ)$_2$ and Cu(II)-(APDTC)$_2$.

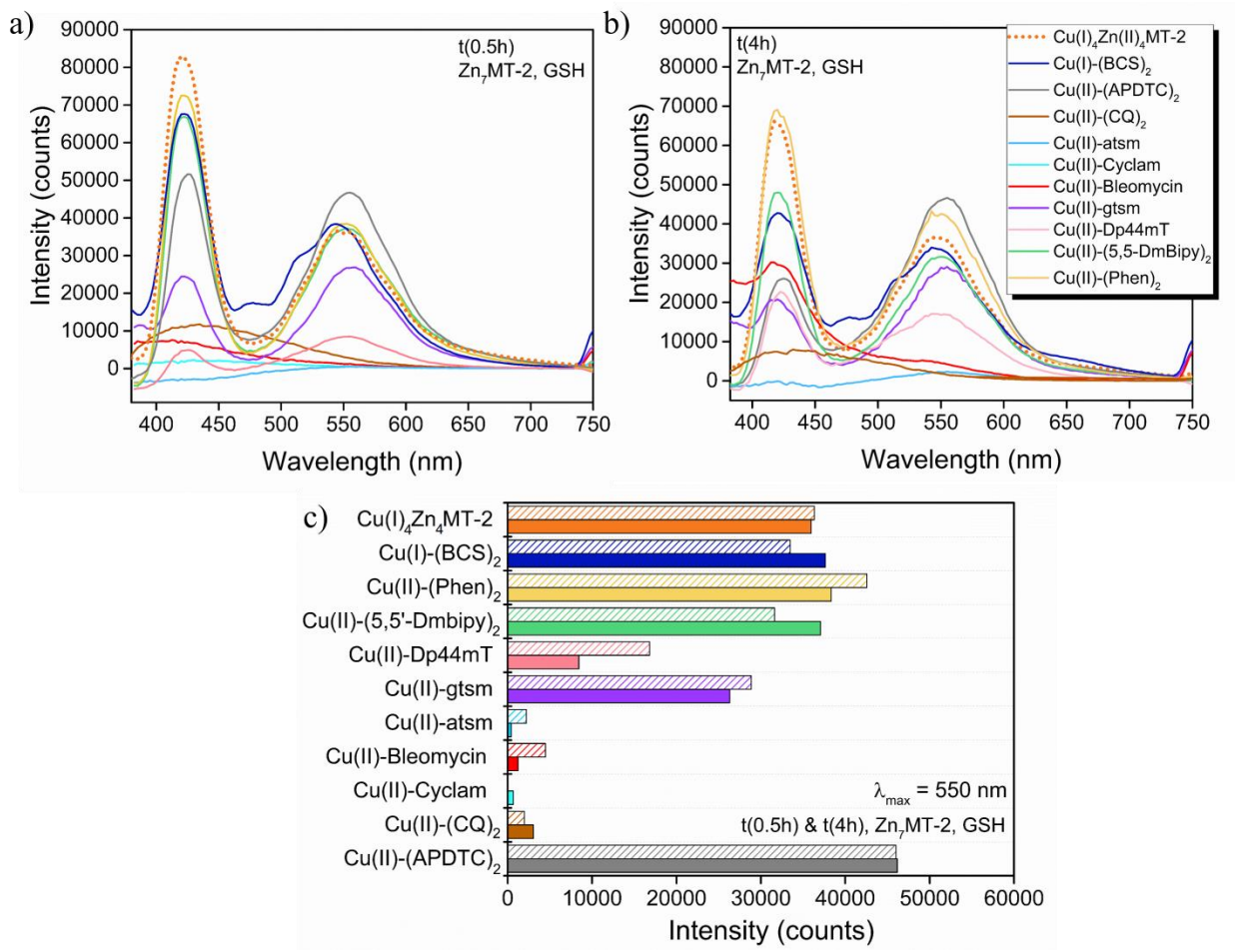

Fig 47 - Reactivity of the Cu-complexes with GSH/$Zn(II)_7$-MT-1 monitored by luminescence. The luminesce emission spectra in the region 280-750 nm were recorded on frozen samples at 77 K upon excitation at λ = 320 nm, for the reactions at a) t(0.5h) and t(4h). Experimental conditions: preformed Cu-complexes at 10 µM concentration were mixed with 2.5 µM $Zn(II)_7$-MT-2 (ratio Cu-complex: $Zn(II)_7$-MT-1, 1:0.25) and 3 mM GSH in 50 mM HEPES, pH 7.4. As a control, the luminesce spectrum of $Cu(I)_4Zn(II)_4$MT-2 complex is presented. c) Histogram displaying the values of intensity of the low energy emissive band centered at 550 nm, for the spectra recorded at t(0.5h) (solid bars) or t(4h) (striped bars) after the addition of GSH and $Zn(II)_7$MT-2 to the preformed Cu-complexes.

The following considerations can be made in terms of stability of the studied Cu-complexes with physiological concentrations of GSH and $Zn(II)_7$-MT :

- upon addition of 3 mM GSH/ 2.5 µM $Zn(II)_7$-MT-1, Cu(I)-$(BCS)_2$ at 10 µM dissociates within mixing-time and Cu(I) binds to MT finally as proven by i) the disappearance of the CT band of Cu(I)-$(BCS)_2$ at λ_{max} = 483 nm (**Fig 46e**) and the appearance of the characteristic LT luminescence spectrum of $Cu(I)_4Zn(II)_4$MT-2 at t(0.5h) (blue spectrum, **Fig 47a**). Under the given experimental conditions Cu(I) binding to MT is thermodynamically favored, thus MT/GSH irreversibly dissociates the complex. Only at higher concentration of hundreds µM Cu(I)-$(BCS)_2$ could resist to MT.[51]

- Cu(II)-$(Phen)_2$ and Cu(II)-(5,5'DmBipy)$_2$ dissociate as well within mixing-time with 3 mM GSH/2.5 µM $Zn(II)_7$-MT-1. This in line with i) their very fast reduction to Cu(I)-$(Phen)_2$ and Cu(I)-(5,5'DmBipy)$_2$[64] and ii) with the much lower thermodynamic stability of the Cu(I)-complexes compared to Cu(I)-MT complex (log β_2 [Cu(I)-$(Phen)_2$] = 15.8; values reported for unsubstituted Cu(I)-$(Bipy)_2$ are generally ~ 2 orders of magnitude lower compared to Cu(I)-$(Phen)_2$.)[65] Thus, as soon as Cu(II)-$(Phen)_2$ and Cu(II)-(5,5'DmBipy)$_2$ are reduced, Cu(I) is immediately taken and stabilized into $Cu(I)_4Zn(II)_4$MT complex. It is important to highlight

that because of the differences between log β_1, and log β_2, at 10 µM concentration the 1:2 complexes Cu(I)-$(Phen)_2$ and Cu(I)-(5,5'DmBipy)$_2$ are only partially formed.

- Reductive dissociation of Cu(II)-Dp44mT and Cu(II)-gtsm with 3 mM GSH/2.5 µM Zn(II)$_7$-MT-1 is slower compared to Cu(II)-$(Phen)_2$ and Cu(II)-(5,5'DmBipy)$_2$, i.e. at 10 µM concentration half of the complexes are dissociated within ~ 4 min and 50 min, respectively. This in line with the more negative redox potentials of Cu(II)-Dp44mT and Cu(II)-gtsm, thus with their slower reduction.[66,67] As seen before, GSH reacts with Cu(II)-Dp44mT with formation of a stable ternary complex, [Dp44mT-Cu(II)-GSH], which does not dissociate. Nevertheless, in the presence of Zn(II)$_7$MT-1 with or without GSH, Cu(II)-Dp44mT is rapidly dissociated and transmetallated, with formation of Zn(II)-(Dp44mT)$_2$. On the other hand, gtsm seems not to form a ternary complex neither with GSH nor with Zn(II)$_7$MT-1, in line with the complete equatorial coordination sphere. Only the axial positions are available for binding of an external ligand, which are much weaker than the equatorial ones. Nevertheless, Cu(II)-gtsm reacted with GSH in the absence of Zn(II)$_7$MT-1, and Cu(II) was reduced to Cu(I) but did only partially dissociate at 10 µM concentration (~ 20% of the complex within 5h) (**Fig 46d**). In contrast, in the presence of Zn(II)$_7$MT-1 the complex was completely dissociated in 4h/5h with Cu(I) irreversibly bound to MT in form of Cu(I)$_4$Zn(II)$_4$MT (violet spectrum, **Fig 46**, **Fig 47**). Results are in line with the reactivity already reported in the literature for Cu(II)-gtsm with GSH and BCS (used as mimic of intracellular Cu(I) binding proteins) and thus with the proposed Cu(II) uptake mechanism mediated by Cu(II)-gtsm, i.e. as it enters the cell it is immediately reduced with consequent Cu(I) dissociation from the ligand.
  Hence, the reason why Cu dissociation from Cu(II)-Dp44mT is faster could be to the fact that i) it can form a stronger ternary complex with MT and ii) to the higher affinity of the corresponding Zn(II)-Dp44mT complex compared to Zn(II)-gtsm. Indeed, as shown in **Fig 46d** after 5h the spectrum characteristic of Zn(II)-gtsm complex (λmax = 434 nm) could not be observed, meaning that Zn(II) released from MT was rather bound to GSH.

- Cu(II)-atsm, Cu(II)-Cyclam and Cu(II)-Bleomycin do not dissociate within 4h/5h in the presence of GSH/Zn(II)$_7$MT as shown by absorbance (only for Cu(II)-atsm) and luminescence spectroscopies. The stability of the complexes with GSH/Zn(II)$_7$MT correlates with the more negative redox potential of the complexes and hence with the fact that they are harder reduce.[67,68]

- Despite the very negative redox potentials, Cu(II)-$(CQ)_2$ and Cu(II)-$(APDTC)_2$ seem to dissociate relatively fast with GSH/Zn(II)$_7$MT-1 (~ 20 and 5 min respectively) as shown by the disappearance of the respective CT bands at λ_{max} = 458 nm and 436 nm. However, 60% of DMSO had to be included in the reaction mixture, because of solubility issues. This behavior would be in line with the lability of the second ligand in both the 1:2 complexes and hence with the possibility to be replaced by an external ligand, i.e. GSH or MT (i.e. *via* associative mechanism). On the other hand, when the reactions were monitored by LT luminescence (brown and grey spectra **Fig 47**), the luminescence spectrum of Cu(I)$_4$Zn(II)$_4$MT-2 complex was only detected for the reaction with Cu(II)-$(APDTC)_2$ but 60% DMSO was not included in the reaction mixture. We are currently repeating the experiments, under the same experimental conditions, to confirm the results obtained.

Finally, we studied the ability of Zn(II)$_7$MT-1 to suppress the Cu(II)-dependent catalyzed ROS production of the Cu(II)-$(Phen)_2$, Cu(II)-(5,5'DmBipy)$_2$ complexes, which would result in the complete deactivation of the Cu-based drugs. The experiment was carried out adding Zn(II)$_7$MT-

1/GSH to the Cu-complexes formed *in situ* during the oxidation of $AscH^-$ (which was monitored by absorbance spectroscopy from the band of $AscH^-$ at λ_{max} = 265 nm), triggered by free Cu (first arrow from the left, **Fig 48**).

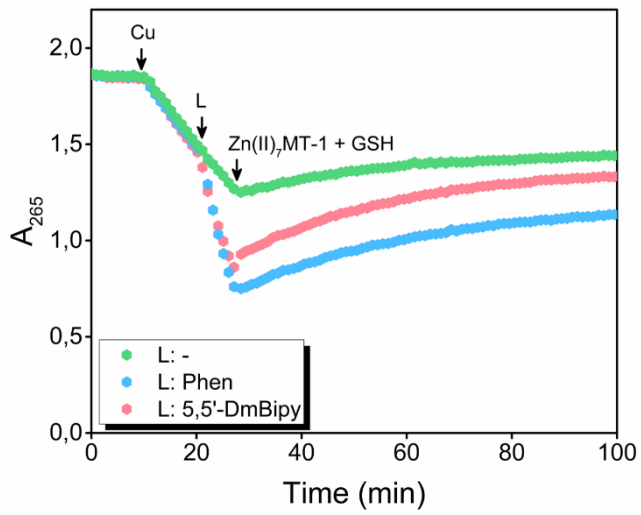

Fig 48 - Impact of $Zn(II)_7$-MT-1 and GSH on the time course of $AscH^-$ oxidation catalyzed by free Cu (green profile), Cu-$(Phen)_2$ (light blue profile), Cu-$(5,5'$-Dmbipy$)_2$ (green profile): evolution of $AscH^-$ absorption at λ_{max}= 265 nm as a function of time. $AscH^-$ oxidation was started by the addiction of free Cu (first arrow from the left) and monitored for 10 min before the addition of Phen or 5,5'-Dmbipy (generation in-situ of the Cu-complexes). Then, $Zn(II)_7$-MT-1 and GSH were added and the reaction monitored over time. Experimental conditions: Cu(II) 1 µM, Ligand 1.2 µM/2.4 µM (ratio 1:1.2/1:2.4), $AscH^-$ 100 µM, GSH 2 mM, $Zn(II)_7$-MT-1 2.5 µM, in HEPES 50 mM, pH 7.4.

When $Zn(II)_7$MT-1 and GSH were added in solution, $AscH^-$ oxidation was immediately arrested, indicating that Cu(I) binding to MT completely stopped the ROS production, redox-silencing Cu(II)-$(Phen)_2$, Cu(II)-$(5,5'$DmBipy$)_2$ complexes.

3.4.3 Summary of the main findings

The results discussed above concerning the reactivity of several Cu-based drugs in terms of catalytic redox-activity in ROS generation (with $AscH^-$ and O_2) and stability with thiol-reducing molecules such as GSH and $Zn(II)_7MT$ are summarized in **Table 6**. The redox-potentials of the Cu-complexes vary significantly depending on the ligand set, and consequently on the geometric arrangement around the Cu center.

Table 6 - Table summarizing the i) $t_{1/2}$ (min or sec) values of Cu release from the selected Cu(II)-complexes, calculated from the experimental kinetics of disappearance of the Cu(II) or Cu(I) CT bands, monitored by absorbance spectroscopy; ii) corresponding molar $AscH^-$ oxidation rates (µM/min), and ii) redox potentials (mV).

Cu-complex	$t_{1/2}$ transfer to MT-1 (with GSH)	r_{obs} $AscH^-$ oxidation (µM min^{-1})	Redox Potential (mV) [NHE]
Background	/	0.11 ± 0.06	/
Cu(II)	< 30 sec	9.5 ± 1.4	160[69]
Cu(II)-ATSM (6)	X	0.05 ± 0.01	-403[67]
Cu(II)-Cyclam (7)	X	0.05 ± 0,02	-736 (E_{pc})[59]
Cu(II)-Bleomycin (11)	X	0.06 ± 0.02	-
Cu(II)-$(CQ)_2$ (13)	~ 20 min	0.16 ± 0.04	-
Cu(II)-$(APDTC)_2$ (12)	~ 5 min	/	-
Cu(II)-GTSM (5)	~ 50 min	0.49 ± 0.10	-241[67]
Cu(II)-Dp44mT (4)	~ 4 min	0.92 ± 0.11	-210[66]
Cu(II)-(5,5'-DmBipy)$_2$ (8)	< 30 sec	10.1 ± 1.0	120[70]
Cu(II)-$(Phen)_2$ (9)	< 30 sec	12.4 ± 1.7	188[64] 170[70]
Cu(I)-$(BCS)_2$ (10)	< 30 sec	0.07 ± 0.01	618[71]

The results obtained show that the potential to have a pro-oxidant Cu-complex, in the presence of elevated concentrations of $AscH^-$, GSH and $Zn(II)_7MT$, as found in the cytosol and nucleus, depends not only on the ability of the Cu-complex to fast redox cycling between Cu(I) and Cu(II)-redox states, in the presence of physiological reductants, but also on the affinity of the ligands for Cu(I). Indeed, considering the reducing intracellular environment and the strong Cu(I) affinity for GSH and MT reaction, reactions of reductive dissociation can be very fast.

Overall, the experiments presented underline the complexity of having Cu(I)/(II) redox systems under conditions encountered in the cytosol/nucleus. Cu(II)-$(Phen)_2$, Cu(II)-(5,5'DmBipy)$_2$ are the complexes that show the highest activity in terms of $AscH^-$ oxidation. This correlates with their favorable redox potential (E° ~ 200 mV vs NHE), that depends on the 2(N,N) Cu-binding donor set provided by aromatic diamines ligands, that is capable of stabilizing both Cu(II) and Cu(I) oxidation states. Nevertheless, in the presence of GSH and $Zn(II)_7MT$, the thermodynamic stability of the Cu(I)-complexes in not high enough to resist to GSH and $Zn(II)_7MT$, resulting in the immediate dissociation of the Cu(I)-complexes as soon as the Cu(II)-complexes are reduced.

The reactivity observed for Cu(II)-ATSM, Cu(II)-Cyclam and Cu(II)-Bleomycin, indicate that Cu-complexes with very negative redox-potentials (< 400 mV vs NHE) could be stable under conditions found in the cytosol/nucleus, as they are very difficult to reduce with physiological reductants. On the other hand, a Cu(I)-complex, will not dissociate in the cytosol/nucleus only if it is thermodynamically more stable than Cu(I)-MT complex, i.e. if the affinity is higher than that of MT ($K_a > 10^{20}$). Studies with tetrathiomolybdate suggest that its affinity is sufficient to sequester Cu from MTs.[72] Besides, more recently, the Cu(I)-complex of PSP-2, a Cu(I) chelator that binds Cu(I) with low zeptomolar dissociation constant (logK = 20, 25 °C), has been shown to selectively reduce cellular Cu levels and to exhibit a significant anti-angiogenic activity.[73,74]

Considering that a Cu(I)/(II) redox system exist in the cytosol and nucleus, i.e. Cu-Zn SOD (SOD1), the question that arises is how nature does it. Once translated the nascent monomeric polypeptide of SOD1 binds one Zn ion, providing structural integrity before the direct interaction with CCS occurs. CCS delivers Cu ion into the active site and catalyzes the formation of an intra-subunit disulfide bond and the dimerization of two subunits (active enzyme).[75] Thus, Cu is kinetically trapped within the positively charged active site of the enzyme, while the rest of the surface is negatively charged.[69] This charge gradient increases the equilibrium concentration of superoxide near the active site channel. Therefore, despite the lower thermodynamic stability of the Cu, Zn SOD complex, MT does not retrieve Cu from the enzyme. However, this is difficult to obtain with small molecule drugs.

3.5 Reference list

1 D. S. Sigman, D. R. Graham, V. D. Aurora, A. M. Stern and D. Aurora, *J. Biol. Chem.*, 1979, **254**, 12269–12272.

2 D. S. Sigman, *Acc. Chem. Res.*, 1986, **19**, 180–186.

3 T. J. P. McGivern, S. Afsharpour and C. J. Marmion, *Inorganica Chim. Acta*, 2018, **472**, 12–39.

4 Z. Yu and J. A. Cowan, *Chem. - A Eur. J.*, 2017, **23**, 14113–14127.

5 K. C. Park, L. Fouani, P. J. Jansson, D. Wooi, S. Sahni, D. J. R. Lane, D. Palanimuthu, H. C. Lok, Z. Kovačević, M. L. H. Huang, D. S. Kalinowski and D. R. Richardson, *Metallomics*, 2016, **8**, 874–886.

6 P. Zhang and P. J. Sadler, *Eur. J. Inorg. Chem.*, 2017, **27**, 1541–1548.

7 V. Murray, J. K. Chen and L. H. Chung, *Int J Mol Sci.*, 2018, **19**, E1372.

8 M. Mital, N. E. Wezynfeld, T. Frączyk, M. Z. Wiloch, U. E. Wawrzyniak, A. Bonna, C. Tumpach, K. J. Barnham, C. L. Haigh, W. Bal and S. C. Drew, *Angew. Chemie Int. Ed.*, 2015, **54**, 10460–10464.

9 P. Gonzalez, K. Bossak, E. Stefaniak, C. Hureau, L. Raibaut, W. Bal and P. Faller, *Chem. - A Eur. J.*, 2018, 8029–8041.

10 Y. Jin and J. A. Cowan, *J. Am. Chem. Soc.*, 2005, **127**, 8408–8415.

11 A. N. Pham, G. Xing, C. J. Miller and T. D. Waite, *J. Catal.*, 2013, **301**, 54–64.

12 L. Perrone, E. Mothes, M. Vignes, A. Mockel, C. Figueroa, M. C. Miquel, M. L. Maddelein and P. Faller, *ChemBioChem*, 2010, **11**, 110–118.

13 T. Miyamoto, Y. Fukino, S. Kamino, M. Ueda and S. Enomoto, *Dalt. Trans.*, 2016, **45**, 9436–9445.

14 M. Pitié and G. Pratviel, *Chem. Rev.*, 2010, **110**, 1018–1059.

15 M. E. Rice, 2000, 209–216.

16 B. Chance, H. Sies and A. Boveris, *Physiol. Rev.*, 1979, **59**, 527–605.

17 K. H. S. Schwab, J. Shearer, S. E. Conklin, B. Alies, *J Inorg Biochem*, 2015, **25**, 368–379.

18 M. Z. Wiloch, U. E. Wawrzyniak, I. Ufnalska, A. Bonna, W. Bal, S. C. Drew and W. Wróblewski, *J. Electrochem. Soc.*, 2016, **163**, G196–G199.

19 Z. Xiao, J. Brose, S. Schimo, S. M. Ackland, S. La Fontaine and A. G. Wedd, *J. Biol. Chem.*, 2011, **286**, 11047–11055.

20 J. F. Perez-Benito, *J. Inorg. Biochem.*, 2004, **98**, 430–438.

21 E. Atrián-Blasco, M. Del Barrio, P. Faller and C. Hureau, *Anal. Chem.*, 2018, **90**, 5909–5915.

22 H. Beraldo and D. Gambino, *Mini-Reviews Med. Chem.*, 2004, **4**, 31–39.

23 F. M. and H. S. G. Domagk, R. Behnisch, *Naturwissenschaften*, 1946, 315–320.

24 R. Wallace, J. Richard Thomson, M. J. Bell and H. E. Skipper, *Cancer Res.*, 1956, **16**, 167–170.

25 F. Lynn, M. Manuel, L. King, M. John, M. Angela, S. Niramol, B. MacDonald, Patricia Plezia and S. Almassian, Elizabeth Colacino, Jessica Fischer, *Cancer Chemother. Pharmacol.*, 2002, **50**, 223–229.

26 C. M. Nutting, C. M. L. van Herpen, a B. Miah, S. a Bhide, J.-P. Machiels, J. Buter, C. Kelly, D. de Raucourt and K. J. Harrington, *Ann. Oncol.*, 2009, **20**, 1275–1279.

27 P. Heffeter, V. F. S. Pape, E. A. Enyedy, B. K. Keppler, G. Szakas and C. R. Kowol, *Antioxid. Redox Signal.*, 2018, ars.2017.7487.

28 S. P. Kunos, Charles; Chu, Edward; Beumer, Jan; Sznol, Mario; Ivy, S.; Kunos, Charles A; Beumer, Jan H; Ivy, *Cancer Chemother. Pharmacol.*, 2017, **79**, 201–207.

29 M. Whitnall, J. Howard, P. Ponka and D. R. Richardson, *Proc. Natl. Acad. Sci. U. S. A.*, 2006, **103**, 14901–14906.

30 É. A. Enyedy, N. V. Nagy, É. Zsigó, C. R. Kowol, V. B. Arion, B. K. Keppler and T. Kiss, *Eur. J. Inorg. Chem.*, 2010, 1717–1728.

31 A. E. Stacy, D. Palanimuthu, P. V. Bernhardt, D. S. Kalinowski, P. J. Jansson and D. R. Richardson, *J. Med. Chem.*, 2016, **59**, 4965–4984.

32 C. R. Kowol, W. Miklos, S. Pfaff, S. Hager, S. Kallus, K. Pelivan, M. Kubanik, É. A. Enyedy, W. Berger, P. Heffeter and B. K. Keppler, *J. Med. Chem.*, 2016, **59**, 6739–6752.

33 K. Ishiguro, Z. P. Lin, P. G. Penketh, K. Shyam, R. Zhu, R. P. Baumann, Y. L. Zhu, A. C. Sartorelli, T. J. Rutherford and E. S. Ratner, *Biochem. Pharmacol.*, 2014, **91**, 312–322.

34 E. C. Moore, B. A. Booth and A. C. Sartorelli, *Cancer Res.*, 1971, **31**, 235–238.

35 A. Popović-Bijelić, C. R. Kowol, M. E. S. Lind, J. Luo, F. Himo, É. A. Enyedy, V. B. Arion and A. Gräslund, *J. Inorg. Biochem.*, 2011, **105**, 1422–1431.

36 Y. Aye, M. J. C. Long and J. Stubbe, *J. Biol. Chem.*, 2012, **287**, 35768–35778.

37 Y. Yu and D. R. Richardson, *J. Biol. Chem.*, 2011, **286**, 15413–15427.

38 P. J. Jansson, P. C. Sharpe, P. V. Bernhardt and D. R. Richardson, *J. Med. Chem.*, 2010, **53**, 5759–5769.

39 J. García-Tojal, R. Gil-García, V. I. Fouz, G. Madariaga, L. Lezama, M. S. Galletero, J. Borrás, F. I. Nollmann, C. García-Girón, R. Alcaraz, M. Cavia-Saiz, P. Muñiz, Ò. Palacios, K. G. Samper and T. Rojo, *J. Inorg. Biochem.*, 2018, **180**, 69–79.

40 W. E. Antholine and F. Taketa, *J. Inorg. Biochem.*, 1984, **20**, 69–78.

41 C. R. Kowol, P. Heffeter, W. Miklos, L. Gille, R. Trondl, L. Cappellacci, W. Berger and B. K. Keppler, *J. Biol. Inorg. Chem.*, 2012, **17**, 409–423.

42 A. Kraker, S. Krezoski, J. Schneider, D. Minkel and H. Petering, *J. Biol. Chem.*, 1985, **260**, 13710–13718.

43 M. T. Morgan, L. A. H. Nguyen, H. L. Hancock and C. J. Fahrni, *J. Biol. Chem.*, 2017, **292**, 21558–21567.

44 A. Krezel and W. Bal, *Bioinorg. Chem. Appl.*, 2004, **2**, 293–305.

45 R. C. Hider and X. L. Kong, *BioMetals*, 2011, **24**, 1179–1187.

46 É. A. Enyedy, M. F. Primik, C. R. Kowol, V. B. Arion, T. Kiss and B. K. Keppler, *Dalt. Trans.*, 2011, **40**, 5895.

47 A. Gaál, G. Orgován, Z. Polgári, 4 Réti, AndreaComplex forming competition and in-vitro toxicity studies on the applicability of di-2-pyridylketone-4, V. G. Mihucz, S. Bosze, N. Szoboszlai and C. Streli, *J. Inorg. Biochem.*, 2014, **130**, 52–58.

48 D. Mahendiran, N. Pravin, N. S. P. Bhuvanesh, R. S. Kumar, V. Viswanathan, D. Velmurugan and A. K. Rahiman, *ChemistrySelect*, 2018, **3**, 7100–7111.

49 R. W. Byrnes, M. Mohan, W. E. Antholine, R. X. Xu and D. H. Petering, *Biochemistry*, 1990, **29**, 7046–7053.

50 J. Peisach and W. E. Blumberg, *Arch. Biochem. Biophys.*, 1974, **165**, 691–708.

51 J. S. Calvo, V. M. Lopez and G. Meloni, *Metallomics*, 2018, **10**, 1777–1791.

52 X. Yu, A. Blanden, A. T. Tsang, S. Zaman, Y. Liu, J. Gilleran, A. F. Bencivenga, S. D. Kimball, S. N. Loh and D. R. Carpizo, *Mol. Pharmacol.*, 2017, **91**, 567–575.

53 M. Sato and I. Bremner, *Free Radic. Biol. Med. Med.*, 1992, **14**, 325–337.

54 G. Meloni, P. Faller and M. Vašák, *J. Biol. Chem.*, 2007, **282**, 16068–16078.

55 W. Maret, *Metallomics*, 2015, **7**, 202–211.

56 Z. Zhang, H. Wang, M. Yan, H. Wang and C. Zhang, *Mol. Med. Rep.*, 2017, **15**, 3–11.

57 M. McCann, A. L. S. Santos, B. A. Da Silva, M. T. V. Romanos, A. S. Pyrrho, M. Devereux, K. Kavanagh, I. Fichtner and A. Kellett, *Toxicol. Res. (Camb).*, 2012, **1**, 47–54.

58 A. R. Hendrickson, R. L. Martin and N. M. Rohde, *Inorg. Chem.*, 1976, **15**, 2115–2119.

59 A. Conte-Daban, M. Beyler, R. Tripier and C. Hureau, *Chem. - A Eur. J.*, 2018, **24**, 8447–8452.

60 D. L. Pountney, I. Schauwecker, J. Zarn and M. Vašák, *Biochemistry*, 1994, **33**, 9699–9705.

61 P. C. Ford, E. Cariati and J. Bourassa, *Chem. Rev.*, 1999, **99**, 3625–3647.

62 M. J. Stillaman, A. S. Zelazowski, J. Szymanska and Z. Gasyna, *Inorganica Chim. Acta*, 1989, **161**, 275–279.

63 G. Meloni, V. Sonois, T. Delaine, L. Guilloreau, A. Gillet, J. Teissié, P. Faller and M. Vašák, *Nat. Chem. Biol.*, 2008, **4**, 366–372.

64 M. Pitié, M. Pitié, B. Donnadieu, B. Donnadieu, B. Meunier and B. Meunier, *Inorg. Chem.*, 1998, **37**, 3486–3489.

65 J. M. Vaal, K. Mechant and R. L. Rill, *Nucleic Acids Res.*, 1991, **19**, 3383–3388.

66 P. V. Bernhardt, P. C. Sharpe, M. Islam, D. B. Lovejoy, D. S. Kalinowski and D. R. Richardson, *J. Med. Chem.*, 2009, **52**, 407–415.

67 Z. Xiao, P. S. Donnelly, M. Zimmermann and A. G. Wedd, *Inorg. Chem.*, 2008, **47**, 4338–4347.

68 C. Esmieu, D. Guettas, A. Conte-Daban, L. Sabater, P. Faller and C. Hureau, *Inorg. Chem.*, 2019, acs.inorgchem.9b00995.

69 R. Rakhit and A. Chakrabartty, *Biochim. Biophys. Acta - Mol. Basis Dis.*, 2006, **1762**, 1025–1037.

70 G. B. Postnikova and E. A. Shekhovtsova, *Biochem.*, 2016, **81**, 1735–1753.

71 D. Chen, D. Jiang, F. Zhou, N. Darabedian, T. Kai and Z. Li, *Anal. Biochem.*, 2015, **497**, 27–35.

72 H. M. Alvarez, Y. Xue, C. D. Robinson, M. A. Canalizo-hernández, J. E. Penner-hahn and T. V. O. Halloran, *Science (80-.).*, 2010, **327**, 331–335.

73 D. M. Heuberger, S. Harankhedkar, T. Morgan, W. Petra, M. Calcagni, B. Lai, C. J. Fahrni and J. Buschmann, 2019, 1–10.

74 F. Saeedifard, M. T. Morgan, J. Bacsa and C. J. Fahrni, *Inorg. Chem.*, , DOI:10.1021/acs.inorgchem.9b00965.

75 J. B. Proescher, M. Son, J. L. Elliott and V. C. Culotta, *Hum. Mol. Genet.*, 2008, **17**, 1728–1737.

76 J. L. J. Dearling, J. S. Lewis, G. E. D. Mullen, M. J. Welch and P. J. Blower, *J. Biol. Inorg. Chem.*, 2002, **7**, 249–259.

77 H. Beraldo, L. P. Boyd and D. X. West, 1998, **71**, 67–71.

CHAPTER 4

General conclusion

4.1 Main findings

The aim of the work presented in this thesis was to get a better knowledge about the impact of MTs and other smaller Cu-binding and reducing biomolecules, such as GSH, Cys, $AscH^-$ and Glu, on the redox-activity and stability of some medicinal relevant Cu-complexes. We decided to focus our study on different groups of complexes, i.e. pathophysiological Cu-complexes of Aβ peptides, which are considered to be neurotoxic in AD, and Cu-based drugs, which have been devolved and studied for their potential application as therapeutics for a variety of diseases, including cancer. The main findings of two respective parts are stated below.

❖ Case study I: pathophysiological Cu(II)-Aβ complex of the N-truncated Aβ peptide, $A\beta_{4\text{-}16}$ (model for $A\beta_{4\text{-}42}$)

- Cys and GSH accelerate the rate of Cu transfer from $A\beta_{4\text{-}16}$ to $Zn(II)_7$MT-3, *via* Cu(II) reduction to Cu(I) and Cu(I) shuttling over MT-3;
- Glu accelerate the kinetic of Cu transfer from $A\beta_{4\text{-}16}$ to MT-3, likely *via* an associative mechanism, i.e. transiently forming a ternary complex [Glu-Cu(II)-$A\beta_{4\text{-}16}$];
- Partially loaded $Zn(II)_{7\text{-}x}$MT-3 species acquire Cu faster from Cu(II)-$A\beta_{4\text{-}16}$, proportionally to extent of Zn depletion and hence the number of available unbound-thiol groups;
- GSH, Cys and Glu indirectly affect the Zn distribution between $A\beta_{4\text{-}16}$ and MT-3, being Zn(II) bound to $A\beta_{4\text{-}16}$ at the end of the reaction. Thus, they are modulators of the Cu/Zn distribution between the two biomolecules;
- Depending on external stimuli or stress Cu/Zn distribution between $A\beta_{4\text{-}16}$ and MT-3 can be influenced by multiple partners which act cooperatively, i.e. a Zn-binding biomolecule could abstract Zn from $Zn(II)_{7\text{-}x}$-MT-3 and indirectly influence Cu-trafficking and/or a Cu-binding biomolecule could accelerate the rate of Cu transfer to MT-3 and indirectly affect Zn-trafficking.

Taken together these results suggest that physiological small biomolecules like Cys, GSH and Glu might be implicated in the trafficking of Cu(II)-$A\beta_{4\text{-}x}$ complex, by impacting the synthesis of the redox-silent complex $Cu(I)_4Zn(II)_4$-MT-3. Considering that fluctuations of these molecules can occur, they could impact the distribution of Cu/Zn ions between the two biomolecules downregulated under AD conditions. Therefore, they are important parameters to be considered. Nevertheless, what Cu binding does to $A\beta_{4\text{-}x}$ peptide is still not clear. Cu(II)-$A\beta_{4\text{-}x}$ complex does not produce ROS, so one could argue that $A\beta_{4\text{-}x}$ might have a protective role. On the other hand, as Cu can influence aggregation, it could potentially increase its toxicity.

❖ Case study 2: Cu-based drugs

- The catalytic redox activity of Cu(II) bound to the motif NH_2–Xxx-Zzz-His (ATCUN) with $AscH^-$ and H_2O_2/O_2 is very low and can be stopped via Cu(I)-chelation with BCS. This result

strongly impacts its application as an artificial Cu-enzyme to degrade biomolecules *via* ROS production in a Cu(I)-chelator rich environment like the cytosol/nucleus.

- Cu(II)-TSC complexes are rapidly (minutes) dissociated with physiological concentrations of GSH and $Zn(II)_7$-MT, found in the cytosol and nucleus, and Cu(I) is taken up by MT, with generation of $Cu(I)_4Zn(II)_4MT$ species.
- In case of Cu(II)-Dp44mT, it is also possible that a transmetallation occurs when entering the cytosol or nucleus, with Cu(II)-Dp44mT being transformed into $Zn(II)\text{-}(Dp44mT)_2$.
- The mechanism of reductive dissociation of Cu(II)-TSCs leads to the complete deactivation of the drugs in terms of the often proposed ROS production, as Cu(I)-binding to $Zn(II)_7MT$ completely stops the ROS production induced by Cu(II)-TSCs.
- A redox active Cu(I)/Cu(II)-complex will exist as Cu-complex in the cytosol and nucleus only if it resists to GSH/$Zn(II)_7$MT, i.e. if the Cu(I)-affinity of the Cu-complex is higher than that of MT (i.e. $K_a > 10^{20}$).

In general, the results obtained, concerning the reactivity of several Cu-complexes that display antineoplastic activity, indicate that the GSH/MT system is very efficient in withdrawing Cu from Cu-complexes at concentrations found in the cytosol and nucleus. Thus, these molecules are very important modulators and partners of Cu-based drugs and should be taken into consideration when designing a Cu-complex with targets in these environments. Moreover, they underly the complexity of designing an efficient pro-oxidant Cu-drug based on small molecules, capable of fast redox cycling between Cu(II)/Cu(I) redox states with intracellular physiological reductants and in the presence of strong Cu(I)-chelators.

In conclusion, the results presented in this thesis show that MTs can have a major impact on the fate of a medicinal Cu-complex, having either a neuroprotective role against toxic Cu-complexes, such as Cu(II)-Aβ under AD conditions, or being modulators and deactivators of Cu-based drugs in the cytosol and nucleus.

4.2 Critical discussion and future directions

The research work that has been presented in this thesis is a chemical study, showing the reactivity of several Cu-complexes under physiological-similar conditions found in cellular and extracellular compartments. In my opinion, these studies although carried out under *in vitro* conditions, which of course could be modulated *in vivo,* are extremely important. Indeed, they can help in understanding the fundamental mechanisms of various complex systems and pathways in biology at the molecular level. This knowledge is required to be able to control and modulate biological processes, especially disease-relevant biological pathways, and thus to develop more efficient therapeutics. Hence, I believe that that the results of this thesis pave the long way for novel therapies that may challenge global problems like dementia and cancer.

When conducting this type of research, one of the most important parameters to consider is the *in vitro* concentration of the various components of the reaction-mixture, which should be at least comparable to that found *in vivo*. Exact concentrations of biomolecules (like MTs, GSH, Cys, and $AscH^-$) are mostly known for the intracellular environments (especially cytosol and nucleus), but much less is known for the extracellular space, and in particular in or around the synaptic cleft, where Aβ aggregates are found. Nevertheless, in our studies, we tried to respect, when possible, physiological relevant concentrations of the different biomolecules. The main limit is the

sensitivity of techniques used (i.e. Uv-Vis, CD, fluorescence ^{1}H-NMR, EPR, ESI-MS) which in some cases is not high enough to allow to work in the very low µM range. Nevertheless, we tried to respect always at least the relative ratios between the different compounds (e.g. Cys, GSH and Glu are more concentrated than $A\beta_{4-x}$ peptide and MT).

Overall, our studies highlight that the existence of a Cu-complex in a biological medium strongly depends on its reactivity with multiple partners. For instance, we were able to show that different small physiological molecules, despite their lower Cu(II) reducing power and Cu(I)-binding affinity compared to MTs, can accelerate the rate of Cu transfer to MT *via* different mechanisms. Moreover, the reaction with Glu and EDTA is particularly interesting, it shows that multiple mechanisms may also act cooperatively (leading to additive effects) or complement each other. Hence, considering the multitude of different small molecules that exist together in a biological media and are present at high concentration, this thesis paves the way for further research in this direction.

Despite there are still many aspects to clarify concerning the function of MTs in the development and progression of AD, it is clear that they play an important role, especially regarding their interaction with metal ions and oxidative stress. Considering this, MTs could serve as inspiration for metal-based therapeutic strategies, either by mimicking their chemistry for the development of new chelators or *via* control of their expression for the optimal regulation of metal ions in the brain.

Concerning the development of Cu-prooxidant complexes to be used as anticancer therapeutics, with our test tube experiments we have shown the challenge to have a redox-active Cu-complex able to efficiently catalyze ROS with physiological concentration of GSH and MT, because of their strong reducing power and Cu(I)-affinity. Nevertheless, in other organelles where MT is not present, like the lysosome or mitochondria, they might be active as Cu-complexes and thus this strategy might be exploited to kill cancer cells.

In collaboration with Dr. Christian Gaiddon, during the preparation of this thesis, we have also attempted to see how the MT concentration affects the activities of Cu-TSC complexes in cells. Experiments were performed using Hela cells and inducing MT expression with dexamethasone. Despite some encouraging results, in which we observed that dexamethasone slightly increases the IC_{50}, suggesting that increased MT reduces the toxicity induced by our complexes, the variability among the different experiments was too high to ascertain a statistical significance. We think that the variability between experiments might be linked to the volatile expression level of MT in cancer cells. Therefore, it would be interesting to correlate the intensity of the protective effect with the actual levels of MT expression in each experiment. Overall, significantly more experiments are needed to be performed to obtain and answer on this interesting question.

More in general, I believe that despite the challenge, inorganic chemists should continue their research in the development of Cu-based drugs. However, there is first an essential need to better understand the role that Cu plays in cancer etiology and pathogenesis, and to delineate which cancer types are appropriate for treatments that target Cu. Afterwards, efforts have to be made to better define the biological features of Cu coordination compounds ideal for their anticancer activity.

CHAPTER 5

Supporting material

5.1 Experimental section

5.1.1 Experimental section chapter 2

a. Materials

Tris base (2-amino-2-(hydroxymethyl)-1,3-propanediol), $CuCl_2 \cdot 7H_2O$, $ZnSO_4 \cdot 7H_2O$, TCEP (tris(2-carboxyethyl)phosphine hydrochloride), HCl (trace metal grade), EDTA ((ethylenedinitrilo)tetraacetic acid), PAR (4-(2-pyridylazo)resorcinol), L-Glutathione reduced, L-Cysteine were purchased from Sigma-Aldrich. L-Glutamic acid (Glu) was purchased from Fluka. KH_2PO_4, K_2HPO_4, HEPES buffer were purchased from Alfa Aesar. Trypton, yeast extract, LB Broth, agar, IPTG (agarose, isopropyl-β-D-1 thiogalactopyranoside), SDS (sodium dodecyl sulfate) were from Lab Empire, NaCl, NaOH, glycerol, $KH_2PO_4 \cdot H_2O$, K_2HPO_4 from POCH (Gliwice Poland), pTYB21 vector and chitin resin from New England BioLabs. DTNB (5,5'-dithiobis-(2-nitrobenzoic acid)) from TCI Europe N.V., DTT (DL-dithiothreitol) from Iris Biotech. All solutions were prepared with milli-Q water obtained with a deionizing water system (Merck Millipore, USA).

b. Peptide synthesis and quantification

The N-truncated $A\beta_{4-16}$ peptide (AA sequence: FRHDSGYEVHHQK-NH_2), model for the full length $A\beta_{4-42}$ peptide, was synthesized according to Fmoc strategy and purified by HPLC as already described in the literature.[1] A stock solution of the $A\beta_{4-16}$ peptide was prepared by dissolving the powder in Milli-Q water (resulting pH = 2). The peptide concentration was determined by absorbance spectroscopy from free Tyr^{10} absorption with $\Delta\varepsilon(\lambda_{276-296}) = 1410\ M^{-1}$ at pH 2. This was confirmed by Cu(II) titration in 50 mM PB, pH 7.4, monitored by absorbance spectroscopy through the d-d band of the 1:1 complex Cu(II)-$A\beta_{4-16}$ at $\lambda_{max} = 525$ nm. The titration was carried out by adding portions of a 10 mM $CuCl_2$ stock solution to $A\beta_{4-16}$ peptide.

c. MT-3 preparation and reconstitution with Zn(II)

$Zn(II)_7$-MT-3 used for the study with Cys and GSH: a pet-3d (Novagen) plasmid encoding for human MT-3 sequence was used for recombinant protein expression. $Zn(II)_7$MT-3 was expressed in Escherichia coli strain BL21(DE3)pLys and purified as previously described in the literature.[2]

A stock solution of $Zn(II)_7$MT-3 was prepared by dissolving the powder in 20 mM Tris-HCl, pH 8.6. In order to remove DTT (previously added to preserve the thiol groups from oxidation), a SEC (size exclusion chromatography) column was run, employing a PD mini trap G10 column, equilibrated with PB 10 mM, pH 7.4.

$Zn(II)_7$-MT-3 used for the study with Glu and EDTA: the coding cDNA sequence of human metallothionein-3 (MT-3) was purchased from GenScript (USA) and cloned into the pTYB21

vector (New England Biolabs). The expression vector was transformed into BL21(DE3)pLysS *E. coli* component cells and the protein was expressed as intein fusion.[3] The bacteria were cultured (4 × 1L) in rich full growth medium (1.1% tryptone, 2.2% yeast extract, 0.45% glycerol, 1.3% K_2HPO_4, 0.38% KH_2PO_4) until OD_{600} reached 0.5 at 37°C, then induced with 0.1 mM IPTG and incubated overnight at 20°C with vigorous shaking. Cells were collected by centrifugation at 4 000 × g for 10 min at 4°C, suspended in 200 ml cold buffer A (20 mM HEPES, pH 8.0, 500 mM NaCl, 1 mM EDTA, 1 mM TCEP) and sonicated for 30 min followed by centrifugation at 20,000 × *g* for 45 min at 4°C. Clear supernatant was incubated with 10 ml of a chitin resin (New England Biolabs) overnight with mild shaking at 4°C. The resin was than washed 5-6 times with 25 ml of the same buffer and the cleavage reaction was initiated by adding DTT to a final concentration of 100 mM in buffer A without TCEP. MT-3 was cleaved from resin for 48 h at room temperature with mild mixing. The eluted supernatant containing MT-3 protein was acidified to pH ca. 2.4 using 7% HCl and concentrated using Amicon Ultra-4 Centrifugal Filter Units (Millipore). The concentrated apo-protein was purified using a SEC-70 column (Bio-Rad) equilibrated with 10 mM HCl using Bio-Rad NGC system. The identity of the protein was confirmed using mass spectrometry, on an API 2000 ESI-MS instrument (Applied Biosystems). The m/z values found/calculated were 6925.3/6921.5. Thionein (apo-MT3) was mixed with 10 molar equivalents of $ZnSO_4$ in the presence of 2 mM TCEP under anaerobic conditions.[4] The pH of the solution was adjusted to 8.6 using 1 M Tris base. The sample was concentrated similarly as above and purified on SEC-70 column equilibrated with 20 mM Tris-HCl, pH 8.6. The collected fractions with MT-3 were concentrated and used immediately for experiments or stored at -80°C.

The concentrations of Zn(II) ions, thiols and the total protein were determined spectrophotometrically using PAR and DTNB assays[5,6] or by UV range measurements at 220 nm. Accordingly, MT-3 contained 7.06 ± 0.10 Zn(II) ions per molecule.

d. General procedures and kinetic studies

A Cu(II) stock solution (100 mM) was prepared in Milli-Q water from $CuCl_2 \cdot 2H_2O$. Its concentration was verified by absorbance spectroscopy at λ = 780 nm, pertaining to the Cu(II) aqua ion d-d band (ε = 12 $M^{-1}cm^{-1}$). A Zn(II) stock solution (100 mM) was prepared in Milli-Q water from $ZnSO_4 \cdot 7H_2O$.

Stock solutions of Cys and GSH (100 mM) were freshly prepared daily by dissolving their powders in to a 72.4 mM solution of HCl in Milli-Q water. An EDTA stock solution (100 mM) was prepared by dissolving the powder in MQ water and increasing the pH up to 8 by adding a 5 M NaOH solution. A Glu stock solution (100 mM) was prepared by dissolving the powder in 100 mM PB at pH 7.4.

PB (500 mM), pH 7.4, was prepared by mixing potassium dihydrogen phosphate 99 % (KH_2PO_4) with potassium hydrogen phosphate 98 % (K_2HPO_4) in Milli-Q water, adjusting the pH with a 5M NaOH solution.

Stock solutions when further diluted to the desired concentration for the following experiments.

The reactions have been performed in triplicate (experiment 1, 2 and 3) at different days with different stock solutions of peptide, protein, Cys or GSH, EDTA and Glu. Kinetics of Cu(II) transfer from $A\beta_{4\text{-}16}$ to MT-3 were reproducible and no significant differences were observed. Representative measurements (1st experiment) are shown in the Figures.

Since the initial kinetic of Cu(II)Aβ_{4-16} + Zn(II)$_7$MT-3 varies with the stock solution of Zn(II)$_7$MT-3, we used the acceleration factor for statistical analysis, i.e. the relative value compared to the different Zn(II)$_7$MT-3 preparations.

5.1.2 Experimental section chapter 3 - part 1

a. Materials

N-α-Fmoc-protected amino acids for peptide synthesis and coupling reagents were obtained from Novabiochem or IrisBiotech. Cu(II) ion source, $Cu(Cl)_2 \cdot 2H_2O$, sodium ascorbate, hydrogen peroxide solution 30 % (w/w) in H_2O, Bathocuproinedisulfonic acid disodium salt (BCS), 3-coumarin carboxylic acid (3-CCA), L-Histidine, POBN spin strap, were purchased from Sigma Aldrich and used without further purification. KH_2PO_4, K_2HPO_4, HEPES (buffer preparation) were purchased from Alfa Aesar. 5,5'-dimethyl-2,2'-dipyridyl (5,5'-DmBipy) and 1,10-Phenantroline (Phen) were a gift from Dr. Romain Ruppert (UMR7177- Institut de Chimie, Strasbourg).

b. Peptide synthesis

H-DAHK-OH and H-FRHD-OH were purchased from Genecust (Dudelange, Luxemburg). The peptide H-KGHK-NH2 was synthesized according to the Fmoc/tBu strategy, purified by RP-HPLC and controlled by ESI-MS: observed monoisotopic m/z: $[M^+H^+]$ = 468.40; calculated monoisotopic m/z: $[M^+H^+]$ = 468.30.

c. General procedures

Stock solutions of the peptides were prepared by dissolving the powder in Milli-Q water (resulting pH = 2). Concentration of the peptides was determined by Cu(II) titration in 50 mM PB, pH 7.4, monitored by absorbance spectroscopy through the d-d band of the 1:1 complex Cu(II)-XZH at λ_{max} = 525 nm. Titrations (shown in FigS 1) were carried out by adding portions of a 10 mM $CuCl_2$ stock solution to the peptides.

A stock solution of His (100 mM) was prepared in Milli-Q water; stock solutions of 5,5'-DmBipy (100 mM) and Phen (100 mM) were prepared in 100 % DMSO and then further diluted in H_2O.

A stock solution of Cu(II) (100 mM) was prepared in Milli-Q water from $CuCl_2 \cdot 2H_2O$ and then further diluted for the different experiments. Its concentration was verified by absorbance spectroscopy from the Cu(II) d-d band at 780 nm (ε = 12 $M^{-1}cm^{-1}$).

A stock solution of PB (500 mM, pH 7.4) was prepared by mixing potassium dihydrogen phosphate 99 % (KH_2PO_4) with potassium hydrogen phosphate 98 % (K_2HPO_4) in Milli-Q water, adjusting the pH with a 5 M solution of NaOH. A stock solution of HEPES buffer (500 mM, pH 7.4) was prepared by dissolving HEPES (free acid) in Milli-Q water, adjusting the pH with a 5 M solution of NaOH.

A stock solution of sodium ascorbate (500 mM) and H_2O_2 (500 mM) were freshly prepared daily in Milli-Q water. A stock solution of BCS (50 mM) was prepared in Milli-Q water. A stock solution of the spin-trap POBN (500 mM) was prepared in 500 mM PB, pH 7.4.

d. $AscH^-$ oxidation followed by absorbance spectroscopy

$AscH^-$ oxidation ($[AscH^-]$ = 100 μM) was monitored by absorbance spectroscopy at λ = 265 nm in 50 mM PB/HEPES, pH 7.4 with or without H_2O_2. After monitoring $AscH^-$ oxidation

for 5-10 min, free Cu(II) or the preformed Cu(II)-complex was added ([Cu(II)] = 10 μM) and the reaction monitored over time. Kinetics of ascorbate oxidation were performed in triplicate at different days with different solutions. $AscH^-$ solutions were prepared freshly every day. Only representative measurements are shown in the figures. The molar $AscH^-$ oxidation rate (μM/min) was obtained by dividing the slope of the variation in $AscH^-$ concentration by the extinction coefficient of $AscH^-$ (ε = 14500 $M^{-1}cm^{-1}$).[7] The average values of r_{obs} (μM/min) with standard deviations are reported in Fig 4b.

e. Fluorescence detection of HO• with CCA assay

Coumarin-3-carboxylic acid (CCA) was used to detect hydroxyl radicals (HO•). HO• generated reacts with CCA to form 7-hydrioxy-coumarin-3-carboxylic acid (7-OH-CCA), which upon excitation at λ = 390 nm emits at λ = 450 nm. To a solution containing 0.5 mM CCA, Cu(II) 25 μM and/or peptide 30 μM (ratio Cu(II):peptide, 1:1.2), and/or H_2O_2 250 μM in PB 50 mM, pH 7.4, $AscH^-$ was added to trigger the reaction. The final concentration of $AscH^-$ in the wells was 250 μM (stock solution 25 mM). Kinetics of HO•generation *via* fluorescence of 7-OH-CCA were performed at least 3 times at different days with different solutions. No significant differences were observed, and hence representative measurements are shown in the figures.

5.1.3. Experimental section chapter 3 - part 2

a. Materials

All solvents and reagents obtained from commercial suppliers were used without further purification. Cu(II) and Zn(II) ion sources, respectively the hydrated salts, $CuCl_2 \cdot 2H_2O$ and $ZnSO_4 \cdot 7H_2O$, L(+)-ascorbic acid sodium salt, L-glutathione reduced (GSH), TCEP (tris(2-carboxyethyl)phosphine hydrochloride), HCl (trace metal grade), PAR (4-(2-pyridylazo)resorcinol), EDTA (ethylenediaminetetraacetic acid), Tris base (Trizma, 2-amino-2-(hydroxymethyl)-1,3-propanediol), POBN (α-(4-pyridyl N-oxide)-N-tert-butylnitrone), tetrakis(acetonitrile)copper(I) hexafluorophosphate (Cu(I) source) were purchased from Sigma-Aldrich. The Fe source was an Fe(III) standard solution purchased from Fluka Analytical (1.001 g/l). Trypton, yeast extract, LB Broth, agar, agarose, IPTG (isopropyl-β-D-1 thiogalactopyranoside), SDS (sodium dodecyl sulfate), HEPES (*N*-2-hydroxyethylpiperazine-*N*'-2-ethanesulfonic acid) were from Lab Empire, NaCl, NaOH, glycerol, $KH_2PO_4 \cdot H_2O$, K_2HPO_4 from POCH (Gliwice Poland), pTYB21 vector and chitin resin from New England BioLabs. DTNB (5,5'-dithiobis-(2-nitrobenzoic acid)) from TCI Europe N.V., DTT (DL-dithiothreitol) from Iris Biotech. All solutions were prepared with Milli-Q water obtained with a deionizing water system (Merck).

Ligands: 3-aminopyridine-2-carboxaldehyde thiosemicarbazone (3-AP), di-2-pyridylketone-4,4,-dimethyl-3-thiosemicarbazone (Dp44mT) were purchased from Sigma Aldrich (purity ≥ 98%). Pyridine-2-carboxaldehyde thiosemicarbazone (PT) was purchased from Enamine Store (purity ≥ 95 %).

b. Protein expression and purification

Two different batches of $Zn(II)_7$MT-1 protein from mouse were used. 1) $Zn(II)_7$MT-1 overexpressed in *Escherichia coli* strain BL21(pLysS) which was purified as previously described. This batch of protein has been used for the experiments monitored by absorbance and EPR spectroscopy.[8] 2) $Zn(II)_7$MT-1 recombinantly produced in the laboratory of Dr. Ricard Albalat

(University of Barcelona) as previously reported.[9] This batch of protein has been used for the experiments followed by ESI-MS.

The coding cDNA sequences of metallothionein-2a (MT-2a) and metallothionein-3 (MT-3) were purchased from GenScript (USA) and cloned into the pTYB21 vector (New England Biolabs). The expression vectors were transformed into BL21(DE3)pLysS *E. coli* component cells and the protein was expressed as intein fusion.[10] The bacteria were cultured (depending on isoform 4-6 × 1 l) in rich full growth medium (1.1% tryptone, 2.2% yeast extract, 0.45% glycerol, 1.3% K_2HPO_4, 0.38% KH_2PO_4) until OD600 reached 0.5 at 37°C, then induced with 0.1 mM IPTG and incubated overnight at 20°C with vigorous shaking.[3] Cells were collected by centrifugation at 4 000 × *g* for 10 min at 4°C, suspended in 200 ml cold buffer A (20 mM HEPES, pH 8.0, 500 mM NaCl, 1 mM EDTA, 1 mM TCEP) and sonicated for 30 min followed by centrifugation at 20,000 × *g* for 45 min at 4°C. Clear supernatants were incubated with 10 ml of a chitin resin (New England Biolabs) overnight with mild shaking at 4°C. The resin was than washed 5-6 times with 25 ml of the same buffer and the cleavage reaction was initiated by adding DTT to a final concentration of 100 mM in buffer A without TCEP. MT proteins were cleaved from resin for 48 h at room temperature with mild mixing. The eluted supernatants containing MT-1e, MT-2 and MT-3 were acidified to pH ca. 2.5 using 7% HCl and concentrated using Amicon Ultra-4 Centrifugal Filter Units (Millipore). The concentrated apoproteins were purified using a SEC-70 column (Bio-Rad) equilibrated with 10 mM HCl using Bio-Rad NGC system. The identity of the protein was confirmed using mass spectrometry, on an API 2000 ESI-MS instrument (Applied Biosystems). The averaged molecular masses found/calculated were 6014.4/6014.1, 6043.3/6042.2 and 6925.2/6927.0 for MT-1e, MT-2 and MT-3, respectively. Apoproteins were mixed with 10 molar equivalents of $ZnSO_4$ in the presence of 2 mM TCEP under anaerobic conditions (argon atmosphere).[4] The pH of the solution was adjusted to 8.6 using 1 M Tris base. The sample was concentrated similarly as above and purified on SEC-70 column equilibrated with 20 mM Tris-HCl, pH 8.6. The collected fractions with MT proteins were concentrated and used immediately for experiments or stored at -80°C. The concentrations of Zn(II) ions, thiols and the total protein were determined spectrophotometrically using PAR and DTNB assays or by UV range measurements at 220 nm.[6] Accordingly, MT-1e, MT-2 and MT-3 contained 6.95 ± 0.11, 7.12 ± 0.07 and 7.06 ± 0.10 Zn(II) ions per molecule, respectively. MT-1e sample was used for the CD measurements.

c. General procedures

Stock solutions of the ligands were prepared in anhydrous DMSO (≥99.9%), as well as further diluted solutions. Concentration of the ligands were confirmed by titration of a Cu(II) solution of known concentration in HEPES buffer 100 mM, pH 7.4, monitored by UV-Visible Spectroscopy. A stock solution of Cu(II) (100 mM) was prepared by dissolving the salt in Milli-Q water. Its concentration was verified by absorbance spectroscopy through the Cu(II) d-d band at 780 nm (ε = 12 $M^{-1}cm^{-1}$). A stock solution of Cu(I) (3 mM) was prepared in CH_3CN under saturated argon atmosphere. A stock solution of Zn(II) (100 mM) was obtained by dissolving the salt in Milli-Q water. A stock solution of HEPES buffer (500 mM, pH 7.4) was prepared by dissolving HEPES (free acid) in Milli-Q water, adjusting the pH with a 5 M solution of NaOH. A Stock solution GSH (100 mM) was freshly prepared daily by dissolving the powder into a 72.4 mM solution of HCl in Milli-Q water. A stock solution of sodium ascorbate (100 mM) was freshly prepared daily in Milli-Q water. Spin-trap POBN stock solution (500 mM) was prepared in 500 mM PB, pH 7.4.

d. Preparation of the reaction mixtures

For all the studies deionized Milli-Q water (18 MW) was employed.
Cu(II)-PT, Cu(II)-3-AP, Cu(II)-Dp44mT complexes were generated by mixing a 30 µM solution of PT/3-AP/Dp44mT with a 27 µM solution of Cu(II), in HEPES 100 mM, pH 7.4.

Zn(II)-PT, Zn(II)-3-AP, Zn(II)-$(Dp44mT)_2$ complexes were generated by mixing a 30 µM solution of PT/3-AP/Dp44mT with a 20 µM solution or 15 µM (in case of Dp44mT) solution of Zn(II), in HEPES 100 mM, pH 7.4

Fe(II)-$(PT)_2$, Fe(II)-$(3\text{-}AP)_2$ and Fe(II)-$(Dp44mT)_2$ complexes were generated by mixing a 30 µM solution of PT/3-AP/Dp44mT with a 15 µM solution of Fe(III) in the presence of $AscH^-$ 5 mM (ratio (PT/Dp44mT:Fe(II), 1:0.5) in HEPES buffer 100 mM, pH 7.4.

Fe(III)-PT was generated by mixing a stock solution a 500 µM solution of Fe(III) with a 1 mM solution of PT in TRIS 50 mM, pH 7.4. The preformed complex was incubated for 30 min at 40° C before its use.

All the reactions monitored *via* absorbance spectroscopy and circular dichroism were carried out in the presence of HEPES buffer 100 mM, pH 7.4. Stock solutions of all the reactants were mixed inside quartz cuvettes (used for spectroscopic characterization) to obtain the final concentration desired and the reactions monitored over time. Reactions were carried out at RT, with or without O_2.

For Low T EPR experiments all samples were supplemented by 10 % v/v glycerol to ensure homogeneous sample distribution. Reaction mixtures were immediately transferred in to a 4 mm outer diameter quartz tubes (Wilmad-Labglass) and immediately freeze-quenched with liquid nitrogen prior to their introduction into the precooled cavity.

For EPR spin-trap experiments POBN was used as primary spin-trap and ~5 % of DMSO (from the ligand stock solution) was present in all samples and used as secondary spin-trap to enhance the EPR signal. Reaction mixtures (containing POBN) were immediately transferred in to a EPR capillary after addition of GSH or GSH/$Zn(II)_7$MT-1.

5.1.4 Experimental section chapter 3 - part 3

a. Materials

All solvents and reagents obtained from commercial suppliers were used without further purification. $CuCl_2 \cdot 2H_2O$, L(+)-ascorbic acid sodium salt, L-glutathione reduced (GSH), were purchased from Sigma-Aldrich. HEPES (buffer preparation) was purchased from Alfa Aesar.

Ligands: di-2-pyridylketone-4,4,-dimethyl-3-thiosemicarbazone (Dp44mT), Clioquinol (CQ), Ammonium pyrrolidinedithiocarbamate (APDTC) were purchased from Sigma Aldrich (purity ≥ 98%); bathocuproinedisulfonic acid disodium salt (BCS) was purchased from Alfa Aesar; Bleomycin sulfate was purchased from ETI; glyoxal-bis(N4-methyl-3-thiosemicarbazone) (GTSM) and diacetylbis(4-methyl-3-thiosemicarbazone) (ATSM) were prepared as described in literature procedures;[11,12] 5,5'-dimethyl-2,2'-dipyridyl (5,5'-DmBipy) and 1,10-Phenantroline (Phen) were a gift from Dr. Romain Ruppert (UMR7177- Institut de Chimie, Strasbourg).

b. Preparation of stock solutions and of the Cu-complexes

A stock solution of Cu(II) (100 mM) was prepared by dissolving the salt in Milli-Q water. Its concentration was verified by absorbance spectroscopy through the Cu(II) d-d band at 780 nm (ε = 12 $M^{-1}cm^{-1}$). A stock solution of HEPES buffer (500 mM, pH 7.4) was prepared by dissolving HEPES (free acid) in Milli-Q water, adjusting the pH with a 5 M solution of NaOH. A stock solution GSH (100 mM) was freshly prepared daily by dissolving the powder into a 72.4 mM solution of HCl in Milli-Q water. A stock solution of sodium ascorbate (100 mM) was freshly prepared daily in Milli-Q water.

Stock solutions of the ligands: Dp44mT, CQ, APDTC, GTSM, ATSM, Phen, 5,5'-DmBipy stock solutions were prepared in DMSO (≥ 99.9%) as well as further diluted solutions; BCS and Bleomycin stock solutions were prepared in H_2O.

Stock solutions of the Cu-complexes for $AscH^-$ oxidation were prepared at 500 µM Cu(II), whereas for luminescence experiments at 77 K at 100 µM Cu(II).

Cu(II)-$(APDTC)_2$, Cu(II)-$(CQ)_2$ complexes were generated in 50 mM HEPES, pH 7.4, with 80% DMSO, by mixing a 500 µM or 100 µM solution of Cu(II) with a 1 mM or 200 µM solution of the ligand (ratio Cu(II):L, 1:2).

Cu(II)-ATSM was generated in 50 mM HEPES, pH 7.4, with 80% DMSO, by mixing a 500 µM or 100 µM solution of Cu(II) with a 600 µM or 120 µM solution of ATSM (ratio Cu(II):L, 1:1.2).

Cu(II)-GTSM was generated in 50 mM HEPES, pH 7.4, with 60% DMSO, by mixing a 500 µM or 100 µM solution of Cu(II) with a 600 µM or 120 µM solution of GTSM (ratio Cu(II):L, 1:1.2).

Cu(II)-Cyclam, Cu(II)-Bleomycin was generated in 50 mM HEPES, pH 7.4, by mixing a 500 µM or 100 µM solution of Cu(II) with a 600 µM or 120 µM solution of GTSM (ratio Cu(II):L, 1:1.2).

Cu(II)-$(Phen)_2$, Cu(II)-$(5,5'DmBipy)_2$ complexes were generated in 50 mM HEPES, pH 7.4, by mixing a 500 µM or 100 µM solution of Cu(II) with a 1.2 mM or 240 µM solution of the ligand (ratio Cu(II):L, 1:2.4).

Cu(I)-$(BCS)_2$, was generated in 50 mM HEPES, pH 7.4, by mixing a 500 µM or 100 µM solution of Cu(II) with a 1.2 mM or 240 µM solution of the ligand (ratio Cu(II):L, 1:2.4).

Cu(II)-Dp44mT was generated in 50 mM HEPES, pH 7.4, with 20% DMSO, by mixing a 500 µM or 100 µM solution of Cu(II) with a 600 µM or 240 µM solution of GTSM (ratio Cu(II):L, 1:1.2).

c. $AscH^-$ oxidation followed by absorbance spectroscopy

$AscH^-$ oxidation ([$AscH^-$] = 100 µM) was monitored by absorbance spectroscopy at λ_{max}=265 nm in 50 mM HEPES, pH 7.4. $AscH^-$ autoxidation with O_2 was measured for 10 min, then the reaction was triggered i) by the addition of the preformed Cu(II)-complexes at 5 µM concentration or ii) by the addition of free Cu(II) at 1 µM before or after the addition of the ligand (ratio Cu:L, 1:1.2 or 1:2.4). The reactions were monitored over time for 100 min. Kinetics of $AscH^-$ oxidation were performed in triplicate, at different days with different stock solutions. The molar ascorbate oxidation rate (µM/min) was obtained by dividing the slope of the first 5 minutes of the variation in AscH- concentration by the extinction coefficient of $AscH^-$ (ε = 14500 M-1cm-1). Average values of r_{obs} (µM/min) and the corresponding standard deviation errors have been calculated.

d. Reactions of Cu-complexes with GSH and $Zn(II)_7MT$ followed by absorbance and luminescence spectroscopies

Absorbance spectroscopy: reaction mixtures were prepared inside quartz cuvette with a final volume of 100 µl. To preformed Cu(II)-complexes at 10 µM concentration, in 50 mM HEPES, pH 7.5 (with 60 DMSO% in case of Cu(II)-$(CQ)_2$ and Cu(II)-$(APDTC)_2$), GSH (100 mM) and $Zn(II)_7$MT-1 (160 µM) were added to obtain a final concentration of 3 mM and 2.5 µM respectively (ratio Cu(II): $Zn(II)_7$MT-1, 1:0.25). Reactions were monitored over time collecting intermediate spectra at 5 min intervals.

Luminescence at 77 K: 500 µl samples of 10 µM Cu-L in 50 mM HEPES, pH 7.4 were reacted with 2.5 µM $Zn(II)_7$MT-2 with or without 3 mM GSH for 0.5 h or 4 h at 25^{o}C, transferred to quartz tubes with 2 mm inner diameter, and immersed in cylindrical quartz Dewar filled with liquid nitrogen.

5.2 Methods

a. Absorbance spectroscopy

UV-Vis measurements were performed on a Cary 60 spectrophotometer at room temperature (~25 °C) or on a Clario Star Plate reader (AscH- oxidation). Stock solutions of all the reactants were mixed directly inside quartz cuvettes of 1 cm path length or inside a 96 wells transparent microplate with a final volume of 100 µl. The obtained spectra are expressed in absorbance.

b. Emission spectroscopy

Fluorescence measurements with 3-CCA were performed on a Clario Star Plate reader. Stock solutions of all the reactants were mixed inside a 384 wells black microplate, with a final volume of 100 µl. The obtained spectra are obtained in fluorescence intensity (counts).

Low-temperature luminescence spectra and decays lifetime were collected using a FluoroMax-4 spectrofluorometer (Horiba Scientific). 500 µl samples (reaction mixtures) were transferred to quartz tubes with 2 mm inner diameter and immersed in cylindrical quartz Dewar filled with liquid nitrogen. Emission spectra (380–750 nm, 5 nm slit) were obtained at 77 K with excitation at 320 nm (5 nm slit), using 10 ms initial delay and 300 ms sample window. Lifetime measurements were performed for the emissive bands at 425 nm and 575 nm using 75 ms initial delay and 300 ms sample window. 10 ms and 20 ms delay increments and 500 ms and 1000 ms maximum delays were used for the 425 nm and 575 nm bands, respectively.

c. Circular dichroism spectroscopy

Circular dichroism measurements were carried out on a Jasco J-810 or on a J-815 sectropolarimeter with a scanning speed of 50 nm/min. Stock solutions of all the reactants were mixed directly inside quartz cuvettes of 1 cm path length (with a final volume of 100 µl). The obtained spectra are express as ellipticity (mdeg).

d. ^{1}H-NMR spectroscopy

^{1}H-NMR experiments were recorded with a Bruker Avance III 400 MHz spectrometer. All spectra were calibrated with respect to the D_2O signal (4.79 ppm). NMR spectra were collected at 298 K in 10% D2O/H2O, 50 mM PB at pH 7.4, using the watergate suppression technique.

e. EPR spectroscopy

Both low temperature (100K) and room temperature (294 ± 1K) spin trapping investigations were performed on an EMX X-band spectrometer (EMXplus from Bruker Biopsin GmbH, Germany), equipped with a high sensitivity resonator (4119HS-W1, Bruker).

The g factor was calibrated in the experimental conditions using the Bruker strong pitch (g = 2.0028). Principal spectrometer settings for spin-trapping: Center Field: 3510 G, Sweep Width: 80 G, Microwave power: 4.5 mW, Modulation Amplitude: 1 G, Gain: 50 dB, Conversion Time: ca 250 ms, Time Constant: ca. 80 ms, 1 scan/720 pts/180sec. Low temperature was achieved using continuous flow liquid nitrogen cryostat. Principal spectrometer settings for low temperature: Center Field: 3100 G, Sweep Width: 1500 G, Microwave power: 0.1 mW, Modulation Amplitude: 5 G, Gain: 30 dB, Conversion Time: ca. 200 ms, Time Constant: ca. 80 ms, 3 scans/1500 pts/300sec each.

The room temperature spin trapping investigations were carried out with α-(4-Pyridyl N-oxide)-N-tert-butylnitrone (POBN), used as primary spin trap, and EtOH (5% v/v), added as hydroxyl scavenger to enhance the detection of the $HO^{\bullet}$ produced.

f. ESI-MS

ESI-MS measurements were performed with a MicroTOF-Q (Brucker Daltonics GmbH, Bremen, Germany) instrument equipped with an electrospray ionization source (ESI) in positive mode, interfaced with a Series 1200 HPLC Agilent pump, equipped with an autosampler. The system was controlled by the Compass Software. Conditions used were those optimized for metal-metallothionein samples analysis: 40 µl/min flow rate, in a spectra collection range 800-2500 m/z. The carrier buffer was a 5:95 mixture of acetonitrile:ammonium acetate/ammonia (15 mM, pH 7.0).

5.3 Supplementary figures

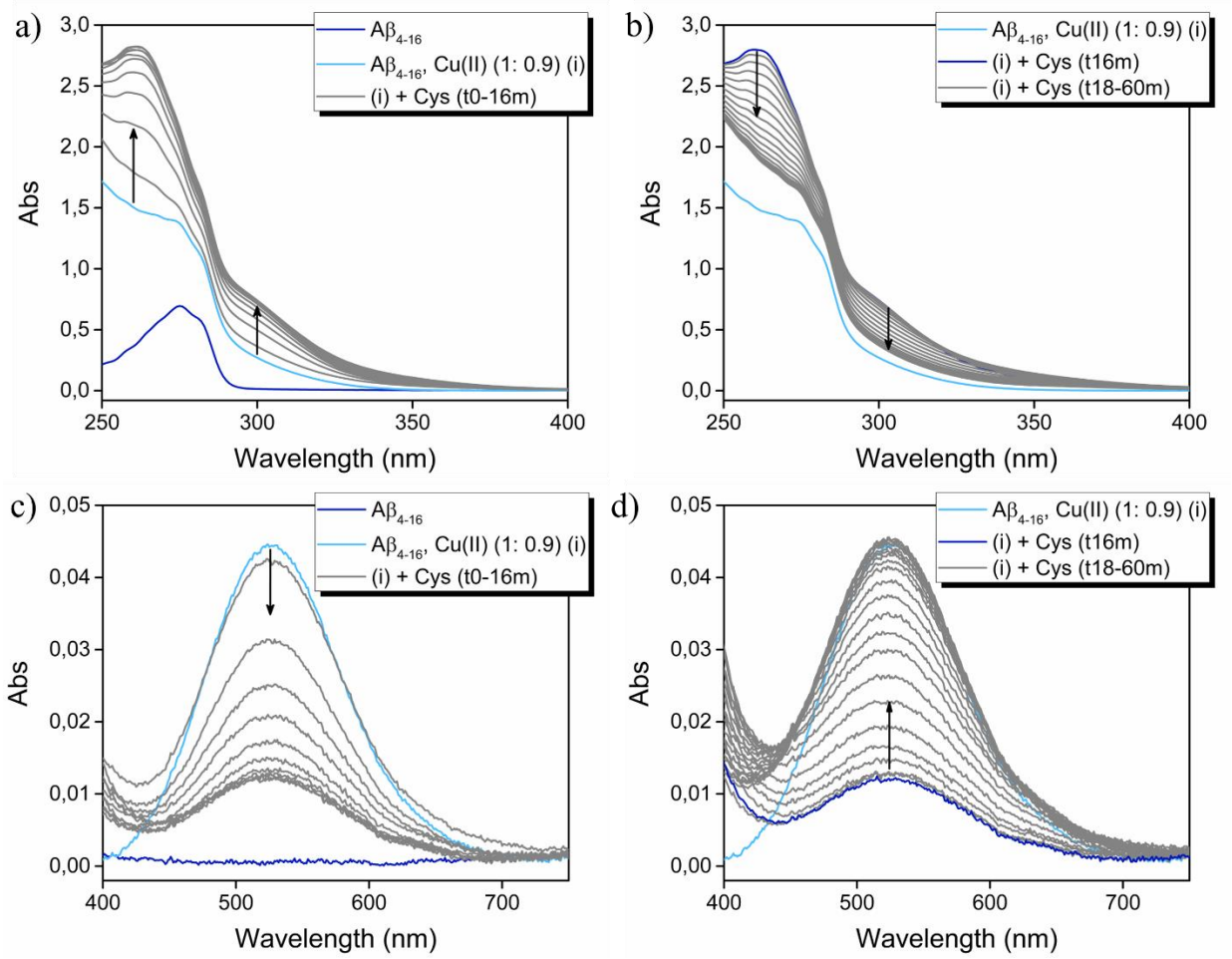

FigS 1 - Absorbance spectroscopy (UV-region, 250-400 nm) of Cu(II) reduction and release from Cu(II)-Aβ$_{4\text{-}16}$ with Cys in the absence of Zn(II)$_7$-MT-3. In a) (UV-region 250-400 nm) and c) (Vis-region, 400-700 nm) spectra of the first 16 min of the reaction after addition of Cys to Cu(II)-Aβ$_{4\text{-}16}$ (light blue spectrum); in b) and d) the corresponding spectra from t(18-60m). Each spectrum was recorded at 2 min intervals. Reaction conditions: Aβ$_{4\text{-}16}$ 500 µM, Cu(II) 450 µM (ratio Aβ$_{4\text{-}16}$/Cu(II), 1:0.9), Cys 3 mM, PB 50 mM, pH 7.4.

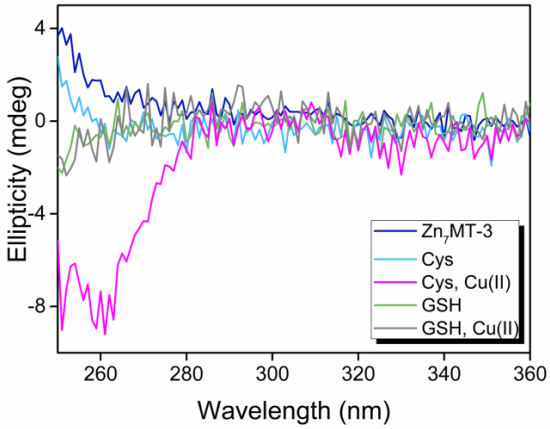

FigS 2 - CD spectra (Uv-region, 250-360 nm) of Zn(II)$_7$-MT-3 (blue profile), Cys (light blue profile), Cu(II)/Cys mixture (purple profile), GSH (green profile), Cu(II)/GSH mixture (grey profile). Final concentration of each component in solution: Zn(II)$_7$-MT-3 20 µM, Cys/GSH 3 mM, Cu(II) 90 µM, PB 50 mM, pH 7.4.

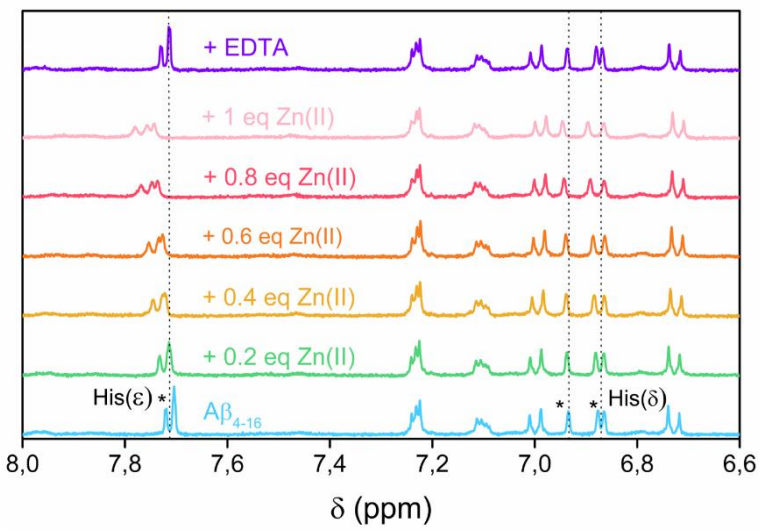

FigS 3 - Zn(II) titration of $A\beta_{4\text{-}16}$ peptide followed by ^{1}H-NMR, through the aromatic region of the spectra, and addition of EDTA to the 1:1 complex Zn(II)-$A\beta_{4\text{-}16}$ (violet profile). Experimental conditions: a 300 µM $A\beta_{4\text{-}16}$ solution (600 µl) was titrated with 2 µl aliquots of a 36 mM stock solution of Zn(II) (0.2 eq Zn(II)/$A\beta_{4\text{-}16}$); to the 1:1 complex Zn(II)-$A\beta_{4\text{-}16}$ (light pink profile) a concentrated solution of EDTA (50 mM, pH 7.4) was added to reach the final concentration of 300 µM.

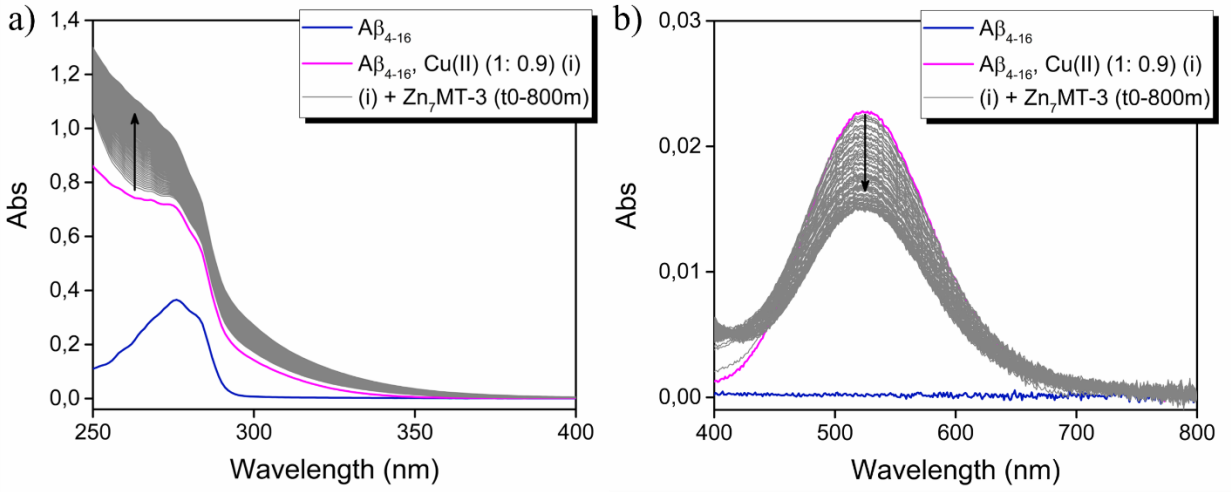

FigS 4 - a) UV and b) Vis regions of the spectra for the reaction of Cu(II)-$A\beta_{4\text{-}16}$ with $Zn(II)_7$-MT-3 monitored by absorbance spectroscopy for 800 min after the addition of $Zn(II)_7$-MT-3 to Cu(II)-$A\beta_{4\text{-}16}$. Intermediate spectra were collected at 10 min intervals Experimental conditions: $A\beta_{4\text{-}16}$ 250 µM, Cu(II) 225 µM, $Zn(II)_7$-MT-3 50 µM, (1:0.9:0.2), PB 50 mM, pH 7.4.

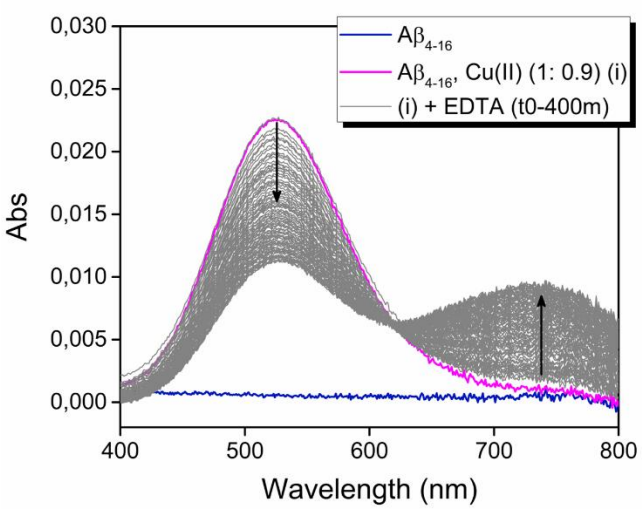

FigS 5 - UV-Vis spectra for the reaction of Cu(II)-$A\beta_{4-16}$ with EDTA monitored by absorbance spectroscopy for 400 min after EDTA addiction to Cu(II)-$A\beta_{4-16}$. Intermediate spectra were collected at 10 min intervals. The corresponding kinetic of disappearance of the d-d band is shown in **Fig 18a** with a blue profile. Experimental conditions: $A\beta_{4-16}$ 250 µM, Cu(II) 225 µM (1:0.9), EDTA 150 µM, PB 50 mM, pH 7.4.

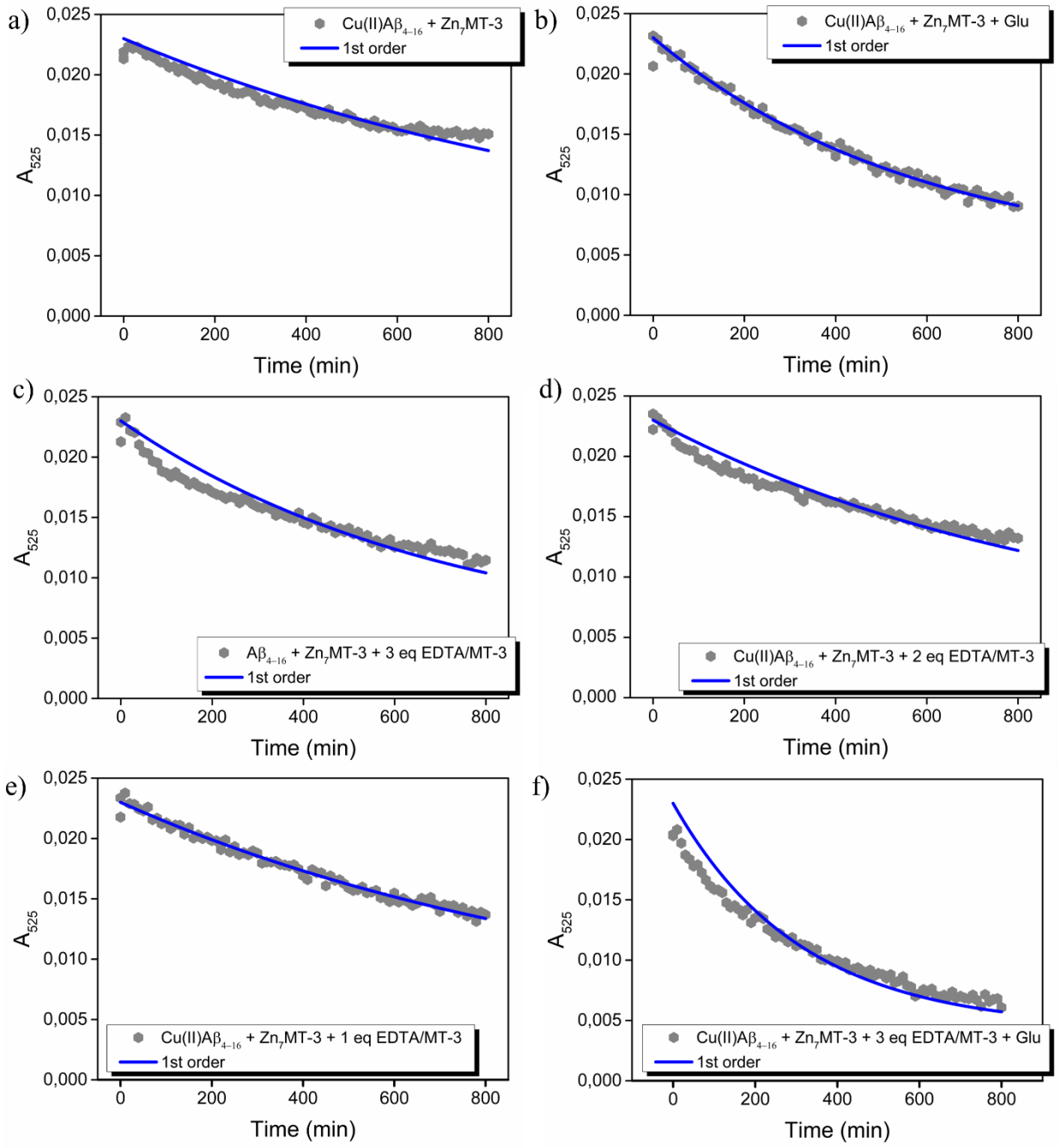

FigS 6 - Experimental kinetics of disappearance of the d-d band of Cu(II)-Aβ$_{4-16}$ for the reactions: a) Cu(II)A-β$_{4-16}$ + Zn(II)$_7$-MT-3, (b) Cu(II)-Aβ$_{4-16}$ + Zn(II)$_7$-MT-3 + Glu, c) Cu(II)-Aβ$_{4-16}$ + Zn(II)$_7$-MT-3 + 3 eq EDTA/ MT-3, d) Cu(II)-Aβ$_{4-16}$ + Zn(II)$_7$-MT-3 + 2 eq EDTA/MT-3, e) Cu(II)-Aβ$_{4-16}$ + Zn(II)$_7$-MT-3 + 1 eq EDTA/MT-3, f) Cu(II)-Aβ$_{4-16}$ + Zn(II)$_7$-MT-3 + 3 eq EDTA/MT-3 + Glu. Kinetics were fitted with the 1st order exponential equation y = W*exp(-k*x)+A. For the first experimental repetition the value of A (plateau of the reaction) was set to 0.0043 (background of the Abs at λ_{max} = 525 nm, due to the Abs of the formed product Cu(I)$_4$Zn(II)$_4$-MT-3 (tail of the band at λ_{max}= 235 nm). The value of W was calculated as X-A where X was set to 0.023 (1st repetition) (experimental value for the Abs at t(0m) from the beginning of the reaction). a) R^2 = 0.91, b) R^2 = 0.99, c) R^2 = 0.91, R^2, d) R^2 = 0.93, e) R^2 = 0.98, f) R^2 = 0.92.

TableS 1 - Table summarizing the $t_{1/2}$ (min) and AF (acceleration factor) values for the different reactions studied, calculated from the experimental kinetics of disappearance of the Cu(II)-Aβ_{4-x} d-d band. Acceleration factors (AFs) were calculated with respect to the reactions Cu(II)-Aβ_{4-16} + Zn(II)$_7$-MT-3 (for the reactions in the presence of Zn(II)$_7$-MT-3) and Cu(II)-Aβ_{4-16} + EDTA (for the reaction Cu(II)-Aβ_{4-16} + EDTA + Glu). Reactions were performed in triplicate (experiment 1, 2, 3), with different stock solutions of peptide, protein, EDTA and Glu, at different days. Representative measurements from the 1st experiment is shown in the figures of the main text of the thesis, as well as in **FigS 6**.

Reaction	Experiment 1		Experiment 2		Experiment 3	
	$t_{1/2}$ (min x 10^2)	AF	$t_{1/2}$ (min x 10^2)	AF	$t_{1/2}$ (min x 10^2)	AF
Cu(II)Aβ_{4-16} + Zn(II)7-MT-3 (i)	7.94	1	7.07	1	5.84	1
(i) + Glu	4.06	1.95	3.28	2.15	2.47	2.36
(i) + EDTA (3eq)	4.95	1.60	4.54	1.56	3.59	1.63
(i) + EDTA (2eq)	6.44	1.23	6.03	1.17	4.77	1.22
(i) + EDTA (1eq)	7.66	1.04	6.38	1.11	4.82	1.21
(i) + EDTA (3eq) + Glu	2.15	3.69	2.30	3.07	1.91	3.06
Cu(II)Aβ_{4-16} + EDTA (ii)	1.94	1	1.64	1	2.08	1
(ii) + Glu	0.98	1.98	1.08	1.52	1.07	1.94

TableS 2 - Calculated molar fractions of Cu(II)-Glu complexes in equilibrium with Aβ_{4-16} and Zn(II)-Glu complexes in equilibrium with the 7th binding site of MT-3 for concentrations used in kinetic experiments.

Cu(II) species	Molar fraction	Zn(II) species	Molar fraction
Cu(II)	1.2×10^{-9}	$Zn(II)^{2+}$	0.0052
Cu(II)-HGlu	4.8×10^{-15}	Zn(II)-Glu	0.0064
Cu(II)-Glu	3.1×10^{-12}	$Zn(II)Glu_2$	0.0012
Cu(II)-Glu_2	5.7×10^{-17}	7th site of MT	0.9872
$Cu(II)_2$-A$\beta 4_{-16}$	0.0000016		
Cu(II)-Aβ_{4-16}	0.999998		

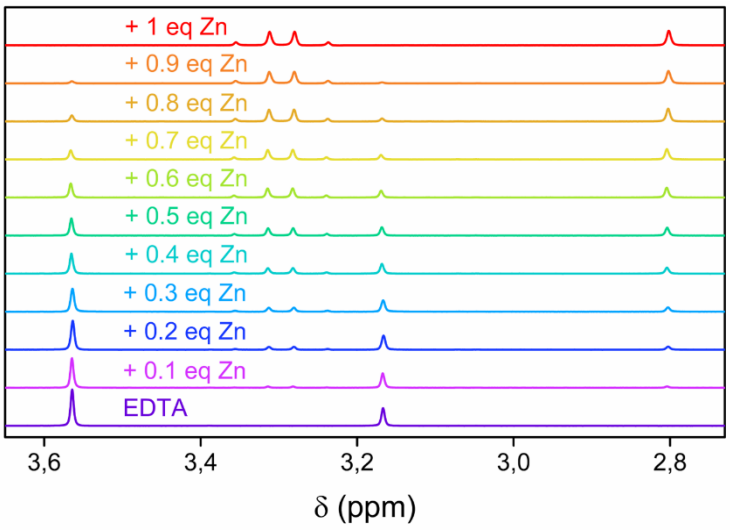

FigS 7 - Zn(II) titration experiment of EDTA monitored by ^{1}H-NMR. Spectra were obtained from 10% D_2O/90% H_2O solution in a 50 mM PB, pH 7.4. A concentrated (60 mM) Zn(II) solution was titrated into a 1 mM solution of EDTA, up to 1 eq of Zn(II)), thus generating the 1:1 complex Zn(II)-EDTA.

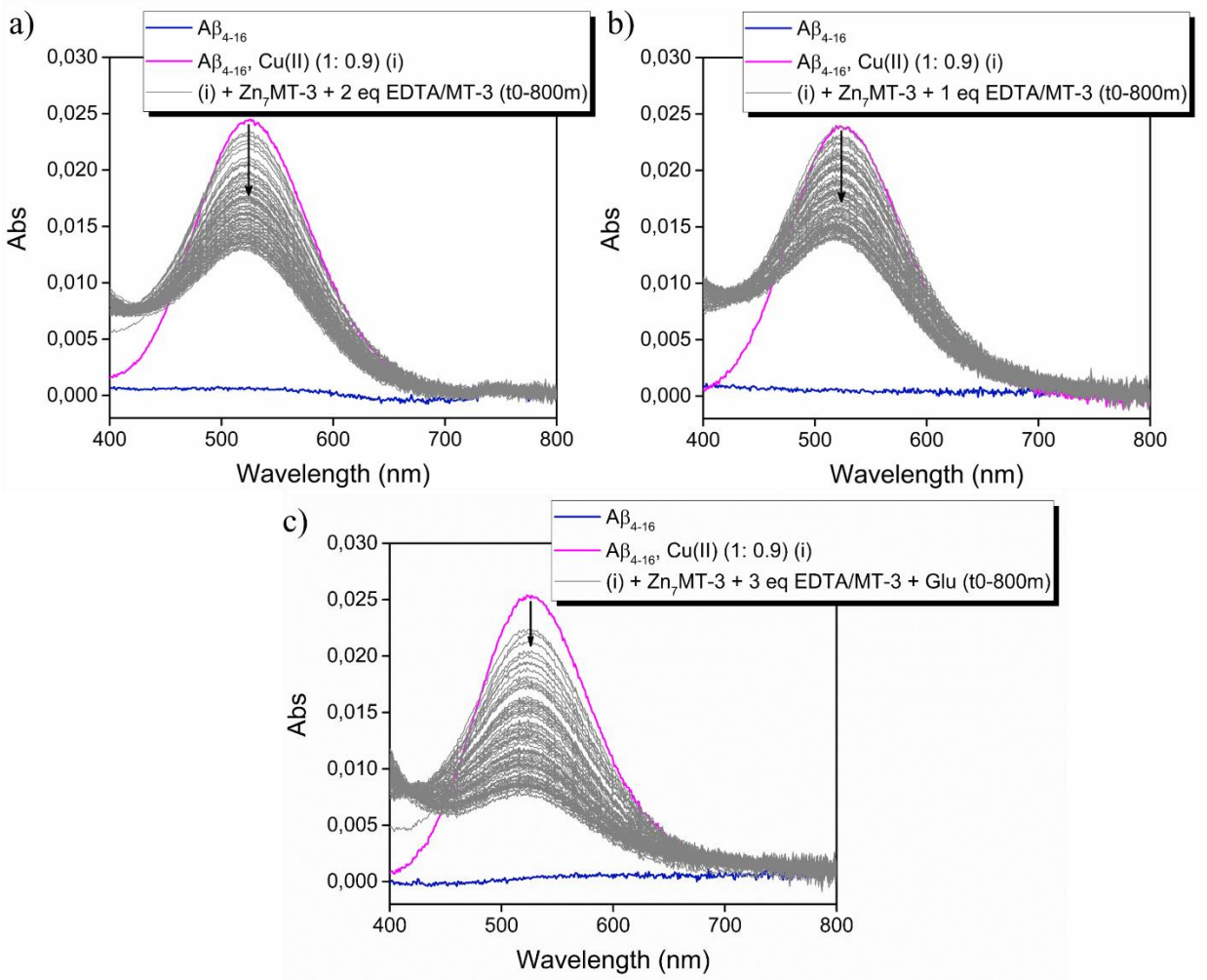

FigS 8 - Source of UV-Vis spectra for the reaction of Cu(II)$A\beta_{4\text{-}16}$ with Zn(II)$_7$-MT-3 and a) 2 eq EDTA/MT-3, b) 1 eq EDTA/MT-3 c) 3 eq EDTA/MT-3, Glu. The scans were collected at 10 min intervals. Experimental conditions: $A\beta_{4\text{-}16}$ 250 µM, Cu(II) 225 µM, Zn(II)$_7$-MT-3 50 µM, (1:0.9:0.2), EDTA a) 100 µM (ratio MT-3:EDTA 1:2), b) 50 µM (ratio MT-3:EDTA, 1:1), c) 150 µM (ratio MT-3:EDTA, 1:3), Glu 5 mM. Reactions were performed in PB 50 mM, pH 7.4.

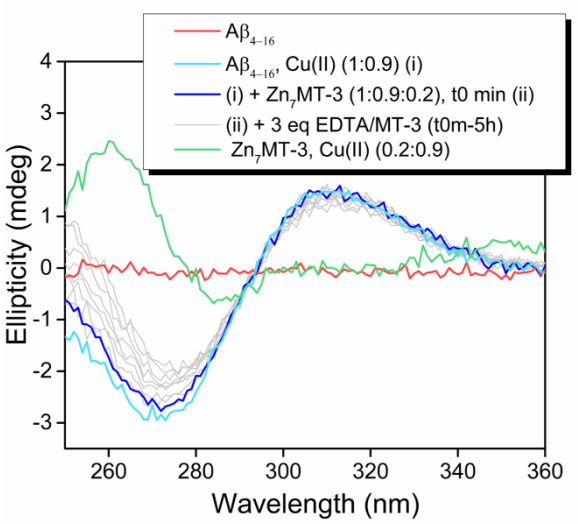

FigS 9 - Reaction between Cu(II)-Aβ$_{4-16}$ and Zn(II)$_4$-MT-3 monitored by circular dichroism (UV-region 250-360 nm). Zn(II)4-MT-3 was generated by adding 3 eq of EDTA/MT-3 to the mixture Cu(II)-Aβ$_{4-16}$/Zn(II)$_4$-MT-3. After addition of EDTA a CD spectrum was recorded every 30 min for 5 hours. Reactions conditions: Aβ$_{4-16}$ 35 µM, Cu(II) 31.5 µM, Zn(II)$_7$-MT-3 7 µM (ratio Aβ$_{4-16}$/Cu(II)/Zn(II)$_7$-MT-3, 1:0.9:0.2), EDTA 21 µM (3 eq/MT-3), PB 50 mM, pH 7.4 .

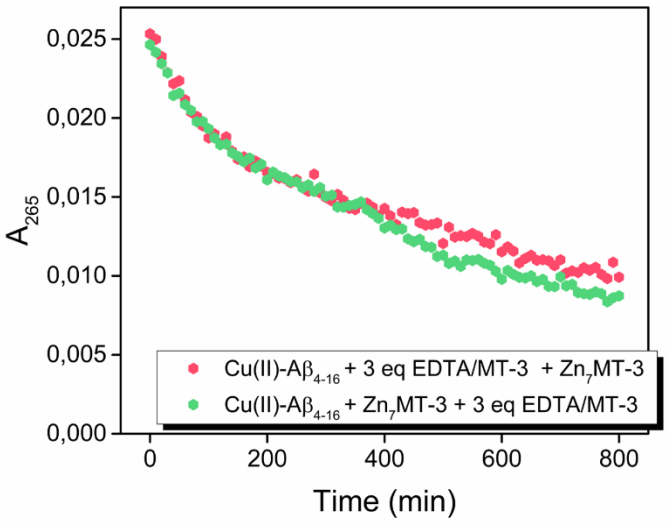

FigS 10 - Effect of the sequence of addictions of Zn(II)$_7$-MT-3 and EDTA to the preformed Cu(II)-Aβ$_{4-16}$ complex on the kinetic of Cu transfer (reaction with 3 eq of EDTA/MT-3). The reaction was monitored by absorbance spectroscopy and kinetics of disappearance of the d-d band of Cu(II)-Aβ$_{4-16}$ complex at λ_{max} = 525 nm are reported. To the Cu(II)-Aβ$_{4-16}$ complex Zn(II)$_7$-MT-3 (1st) and EDTA (2nd) (green profile) or EDTA (1st) and Zn(II)$_7$-MT-3 (2nd) (purple profile) were respectively added and the reaction monitored over time for 800 min, collecting intermediate spectra at 10 min intervals. The second addiction was performed 30 sec after mixing the reaction mixture Cu(II)Aβ$_{4-16}$/Zn(II)$_7$-MT-3 or Cu(II)Aβ$_{4-16}$/EDTA. Experimental conditions: Aβ$_{4-16}$ 250 µM, Cu(II) 225 µM, Zn(II)$_7$-MT-3 50 µM (1:0.9:0.2), EDTA 150 µM (3 eq/MT-3), PB 50 mM, pH 7.4.

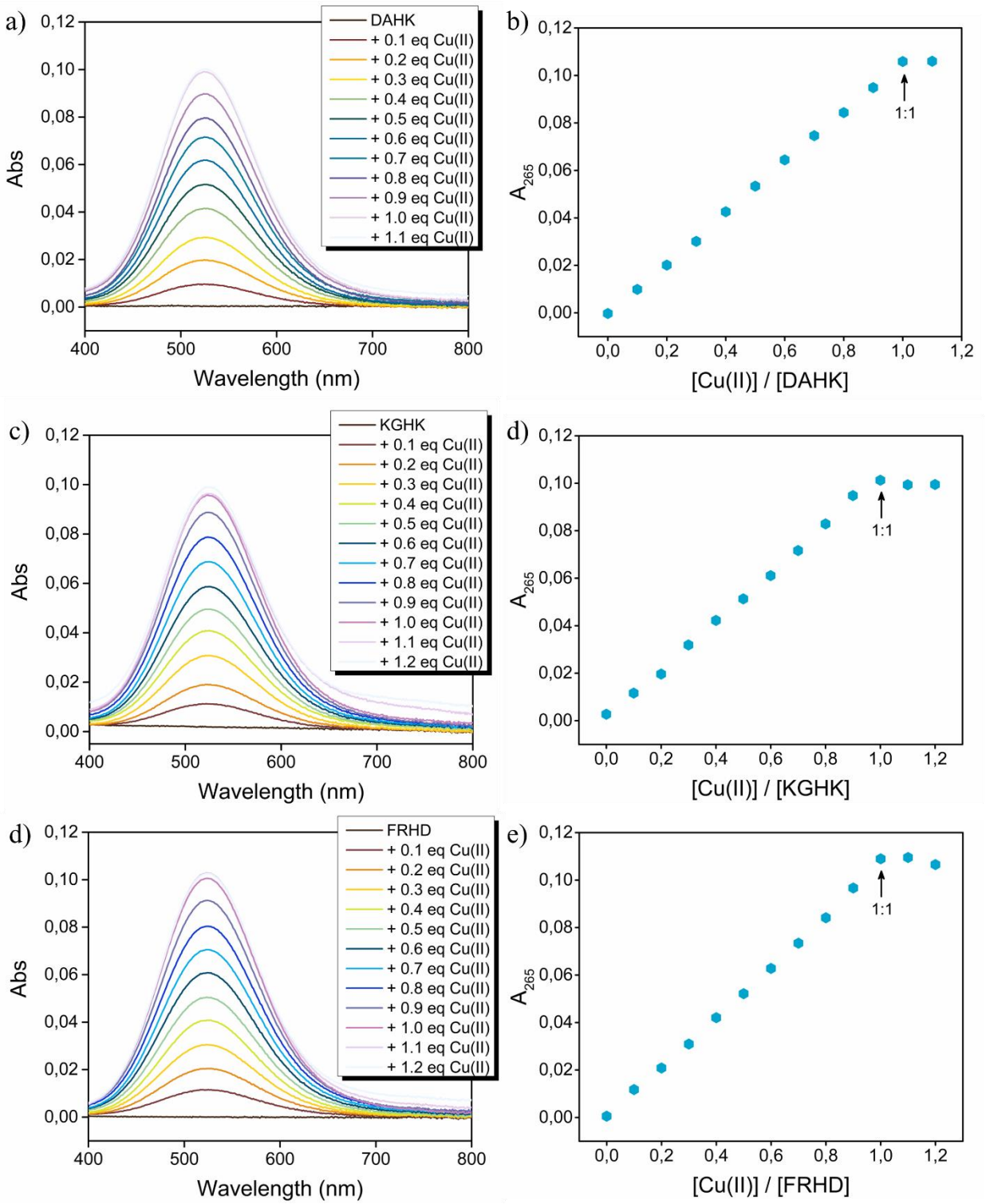

FigS 11 - Cu(II)-titration experiments of a) DAHK, b) KGHK and c) FRHD, monitored by absorbance spectroscopy. In b), d) and e) the corresponding binding curves are reported (A_{525} nm, i.e. λ_{max} of the d-d band Cu(II)-ATCUN, vs [Cu(II) / [XZH] peptide]). Experimental conditions: XZH peptide 1 mM, in PB 50 mM, pH 7.4. Titrations were carried out adding 1 µl aliquotes of a 10 mM Cu(II) stock solution.

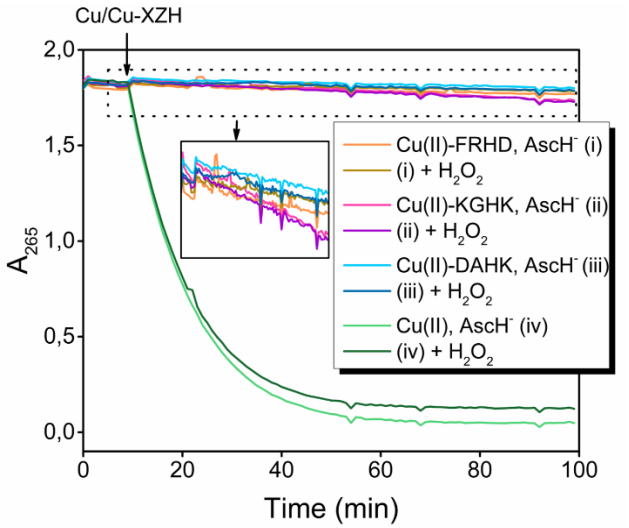

FigS 12 - Evolution of the $AscH^-$ absorption (λ_{max} = 265 nm) as a function of time, after exposure to the three Cu(II)-XZH ATCUN complexes (ratio Cu(II):peptide, 1:1.2) and free Cu(II), with and without H_2O_2. $AscH^-$ oxidation was triggered by the addition of free Cu(II) or the preformed Cu(II)-XZH complexes after 10 min. Experimental conditions: Cu(II) 10 µM, XZH peptide 12 µM, $AscH^-$ and H_2O_2 100 µM, in PB 50 mM, pH 7.4. Inset: zoom of the ascorbate oxidation profile for Cu(II)-XHZ complexes.

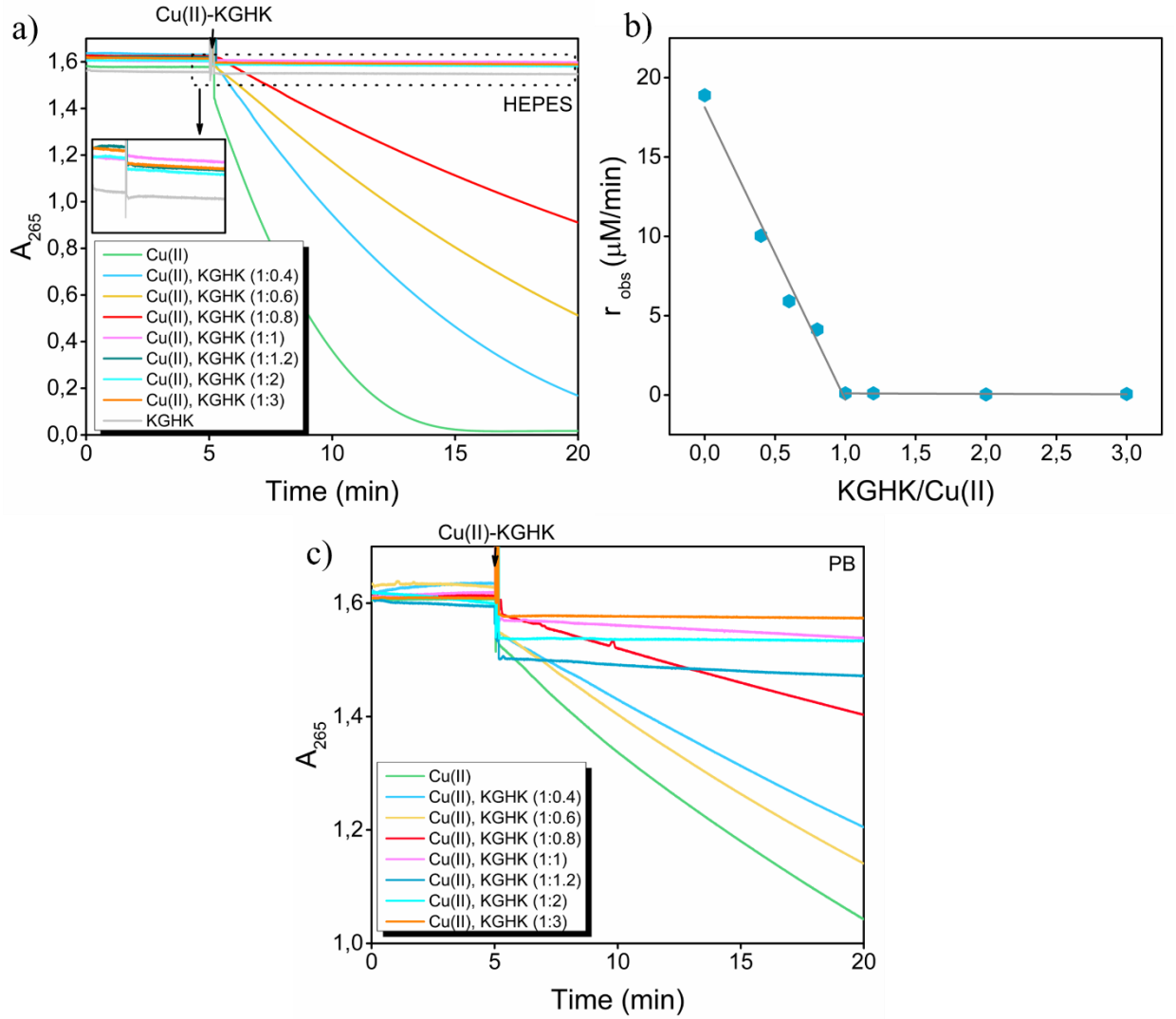

FigS 13 - Kinetics of $AscH^-$ oxidation for Cu(II)-KGHK at different ratios Cu(II):KGHK (1:0, 1:0.4, 1:0.6, 1:0.8, 1:1, 1:1.2, 1:2, 1:3), monitored by absorbance spectroscopy at λ_{max} = 265 nm, in a) HEPES, c) PB 50 mM pH 7.4. $AscH^-$ oxidation was started by the addition of the preformed Cu(II)-KGHK complex at t(5min). In b) corresponding plot of molar $AscH^-$ oxidation rate (µM/min) as a function of KGHK to Cu(II) ratio, for the reactions in HEPES. Experimental conditions: Cu(II) 10 µM, XZH peptide 0-30 µM, $AscH^-$ 100 µM, in a) HEPES, c) PB 50 mM, pH 7.4.

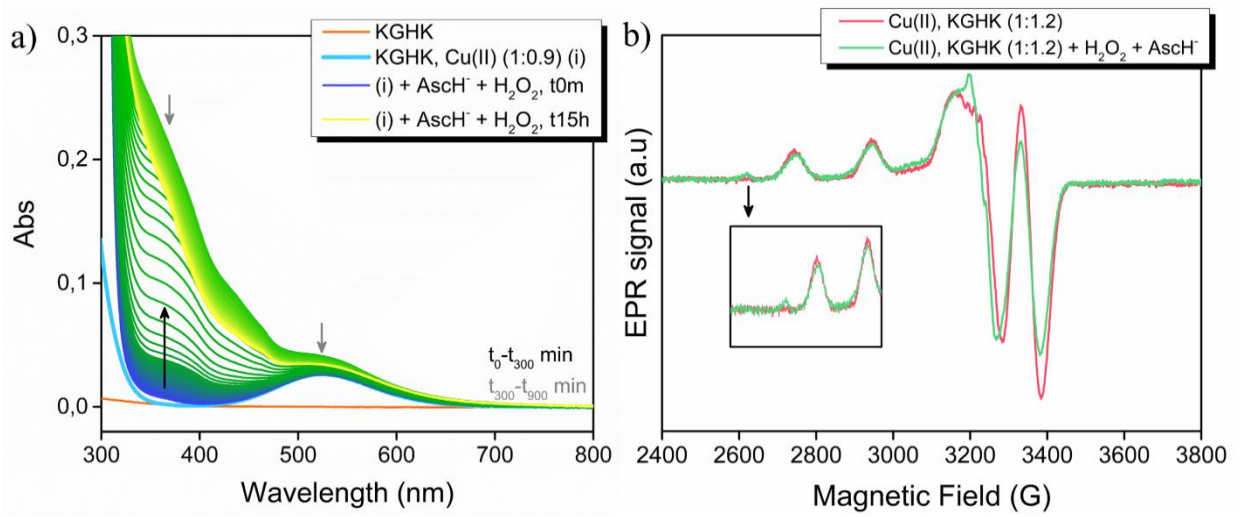

FigS 14 - Partial degradation of KGHK peptide during the reaction of Cu(II)-KGHK (ratio 1:1.2, Cu(II):KGHK) with $AscH^-$ and H_2O_2 shown by a) absorbance and b) EPR spectroscopies at low temperature. Experimental conditions a): Cu(II) 250 µM, KGH 300 µM, $AscH^-$ and H_2O_2 5 mM, in PB 50 mM, pH 7.4. The reaction was monitored for 15 h, collecting intermediate spectra at 10 min intervals. Experimental conditions b): Cu(II) 200 µM, KGH 240 µM, $AscH^-$ and H_2O_2 4 mM, in PB 80 mM, pH 7.4. Reaction mixtures were incubated for 24h under aerobic conditions and then transferred into a 4 mm outer diameter quartz tubes (Wilmad-Labglass) and freeze-quenched with liquid nitrogen before their introduction into the precooled cavity.

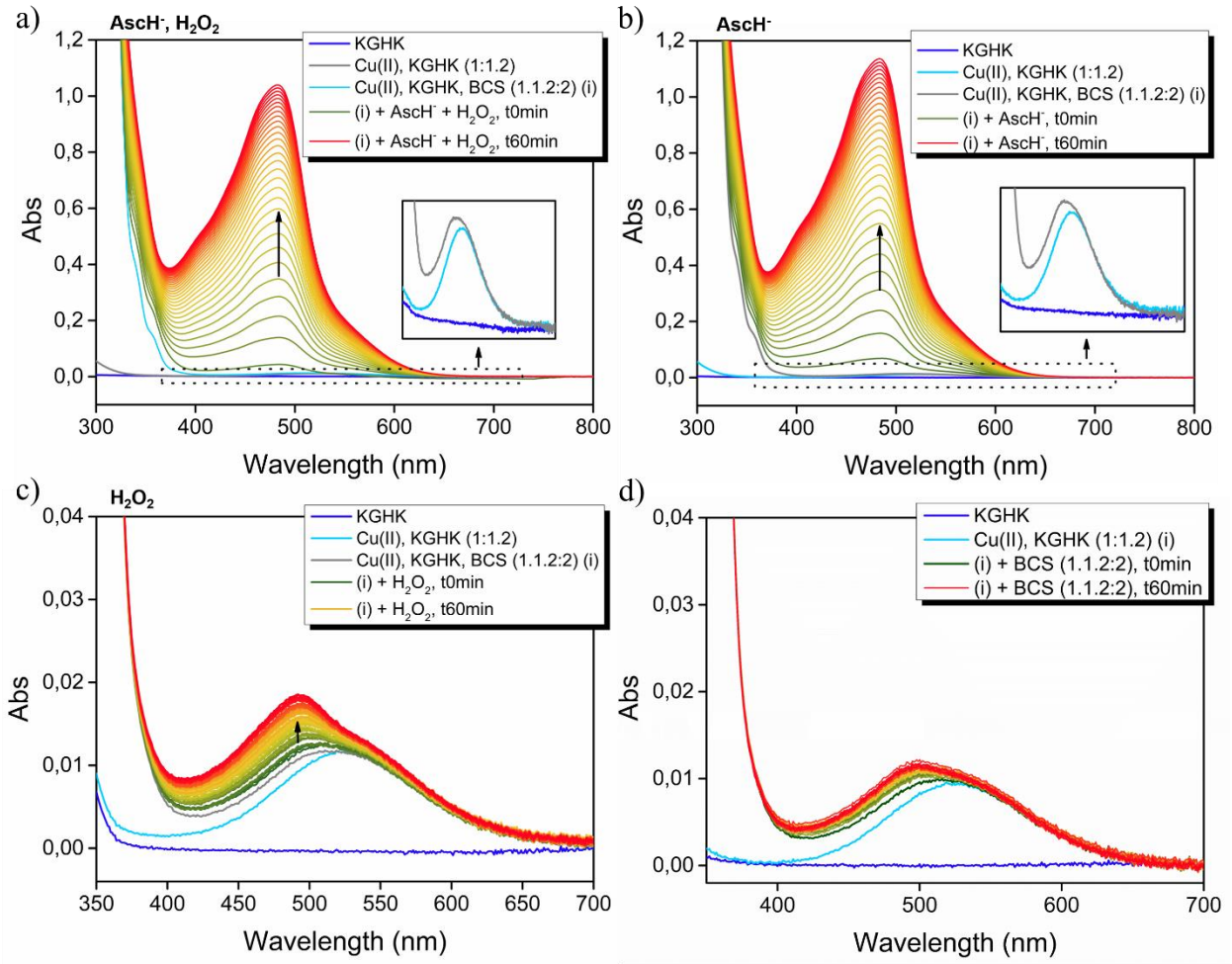

FigS 15 - Uv-Vis spectra for the reaction of Cu(II)-KGHK (ratio 1:1.2, Cu(II):KGHK) with a) $AscH^-$ and H_2O_2 , b) $AscH^-$, c) H_2O_2, d) blank (i.e. with no $AscH^-$ and/or H_2O_2) in the presence of BCS. Experimental conditions: Cu(II) 100 µM, KGHK 1200 µM, $AscH^-$ and H_2O_2 10 mM, BCS 200 µM, in PB 50 mM, pH 7.4. Reactions were monitored over 1h, collecting intermediate spectra at 2 min intervals.

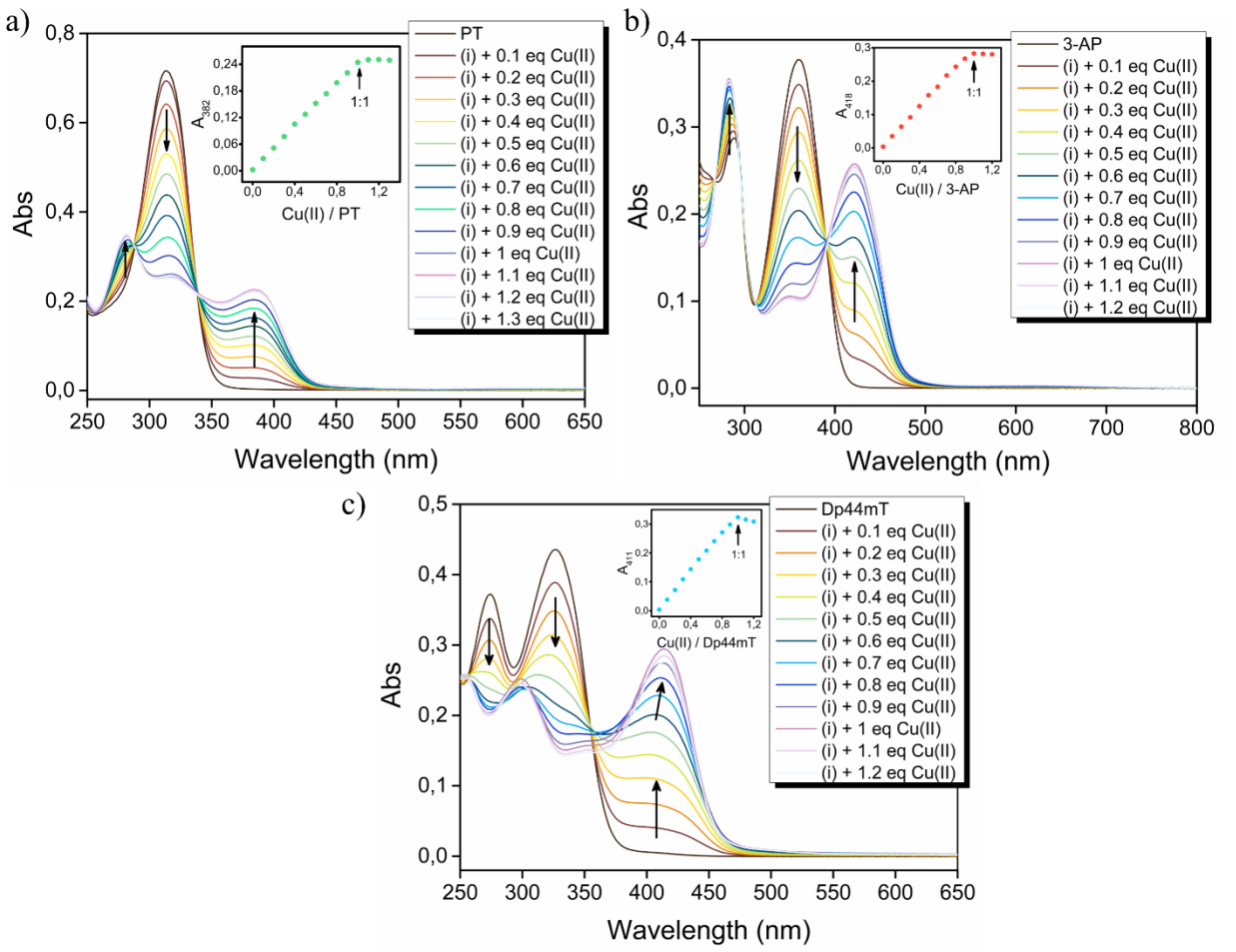

FigS 16 - Cu(II) titration experiments to determine the binding stoichiometry a) Cu(II)/PT, b) Cu(II)/3-AP, c) Cu(II)/Dp44mT. Insets: corresponding binding curves at λ_{max} = 411 nm**.** Experimental conditions: a 30 µM solution of PT/3-AP/Dp44mT in HEPES buffer 100 mM, pH 7.4, was titrated with 1 µl aliquots of a 300 µM Cu(II) stock solution.

- Cu(II)-PT: λ_{max} = 382 nm, λ_{max} = 318 nm, λ_{max} = 280 nm, isosbestic points at λ = 338 nm, λ = 287 nm.
- Cu(II)-3-AP: λ_{max} = 418 nm, λ_{max} = 349 nm, λ_{max} = 283 nm, isosbestic points at λ = 393 nm, λ = 311 nm, λ = 366 nm.
- Cu(II)-$(Dp44mT)_2$: λ_{max} = 403 nm, λ_{max} = 310 nm, λ_{max} = 304 nm; Cu(II)-Dp44mT: λ_{max} = 411 nm, λ_{max} = 298 nm, λ_{max} = 253 nm.

TableS 3 - Principal EPR simulations parameters. [a,b] Simulations were achieved with Easyspin Toolbox under Matlab environment (Stoll et al JMR, 178(1), 42-55, 2006). A broad Cu(II) EPR fingerprint was implemented to the simulation of the orange and blue spectra to account for the observed baseline, arising from the sample solubility limit.

Species	**PT, Cu(II) (1:0.9) (i)[c]**	**(i) + GSH**	**(i) +$Zn(II)_7$MT-1[b]**
$g_{//}$	2.205	2.142	2.147
$A_{//}$ (Cu(II)) (MHz)	544	520	515

[a] field strain and linewidth parameters were used to account for the experimental line-broadening.

[b] Isotropic superhyperfine coupling constants for accounting for 2 nitrogen atoms of 40±5 MHz were implemented to the computation.

[c] broad Cu(II) EPR fingerprint was implemented to the simulation to account for the observed baseline, arising from the solubility limit of our sample.

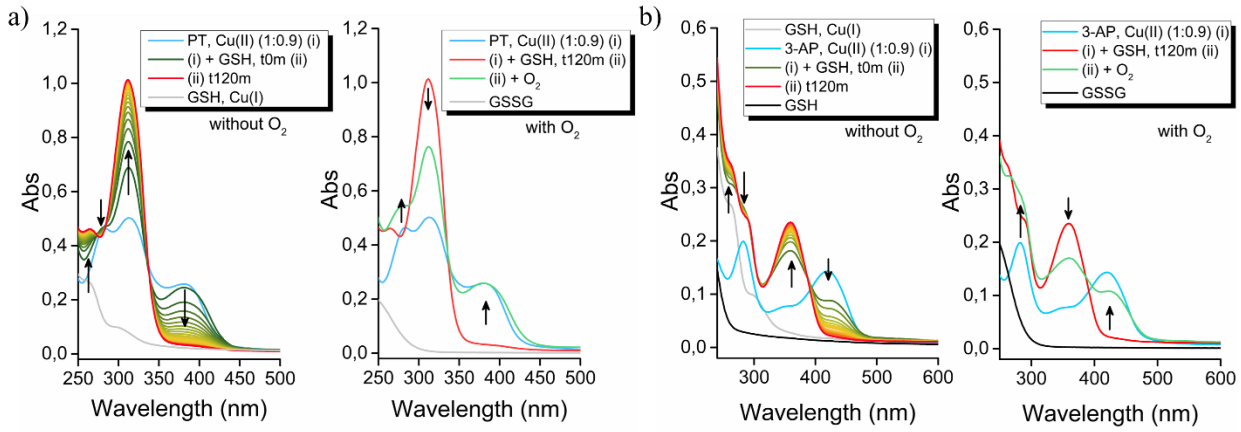

FigS 17 - Reactivity of a) Cu(II)-PT, b) Cu(II)-3-AP complexes with GSH under anaerobic conditions (left panels) and after bubbling O_2 through the solution (right panels). Left panels: UV-Vis spectra for the reaction between Cu(II)-PT/3-AP and 1 mM GSH under anaerobic conditions. The reactions were monitored over time from t_0 min after GSH addition to the preformed Cu(II)-PT/3-AP complexes (ratio PT/3-AP:Cu(II), 1:0.9) to t(120m), collecting intermediate spectra at 4 min intervals. The dark arrows indicate the changes observed in the spectra after GSH addition to the preformed Cu(II)-PT/3-AP complexes (light blue lines) i.e. the disappearance of the CT bands of the ternary adduct [TSC-Cu(II)-GSH] (λ_{max} (PT) = 386 nm, λ_{max} (3-AP) = 425 nm), the appearance of the UV band of the free ligand (λ_{max} (PT) = 313 nm, λ_{max} (3-AP) = 359 nm) and of characteristic CT band of the Cu(I)-GSH complex at λ_{max} = 265 nm. Right panels: corresponding spectra (green lines) obtained after bubbling O_2 through the solution. The dark arrows indicate the changes from the red spectrum (Cu(II)-PT/3-AP + GSH, t(120m) in anaerobic conditions) to the green spectrum. Experimental conditions: reaction mixtures (b) 30 µM PT, 27 µM Cu(I)/15 µM 3-AP, 12 µM Cu(I) (ratio TSC:Cu(I), 1:0.9), GSH 1 mM, 100 mM HEPES buffer, pH 7.4) were prepared under saturated argon atmosphere in a screw cap cell cuvette equipped with septum, containing 1 ml of solution. After addition of Cu(I) to the ligand solution, the characteristic UV spectra of the Cu(II)-PT/3-AP complexes were immediately detected.

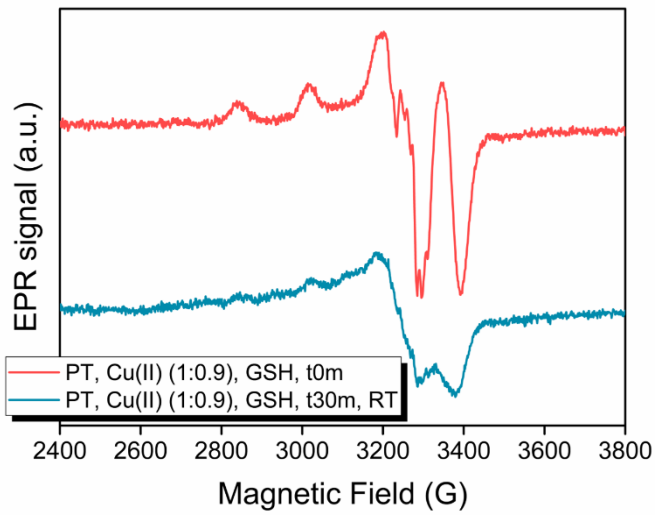

FigS 18 - EPR spectrum of the snap-frozen solution of Cu(II)-PT after the addition of GSH (red line) and of the room temperature solution after 30 min from GSH addition to Cu(II)-PT complex (red line). Experimental conditions: 1 mM PT, 900 µM Cu(II) (ratio PT:Cu(II), 1:0.9) in HEPES buffer 100 mM, pH 7.4, GSH 3 mM.

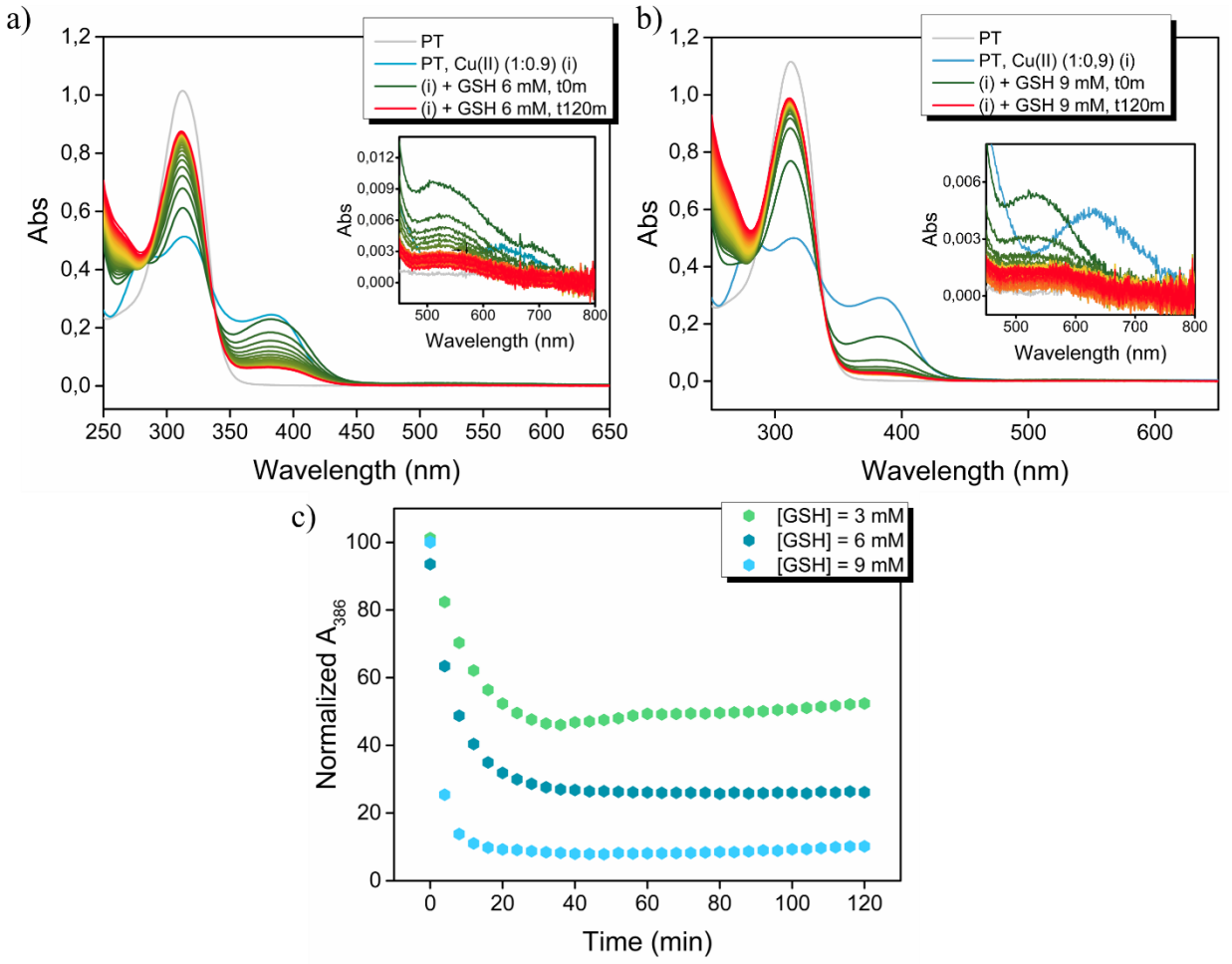

FigS 19 - Concentration dependence of Cu(II)-PT complex reactivity with GSH. a) UV-Vis spectra for the reaction between Cu(II)-PT and 6 mM GSH, b) 9 mM GSH. The reactions were monitored over time from t_0 min after GSH addition to the preformed Cu(II)-PT complex (ratio PT:Cu(II), 1:0.9) to t_{120} min, collecting intermediate spectra at 4 min intervals. Insets refer to the Vis region of the spectra 450-800 nm. c) Corresponding experimental kinetics for the reactions of the Cu(II)-PT complex with different concentrations of GSH, respectively 3 mM (green profile), 6 mM (dark blue profile), 9 mM (light blue profile): normalized absorbance at λ_{max} = 386 nm (CT band of the ternary complex [PT-Cu(II)-GSH]) versus time. Experimental conditions 30 µM PT, 27 µM Cu(II) (ratio PT:Cu(II), 1:0.9), GSH a) 3 mM, b) 9 mM, HEPES buffer 100 mM, pH 7.4.

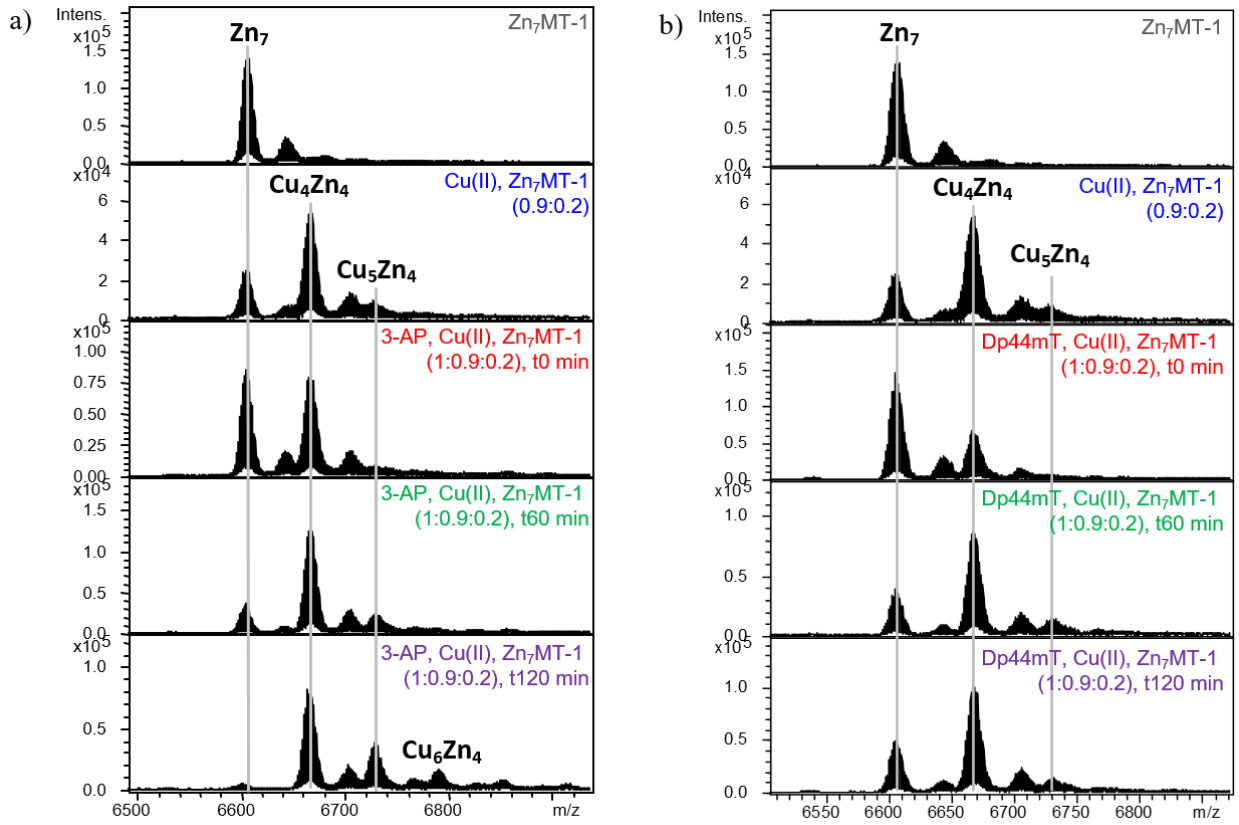

FigS 20 - Reactivity of a) Cu(II)-3-AP, b) Cu(II)-Dp44mT with Zn(II)$_7$MT-1. Deconvoluted ESI-MS spectra of Zn(II)$_7$MT-1, Cu(II)/Zn(II)$_7$MT-1, 0.9:0.2, 3-AP or 3-AP or Dp44mT/Cu(II)/Zn(II)$_7$MT-1, 1:0.9:0.2, collected at t(0m), t(60m) min and t(120m) min from the addition of Zn(II)$_7$MT-1 to the preformed Cu(II)-3-AP/Dp44mT complex. Experimental conditions: 50 µM 3-AP/Dp44mT, 45 µM Cu(II), 10 µM Zn(II)$_7$MT-1, 50 mM ammonium acetate, pH 7.4. The main peak in of m/z ~ 6610 has the mass expected for Zn(II)$_7$MT-1 at neutral pH; the main peak at m/z ~6671 corresponds to a substitution of three Zn(II) ions with four Cu(I) ions; the peaks at m/z ~6732 and ~6792 correspond to a substitution of three Zn(II) ions with respectively five and six Cu(I) ions.

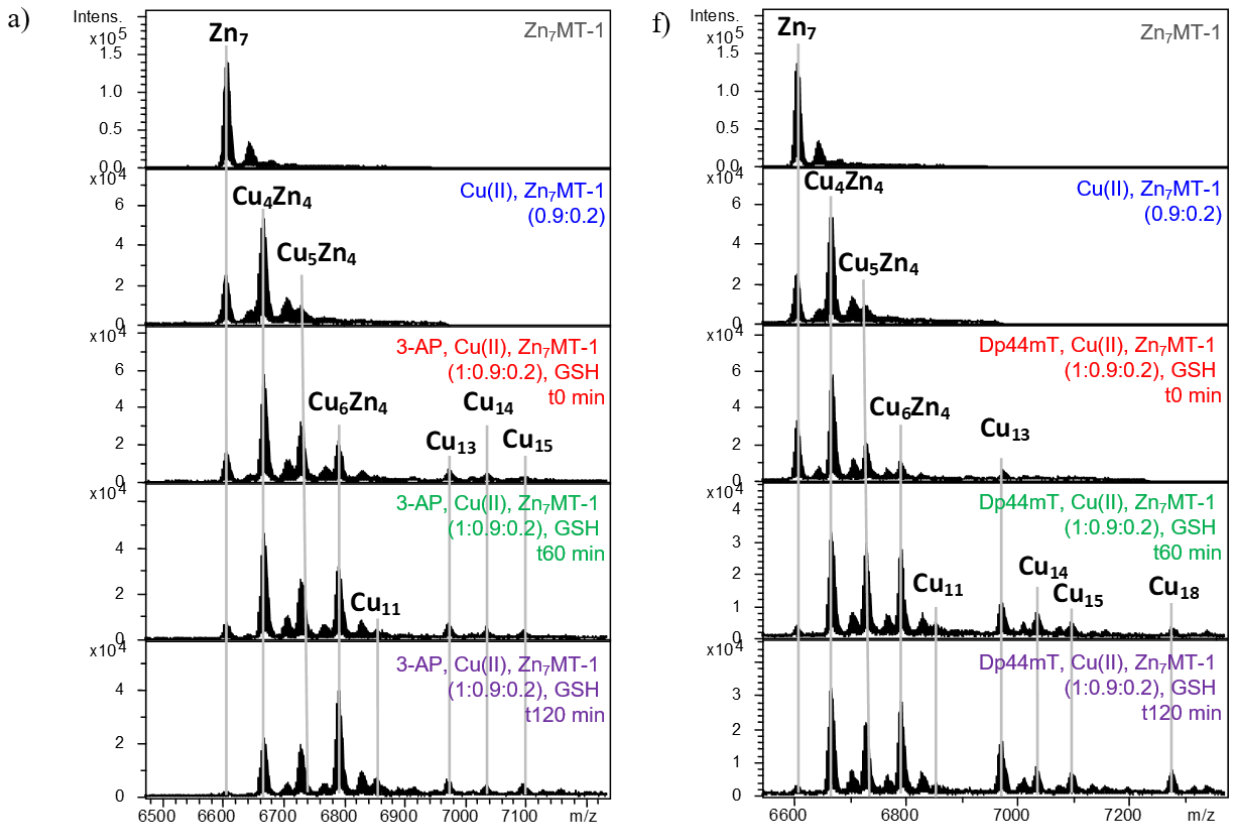

FigS 21 - Reactivity of a) Cu(II)-3-AP, b) Cu(II)-Dp44mT with $Zn(II)_7MT$-1/GSH. Deconvoluted ESI-MS spectra of $Zn(II)_7MT$-1, Cu(II)/$Zn(II)_7MT$-1, 0.9:0.2, 3-AP or Dp44mT/Cu(II)/$Zn(II)_7MT$-1, 1:0.9:0.2, GSH at t(0m), t(60m) min and t(120m) from the addition of $Zn(II)_7MT$-1/GSH to the preformed Cu(II)-3-AP/Dp44mT complex. Experimental conditions: 50 µM 3-AP, 45 µM Cu(II) , 10 µM $Zn(II)_7MT$-1 (ratio 3-AP:Cu(II):$Zn(II)_7MT$-1, 1:0.9:0.2), 3 mM GSH, 50 mM ammonium acetate, pH 7.4. The main peak in a) of m/z ~6610 has the mass expected for $Zn(II)_7MT$-1 at neutral pH; the main peak at m/z ~6671 in b, c, d, e) corresponds to a substitution of three Zn(II) ions with four Cu(I) ions; the peaks at m/z ~6732 and ~6792 correspond to a substitution of three Zn(II) ions with respectively five and six Cu(I) ions. The peaks at m/z ~6860, ~6880, ~7040 and ~7100 correspond to a substitution of seven Zn(II) ions with respectively eleven, thirteen, fourteen, fifteen Cu ions.

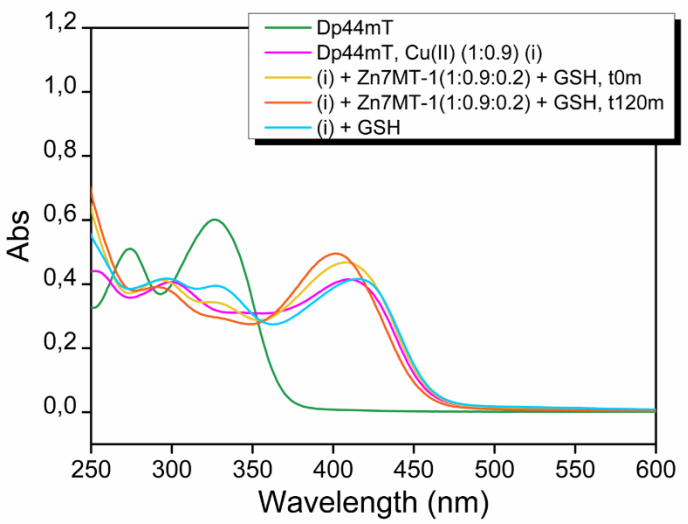

FigS 22 - Comparison of the spectra for the reaction of Cu(II)-Dp44mT with GSH (light blue line, t(0m) and for the reaction of Cu(II)-Dp44mT with GSH and $Zn(II)_7MT$-1 (yellow line, t_0 min, orange line, t(120m)). Experimental conditions: Dp44mT 30 µM (grey line), Dp44mT 30 µM, Cu(II) 27 µM (1:0.9) (orange line), Dp44mT 30 µM, Cu(II) 27 µM, $Zn(II)_7MT$-1 6 µM (1:0.9:0.2) ± GSH 3 mM, HEPES 100 mM, pH 7.4.

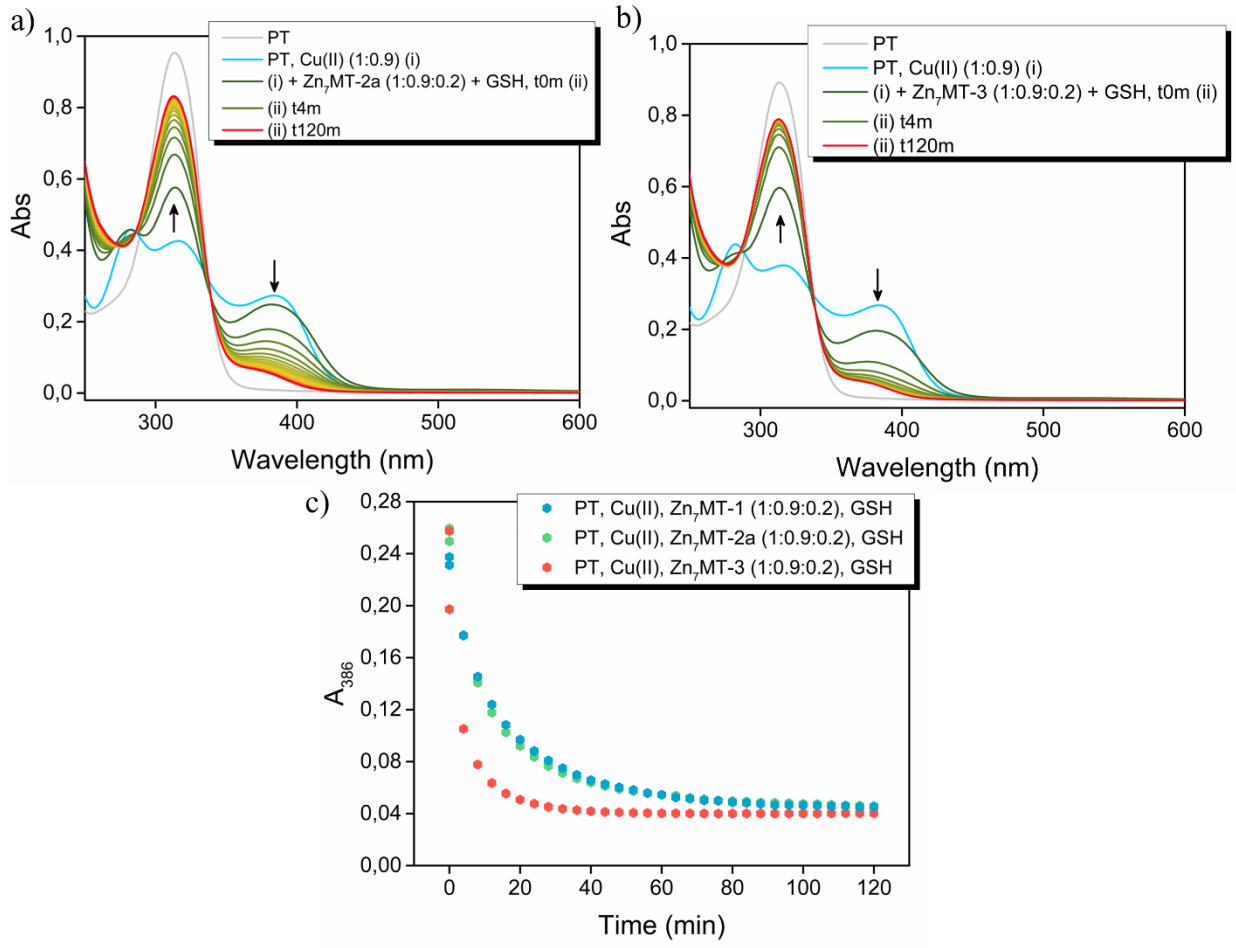

FigS 23 - Uv-Vis spectra of for the reaction of Cu(II)-PT with a) GSH/$Zn(II)_7$MT-2a, b) GSH/$Zn(II)_7$MT-3 monitored over time after GSH/ $Zn(II)_7$MT addition to the preformed Cu(II)-PT complex (for the reaction with $Zn(II)_7$MT-1, see **Fig 36**). c) Corresponding experimental kinetics, i.e. absorbance at λ_{max} = 386 nm (CT band of the ternary complex [PT-Cu(II)-GSH]) versus time: $Zn(II)_7$MT-1 isoform (blue profile), $Zn(II)_7$MT-2a isoform (green profile), $Zn(II)_7$MT-3 isoform (red profile). Experimental conditions: 30 µM PT, 27 µM Cu(II) (ratio PT:Cu(II), 1:0.9) in HEPES buffer 100 mM, pH 7.4, 3 mM GSH and 6 µM $Zn(II)_7$MT-1/$Zn(II)_7$MT-2a/$Zn(II)_7$MT-3. Intermediate spectra have been collected at 4 min intervals.

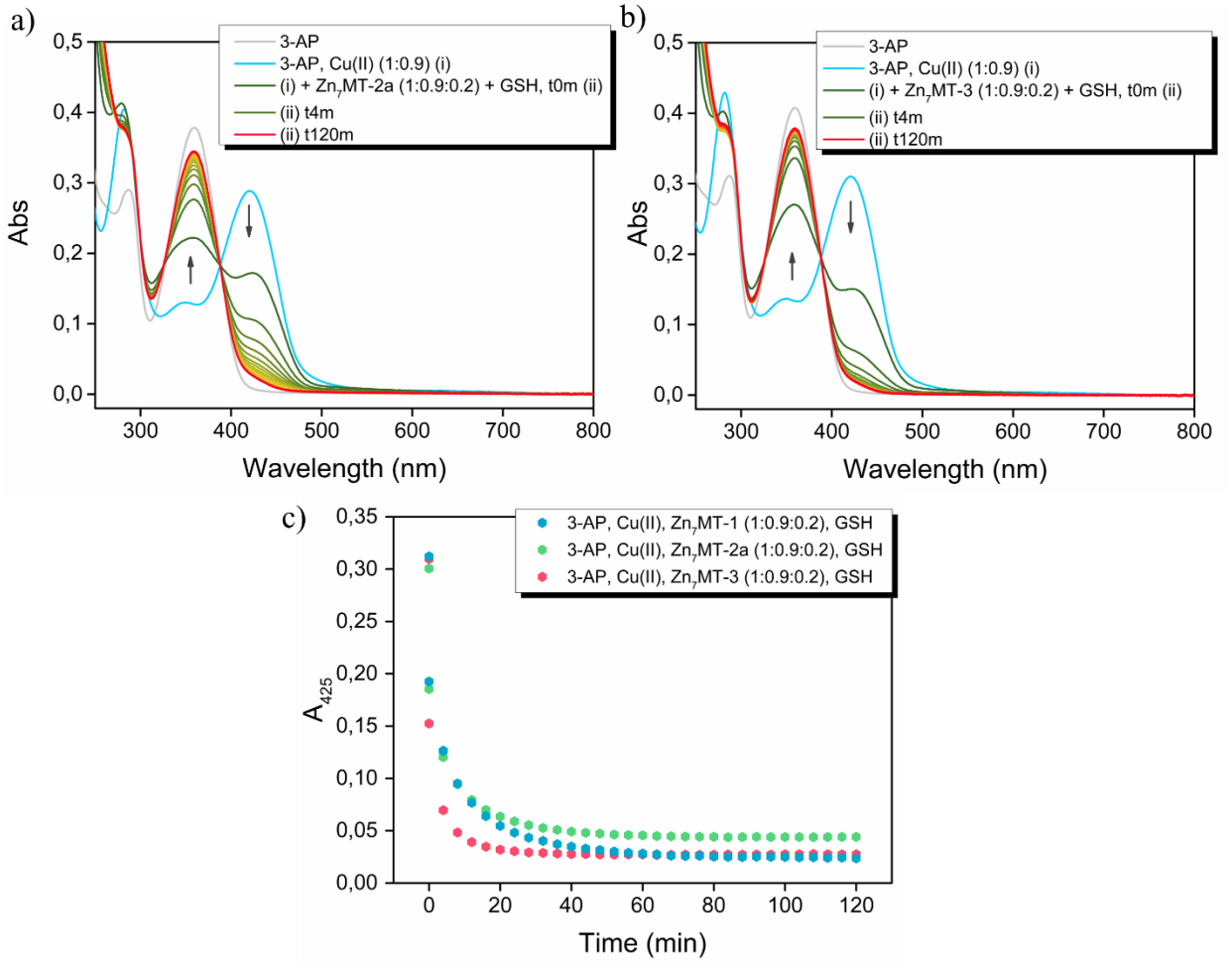

FigS 24 - Uv-Vis spectra of for the reaction of Cu(II)-3-AP with a) GSH/$Zn(II)_7$MT-2a, b) GSH/$Zn(II)_7$MT-3 monitored over time after GSH/$Zn(II)_7$MT addition to the preformed Cu(II)-3-AP complex (for the reaction with $Zn(II)_7$MT-1, see **Fig 36**). c) Corresponding experimental kinetics, i.e. absorbance at λ_{max} = 425 nm (CT band of the ternary complex [3-AP-Cu(II)-GSH]) versus time: $Zn(II)_7$MT-1 isoform (blue profile), $Zn(II)_7$MT-2a isoform (green profile), $Zn(II)_7$MT-3 isoform (red profile). Experimental conditions: 30 µM 3-AP, 27 µM Cu(II) (ratio PT:Cu(II), 1:0.9) in HEPES buffer 100 mM, pH 7.4, 3 mM GSH and 6 µM $Zn(II)_7$MT-1/$Zn(II)_7$MT-2a/$Zn(II)_7$MT-3. Intermediate spectra have been collected at 4 min intervals.

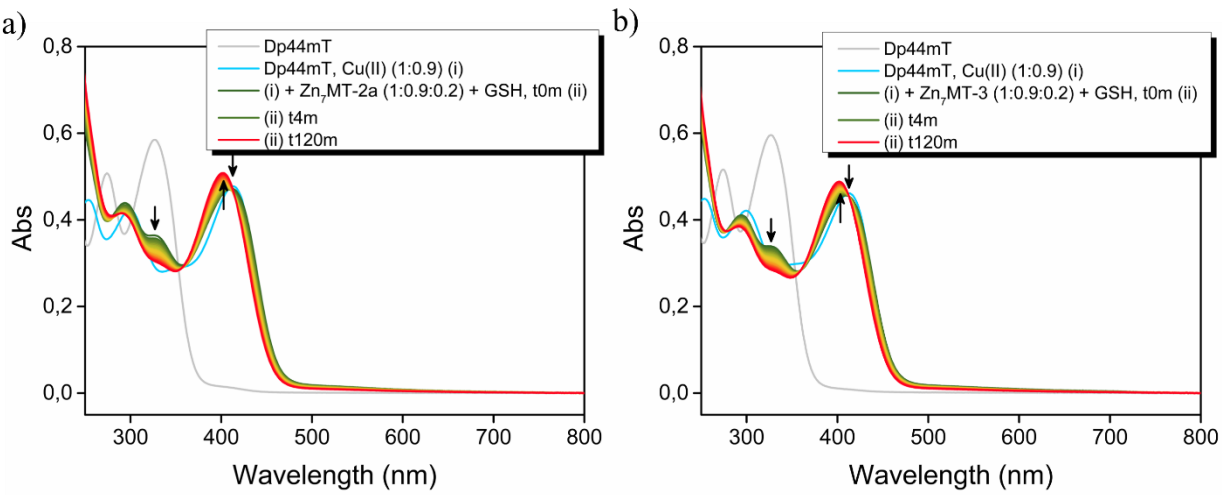

FigS 25 - Uv-Vis spectra of for the reaction of Cu(II)-Dp44mT with a) GSH/$Zn(II)_7$MT-2a, b) GSH/$Zn(II)_7$MT-3 monitored over time after GSH/$Zn(II)_7$MT addition to the preformed Cu(II)-Dp44mT complex (for the reaction with $Zn(II)_7$MT-1, see **Fig 36**). Experimental conditions: 30 µM Dp44mT, 27 µM Cu(II) (ratio Dp44mT:Cu(II), 1:0.9) in HEPES buffer 100 mM, pH 7.4, 3 mM GSH and 6 µM $Zn(II)_7$MT-1/$Zn(II)_7$MT-2a/$Zn(II)_7$MT-3. Intermediate spectra have been collected at 4 min intervals.

TableS 4 - Table summarizing the $t_{1/2}$ (min) values for the reactions of Cu(II)-PT and Cu(II)-3-AP with GSH and $Zn(II)_7$MT-1/$Zn(II)_7$MT-2a/$Zn(II)_7$MT-3. $t_{1/2}$ values were calculated from the experimental kinetics of disappearance of the of CT bands of the [PT/3-AP- Cu(II)-GSH] complexes (λ_{max} [PT-Cu(II)-GSH] = 386 nm, λ_{max} [3-AP-Cu(II)-GSH] = 424 nm). Experimental kinetics were fitted with a 1st order exponential equation y = W*exp(-k*x)+A.

Reaction	**$t_{1/2}$ (min)**
Cu(II)-PT + $Zn(II)_7$MT-1 + GSH	10.4
Cu(II)-PT + $Zn(II)_7$MT-2a + GSH	8.2
Cu(II)-PT + $Zn(II)_7$MT-3 + GSH	3.1
Cu(II)-3-AP + $Zn(II)_7$MT-1 + GSH	5.0
Cu(II)-3-AP + $Zn(II)_7$MT-2a + GSH	3.8
Cu(II)-3-AP + $Zn(II)_7$MT-3 + GSH	1.9

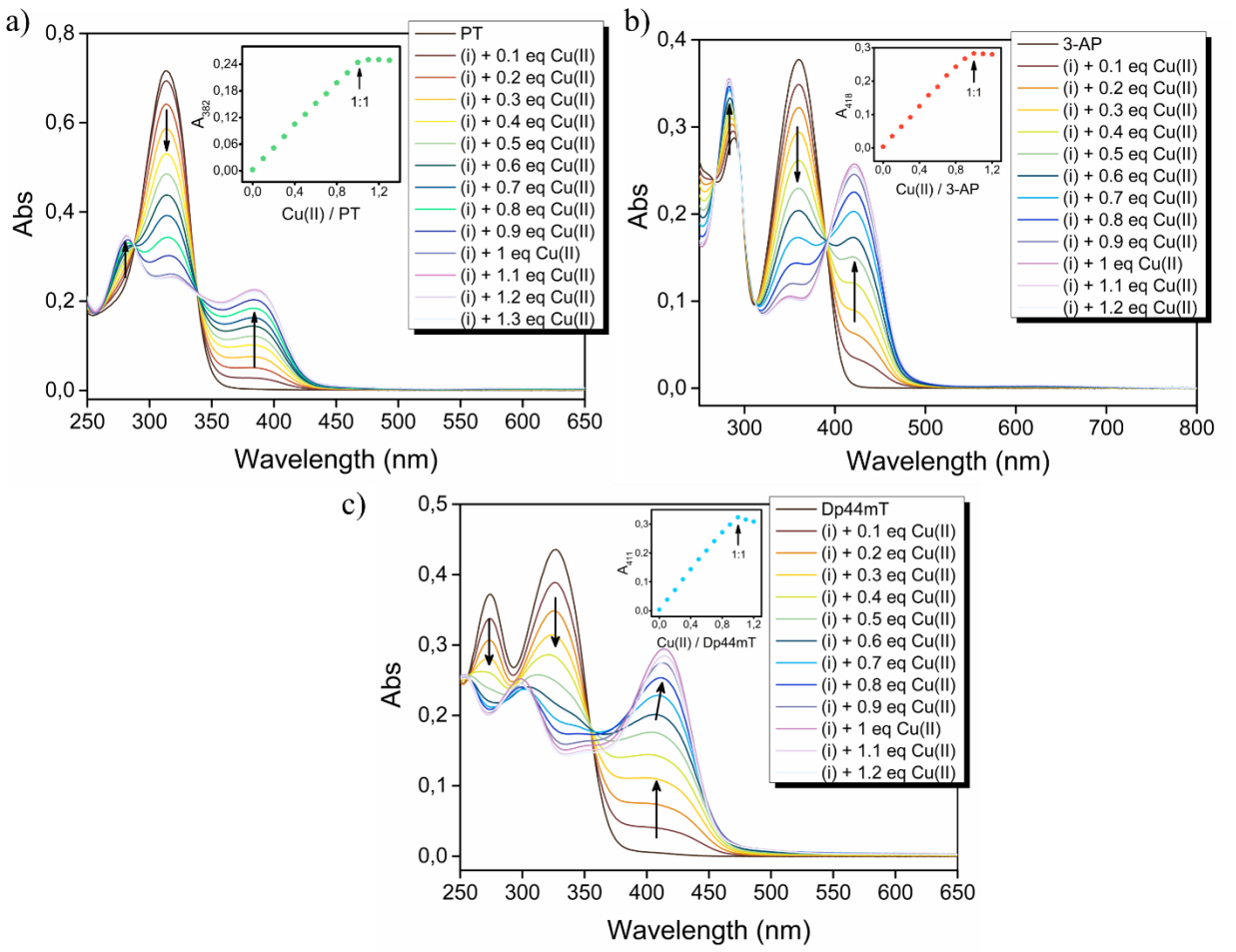

FigS 26 - Zn(II) titration experiments to determine the binding stoichiometry a) Zn(II)/PT, b) Zn(II)/3-AP, c) Zn(II)/Dp44mT. Insets: corresponding binding curves at λ_{max} = 364 nm. Experimental conditions: a solution of 30 µM ùof PT/3-AP/Dp44mT in HEPES buffer 100 mM, pH 7.4, was titrated with 1 µl aliquots of a 300 µM Zn(II) stock solution. Zn(II)-PT: λ_{max} = 364 nm, λ_{max} = 275 nm, isosbestic point, λ = 337 nm.

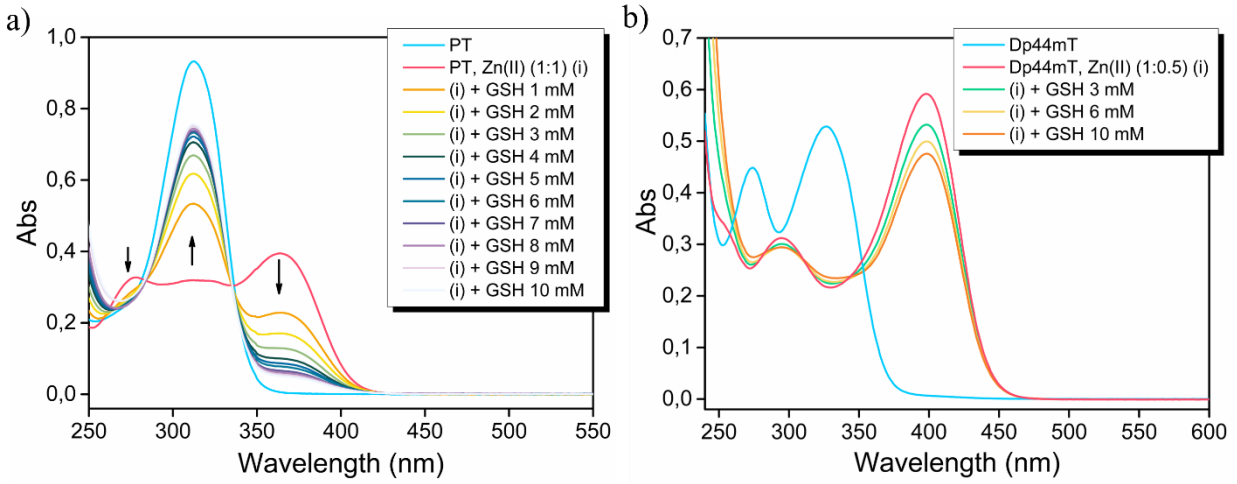

FigS 27 - Uv-Vis spectra corresponding to the reaction of a) Zn(II)-PT, b) Zn(II)-$(Dp44mT)_2$ with increasing concentration of GSH (up to 10 mM). Experimental conditions: a) 30 µM 3-AP, 30 µM Zn(II), b) 30 µM Dp44mT, 15 µM Zn(II) in HEPES buffer 100 mM, pH 7.4, GSH (1-10 mM).

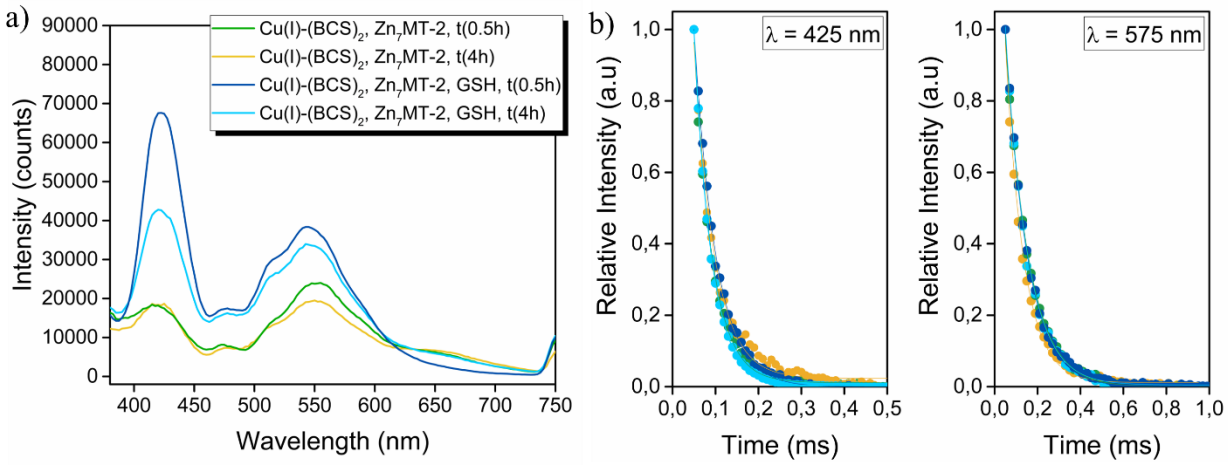

FigS 28 - a) Low-temperature luminescence spectra obtained after the addition of $Zn(II)_7$-MT-1 with or without GSH to the preformed Cu(I)-$(BCS)_2$ complex. b) Emission lifetimes obtained from the decay fits of the emissive bands at 425 nm (left panel) and at 575 nm (right panel). Experimental conditions: 10 µM Cu(I)-$(BCS)_2$ (ratio 1:2.4), 2.5 µM $Zn(II)_7$-MT-1 (ratio Cu-complex: $Zn(II)_7$-MT-1, 1:0.25), 3 mM GSH, HEPES 50 mM, pH 7.4.

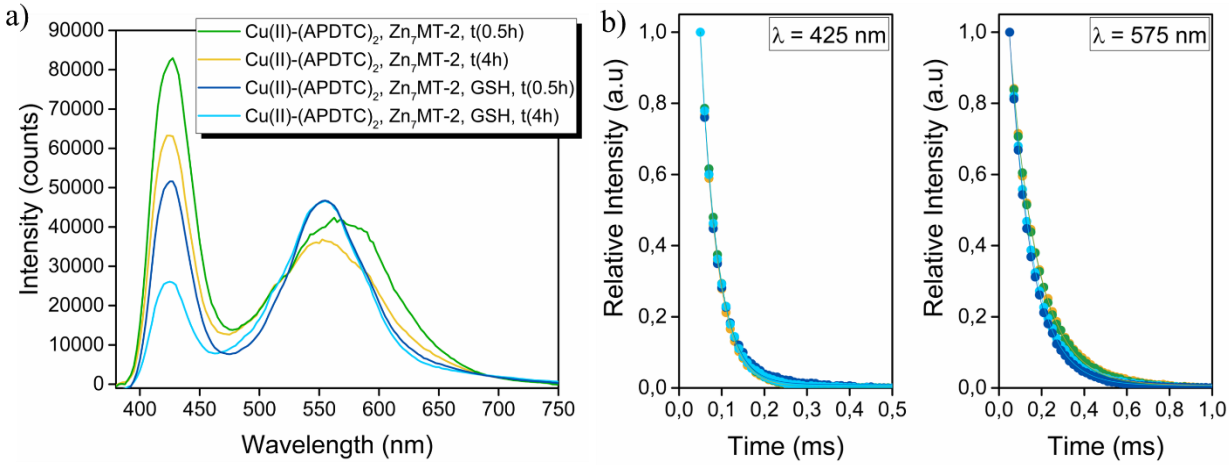

FigS 29 - a) Low-temperature luminescence spectra obtained after the addition of $Zn(II)_7$-MT-1 with or without GSH to the preformed Cu(II)-$(APDTC)_2$ complex. b) Emission lifetimes obtained from the decay fits of the emissive bands at 425 nm (left panel) and at 575 nm (right panel). Experimental conditions: 10 µM Cu(II)-$(APDTC)_2$ (ratio 1:2), 2.5 µM $Zn(II)_7$-MT-1 (ratio Cu-complex: $Zn(II)_7$-MT-1, 1:0.25), 3 mM GSH in HEPES 50 mM, pH 7.4.

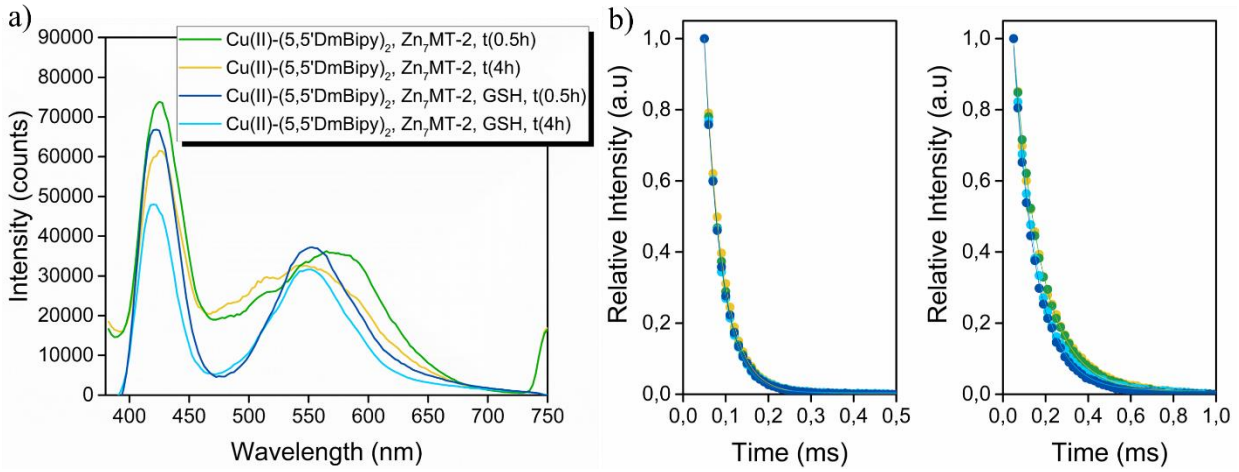

FigS 30 - a) Low-temperature luminescence spectra obtained after the addition of $Zn(II)_7$-MT-1 with or without GSH to the preformed Cu(II)-(5,5'DmBipy)$_2$ complex. b) Emission lifetimes obtained from the decay fits of the emissive bands at 425 nm (left panel) and at 575 nm (right panel). Experimental conditions: 10 µM Cu(II)-(5,5'DmBipy)$_2$ (ratio 1:2.4), 2.5 µM $Zn(II)_7$-MT-1 (ratio Cu-complex: $Zn(II)_7$-MT-1, 1:0.25), 3 mM GSH, HEPES 50 mM, pH 7.4.

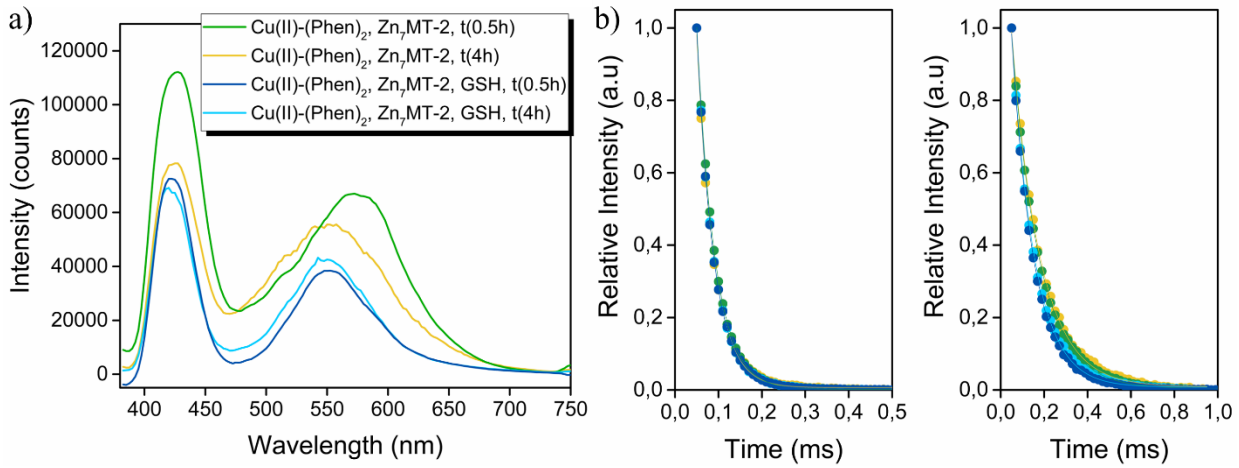

FigS 31 - a) Low-temperature luminescence spectra obtained after the addition of $Zn(II)_7$-MT-1 with or without GSH to the preformed Cu(II)-(Phen)$_2$ complex. b) Emission lifetimes obtained from the decay fits of the emissive bands at 425 nm (left panel) and at 575 nm (right panel). Experimental conditions: 10 µM Cu(II)-(Phen)$_2$ (ratio 1:2.4), 2.5 µM $Zn(II)_7$-MT-1 (ratio Cu-complex: $Zn(II)_7$-MT-1, 1:0.25), 3 mM GSH, HEPES 50 mM, pH 7.4.

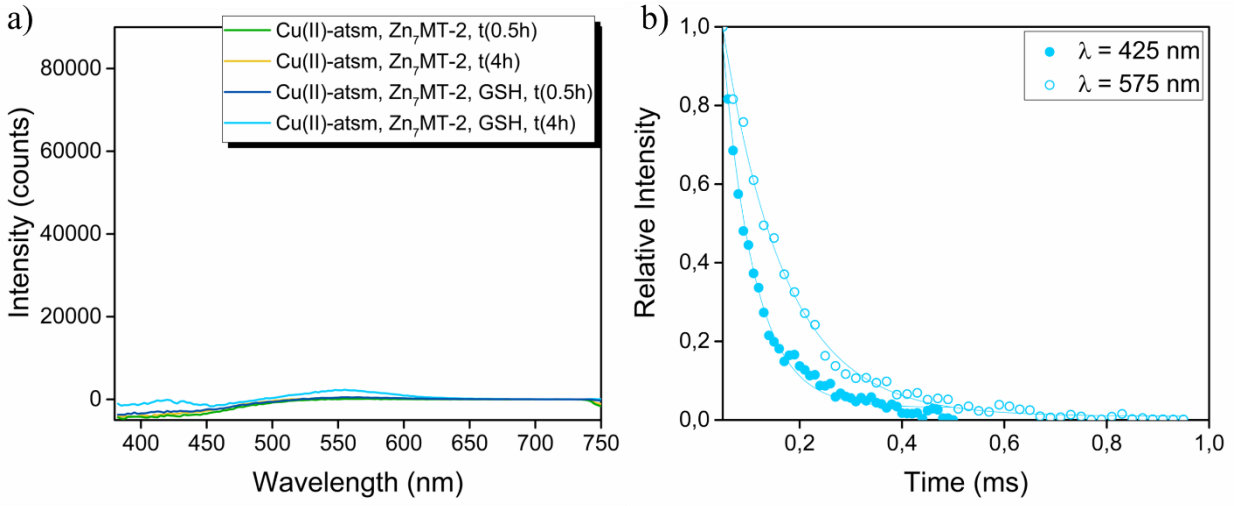

FigS 32 - a) Low-temperature luminescence spectra obtained after the addition of $Zn(II)_7$-MT-1 with or without GSH to the preformed Cu(II)-atsm complex. b) Emission lifetimes obtained from the decay fits of the emissive bands at 425 nm (left panel) and at 575 nm (right panel). Experimental conditions: 10 µM Cu(II)-$(Phen)_2$ (ratio 1:1.2), 2.5 µM $Zn(II)_7$-MT-1 (ratio Cu-complex: $Zn(II)_7$-MT-1, 1:0.25), 3 mM GSH in HEPES 50 mM, pH 7.4.

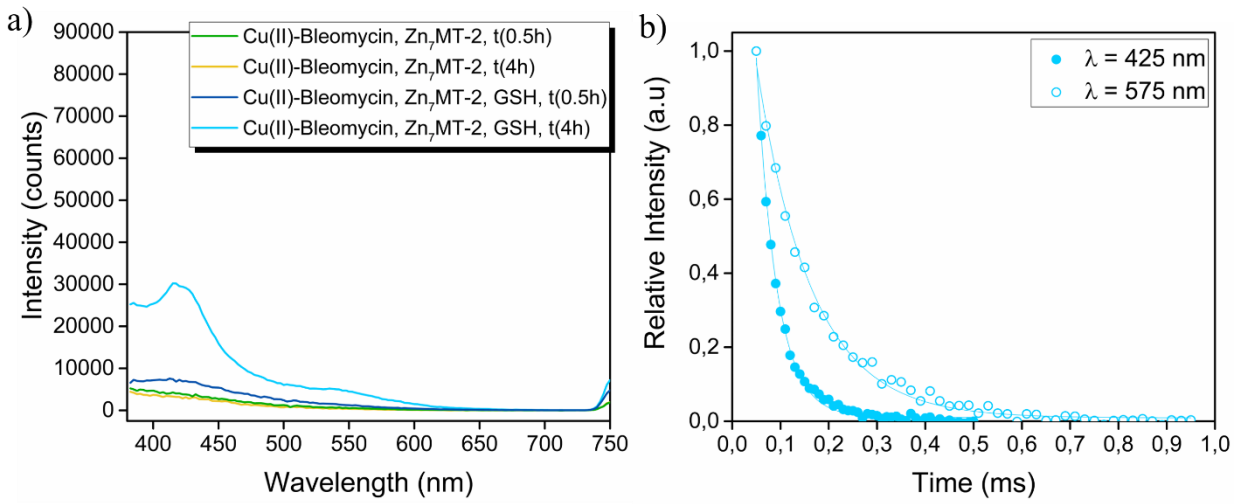

FigS 33 - a) Low-temperature luminescence spectra obtained after the addition of $Zn(II)_7$-MT-1 with or without GSH to the preformed Cu(II)-Bleomycin complex. b) Emission lifetimes obtained from the decay fits of the emissive bands at 425 nm (left panel) and at 575 nm (right panel). Experimental conditions: 10 µM Cu(II)-Bleomycin (ratio 1:1.2), 2.5 µM $Zn(II)_7$-MT-1 (ratio Cu-complex: $Zn(II)_7$-MT-1, 1:0.25), 3 mM GSH in HEPES 50 mM NaCl, pH 7.4.

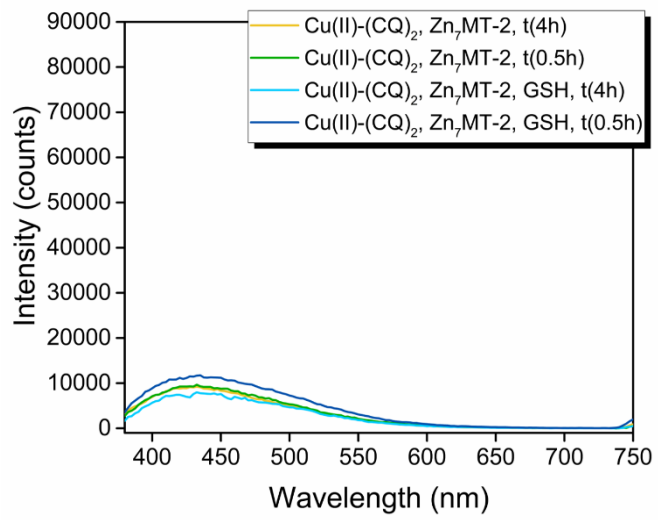

FigS 34 - a) Low-temperature luminescence spectra obtained after the addition of $Zn(II)_7$-MT-1 with or without GSH to the preformed Cu(II)-$(CQ)_2$ complex. Experimental conditions: 10 µM Cu(II)-CQ (ratio 1:2), 2.5 µM $Zn(II)_7$-MT-1 (ratio Cu-complex: $Zn(II)_7$-MT-1, 1:0.25), 3 mM GSH in HEPES 50 mM, pH 7.4.

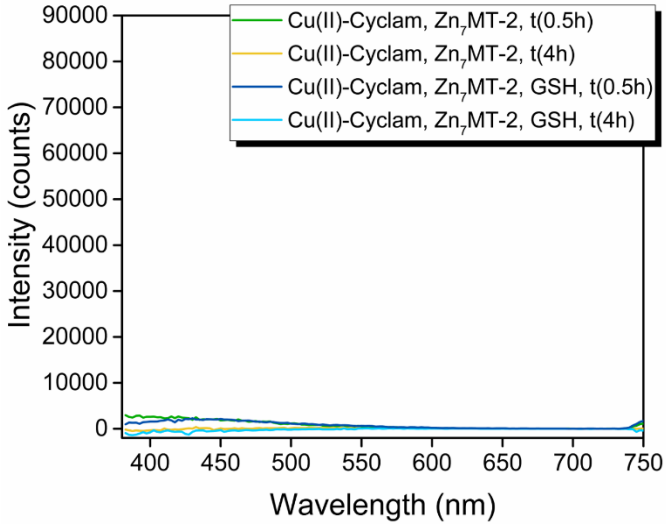

FigS 35 - Low-temperature luminescence spectra obtained after the addition of $Zn(II)_7$-MT-1 with or without GSH to the preformed Cu(II)-Cyclam complex. Experimental conditions:10 µM Cu(II)-Cyclam (ratio 1:1.2), 2.5 µM $Zn(II)_7$-MT-1 (ratio Cu-complex: $Zn(II)_7$-MT-1, 1:0.25), 3 mM GSH in HEPES, 50 mM, pH 7.4.

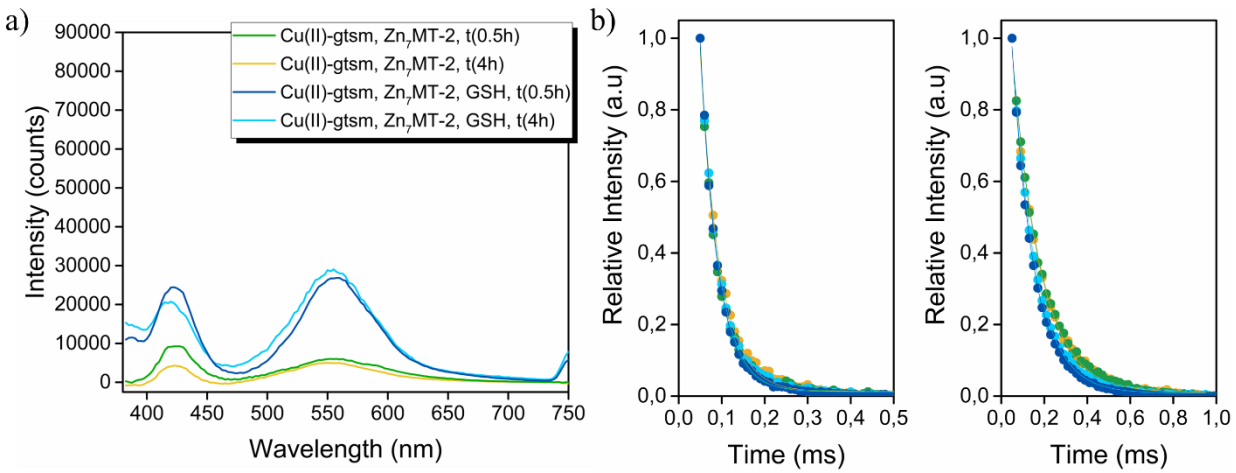

FigS 36 - a) Low-temperature luminescence spectra obtained after the addition of $Zn(II)_7$-MT-1 with or without GSH to the preformed Cu(II)-gtsm complex. b) Emission lifetimes obtained from the decay fits of the emissive bands at 425 nm (left panel) and at 575 nm (right panel). Experimental conditions: 10 µM Cu(II)-gtsm (ratio 1:1.2), 2.5 µM $Zn(II)_7$-MT-1 (ratio Cu-complex: $Zn(II)_7$-MT-1, 1:0.25), 3 mM GSH in HEPES, 50 mM, pH 7.4.

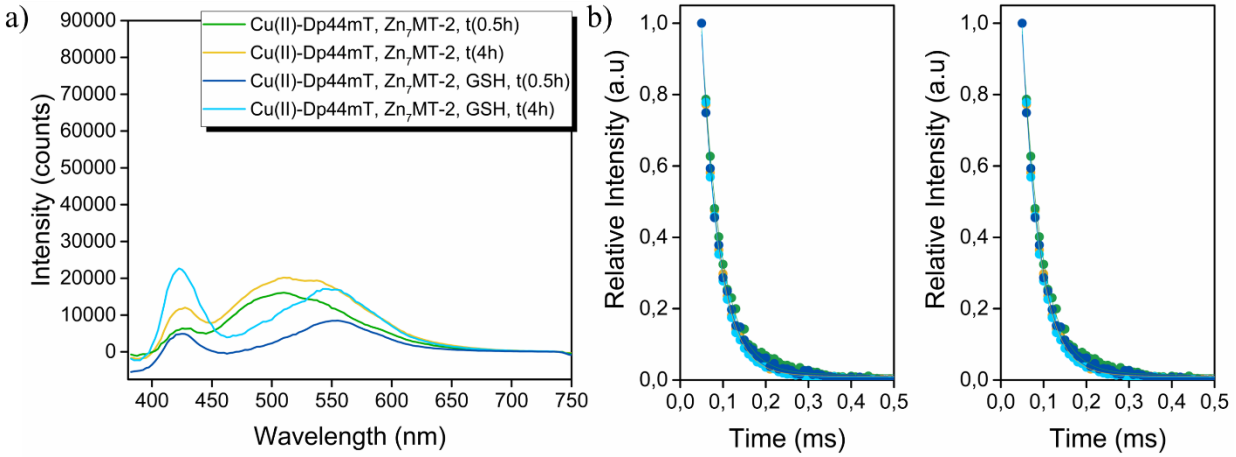

FigS 37 - a) Low-temperature luminescence spectra obtained after the addition of $Zn(II)_7$-MT-1 with or without GSH to the preformed Cu(II)-Dp44mT complex. b) Emission lifetimes obtained from the decay fits of the emissive bands at 425 nm (left panel) and at 575 nm (right panel). Experimental conditions: 10 µM Cu(II)-Dp44mT (ratio 1:1.2), 2.5 µM $Zn(II)_7$-MT-1 (ratio Cu-complex: $Zn(II)_7$-MT-1, 1:0.25), 3 mM GSH in HEPES, 50 mM, pH 7.4.

5.4 Reference list

1 N. E. Wezynfeld, E. Stefaniak, K. Stachucy, A. Drozd, D. Płonka, S. C. Drew, A. Krężel and W. Bal, *Angew. Chemie - Int. Ed.*, 2016, **55**, 8235–8238.

2 P. Faller, D. W. Hasler, O. Zerbe, S. Klauser, D. R. Winge and M. Vaăák, *Biochemistry*, 1999, **38**, 10158–10167.

3 A. Krezel and W. Maret, *J. Am. Chem.Soc*, 2007, **129**, 10911–10921.

4 A. Krężel, R. Latajka, G. D. Bujacz and W. Bal, *Inorg. Chem.*, 2003, **42**, 1994–2003.

5 A. Kocyła, A. Pomorski and A. Krężel, *J. Inorg. Biochem.*, 2015, **152**, 82–92.

6 P. Eyer, F. Worek, D. Kiderlen, G. Sinko, A. Stuglin, V. Simeon-Rudolf and E. Reiner, *Anal. Biochem.*, 2003, **312**, 224–227.

7 E. Atrián-Blasco, M. Del Barrio, P. Faller and C. Hureau, *Anal. Chem.*, 2018, **90**, 5909–5915.

8 N. Romero-Isart, L. T. Jensen, O. Zerbe, D. R. Winge and M. Vaák, *J. Biol. Chem.*, 2002, **277**, 37023–37028.

9 N. Cols, N. Romero-Isart, M. Capdevila, B. Oliva, P. Gonzàlez-Duarte, R. Gonzàlez-Duarte and S. Atrian, *J. Inorg. Biochem.*, 1997, **68**, 157–166.

10 A. Drozd, D. Wojewska, M. D. Peris-Díaz, P. Jakimowicz and A. Krężel, *Metallomics*, 2018, **10**, 595–613.

11 J. L. J. Dearling, J. S. Lewis, G. E. D. Mullen, M. J. Welch and P. J. Blower, *J. Biol. Inorg. Chem.*, 2002, **7**, 249–259.

12 H. Beraldo, L. P. Boyd and D. X. West, 1998, **71**, 67–71.